NASA CONTRACTOR REPORT

NASA CR-1515

A STUDY OF THE VIBRATION RESPONSES OF SHELLS AND PLATES TO FLUCTUATING PRESSURE ENVIRONMENTS

by D. J. Bozich and R. W. White

Prepared by
WYLE LABORATORIES
Huntsville, Ala.
for Manned Spacecraft Center

NATIONAL AERONAUTICS AND SPACE ADMINISTRATION • WASHINGTON, D. C. • MARCH 1970

NASA CR-1515

A STUDY OF THE VIBRATION RESPONSES OF SHELLS AND PLATES TO FLUCTUATING PRESSURE ENVIRONMENTS

By D. J. Bozich and R. W. White

Issued by Originator as Report No. WR 69-19

Prepared under Contract No. NAS 9-7484 by
WYLE LABORATORIES
Huntsville, Ala.

for Manned Spacecraft Center

NATIONAL AERONAUTICS AND SPACE ADMINISTRATION

For sale by the Clearinghouse for Federal Scientific and Technical Information
Springfield, Virginia 22151 – Price $3.00

SUMMARY

Effects of modal cross-correlations on the spatial distributions of vibration amplitudes are investigated for a damped, uniform beam having localized excitation. Using a computerized modal analysis method, analytical estimates of the space-average mean-square acceleration response spectra were determined for a variety of uniform cylindrical shells and flat plates exposed to ducted progressive acoustic wave fields, a reverberant acoustic field, and boundary layer turbulence. Several approximations of the series response equation are introduced in order to show how special situations can be treated by elementary methods. A comparison between the modal analysis and statistical energy methods is presented for shell response to reverberant acoustic excitation.

ACKNOWLEDGEMENTS

The authors wish to express their appreciation to Mr. K. McK. Eldred of Wyle Laboratories for many helpful discussions during the course of this investigation. The authors wish to thank Mr. D. Lister of Wyle for performing the extensive programming efforts and numerical computations required for this study; Mr. V. Conticelli for providing the technical material for Section 3.1.6 and for the statistical energy evaluations used in this report; and Mr. J. Matzkiw for documentation assistance.

TABLE OF CONTENTS

1.0 INTRODUCTION

During 1967 and 1968, acoustic and vibration qualification tests were performed on the Apollo structure at NASA's Manned Space Center in Houston, Texas. The structure tested included the stacked configuration of the Command Module, Service Module, Spacecraft Lunar Module Adapter (SLA), the Lunar Module mounted within the SLA, and the Instrument Unit. These tests were performed in the Spacecraft Acoustic Laboratory (SLA) which is housed in Building 39 at the NASA complex. The SAL facility was designed to subject the structure to two types of acoustic environments, namely:

a) A reverberant acoustic field.

b) A progressive wave field generated within sixteen, axially oriented ducts that are close coupled to the skin of the vehicle and which are independently driven at one end by random acoustic noise sources.

These two acoustic environments were used to simulate the fluctuating pressure environments on the vehicle due to rocket noise at launch and due to in-flight boundary layer turbulence. By limiting the acoustic correlation lengths around the circumference of the vehicle, the sixteen ducts provided a measure of simulation of aerodynamic turbulence over the vehicle skin.

In support of the above testing program, an analytical study was made of the vibration responses of a portion of the Apollo structure when exposed to various types of fluctuating pressure environments, including:

- Axially oriented ducts of various circumferential widths
- Reverberant acoustic field
- Boundary layer pressure fluctuations

Comparisons of responses to acoustic and boundary layer turbulence fields allowed the acoustic spectrum levels to be adjusted as a function of frequency so that the acceleration response spectrum to acoustic excitation is similar to that expected for in-flight turbulence. Response to the acoustic launch environment was expected to be similar to that of a reverberant or duct field. In order for the analyses to be tractable, the portion of the structure selected for analysis was the SLA which is a uniform, truncated conical shell constructed of 1.7 in. thick aluminum honeycomb. The short angle of the shell is only 9 degrees so the analyses were conducted for an equivalent cylindrical shell having the same length and same average radius of the SLA.

The method of analysis used is a classical modal analysis of the shell in which all modes were included whose resonance frequencies were between 10 and 1000 Hz. An exception is that all (m,n)-modes of the shell for which n = 1 were deleted because it was felt that constraints on the ends of the SLA were insufficient to permit such modes to respond. A detailed discussion of the method of analysis and of the analytical results are presented in References 1 and 2.

During the course of this analytical study, a computer program was developed at Wyle Laboratories, Huntsville Division, for the purpose of performing the detailed calculations of the modal forcing functions, resonance frequencies, dynamic magnification factors and the summation of the space-average acceleration responses of all of the modes of the shell. Since the submission of Reference 1, the authors have extended this computer program to include:

Analyzeable Structures

- Uniform Cylindrical Shells
- Uniform Rectangular Plates

Excitation Fields

- Point Force
- Axially Oriented Ducts
- Reverberant Acoustic Field
- Boundary Layer Turbulence

Distributed over entire surface or localized to any rectangular area.

Printouts

- Resonance Frequencies
- Deflection, Velocity, or Acceleration Spectrum for Space-Average or Pointwise Responses
- Third Octave Responses
- Tables of Individual Modal Responses Ordered by Response Amplitude
- Joint Acceptances
- Dynamic Magnification Factors

Plots

- Resonance Frequencies Versus Either Mode Number m or n
- Response Spectra
- Joint Acceptances

Since the development of this computer program, it has been used to analyze the responses of a variety of plate and shell structures. Included among these are the Apollo SLA, Supersonic Transport (SST) (Reference 9), and the Manned Orbital Laboratory (Reference 10).

This report has several purposes. First, an assumption is made in Reference 1 that the effects of cross-correlations between responses of different modes are small and can be neglected, and hence that the space-average response of the SLA is a good measure of the response at any point on the shell. Some interest has been generated in these cross-correlations. In reference 3, Wilby investigates the magnitudes of such terms for flat plates exposed to boundary layer turbulence and he finds that in general their contributions can be neglected. As discussed by Powell in Reference 7, these cross-correlations account for the difference between the space-average response level and the response at a point; and if the differences between these are significant, then the modal cross-correlations can be expected to be significant. As an example of such a circumstance, response of a damped plate or shell to a localized excitation will display vibration levels at the source location (area of application of excitation) which are high relative to levels at some distance from the source. This decay of vibration levels with distance is expected to increase with increasing frequency. Thus, for response of a structure to a point force, or any other localized excitation, the modal cross-correlations will be important at high frequencies. Such cases can be of practical significance when aerospace shells are exposed to localized, high level turbulence and buffet loads in the neighborhood of a protuberance.

In an attempt to study the modal cross-correlations in a simple manner, an analysis is presented in Section 2.0 of the vibration responses of a damped, uniform, pinned-pinned beam excited by a harmonic couple at one end. This vibration problem is solved analytically by an exact method which leads to a closed form expression for the distribution of deflection amplitudes along the span of the beam. The problem is then solved by the modal analysis method in which the effects of modal cross-correlations are included. The results of both methods were numerically evaluated for excitation frequencies equal to the undamped resonance frequencies of the first and third modes of the beam, and it was found that the results were exactly equal. Graphs are presented which show how the cross-correlations control the dissipation of response levels with distance along the span of the beam.

As discussed in Reference 1, in the modal analysis technique, a large number of modes of a plate or shell are employed in the computation of a response spectrum. At each frequency, the space-average mean-square response of each mode is computed by accounting for dynamic magnitication factors and the structural pressure field coupling factors (joint acceptances) for the two principal directions of the structure. The total mean-square response at the given frequency is then found by summing the responses of all the modes. This procedure is repeated at 100 excitation frequencies per decade for two or three decades. Although this large amount of computation appears to be a formidable and expensive task, Wyle Laboratories computer program is designed so that the entire computation for a single analysis can generally be performed in about 2-3 minutes on a high speed digital computer.

This computer program was used to determine acceleration response spectra for a variety of cylindrical shells and plates exposed to various fluctuating pressure environments. These environments include ducted progressive acoustic wave fields, a reverberant acoustic field and boundary layer turbulence. For the duct excitation, responses were determined for different numbers of ducts (one to sixty-four ducts) and a special study was made to determine the effect on high frequency responses of an exponentially damped correlation function for one sixteen duct field. The results of these computations are presented in this report in order to show the variability of responses of different types of structures and different types of excitation.

Section 3.1 of this report contains a summary type description of the shell and plate structures that were analyzed. These structures were chosen with sufficient variability of geometry, stiffnesses and masses such that general trends in response characteristics can be noted from the computed acceleration spectra.

Mode shapes and generalized masses for uniform shells and plates are discussed in Section 3.2. This section is included since the mode shape functions assumed for cylindrical shells have been improved relative to those employed in Reference 1. In particular, the amplitude of the tangential mode shape is varied with circumferential mode number so that the cylindrical shell asymptotically approaches a flat plate for a large number of circumferential modes. The resulting effect on generalized mass is also discussed.

Resonance frequencies and modal densities of these structures are analyzed in Section 3.3. Characteristics of the various fluctuating pressure environments are briefly reviewed in Section 3.4 and this is followed by a discussion of the coincidence phenomena in Section 3.5. Appendices A and B, in which the mathematical forms for joint acceptance are developed, are included as supplements to the discussions in Sections 3.4 and 3.5. The general series equation used for the acceleration spectrum computations is presented in Section 3.6, and this is followed in Section 3.7 by the development of several simplifying approximations of the general response equation.

During the past few years, significant advances have been made in the development of statistical energy methods as applied to structural vibrations. Such methods provide an alternate technique for computing vibration responses of shells and plates exposed to fluctuating pressure environments. It is of interest to compare results obtained by the modal analysis method and the statistical energy method, and for this purpose, the equations used in the latter approach are reviewed in Section 3.8.

Section 4.0 contains a summary type discussion of the many acceleration spectra computed during the course of this study. SLA responses to acoustic excitation within 1, 2, 4, 8, 16, 32, and 64 ducts are presented in Section 4.1.1. Here it is shown that theoretically a rapid roll-off of response occurs above the ring (actually coincidence) frequency. A comparison is made between these predicted responses and a comparable experimentally measured response which shows no such roll-off. The possibility exists that actual space conditions differ from those assumed in the analysis; and as a possible explanation of this difference, acceleration spectra are presented in Section 4.1.2 for an acoustic field with an exponentially damped correlation function for each duct.

An investigation of the modes of the SLA shows that this shell is a rather special case shell in that all shell modes are acoustically fast in the axial direction, and the flat plate acoustic coincidence frequency occurs at approximately twice the ring frequency, whereas for thin wall cylinders this factor is five to ten times. It is interesting, therefore, to consider how the response changes as various structural parameters are altered, such as the radius, extensional and bending stiffnesses and the mass per unit area. Several such cases are analyzed and discussed in Section 4.1.3 for acoustic duct excitation. For purposes of comparison, this section includes the analysis of several other smaller shells with homogeneous skins and a few flat plates.

The basic SLA shell and the other cylinders and plates are analyzed for response to a reverberant acoustic field and to boundary layer turbulence in Sections 4.2 and 4.3. Reverberant responses of these structures are similar to responses for duct excitation; however, there are differences which warrant presenting responses for both types of acoustic fields. The essential difference in response to reverberant and duct acoustic fields lies in the circumferential correlation lengths, which for a reverberant field are quite different from those at a ducted progressive wave field. Structural responses of plates and shells are often analyzed by statistical energy analysis methods; and for purposes of comparison with the modal analysis techniques, several reverberant response spectra are computed by both methods. Responses to boundary layer turbulence are presented for different Mach numbers and different boundary layer thicknesses. Comparisons of the response of a given structure to different types of excitation are made throughout Section 4.0.

In the computerized version of the modal analysis technique used for the above response studies, no attempt is made to predict those modes which are expected to be dominant. The computation procedure could be made more efficient if the significant modes responding at any frequency could be predetermined. Several example structures were selected for a detailed mode-by-mode analysis by the digital computer, and printouts of the first 40 most important modes are made at four frequencies for duct, reverberant and turbulence excitation. The printouts include mode number, joint-acceptance dynamic magnification factors, wavelength ratios and accumulation percentage contributions of the modes to the total response. In addition, plots are presented of the number of modes required to achieve various percentages of the total response. (These data are discussed in Section 4.0.)

2.0 RESPONSE OF A DAMPED BEAM FOR LOCALIZED EXCITATION

This section of the report contains an analysis of the steady-state vibration response of a damped, uniform, pinned-pinned beam for a harmonic point-couple applied to one end of the beam. The absolute value of the deflection amplitude is determined as a function of position along the span of the beam; and the space-average value of this amplitude over the length of the beam is also determined. For purposes of comparison, the beam analysis is performed by two different methods, namely:

1. An exact analysis which leads to a closed form expression for the deflection amplitude.
2. A modal analysis which leads to a Fourier series type expression for the deflection amplitude.

Due to the presence of damping, the vibration levels in the neighborhood of the excited end of the beam are expected to be higher than the vibration levels near the other end; and in general, the vibration levels should decay with distance from the source of excitation. Furthermore, the rate at which deflection amplitudes decay with distance along the span depends upon the magnitude of internal damping and upon the excitation frequency such that the decay rate increases with either damping level or excitation frequency. For nominal values of damping, the spatial decay rate is not large at low frequencies such as the resonance frequency of the fundamental mode of the beam; however, at higher frequencies, the spatial decay is pronounced. For a fixed value of beam damping, this effect is often described simply as a constant decrease in vibration amplitude across each elastic wave length of the beam so that the decay rate increases with an increasing number of elastic waves along the span of the beam.

The exact analysis method provides a closed form expression for the spatially decaying vibration levels; and the functional control of damping and frequency upon the decaying vibration levels is readily apparent. The primary purpose of this analysis is to show that a modal analysis technique, which involves a series of non-decaying response quantities, can be accurately used to predict the same spatial decay of vibration levels along the span of the beam. In particular, it is shown that the cross-correlations of responses of different modes of the beam are responsible for this decay.

Numerical examples are constructed for each of the two methods of analysis. Using the exact method of analysis, two numerical examples are presented in which the excitation frequency is chosen so as to be approximately equal to the resonance frequencies of the first and third modes, respectively, of the undamped beam. For purposes of comparison, the second of these two numerical examples is repeated by using equations developed from the modal analysis. Comparable values of damping are used in all of the examples; and in order to emphasize the spatial decay of vibration levels, a relatively large value of damping is employed, namely, a damping value which is approximately equal to one-half of critical damping for the resonant mode of interest.

Equations of motion for the two methods of analysis are developed in Section 2.1. Here, for the exact method of analysis, the excitation couple is introduced as a boundary condition on the bending moment at the driven end of the beam; while for the modal analysis method, the excitation couple is treated as the limit of a distributed force along the beam span. Based on the equations of motion, exact response equations are developed in Section 2.2 and modal analysis response equations are developed in Section 2.3.

2.1 Equations of Motion

Consider a uniform pinned-pinned beam whose basic properties are defined as:

L = length

μ = mass per unit length

I = moment of inertia of cross-section area

E = Young's modulus of elasticity

c = equivalent viscous damping per unit length.

Such a beam is shown in Figure 1, wherein the following quantities are used to describe the excitation and dynamic response of the beam:

x = axial coordinate; $0 \leq x \leq L$

t = time

U(x,t) = bending deflection

θ(x,t) = bending slope

$$= \partial U(x,t)/\partial x \tag{1a}$$

C(0,t) = external point couple applied at x = 0.

Internal beam bending moments and shear forces are shown in Figure 2 and are defined as:

M(x,t) = internal bending moment

$$= E I \, \partial^2 U(x,t)/\partial x^2 \tag{1b}$$

V(x,t) = internal shear force

$$= - \partial M(x,t)/2x = - E I \, \partial^3 U(x,t)/\partial x^3 \tag{1c}$$

An alternate form of excitation of the beam is shown in Figure 3, where:

$$\left.\begin{aligned} F(x,t) &= \text{applied force, per unit length, centered at } x_0 \\ &= F(t) \cdot [(x-x_0)/\epsilon], \quad |x-x_0| \leq \epsilon \\ &= 0 \qquad\qquad\qquad\quad , \quad |x-x_0| > 0 \end{aligned}\right\} \tag{2a}$$

F(t) = maximum value of F(x,t) at $x_0 + \epsilon$

$C(x_0,t)$ = point couple at x_0 which is equivalent to F(x,t)

$$= \int_{x_0-\epsilon}^{x_0+\epsilon} (x-x_0)\, F(x,t)\, dx = \frac{2}{3} F(t) \cdot \epsilon^2 \tag{2b}$$

In the limit as $F(t) \rightarrow \infty$ and $\epsilon \rightarrow 0_x$ such that $F(t) \cdot \epsilon^2$ remains finite, and as $x_0 \rightarrow 0$, the force distribution F(x,t) and the point couple $C(x_0,t)$ reduce to:

$$\left.\begin{aligned} \text{Lim } F(x,t) &= - C(0,t) \cdot d\delta(x)/dx \\ \text{Lim } C(x_0,t) &= C(0,t) \end{aligned}\right\} \begin{aligned} &\epsilon \rightarrow 0 \\ &F(t) \rightarrow \infty \\ &x_0 \rightarrow 0 \end{aligned} \tag{2c}$$

$\delta(x)$ = Dirac delta function

$$= \infty, \quad x = 0 \qquad (2d)$$

$$= 0, \quad x \neq 0$$

$d\delta(x)/dx$ = derivative of $\delta(x)$

$$= -\delta(x)/x \text{ (see Page 743 of Reference 8)} \qquad (2e)$$

The equation of motion of the beam can be written in either of the following homogeneous or inhomogeneous forms:

$$\mu \frac{\partial^2 U(x,t)}{\partial t^2} + c \frac{\partial U(x,t)}{\partial t} + EI \frac{\partial^4 U(x,t)}{\partial x^4} = 0 \qquad (3a)$$

$$\mu \frac{\partial^2 U(x,t)}{\partial t^2} + c \frac{\partial U(x,t)}{\partial t} + EI \frac{\partial^4 U(x,t)}{\partial x^4} = F(x,t) \qquad (3b)$$

Assuming that the excitation and response are steady-state and harmonic at frequency ω, any function $G(x,t)$ can be expressed as

$$G(x,t) = G(x)\, e^{i\omega t} = \left\{U(x,t),\ \theta(x,t),\ M(x,t),\ V(x,t),\ C(x_0,t),\ F(x,t),\ F(t)\right\} \qquad (4a)$$

$$G(x) = \text{complex amplitude} = \left\{U(x),\ \theta(x),\ M(x),\ V(x),\ C(x_0),\ F(x),\ F\right\} \qquad (4b)$$

In this case, Equations (3) reduce to the following ordinary differential equations:

$$\frac{d^4 U(x)}{dx^4} = \left(\frac{\lambda}{L}\right)^4 U(x) \qquad (5a)$$

$$\frac{d^4 U(x)}{dx^4} = \left(\frac{\lambda}{L}\right)^4 U(x) + \frac{F(x)}{EI} \qquad (5b)$$

where

$$\lambda^4 = \frac{L^4}{EI}\, \mu\, \omega^2\, (1 - i\,\delta) \qquad (6a)$$

$$= \lambda_0^4 \exp\left[-i\, 4\, \psi \pm i\, 2 n \pi\right], \quad n = 0,1,2,3 \qquad (6b)$$

$$\left.\begin{aligned} \lambda_0 &= L\, [\omega]^{\frac{1}{2}} \cdot [\mu/EI]^{\frac{1}{4}} \cdot [1 + \delta^2]^{1/8} \\ &= [\alpha^2 + \beta^2]^{\frac{1}{2}} \text{ (from Equations (9e) and (9f))} \\ \omega &= \left(\frac{\lambda_0}{L}\right)^2 \cdot \sqrt{\frac{EI}{\mu}} \cdot [1 + \delta^2]^{-\frac{1}{4}} \end{aligned}\right\} \qquad (6c)$$

$$\delta = c/\mu\,\omega = \text{damping factor } (0 \le \delta \le \infty) \qquad (6d)$$

$$\psi = \frac{1}{4} \tan^{-1} \delta = \text{phase angle } (0 \le \psi \le 22.5^\circ) \qquad (6e)$$

Equation (6b) implies that for $\delta > 0$, λ has the following four distinct complex values:

$$\lambda = \alpha - i\beta, \qquad n = 0 \tag{7a}$$
$$= -\beta - i\alpha, \qquad n = 1 \tag{7b}$$
$$= -\alpha + i\beta, \qquad n = 2 \tag{7c}$$
$$= \beta + i\alpha, \qquad n = 3 \tag{7d}$$

$$\alpha = \lambda_0 \cos\psi, \quad (1.0 \geq \cos\psi \geq 0.92388) \tag{7e}$$
$$\beta = \lambda_0 \sin\psi, \quad (0 \leq \sin\psi \leq 0.38268) \tag{7f}$$

Equation (5a) can be used to describe the response of the beam to the end couple by introducing C(0,t) as a boundary condition on the bending moment at $x = 0$; and this approach leads to an exact closed form solution as discussed in Section 2.2. Equation (5b) can be used to obtain an equivalent infinite series solution in terms of modal responses to the line force F(x,t), and in the limit to the end couple C(0,t); and this type of solution is developed in Section 2.3.

2.2 Closed Form Equation for Response

The general solution of Equation (5a) is:

$$U(x) = A \cosh\lambda\bar{x} + B \sinh\lambda\bar{x} + C \cos\lambda\bar{x} + D \sin\lambda\bar{x} \tag{8a}$$

$$\bar{x} = x/L = \text{nondimensional coordinate; } 0 \leq \bar{x} \leq 1 \tag{8b}$$

A,B,C,D = constants of integration.

Boundary conditions at the two ends of the pinned-pinned beam are:

$$U(x) = 0 \quad \text{at} \quad x = 0 \quad \text{and} \quad x = L \tag{9a}$$

$$\left.\begin{aligned} EI\, d^2U(x)/dx^2 = M(x) &= -C(0) \quad &\text{at } x = 0 \\ &= 0 &\text{at } x = L \end{aligned}\right\} \tag{9b}$$

Note that the negative sign is used in Equation (9b) because the applied couple C(0) is opposite in direction to the beam bending moment M(0) at $x = 0$. From Equations (8a) and (9a,b) the constants of integration are:

$$\left.\begin{aligned} A &= -C = -L^2 C(0)/2EI\lambda^2 \\ B &= -A \operatorname{ctnh}\lambda \\ D &= A \operatorname{ctn}\lambda \end{aligned}\right\} \tag{9c}$$

Substituting Equation (9c) into Equation (8a) gives the following closed form expression for the deflection amplitude of the damped pinned-pinned beam to the end couple:

$$U(x) = \frac{L^2 C(0)}{2EI\lambda^2} \bar{U}(x) \tag{10a}$$

$\bar{U}(x)$ = normalized deflection response

$$= \frac{\sin\lambda\bar{y}}{\sin\lambda} - \frac{\sinh\lambda\bar{y}}{\sinh\lambda} \tag{10b}$$

$$\bar{y} = 1 - \bar{x} \tag{10c}$$

As a partial check on the validity of Equations (10), the excitation frequency can be set equal to zero giving an expression for the static deflection, $U_s(x)$, due to a static end couple $C_s(0)$; and the resulting equation can be compared with well known solutions. Equations (6) show that $\lambda \to 0$ as $\omega \to 0$; and for vanishingly small values of λ, the functions in Equation (10b) can be approximated by the first few terms of their power series expansions, namely:

$$\left.\begin{aligned}
\sin \lambda \bar{y} &\doteq \lambda \bar{y} \left[1 - \frac{1}{6} (\lambda \bar{y})^2 + \ldots\right] \\
(\sin \lambda)^{-1} &\doteq \lambda^{-1} \left[1 - \frac{1}{6} \lambda^2 + \ldots\right] \doteq \lambda^{-1} \left[1 + \frac{1}{6} \lambda^2 - \ldots\right] \\
\sinh \lambda \bar{y} &\doteq \lambda \bar{y} \left[1 + \frac{1}{6} (\lambda \bar{y})^2 + \ldots\right] \\
(\sinh \lambda)^{-1} &\doteq \lambda^{-1} \left[1 + \frac{1}{6} \lambda^2 + \ldots\right] \doteq \lambda^{-1} \left[1 - \frac{1}{6} \lambda^2 - \ldots\right]
\end{aligned}\right\} \qquad (11)$$

Substituting Equations (11) into Equation (10b), and taking the limit as $\lambda \to 0$ gives:

$$U_s(x) = \frac{L^2\, C_s(0)}{6\, E I} (2 - \bar{x})(1 - \bar{x})\, \bar{x} \qquad (12a)$$

$$\left.\begin{aligned} U_s(x) &= U(x) \\ C_s(0) &= C(0) \end{aligned}\right\} \text{ at } \omega = 0 \qquad (12b)$$

Equation (12a) is equivalent to that presented under condition 19 in Table III on Page 104 of Reference 6. Note that a positive couple $C_s(0)$ yields a positive deflection $U_s(x)$ as expected on the basis of the sign convention shown in Figure 1.

Another special case of interest is that which corresponds to zero damping. In this case, $c = \delta = \psi = \beta = 0$ according to Equations (6a,b,c). Thus, Equations (10a,b) reduce to:

$$U(x) = \frac{L^2 C(0)}{2\, E I \lambda_0^2}\, \bar{U}(x) \qquad (13a)$$

$$\bar{U}(x) = \frac{\sin \lambda_0 \bar{y}}{\sin \lambda_0} - \frac{\sinh \lambda_0 \bar{y}}{\sinh \lambda_0} \qquad \delta = 0 \qquad (13b)$$

When $\lambda_0 = m\pi$, $m = 1, 2, 3, \ldots$, the first term in Equation (13b) becomes infinitely large implying that $\lambda_0 = m\pi$ corresponds to a resonance frequency of the undamped beam, with $\sin m\pi y$, or $\sin m\pi x$, being the associated resonant deflection shape of the beam. Thus, the resonance frequency and mode shape of the m-th mode of the undamped, pinned-pinned beam are:

ω_m = undamped resonance frequency of m-th mode

$$= \left(\frac{m\pi}{L}\right)^2 \cdot \left[\frac{EI}{\mu}\right]^{\frac{1}{2}} \qquad (13c)$$

$\phi_m(\bar{x})$ = mode shape of the m-th mode

$$= \sin m\pi \bar{x} \qquad (13d)$$

From Equations (10a,b), the functions U(x) and $\bar{U}(x)$ are even functions of λ, so that from Equations (7), only $\lambda = \alpha - i\,\beta$ and $\lambda = \beta + i\,\alpha$ need be considered. However, it can be shown that

$$\left[\frac{\sin\lambda\bar{y}}{\sin\lambda}\right]_{\lambda=\alpha-i\beta} = \left[\frac{\sinh\lambda\bar{y}}{\sinh\lambda}\right]_{\lambda=\beta+i\alpha}$$

$$\left[\frac{\sin\lambda\bar{y}}{\sin\lambda}\right]_{\lambda=\beta+i\alpha} = \left[\frac{\sinh\lambda\bar{y}}{\sinh\lambda}\right]_{\lambda=\alpha-i\beta} \qquad (14)$$

$$\left[\frac{1}{\lambda^2}\right]_{\lambda=\alpha-i\beta} = -\left[\frac{1}{\lambda^2}\right]_{\lambda=\beta+i\alpha}$$

It follows from Equations (14) that the combined form of Equations (10a,b) is identically the same for $\lambda = \alpha - i\,\beta$ and $\lambda = \beta + i\,\alpha$; *and hence, the four complex values of λ defined by Equations (7) lead to the same deflection equation. It is sufficiently general then to let $\lambda = \alpha - i\,\beta$; and in this case, it is readily shown that the real* ($\mathscr{R}$) and imaginary ($\mathscr{I}$) parts of the two terms in Equation (10b) are:

$$\mathscr{R}\left[\frac{\sin\lambda\bar{y}}{\sin\lambda}\right] = \frac{\cos\alpha\bar{x}\cdot\cosh\beta(2-\bar{x}) - \cos\alpha(2-\bar{x})\cdot\cosh\beta\bar{x}}{\cosh 2\beta - \cos 2\alpha} = \begin{cases}1.0 & \text{at } \bar{x}=0\\ 0 & \text{at } \bar{x}=1\end{cases} \qquad (15a)$$

$$\mathscr{I}\left[\frac{\sin\lambda\bar{y}}{\sin\lambda}\right] = \frac{-\sinh\beta(2-\bar{x})\cdot\sin\alpha\bar{x} + \sinh\beta\bar{x}\cdot\sin\alpha(2-\bar{x})}{\cosh 2\beta - \cos 2\alpha} = \begin{cases}0 & \text{at } \bar{x}=0\\ 0 & \text{at } \bar{x}=1\end{cases} \qquad (15b)$$

$$\mathscr{R}\left[\frac{\sinh\lambda\bar{y}}{\sinh\lambda}\right] = \frac{\cosh\alpha(2-\bar{x})\cdot\cos\beta\bar{x} - \cosh\alpha\bar{x}\cdot\cos\beta(2-\bar{x})}{\cosh 2\alpha - \cos 2\beta} = \begin{cases}1.0 & \text{at } \bar{x}=0\\ 0 & \text{at } \bar{x}=1\end{cases} \qquad (15c)$$

$$\mathscr{I}\left[\frac{\sinh\lambda\bar{y}}{\sinh\lambda}\right] = \frac{\sinh\alpha(2-\bar{x})\cdot\sin\beta\bar{x} - \sinh\alpha\bar{x}\cdot\sin\beta(2-\bar{x})}{\cosh 2\alpha - \cos 2\beta} = \begin{cases}0 & \text{at } \bar{x}=0\\ 0 & \text{at } \bar{x}=1\end{cases} \qquad (15d)$$

In terms of the quantities defined by Equations (15), the real and imaginary parts of $\bar{U}(x)$, as well as the absolute value of $\bar{U}(x)$, are:

$$\mathscr{R}[\bar{U}(x)] = \mathscr{R}\left[\frac{\sin\lambda\bar{y}}{\sin\lambda}\right] - \mathscr{R}\left[\frac{\sinh\lambda\bar{y}}{\sinh\lambda}\right] \qquad (15e)$$

$$\mathscr{I}[\bar{U}(x)] = \mathscr{I}\left[\frac{\sin\lambda\bar{y}}{\sin\lambda}\right] - \mathscr{I}\left[\frac{\sinh\lambda\bar{y}}{\sinh\lambda}\right] \qquad (15f)$$

$$\left|\bar{U}(x)\right| = \left[\left\{\mathscr{R}[\bar{U}(x)]\right\}^2 + \left\{\mathscr{I}[\bar{U}(x)]\right\}^2\right]^{\frac{1}{2}} \qquad (15g)$$

From Equations (6) and (7), it is readily shown that the absolute value of λ^2 is:

$$\left|\lambda^2\right| = \alpha^2 + \beta^2 = \lambda_0^2 \qquad (15h)$$

Finally, from Equations (13a) and (18h) the absolute value of $U(x)$ is

$$\left|U(x)\right| = \frac{L^2 C(0)}{2\,E\,I\,\lambda_0^2}\;\left|\bar{U}(x)\right| \tag{15i}$$

Equation (15i) defines the magnitude and the spanwise distribution of deflection along the beam. In order to simplify the theoretical results of a structural analysis, it is common practice to determine the mean-square value of the space-average response. From Equations (15a-i), the mean-square space-average deflection of the beam is:

$\overline{\left|U(x)\right|^2}$ = mean-square space-average deflection of beam

$$\equiv \int_0^1 \left|U(x)\right|^2 \cdot dx = \left[\frac{L^2 C(0)}{2\,E\,I\,\lambda_0^2}\right]^2 \cdot \overline{\left|\bar{U}(x)\right|^2} \tag{15j}$$

$\overline{\left|\bar{U}(x)\right|^2}$ = space-average of normalized deflection of beam

$$\equiv \int_0^1 \left|\bar{U}(x)\right|^2 \cdot d\bar{x}$$

$$= \int_0^1 \left\{\mathscr{R}[\bar{U}(x)]\right\}^2 + \left\{\mathscr{I}[\bar{U}(x)]\right\}^2 \cdot d\bar{x}$$

$$= \int_0^1 \left[\left\{\mathscr{R}\left[\frac{\sin\lambda\bar{y}}{\sin\lambda}\right]\right\}^2 + \left\{\mathscr{I}\left[\frac{\sin\lambda\bar{y}}{\sin\lambda}\right]\right\}^2\right] \cdot d\bar{x}$$

$$-2\int_0^1 \left[\mathscr{R}\left[\frac{\sin\lambda\bar{y}}{\sin\lambda}\right] \cdot \mathscr{R}\left[\frac{\sinh\lambda\bar{y}}{\sinh\lambda}\right] + \mathscr{I}\left[\frac{\sin\lambda\bar{y}}{\sin\lambda}\right] \cdot \mathscr{I}\left[\frac{\sinh\lambda\bar{y}}{\sinh\lambda}\right]\right] \cdot d\bar{x}$$

$$+\int_0^1 \left[\left\{\mathscr{R}\left[\frac{\sinh\lambda\bar{y}}{\sinh\lambda}\right]\right\}^2 + \left\{\mathscr{I}\left[\frac{\sinh\lambda\bar{y}}{\sinh\lambda}\right]\right\}^2\right] \cdot d\bar{x}$$

$$= \frac{\left(\frac{\sinh 2\beta}{2\beta}\right) - \left(\frac{\sin 2\alpha}{2\alpha}\right)}{\cosh 2\beta - \cos 2\alpha} + \frac{\left(\frac{\sinh 2\alpha}{2\alpha}\right) - \left(\frac{\sin 2\beta}{2\beta}\right)}{\cosh 2\alpha - \cos 2\beta}$$

$$-\frac{1}{2}\,\frac{\left(\frac{\sinh 2\alpha - \sin 2\beta}{\alpha+\beta}\right) + \left(\frac{\sinh 2\alpha + \sin 2\beta}{\alpha-\beta}\right)}{\cosh 2\alpha - \cos 2\beta} \tag{15k}$$

$$-\frac{1}{2}\,\frac{\left(\frac{\sinh 2\beta - \sin 2\alpha}{\alpha+\beta}\right) - \left(\frac{\sinh 2\beta + \sin 2\alpha}{\alpha-\beta}\right)}{\cosh 2\beta - \cos 2\alpha}$$

For the special case of zero-damping for which $\delta = \beta = 0$ and $\lambda = \lambda_0 = \alpha$, Equation (15k) reduces to:

$$\overline{|\bar{U}(x)|^2}_{\delta=0} = \frac{1 + \left(\frac{\sin 2\alpha}{2\alpha}\right)}{1 - \cos 2\alpha} - \frac{1 + \left(\frac{\sinh 2\alpha}{2\alpha}\right)}{\cosh 2\alpha - 1} \tag{15l}$$

Equation (15l) can be verified by direct integration of the square of Equation (13b) for $\lambda = \alpha$ = real quantity. The root-mean-square value of the space-average deflection (normalized) of the beam is:

$$\overline{|\bar{U}(x)|} = \text{rms space-average of normalized deflection}$$

$$= \left[\overline{|\bar{U}(x)|^2}\right]^{\frac{1}{2}} \tag{15m}$$

Resonance frequencies of the damped beam may be defined as those frequencies for which $\overline{|\bar{U}(x)|}$ is a maximum; and it is expected that these frequencies will vary with the damping factor δ. From Equations (6c), (7e,f), (17b) and (18), it is seen that $\overline{|\bar{U}(x)|}$ is a complex function of frequency and damping; and hence maximum values of $\overline{|\bar{U}(x)|}$ are most easily obtained by numerical or graphical techniques. As an example, $\overline{|\bar{U}(x)|}$ is shown in Figure 4 as a function of α for three different values of δ, namely $\delta = 0.10$, 0.50 and 1.00. Here, α is used as a frequency parameter, which by Equations (6c,e) and (7e), is related to ω through the following relationship:

$$\omega = \left(\frac{\alpha}{L}\right)^2 \cdot \sqrt{\frac{EI}{\mu}} \cdot g(\delta) \tag{16a}$$

$$g(\delta) = \frac{1}{[1 + \delta^2]^{\frac{1}{4}} \cos^2 \psi} = \frac{2\sqrt{2}}{\sqrt{2}\,[1 + \delta^2]^{\frac{1}{4}} + \left[1 + \sqrt{1 + \delta^2}\right]^{\frac{1}{2}}} \tag{16b}$$

$= 1.0$ for $\delta = 0$

$= 0.9975$ for $= 0.10$

$= 0.9459$ for $= 0.50$

$= 0.9040$ for $= 1.00$

Figure 4 shows that as $\delta \to 0$, the resonance values of $\alpha \to m\pi$, $m = 1,2,3, \ldots$. This is in agreement with Equation (13c) since $\alpha \to \lambda_0$ as $\delta \to 0$. As damping increases, the resonance values of α decrease slightly but remain approximately equal to $m\pi$. The curves in Figure 4 show that the space average deflection decreases with increasing damping and generally decreases with increasing frequency. Furthermore, as frequency increases, resonant response peaks become less dominant; and for any given value of δ, there exists a frequency which is sufficiently large so that the resonant peaks essentially disappear. This effect results from the fact that, as shown in Equation (6d), the damping c increases with frequency for a constant value of δ. Curves similar to those shown in Figure 4 have been developed by Snowdon for beams with other boundary conditions; and these are reported in Reference 4.

Using Equations (16), two numerical examples are constructed which show the spanwise distributions of $|\bar{U}(x)|$ at two different frequencies. The excitation frequencies are chosen to be approximately equal to the undamped resonance frequencies of the first and third modes of the beam. Specifically the excitation frequencies are selected by setting $\alpha = \pi$ and $\alpha = 3\pi$. The value of damping is chosen as $\delta = 1.0$. Numerical values of the various parameters used in these two examples are listed in Table 1. The distributions of $|\bar{U}(x)|$ and of its real and imaginary components are shown graphically in Figure 5 for $\alpha = \pi$ (first mode) and in Figure 6 for $\alpha = 3\pi$ (third mode). It is seen in Figure 5 that $|\bar{U}(x)|$ is approximately equal to $\mathcal{I}[-\sin\lambda\,\bar{y}/\sin\lambda]$, and that the distribution of $|\bar{U}(x)|$ is approximately equal to that for the fundamental mode of an undamped beam, namely, a half-cycle sine wave. Thus, even for the relatively large damping factor of $\delta = 1.0$, the deflection distribution is not significantly altered by damping. Conversely, Figure 6 shows that a significant decay of vibration amplitudes occurs along the beam for the third mode. It should be noted that $|\bar{U}(x)|$ represents the envelope of the maximum positive deflection (normalized) of the beam and that this maximum deflection is achieved at different times for different points along the span. Thus, $|\bar{U}(x)|$ does not represent a mode shape for the beam. The root-mean-square value of the space average deflection is shown for both modes in Figures 5 and 6.

For excitation frequencies $\omega \gg \omega_1$, and for $\delta > 0$, Equation (6c) shows that $\lambda_0 \gg 1$, and Equations (7e) and (7f) show that $\alpha \gg 1$ and $\beta \gg 1$. In this case, the first term in the numerators and denominators of each of the four Equations (15a-d) dominate the second term, except at $\bar{x} = 1.0$. Furthermore, the sinh ( ) and cosh ( ) functions can be approximated by $(1/2)\, e^{(\ )}$; and hence, it can be shown that

$$\left.\begin{aligned} |\bar{U}(x)| &\doteq e^{-\beta\bar{x}}\left[1 - 2\,e^{-(\alpha-\beta)\bar{x}}\cos(\alpha-\beta)\,\bar{x} + e^{-2(\alpha-\beta)\,\bar{x}}\right]^{\frac{1}{2}} \\ &= 0 \qquad \text{at} \quad \bar{x} = 0 \\ &\doteq e^{-\beta\bar{x}} \quad \text{at} \quad \bar{x} = 1.0 \end{aligned}\right\} \quad \omega \gg \omega_1 \tag{17}$$

Equation (17), for which beam boundary conditions are only approximately satisfied, shows directly how the vibration amplitudes decay with distance from the point of excitation, for high frequency excitation. This decay is controlled by the factor $\exp(-\beta\bar{x})$.

2.3 Infinite Series Equation for Response

The general solution of Equation (5b) can be developed in an infinite series of modal responses by assuming the solution:

$$U(x) = \sum_{m=1}^{\infty} q_m\, \phi_m(\bar{x}) \tag{18}$$

where q_m is the complex response amplitude of the m-th mode and $\phi_m(\bar{x})$ is the mode shape defined by Equation (13d). Substituting Equation (18) into Equation (5b) and collecting terms gives

$$\sum_{m=1}^{\infty}\left[\left(\frac{m\pi}{L}\right)^4 - \left(\frac{\lambda}{L}\right)^4\right]\phi_m(\bar{x})\, q_m = \frac{F(x)}{EI} \tag{19}$$

The mode shapes $\phi_m(\bar{x})$ satisfy the orthogonality condition

$$\begin{aligned} \int_0^1 \phi_m(\bar{x})\,\phi_r(\bar{x})\,d\bar{x} &= 1/2 \quad \text{if} \quad m = r \\ &= 0 \quad\;\; \text{if} \quad m \neq r \end{aligned} \tag{20}$$

Thus, multiplying both sides of Equation (19) by $\phi_m(\bar{x})$, integrating term-by-term, and invoking the orthogonality condition of Equation (20) leads to the following expression for q_m:

$$q_m = \frac{2}{EI} \frac{\int_0^1 F(x) \cdot \phi_m(\bar{x})\, d\bar{x}}{\left[\left(\frac{m\pi}{L}\right)^4 - \left(\frac{\lambda}{L}\right)^4\right]} \tag{21}$$

The integral in Equation (21) represents the generalized force for the m-th mode; and using Equations (2a,b) and (13d), this integral can be expressed algebraically as follows:

$$\int_0^1 F(x) \cdot \phi_m(\bar{x})\, d\bar{x} = \frac{2\, F \cos m\pi\, \bar{x}_0}{m\pi} \left[\frac{\sin m\pi\, \bar{\epsilon}}{m\pi\bar{\epsilon}} - \cos m\,\pi\,\bar{\epsilon}\right] \tag{22a}$$

$$\doteq \left\{\frac{2}{3}\, F\, \epsilon^2\right\} \frac{m\pi}{L^2} \cos m\pi\, \bar{x}_0 \quad \text{for} \quad \epsilon \approx 0 \tag{22b}$$

$$= C(x_0)\, \frac{m\pi}{L^2} \cos m\pi\, \bar{x}_0 \tag{22c}$$

$$= C(0)\, m\pi/L^2 \quad \text{for} \quad x_0 = 0 \tag{22d}$$

The above integral could also be evaluated by using Equations (2c-e) as follows:

$$\int_0^1 F(x)\, \phi_m(\bar{x})\, d\bar{x} = -\frac{C(0)}{L} \int_0^L \frac{d\delta(x)}{dx} \sin(m\pi\bar{x})\, dx$$

$$= \frac{m\pi\, C(0)}{L^2} \int_0^L \delta(x)\, \frac{\sin(m\pi\,\bar{x})}{(m\pi x)}\, dx$$

$$= \frac{m\pi\, C(0)}{L^2} \lim_{x \to 0} \left[\frac{\sin(m\,\pi x)}{(m\pi x)}\right]$$

$$= \frac{m\pi\, C(0)}{L^2} \tag{22e}$$

Now, substituting Equation (22e) into Equation (21), and using Equations (6a) and (13c), the expression for q_m reduces to the form:

$$q_m = \frac{2L^2\, C(0)}{(m\pi)^3\, EI}\, H\left(\frac{\omega}{\omega_m}\right) e^{-i\,\theta\,(\omega/\omega_m)} \tag{23}$$

$H(\omega/\omega_m)$ = single degree of freedom dynamic magnification factor for the m-th mode

$$= \left[\left\{1 - \left(\frac{\omega}{\omega_m}\right)^2\right\}^2 + \delta^2 \left(\frac{\omega}{\omega_m}\right)^4\right]^{-\frac{1}{2}} \tag{24a}$$

$$= \left[\left\{1 - \left(\frac{\omega}{\omega_m}\right)^2\right\}^2 + (2\,\zeta_m)^2 \left(\frac{\omega}{\omega_m}\right)^2\right]^{-\frac{1}{2}} \tag{24b}$$

$\theta(\omega/\omega_m)$ = phase angle for m-th mode

$$= \tan^{-1}\left[\frac{\delta\,(\omega/\omega_m)^2}{1 - (\omega/\omega_m)^2}\right] \tag{24c}$$

$$= \tan^{-1}\left[\frac{2\,\zeta_m\,(\omega/\omega_m)}{1 - (\omega/\omega_m)^2}\right] \tag{24d}$$

ζ_m = ratio of actual damping to critical damping for the n-th mode

$$= \omega\,\delta/2\,\omega_m = c/2\,\mu\,\omega_m \qquad \text{(See Equation (6d))} \tag{24e}$$

If the modal analysis is to be consistent with the exact analysis described in Section 2.2, then δ must have the same value for all beam modes, although this value of δ may vary with ω. From Equation (6d), this condition implies that c is the same for all modes vibrating at frequency ω. Thus, Equations (24a) and (24c) are desired forms of $H(\omega/\omega_m)$ and $\theta(\omega/\omega_m)$ when comparing results of the exact and modal analyses.

In many dynamic analyses, such as those described in Reference ( ), constant percentage bandwidths are often assumed for the various modes; and in this case, ζ_m has the same value for all modes, which from Equation (24e) implies that c increases with ω_m. In the latter case, Equations (24b) and (24d) with $\zeta_m = \zeta$ = constant are the appropriate forms of $H(\omega/\omega_m)$ and $\theta(\omega/\omega_m)$. In the numerical examples discussed at the end of this section, a comparison is made between responses computed for both types of damping.

It is interesting to note that the maximum values of $H(\omega/\omega_m)$ and the corresponding damped resonance frequencies for the two different types of damping are:

$$\text{Max } H(\omega/\omega_m) = \sqrt{1+\delta^2}/\delta \qquad \text{at} \quad \omega/\omega_m = 1\Big/\sqrt{1+\delta^2} \tag{25a}$$

$$= 1\Big/2\zeta\sqrt{1-\zeta^2} \qquad \text{at} \quad \omega/\omega_m = \sqrt{1-2\,\zeta^2} \tag{25b}$$

From Equation (18), the absolute value of the deflection is:

$$|U(x)| = \left[\left\{\sum_{m=1}^{\infty} \mathscr{R}(q_m)\,\phi_m(\bar{x})\right\}^2 + \left\{\sum_{m=1}^{\infty} \mathscr{I}(q_m)\,\phi_m(\bar{x})\right\}^2\right]^{\frac{1}{2}}$$

$$= \left[\sum_{m=1}^{\infty}\sum_{r=1}^{\infty} \left\{\mathscr{R}(q_m)\,\mathscr{R}(q_r) + \mathscr{I}(q_m)\,\mathscr{I}(q_r)\right\}\,\phi_m(\bar{x})\,\phi_r(\bar{x})\right]^{\frac{1}{2}}$$

The real and imaginary parts of q_m can be obtained from Equation (23), and are:

$$\mathscr{R}(q_m) = \frac{2L^2 C(0)}{(m\pi)^3 EI} H\left(\frac{\omega}{\omega_m}\right) \cos\theta(\omega/\omega_m) \tag{27a}$$

$$\mathscr{I}(q_m) = -\frac{2L^2 C(0)}{(m\pi)^3 EI} H\left(\frac{\omega}{\omega_m}\right) \sin\theta(\omega/\omega_m) \tag{27b}$$

Substituting Equations (27) into Equations (26) gives

$$|U(x)| = \frac{2L^2 C(0)}{EI}\left[\sum_{m=1}^{\infty}\sum_{r=1}^{\infty} \frac{\phi_m(\bar{x})\,\phi_r(\bar{x})}{(m\pi)^3 (r\pi)^3} H\left(\frac{\omega}{\omega_m}\right) H\left(\frac{\omega}{\omega_r}\right) \cdot \cos\left[\theta(\omega/\omega_m) - \theta(\omega/\omega_r)\right]\right]^{\frac{1}{2}} \tag{28}$$

It is convenient now to write Equation (28) in a form similar to Equation (15i), namely:

$$|U(x)| = \frac{L^2 C(0)}{2EI\lambda_0^2} |\bar{U}(x)|$$

$$|\bar{U}(x)| = A_1\left[\sum_{m=1}^{\infty}\sum_{r=1}^{\infty} \beta_{mr}(\omega)\,\phi_m(\bar{x})\,\phi_r(\bar{x})\right]^{\frac{1}{2}} \tag{29b}$$

$$A_1 = 4\lambda_0^2/\alpha^3 = 4/\alpha \cos^2\psi \tag{29c}$$

$$\beta_{mr}(\omega) = \left(\frac{\alpha}{m\pi}\right)^3 \left(\frac{\alpha}{r\pi}\right)^3 H\left(\frac{\omega}{\omega_m}\right) \cdot H\left(\frac{\omega}{\omega_r}\right) \cdot \cos\left[\theta(\omega/\omega_m) - \theta(\omega/\omega_r)\right] \tag{29d}$$

From Equations (6c) and (13a), the frequency ratio ω/ω_m is:

$$\frac{\omega}{\omega_m} = \frac{(\lambda_0/m\pi)^2}{[1+\delta^2]^{\frac{1}{4}}} \tag{29e}$$

Space average responses are often used to define the response level of a structure because this provides a single value which is independent of location on the structure and because it is more easily computed. Using Equations (20 and (29b), such a space average is:

$$\overline{|\bar{U}(x)|} = \left[\int_0^1 |\bar{U}(x)|^2 \, d\bar{x}\right]^{\frac{1}{2}}$$

$$= A_1\left[\frac{1}{2}\sum_{m=1}^{\infty} \beta_{mm}(\omega)\right]^{\frac{1}{2}} \tag{29f}$$

It is of interest now to compare the modal analysis method developed above with the exact method of analysis developed in Section 2.2. This comparison is made by using Equations (29) to compute $|\bar{U}(x)|$ for the third mode of the beam for which $\alpha = 3\pi$ and $\delta = 1.0$, and comparing this $|\bar{U}(x)|$ with that shown in Figure 5. Based on the numerical values of parameters listed in Table 1, the quantities A_1 and ω/ω_m defined by Equations (29c,e) become:

$$\left.\begin{aligned} A_1 &= 4/(3\pi)\,(0.98079)^2 = 0.442 \\ \omega/\omega_m &= 0.873\,(3/m)^2 \end{aligned}\right\} \qquad (30)$$

Table 2 contains a list of numerical values of ω/ω_m, $H(\omega/\omega_m)$, $(\alpha/m\pi)^3\ H(\omega/\omega_m)$, $\theta(\omega/\omega_m)$ for the modes $m = 1\text{-}6$. Note that for modes $m > 6$, $H(\omega/\omega_m) \approx 1.0$ and $\theta(\omega/\omega_m) \approx 0$. Table 3 contains a list of values of β_{mr} for $m = 1\text{-}6$ and $r = 1\text{-}6$, where it is to be noted that $\beta_{mr} = \beta_{rm}$.

Numerical values of $|\bar{U}(x)|$ were computed using five, ten and thirty modes of the beam; and these values are listed in Table 4 along with comparable values obtained from the exact analysis of the beam. Here, reference is made to those cases for which $\delta = 1.0$. Table 4 shows that values of $|\bar{U}(x)|$ for thirty modes ($m = 1\text{-}30$) are within 0.5 percent of those obtained by the exact analysis method, which implies excellent agreement. When ten modes are used, the maximum error in the modal analysis is only 2 percent. A graphical comparison of the exact values of $|\bar{U}(x)|$ with those for only five ($m = 1\text{-}5$) modes of the beam is shown in Figure 7; and here it is seen that a five mode approximation gives reasonably accurate values of $|\bar{U}(x)|$.

The exact analysis of the beam as developed in Section 2.2 implies that the damping factor δ is constant for all modes of the beam; and this assumption leads to the modal dynamic magnification factor and phase angle as defined by Equations (24a) and (24c). These expressions were used in the modal analysis for the cases when $\delta = 1.0$. The deflection distribution $|\bar{U}(x)|$ was also computed for $2\zeta = 1.0$ and for thirty modes of the beam, and the results are listed in Table 4 and are shown graphically in Figure 8. It is seen that a constant value of ζ for all modes leads to values of $|\bar{U}(x)|$ which are approximately the same as values for a constant δ, except at certain points along the span. The general rate of decay of vibration levels along the beam is approximately the same for both forms of damping.

The main conclusion to be drawn from the above numerical evaluations is that the modal analysis method is capable of accurately predicting the spatial decay of vibration levels along a damped structure such as a beam. This is possible only when terms in Equation (29b) for which $m \neq r$ are included in the computations. Those terms for which $m = r$ (self-terms) are positive at all points along the span of the beam, whereas the terms for which $m \neq r$ (cross-terms) may be negative along the span. All significant terms in this series tend to be positive and to add in the neighborhood of the source of excitation, which for the beam under discussion is in the neighborhood of $\bar{x} = 0$. However, at some distance along the span, most of the cross-terms are negative and subract from the self-terms, and thus lead to a lower response level at some distance from the source of excitation. The contirbutions of six of the major terms in the series are shown in Figure 9, three terms being self-terms and the other three being cross-terms. It is seen that the cross-terms are quite large and hence they are significant to the computations of response.

3.0 ANALYSIS METHODS

This section presents and discusses the various components of the methods used for analyzing the responses of shell and plate structures to fluctuating pressure fields. These components of the modal analysis method comprise structural configurations, mode shapes, resonance frequencies, fluctuating pressure environments, coincidence conditions, and associated response equations. A section on approximation forms of the response equations is also included. The statistical energy analysis method extensively utilized by other researchers and presented in the literature (References 14-17) is summarized herein.

3.1 Structural Configurations

The following all-aluminum structures are considered:

- Uniform cylindrical shell equivalent of Spacecraft Lunar Module Adaptor (SLA) segment of Apollo Spacecraft. (The shell wall is 1.70 in. thick honeycomb with 0.015 in. and 0.032 in. face sheets - References 1 and 2.)

- Several shells similar in all structural details to cylindrical equivalent of SLA except for changes in one or two structural parameters such as radius, stiffness or mass.

- Republic Cylinder No. 12, which is a relatively small shell with homogeneous wall (Reference 11).

- Two uniform cylindrical shells with homogeneous walls which have dimensions similar to, but different from, those of Republic Cylinder No. 12. (These shells, and stiffened versions of these shells are presently being used in impedance experiments at Wyle Laboratories.)

- A flat rectangular panel (9-bay panel) with orthogonal stiffeners uniformly spaced so as to consist of 9 equal sized uniform rectangular plates.

- Two thin rectangular plates of equal size, except for thickness, one of which is a typical (center) plate segment of the above 9-bay panel.

- Several flat plate sections of the above uniform cylinders.

For purposes of analytical simplicity, it is assumed that the two circular edges of each of the cylindrical shells, and the four straight edges of each rectangular panel (or plate) are tangentially pinned. A summary of the dimensions, stiffnesses, masses and damping factors used for these structures are summarized in Tables 6 and 7. Symbols appearing in these tables are defined below:

L_x = axial length of cylindrical shell or rectangular plate

L_y = lateral width of rectangular plate

R = shell radius

D = isotropic bending stiffness of shell wall

D_x, D_y = orthotropic bending stiffnesses of rectangular plate along the (x,y)-axes, respectively. (For isotropic plates, $D_x = D_y$ = isotropic bending stiffness.)

K_e = extensional (membrane) stiffness of shell wall.

μg = (average) weight per unit area of shell or plate.

Q = dynamic magnification factor at resonance. (It is assumed that Q is the same for all modes of a given plate or shell.)

= $1/2\zeta$, where ζ is the ratio of actual damping to critical damping (ζ = 1.0 for critical damping).

Tables 6 and 7 also contain summaries of the types of excitation fields employed for each structure; and the corresponding figure number refers to the figure containing a graph of the comparable acceleration spectrum. Brief descriptions of the various excitation fields used are presented in Section 3.4.

3.2 Mode Shapes

In References 1 and 2, elementary sinusoidal mode shapes were assumed for the resonant deflection distributions along the axis and around the circumference of the cylindrical shell. A single mode of vibration of the shell involved both radial and circumferential deflections; and in the above references, the amplitude of the circumferential deflection is assumed to be equal to the amplitude of the radial deflection. This assumption is valid for the low order circumferential modes; however, the resulting generalized mass is too large for the higher order circumferential modes. If the vibration characteristics of the shell are to approach those of a flat plate at high frequencies, the generalized mass of the cylinder must approach the generalized mass of a flat plate as the ring mode number becomes large. This flat plate asymptote can be achieved by introducing the approximation given by Forsberg on page 19 of Reference 18, namely, that the circumferential deflection of the (m,n)-mode is (1/n) times the radial deflection of this mode. It follows that the mode shape equations in References 1 and 2 should be altered to the following form:

$$\left.\begin{aligned} \phi_{mn1}(x,y) &= \sin(m\pi\bar{x}) \cdot \sin(2n\pi\bar{y}) \\ \phi_{mn2}(x,y) &= \sin(m\pi\bar{x}) \cdot \cos(2n\pi\bar{y}) \end{aligned}\right\} \quad \text{Radial Modes} \qquad (31)$$

$$\left.\begin{aligned} \psi_{mn1}(x,y) &= \sin(m\pi\bar{x}) & n &= 0 \\ &= \frac{1}{n}\sin(m\pi\bar{x}) \cdot \cos(2n\pi\bar{y}), & n &\geq 1 \\ \psi_{mn2}(x,y) &= 0 \qquad , & n &= 0 \\ &= \frac{1}{n}\sin(m\pi\bar{x}) \cdot \sin(2n\pi\bar{y}), & n &\geq 1 \end{aligned}\right\} \quad \text{Circumferential Modes} \qquad (32)$$

These equations imply that the amplitudes of the circumferential deflection components approach zero as n increases. Thus, at high frequencies, only the radial deflection components are significant (for the particular modes of interest in this report) so that the shell characteristics reduce to those of a flat plate. As discussed by Weingarten in Reference 19, the mode shapes defined by Equations (31) and (32) are approximate and are valid only for large values of n. However, the errors in the final response computations due to the assumption of elementary modes is expected to be small. If the analysis in this report were to be extended to computations of internal loads and stresses near the edges of the shell, it would be necessary to refine the mode shape equations.

The generalized mass, M_{mni}, of the (mni)-mode of the shell is defined in terms of a generalized mass fraction, ξ_{mni}, and the total mass, M_0, of the shell as follows:

$M_{mni} = \xi_{mni} M_0$ = generalized mass of (mni)-mode

M_0 = μA = total mass of shell

μ = *mass per unit area of shell wall*

A = total surface area of shell wall

$$\xi_{mni} = \int_{\bar{x}=0}^{1} \int_{\bar{y}=0}^{1} \left[\phi_{mni}^2(x,y) + \psi_{mni}^2(x,y)\right] d\bar{x}\, d\bar{y}$$

$$= 1/2, \qquad n = 0$$

$$= [1 + 1/n^2]/4, \quad n \geq 1 \tag{33}$$

3.3 Resonance Frequencies and Modal Densities

The equation given in Reference 1 for the resonance frequency, f_{mn}, of the (m,n)-mode of a pinned-end cylindrical shell can be written in the following alternate form:

$$\frac{f_{mn}}{f_0} = \left[\left\{\frac{\lambda_m^2}{\lambda_m^2 + n^2}\right\}^2 + \beta^2 \left\{\lambda_m^2 + n^2 - 1\right\}^2\right]^{\frac{1}{2}} \tag{34}$$

where

m = number of elastic half-waves along axis of shell

n = number of elastic full-waves around the circumference of shell

$\lambda_m = m \pi R/L_x$

$\beta = [D/K_e]^{\frac{1}{2}}/R$ for general shell

$= (h/R)/2\sqrt{3(1 - \nu^2)}$ for homogeneous shell

f_0 = resonance frequency of ring breathing mode ($n = \beta = 0$)

$= [K_e/\mu]^{\frac{1}{2}}/2\pi R$ for general shell

$= C_L/2\pi R$ for homogeneous shell

h = wall thickness for homogeneous shell

C_L = material speed of sound

ν = Poisson's ratio.

Equation (34) is used in the computer program which numerically evaluated the acceleration response spectra presented in this report. Except for small values of m and n, the (-1) in the second term on the right-hand side of Equation (34) can be neglected so that Equation (34) can be written in the following approximate form:

$$\frac{f_{mn}}{f_0} \doteq \left[\left\{\frac{\mathscr{X}^2}{\mathscr{X}^2+\mathscr{Y}^2}\right\}^2 + \left\{\mathscr{X}^2 + \mathscr{Y}^2\right\}^2\right]^{\frac{1}{2}} \tag{35}$$

$$\left.\begin{aligned} \mathscr{X} &= \sqrt{\beta}\,\lambda_m \\ \mathscr{Y} &= \sqrt{\beta}\,n \end{aligned}\right\} \tag{36}$$

Following the approach used in Reference 14, contours of constant values of f_{mn}/f_0 can be constructed in a graph of $\mathscr{X}$ vs $\mathscr{Y}$, or $\sqrt{\beta}\,\lambda_m$ vs $\sqrt{\beta}\,n$. These contours can be found, for example, in Figure 14. Similar contours are shown in Figures 15-27. The advantage in using such a graph is that the shapes and numerical values of the contours are the same for all shells. Resonance frequencies of a given cylinder can be located on the graph by numerically evaluating $\mathscr{X}$ and $\mathscr{Y}$ for integer values of m and n.

The first term on the right-hand side of Equation (35) is associated with extensional (or membrane) deformations of the shell while the second term is associated with bending of the shell wall. In general, low order modes of the shell are of the membrane type, while high order modes are of the bending (plate) type. The division between membrane and bending deformations of the shell occurs when the two terms in Equation (35) are equal. Equating these two terms leads to Equation (36) which defines a circle of radius 1/2 centered at $\mathscr{X} = 1/2$, $\mathscr{Y} = 0$.

$$\left[\mathscr{X} - \frac{1}{2}\right]^2 + \mathscr{Y}^2 = \left[\frac{1}{2}\right]^2 \qquad \text{Membrane-Bending Contour} \tag{37}$$

This circle is shown as a dotted line in Figure 13. Within the circle the shell modes are controlled by extension while outside of this circle the modes are controlled by bending. It is easily shown that the f_{mn}/f_0 contours have a zero slope on this circle.

The equation used for the resonance frequencies of a flat, rectangular plate with simply supported edges is:

$$f_{mn} = \frac{\pi}{2}\sqrt{\frac{D}{\mu}}\left[\left(\frac{m}{L_x}\right)^2 + \left(\frac{n}{L_y}\right)^2\right] \tag{38}$$

Frequency graphs similar to those for a cylindrical shell can also be developed for the flat plate.

The low frequency modes of a shell or plate are generally well separated in frequency space, and as a result, response levels are governed by the response levels of individual modes. At higher frequencies, the separations between resonance frequencies may decrease to such an extent that modal bandwidths overlap thus leading to an overall response which is greater than the responses of the individual contributing modes. In the latter case, the overall (mean-square) response is proportional to modal density. A knowledge of the modal densities of the various shells and plates analyzed in this section is helpful in the interpretation and understanding of their acceleration spectra. Formulas for the approximate values of modal density are summarized below for cylindrical shells and flat rectangular plates.

In Reference (16), Miller, et al., present two expressions for the approximate overall modal density of a uniform, thin cylindrical shell with homogeneous wall of finite length. One of these expressions is valid in the frequency range below ring resonance where the modal density is proportional to $\sqrt{f}$; and the other expression is valid in the frequency range above ring resonance where the modal density is constant and is equal to one-half of the modal density of an equivalent flat plate with the same surface area. These expressions are easily generalized to include honeycomb and stiffened shell walls for which the stiffness distributions are assumed to be uniform and isotropic. The resulting equations are summarized below:

$\mathcal{N}(f)$ = modal density of cylindrical shell

$$= \frac{9A}{16\pi}\left[\frac{\mu}{D}\cdot\frac{f}{f_0}\right]^{\frac{1}{2}} \quad \text{(General Shell)} \qquad f < f_0 \tag{39}$$

$$= \frac{9A\sqrt{3(1-\nu^2)}}{8\pi\, h\, C_L} \quad \text{(Homogeneous Shell)} \qquad f < f_0 \tag{40}$$

$$= \frac{A}{4}\left[\frac{\mu}{D}\right]^{\frac{1}{2}} \quad \text{(General Shell)} \qquad f_0 < f \tag{41}$$

$$= \frac{A\sqrt{3(1-\nu^2)}}{2\, h\, C_L} \quad \text{(Homogeneous Shell)} \qquad f_0 < f \tag{42}$$

The above expressions show that modal density increases with increasing surface area and mass per unit area, and decreases with increasing stiffnesses. Equivalently, if a given structure is altered in such a manner that resonance frequencies are lowered/increased, then the modal density is increased/lowered. More exact integral equations for modal densities of thin circular cylinders have been developed by Bolotin and these are discussed in Reference (16) along with comparisons between Bolotin's and Heckl's equations. It is sufficient to note here that Heckl's equations underestimate the modal density by about 33 percent for $f < f_0$; however, they are reasonably accurate for $f > 2 f_0$. At the ring frequency, Bolotin predicts a modal density of about 1.5 times that of Heckl.

Comparable equations for the modal density of a uniform, flat rectangular plate are:

$\mathcal{N}(f)$ = modal density of plate

$$= \frac{A}{2}\left[\frac{\mu}{D}\right]^{\frac{1}{2}} \quad \text{(General Plate)} \tag{43}$$

$$= \frac{A\sqrt{3(1-\nu^2)}}{h\, C_L} \quad \text{(Homogeneous Plate)} \tag{44}$$

Using Equations (39)-(44), modal density values were calculated and are summarized in Tables 6 and 7 for the various shell and plate structures analyzed in this report. Note that because of their relatively small surface areas, the flat panels have modal densities which are significantly lower than those of the cylindrical shells, with the exception of the equivalent SLA panel.

The frequency separation, δf, between adjacent resonance frequencies, and the bandwidth, Δf, of any mode resonant at f, are:

$$\left.\begin{aligned} \delta f &= 1/\mathcal{N}(f) = \text{separation between resonance frequencies} \\ \Delta f &= f/Q = \text{modal bandwidth} \end{aligned}\right\} \tag{45}$$

Modal bandwidths overlap when $\Delta f > \delta f$, or equivalently when the modal density satisfies the inequality:

$$\mathcal{N}(f) > Q/f \qquad \text{(Modal Bandwidth Overlap)} \tag{46}$$

3.4 Fluctuating Pressure Environments

This section briefly describes the characteristics of various fluctuating pressure environments in terms of space correlation functions. These functions are used in Appendices A and B to develop expressions for joint acceptance.

3.4.1 Boundary Layer Turbulence

A discussion of the spatial correlation properties associated with corrected boundary layer turbulence is presented in References 1 and 2, where experimental data are presented in support of the mathematical model selected for the correlation functions. An additional reference which can be cited for a more detailed discussion of this environment is Reference 3.

It is of interest here, however, to review the assumptions made in the treatment of this environment; and these are summarized below:

- The fluctuating pressure field is statistically ergodic and stationary.
- The PSD of the fluctuating pressure field is uniform over the area of excitation.
- The field of turbulence is spatially homogeneous in directions parallel and normal to the flow axis so that the spatial correlations are dependent only on the distance between two points.
- The convection velocity, U_c, and the boundary layer thickness are independent of frequency and position on the structure.
- The narrow-band spatial correlation function is independent of time and can be expressed as a product of longitudinal (along flow axis) and lateral (normal to flow axis) correlation functions.
- The low frequency correlation lengths are limited approximately to the thickness of the boundary layer.
- The narrow-band longitudinal correlation function can be approximated by an exponentially damped cosine function; and the narrow-band lateral correlation function can be approximated by an exponential function.

The correlation functions are represented as follows:

$$C(\bar{\xi};\omega) = \exp\left[-\delta_x \left|\bar{\xi}\right|\right] \cdot \cos\gamma_x\ \bar{\xi} = \text{longitudinal correlation function}$$

$$C(\bar{\eta};\omega) = \exp\left[-\delta_y \left|\bar{\eta}\right|\right] \qquad = \text{lateral correlation function}$$

$$\gamma_x = \omega\, L_x/U_c$$

$$\gamma_y = \omega\, L_y/U_c$$

$$\delta_x = a\ \gamma_x + b\, L_x/\delta_b$$

$$\delta_y = c\ \gamma_y + d\, L_y/\delta_b$$

a, b, c, d = constants that may be selected from a knowledge of the characteristics of the boundary layer flow field.

Numerical values of U_c, δ_b, a, b, c, d used in References 1 and 2 for the analysis of the SLA are:

U_c = 9810 in./sec = Mach 1

= 15,900 in./sec = Mach 2

δ_b = 12.0 in.

a = 0.10

b = 0.265

c = d = 2.0

In the computer program, the constants a, b, c, d can be altered to represent various types of pressure fields. From example, a = b = c = d = 0 implies an acoustic progressive wave field along the x-axis.

3.4.2 Ducted Progressive Wave Field

The ducted progressive wave field consists of N independent plane wave fields that propagate at parallel incidence along the length, L_x, of a cylindrical shell or rectangular plate. This field is formed within a rigid shroud that completely covers the structural surface and that is internally baffled so as to create a set of N straight, parallel ducts which act as acoustic wave guides. The intermediate walls between adjacent ducts are separated from the structural surface by a set of flexible seals that minimize acoustic leakage between adjacent ducts and minimize structural constraints introduced by the shroud. The ducts have uniform widths of $2\pi R/N$ around the circumference of the shell, and L_y/N across the width of a rectangular plate. Sketch 1 below shows a four (N = 4) duct system on a flat plate. Each duct is driven at one end by a broadband random acoustic noise source and has an anechoic termination at the other end. The N acoustic noise sources are driven by uncorrelated random signals in order to produce N uncorrelated progressive wave fields. In the analysis, it is assumed that plane wave fronts exist in each duct. The acoustic field along the axis of any one duct is said to be axially correlated if at any frequency the axial pressure distributions are sinusoidal. Due to various acoustic phenomena in the ducts, these axial pressure distributions may not be sinusoidal, in which case axial correlation lengths may be limited.

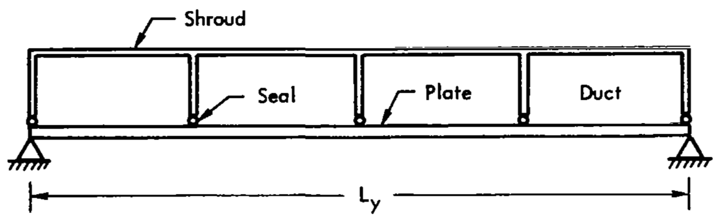

Sketch 1. Flat Plate with Four-Duct Shroud

3.4.3 Reverberant Acoustic Field

The reverberant acoustic field is assumed to be an ideal diffuse field that is composed of plane waves which impinge on the structural surface with an equal probability for all angles of incidence. In an ideal reverberation room, the narrow band space correlation function relative to any two points separated by a distance r is $[\sin k r]/k r$ where $k = \omega/c_0$ = acoustic wave number. The presence of the structure being analyzed is assumed to have no influence on the impinging wave field, as for example, a small flat plate flush mounted in a wall of the room.

For both flat and cylindrical surfaces, the narrow band space correlation functions are:

$$C(\bar{\zeta};\omega) = \frac{\sin k \bar{\zeta}}{k \bar{\zeta}}$$

$$C(\bar{\eta};\omega) = \frac{\sin k \bar{\eta}}{k \bar{\eta}}$$

In Reference 20, Wenzel shows that the above equation for $C(\bar{\zeta};\omega)$ is quite accurate for a cylinder even when scattering is considered. Because of scattering, the above equation for $C(\bar{\eta};\omega)$ introduces some errors for a cylinder; however, the errors diminish with increasing frequency.

Reflections of the acoustic waves from the surface cause effective increases in surface pressures. At low frequencies, the reflection factor on pressure level is unity, while at high frequencies this factor is 2.0. An average value of $\sqrt{2}$ is used in the analysis.

3.5 Acoustic Coincidence Conditions

The modes of the shell which exhibit the greatest response levels for acoustic excitation at a single frequency f are those modes whose resonance frequencies $f_{mn} = f$ and whose elastic wavelengths λ_e are equal to the acoustic wave length λ. (This is equivalent to saying that the elastic wave speed of the shell is equal to the speed of sound c_0 in air.) Such a condition is often referred to as acoustic coincidence; the frequencies at which the condition occurs are called coincidence frequencies; and the modes satisfying this condition are called coincident modes. Those modes for which the coincidence condition is almost, but not exactly, satisfied are called near-coincident modes.

Acoustic coincidences or near coincidences can occur along the axis of the shell or around the circumference, or both. Frequencies associated with axial coincidence are denoted as f_{cm} and those associated with circumferential coincidence are denoted as f_{cn}. Using the resonance frequency contour graph of $\mathscr{X}$ vs $\mathscr{Y}$, it is possible to develop a simple graphical method for determining the frequencies f_{cm}. If the acoustic wavelength is equal to the axial elastic wavelength, then one equation for f_{cm} is:

$$f_{cm} = c_0/\lambda = c_0/\lambda_{ex} = m\, c_0/2\, L_x = \sqrt{2}\, f_0\ \ \mathscr{X}/\mathscr{P}^{\frac{1}{4}} \tag{47}$$

λ = acoustic wavelength

λ_{cx} = $2\, L_x/m$ = elastic wavelength along shell axis

c_0 = speed of sound in air

$$\mathscr{P} = 4\, \beta^2\ [2\, \lambda_1\, L_x\, f_0/c_0\,]^4 = 4\, K_e\, D/R^2\, \mu^2\, c_0^4 \tag{48}$$

$$= \frac{1}{3(1-\nu^2)} \left(\frac{h}{R}\right)^2 \left(\frac{C_L}{c_0}\right)^4 \qquad \text{for homogeneous shell.}$$

Setting $f_{cm} = f_{mn}$ and using Equations (35) and (47), a relationship between $\mathscr{X}$ and $\mathscr{Y}$ can be developed as follows:

$$(\mathscr{X}^2 + \mathscr{Y}^2)^4 - \frac{2\mathscr{X}}{\sqrt{\mathscr{P}}}\, (\mathscr{X}^2 + \mathscr{Y}^2)^2 + \mathscr{X}^4 = 0$$

$$(\mathscr{X}^2 + \mathscr{Y}^2)^2 = \mathscr{X}_0^2\, \mathscr{X}^2$$

$$\left[\mathscr{X} - \frac{1}{2}\, \mathscr{X}_0\right]^2 + \mathscr{Y}^2 = \left[\frac{1}{2}\, \mathscr{X}_0\right]^2 \qquad \text{Axial Coincidence Condition} \tag{49}$$

$$\mathscr{X}_0 = \left[\frac{1 \pm \sqrt{1-\mathscr{P}}}{\sqrt{\mathscr{P}}}\right]^{\frac{1}{2}} \tag{50}$$

A graph of $\mathscr{X}_0$ as a function of $\mathscr{P}$ was developed from Equation (50) and is shown in Figure 10 for $\mathscr{P} \leq 1$. Note that $\mathscr{X}_0$ has two real values when $\mathscr{P} < 1$, $\mathscr{X} = 1$ when $\mathscr{P} = 1$, and $\mathscr{X}_0$ is complex when $\mathscr{P} > 1$. Thus for $\mathscr{P} \leq 1$, Equation (49) shows that the axial coincidence condition appears on an $\mathscr{X}$, $\mathscr{Y}$ graph in the form of two circles of radii $\mathscr{X}_0/2$ and centered at $(\mathscr{X}, \mathscr{Y}) = (\mathscr{X}_0/2,\ 0)$. When $\mathscr{P} = 1$, the two circles coalesce to the circular membrane-bending contour defined by Equation (37). Pairs of contours are shown in Figure 11 for several values of $\mathscr{P}$. Note that these contours do not exist when $\mathscr{P} > 1$ which implies that axial coincidence conditions do not exist.

A similar procedure can be used to develop the circumferential coincidence contours shown in Figure 12. In this case f_{cn} is defined by the equation:

$$f_{cn} = c_0/\lambda = c_0/\lambda_{ey} = n\, c_0/2\,\pi R = \mathscr{Y}_0\ \mathscr{Y}\ f_0 \tag{51}$$

$$\mathscr{Y}_0 = c_0/2\pi R\, f_0\ \sqrt{\beta} \tag{52}$$

Now set $f_{cn} = f_{mn}$ and use Equations (35) and (51) to obtain the following relationship between $\mathscr{X}$ and $\mathscr{Y}$:

$$(\mathscr{X}^2 + \mathscr{Y}^2)^4 - \mathscr{Y}_0^2 (\mathscr{X}^2 + \mathscr{Y}^2)^3 + \mathscr{Y}_0^2 \mathscr{X}^2 (\mathscr{X}^2 + \mathscr{Y}^2)^2 + \mathscr{X}^4 = 0 \qquad (53)$$

The contours defined by Equation (53) were obtained by use of a digital computer for several values of the parameter $\mathscr{Y}_0$; and these contours are shown in Figure 12. Note that there is only one contour for each value of $\mathscr{Y}_0$; and $\mathscr{Y} = \mathscr{Y}_0$ when $\mathscr{X} = 0$.

Acoustically fast (AF) modes are defined as those modes for which the elastic wave speed in the shell is greater than the speed of sound, when the excitation frequency is equal to the resonance frequency. The opposite is true for acoustically slow (AS) modes. This implies that $\lambda < \lambda_e$ for (AF)-modes and $\lambda_e < \lambda$ for (AS)-modes. The coincidence, or resonance frequencies of modes which are (AF) or (AS) along the x-axis or along the y-axis can be found from the following inequalities: (see Equations (47) and (51))

$$\left.\begin{array}{lll}
f_{cm}/f_0 = c_0/f_0\ \lambda > c_0/f_0\ \lambda_{ex} = \sqrt{2}\ \mathscr{X}/\mathscr{P}^{\frac{1}{4}} & & (AF)_m\text{-modes} \\
f_{cn}/f_0 = c_0/f_0\ \lambda > c_0/f_0\ \lambda_{ey} = \mathscr{Y}_0\ \mathscr{Y} & & (AF)_n\text{-modes} \\
f_{cm}/f_0 = c_0/f_0\ \lambda < c_0/f_0\ \lambda_{ex} = \sqrt{2}\ \mathscr{X}/\mathscr{P}^{\frac{1}{4}} & & (AS)_m\text{-modes} \\
f_{cn}/f_0 = c_0/f_0\ \lambda < c_0/f_0\ \lambda_{ey} = \mathscr{Y}_0\ \mathscr{Y} & & (AS)_n\text{-modes}
\end{array}\right\} \qquad (54)$$

The regions of (AF) and (AS)-modes can be determined most easily by means of an example. Figure 13 contains a pair of axial coincidence contours for $\mathscr{P} = 0.6$, a circumferential coincidence contour for $\mathscr{Y}_0 = 1.8$, and the membrane-bending contour. Now the f_{mn}/f_0 contours (not shown on this graph) have a zero slope on the membrane-bending contour; and as a result, the double arrows shown on the three coincidence contours in Figure 13 are approximately tangent to the corresponding f_{mn}/f_0 contours which intersect the coincidence contours at the locations of the arrows. Then if f_{cm}/f_0 or f_{cn}/f_0 is held constant and $\mathscr{X}$ or $\mathscr{Y}$ varied in Equations (54) the regions in which the inequalities hold become obvious. $(AF)_m$-modes exist within the inner $\mathscr{P} = 0.6$ circle; $(AS)_m$-modes exist between the pair of $\mathscr{P} = 0.60$ contours; $(AF)_m$-modes exist outside of the outer $\mathscr{P} = 0.6$ contour; $(AS)_n$-modes exist below the $\mathscr{Y}_0 = 1.8$ contour; and $(AF)_n$-modes exist above the $\mathscr{Y}_0 = 1.8$ contour. These regions are identified in Figure 13. Note that if $\mathscr{P} \geq 1.0$ all of the shell modes are $(AF)_m$-modes. The $(\mathscr{X}, \mathscr{Y})$-space in Figure 13 can be divided into the following four regions based on the types of modes within the region:

Region 1 – $(AS)_m$, $(AS)_n$
Region 2 – $(AS)_m$, $(AF)_n$
Region 3 – $(AF)_m$, $(AS)_n$
Region 4 – $(AF)_m$, $(AF)_n$

Since (AS)-modes have lower response levels than (AF) modes, it is expected that modes in Region 1 can be neglected relative to modes in Region 4.

Another method for identifying modes which are (AF) or (AS) is to construct contours of constant values of n in a graph of f_{mn} vs m, and contours of constant values of m in a graph of f_{mn} vs n. Examples of such graphs (drawn by the computer) are shown in Figures 28 and 29 for the SLA. Also plotted on these graphs are the coincidence curves defined by Equations (47) and (51). In both Figures 28 and 29, (AF) modes lie above the coincidence curves while (AS) modes lie below the curves.

3.6 Response Equations

The equation used to compute the space-average acceleration response spectrum is derived in Reference 1. This *equation is presented below for convenience:*

$$\frac{S[\ddot{U};f]}{S[P;f]} = \frac{1}{(\mu g)^2} \sum_{m=1}^{\infty} \sum_{n=0}^{\infty} \beta_{mn} H^2\left(\frac{f_{mn}}{f}\right) \cdot j_m^2(f) \cdot j_n^2(f) \tag{55}$$

$S[\ddot{U};f]$ = space-average power spectral density of acceleration; g^2/Hz

$S[P;f]$ = pressure power spectral density; $(psi)^2/Hz$

μg = weight per unit area of surface of shell or plate; (lb/in^2)

β_{mn}	$= 2,$	$m = 1,2,3, \ldots;$	$n = 0$	Cylindrical Shell
	$= 4n^4/(1+n^2)^2,$	$m = 1,2,3, \ldots;$	$n = 1,2,3, \ldots$	
	$= 4,$	$m = 1,2,3, \ldots;$	$n = 1,2,3, \ldots$	Plate

$H\left(\frac{f_{mn}}{f}\right)$ = single degree of freedom dynamic magnification factor for acceleration response of the (m,n)-mode

$$= \left[\left\{\left(\frac{f_{mn}}{f}\right)^2 - 1\right\}^2 + \frac{1}{Q^2}\left(\frac{f_{mn}}{f}\right)^2\right]^{-\frac{1}{2}}$$

$j_m^2(f)$ = joint acceptance for mth mode

$j_n^2(f)$ = joint acceptance for nth mode.

Note that the above equation for β_{mn} has been altered to reflect the changes in mode shape as discussed in Section 3.2. Equation (55) may be used for estimating the response of a plate or cylindrical shell. Assumptions inherent in Equation (55) include:

- Mode shapes can be expressed as products of modes along the principal axes of the plate or shell.

- Space-correlation functions for the fluctuating pressure fields can be expressed as products of space-correlation functions along the two principal axes of the plate or shell.

- Mode shapes of the plate or shell are orthogonal with respect to the mass, stiffness and damping distributions of the structure; and this condition is valid if the structure is uniform.

This equation treats each mode of the structure as a single degree of freedom system whose response is independent of the responses of all other modes. The total mean-square response of the structure is then equal to the sum of the ensemble of mean-square responses of all of the structural modes.

The influence of cross-correlations between the responses of any pair of modes is automatically deleted by space averaging the response. Thus, Equation (55) contains no cross-product terms associated with two different modes. The influence of modal cross-correlations in response is demonstrated in Section 2 for a pinned beam. There it is seen that these cross-correlations describe the variation of response from the space average, and such variations are expected to be important for structures with localized excitations. In the latter case, response levels are expected to be high near the source of excitation and to decrease with increasing distance from the source. As a result, Equation (55) cannot be used to show this dissipation effect with distance and must be used with care when localized excitations are employed. When the plate or shell is well coupled, the space average response level should be approximately proportional to the area of excitation. This is shown by the joint acceptance equation for localized excitation discussed in Appendices A and B. These joint acceptances might be written as:

$$j_m^2(\omega) = \left(\frac{\Delta x}{L_x}\right)^2 J_m^2(\omega)$$

$$j_n^2(\omega) = \left(\frac{\Delta y}{L_y}\right)^2 J_n^2(\omega)$$

where Δx and Δy are the length and width of a rectangular area over which the excitation is applied. Substituting this equation into Equation (55) gives:

$$\frac{S[\ddot{U};f]}{S[P;\omega]} = \frac{(A_e/A)^2}{(\mu g)^2} \sum_{m=1}^{\infty} \sum_{n=0}^{\infty} \beta_{mn} H^2 \left(\frac{f_{mn}}{f}\right) J_m^2(\omega)\, J_n^2(\omega) \tag{55a}$$

$A_e = \Delta x\, \Delta y$ = excitation area

$A = L_x L_y$ = total area of structure.

The joint acceptance $J_m^2(\omega)$ and $J_n^2(\omega)$ are relatively insensitive to Δx and Δy.

If a localized excitation is to be used, responses should be computed by two methods. First, Equation (55) can be used to give a reasonably good estimate of the average response of the unforced portion of the structure. Secondly, the response of only the forced portion of the structure should be computed to give an upper bound on the localized response levels. Actual response levels near the source will be lower than those computed in the second calculation, while response levels far from the source should be higher than those predicted by the first calculation. A single example of this method is presented in Figures 117 and 118 and is discussed in Section 4.3.

3.7 Approximations of the Response Excitation

Special cases are often encountered in which the series response equation, Equation (55), can be simplified by means of various approximations. The resulting equation may be a relatively simple closed form expression for response; or several equations may result that indicate a simple arithmetic procedure by which the responses can be computed. These special cases are generally associated with the low frequency range where modes are well separated in frequency space, higher frequency ranges in which only certain types of modes dominate the response, and very high frequency ranges in which a large number of closely spaced modes respond with approximately the same amplitude. Several of these approximations are developed below and are validated by means of examples. Approximations of the type discussed here have also been made by other investigators and can be found in the literature.

An obvious simplification of Equation (55) can be introduced at low frequencies where modal bandwidths are relatively small and where resonance frequencies are sufficiently well separated to ensure that modal bandwidths do not overlap. In this frequency range, the response is dominated by a set of distinct resonance response peaks each of which is due to the response of a single mode; and in this case the peak amplitudes can be calculated by using a single term in Equation (55). The first few response peaks of most of the acceleration spectra shown in Figures 37-118 are of this type. In several of these graphs, the peaks are identified by mode numbers (m,n). For most structures, the modes tend to coalesce at higher frequencies due to increases in modal bandwidths, modal densities and the number of modes excited; however, Figure 65 shows an example of a thin flat plate whose response to a progressive acoustic wave is distinctly modal over a two and one-half decade frequency range; that is, the entire spectrum could have been calculated by using a single term in Equation (55) at each of the response peaks. In this example, the modal density is constant with a 10 Hz average separation between modes, the damping is relatively light with $Q = 30$, and the progressive acoustic wave field is rather selective in the types of modes excited. As an example of how Equation (55) can be used to calculate individual response peaks, a sample calculation is given below for the (1,1)-mode of the plate whose response is shown in Figure 65:

L_x = 24.0 in. = length along propagation axis

L_y = 16.0 in. = width normal to propagation axis

h = 0.10 in. = plate thickness

μg = 0.01 lb/in.^{2} = weight per unit area

μ = $2.58 \cdot 10^{-5}$ lb-sec^2/in.^{3} = mass per unit area

D = 956.0 lb-in. = plate bending stiffness

Q = 30 = resonant dynamic magnification factor

$m = n = 1$ = mode numbers

$$f_{mn} = (\pi/2) \cdot [D/\mu]^{\frac{1}{2}} \cdot [(m/L_x)^2 + (n/L_y)^2]$$

$$= 149.0\,[(m/3)^2 + (n/2)^2]$$

$$= 55.5 \text{ Hz for } (1,1)\text{-mode}$$

c_0 = 13,440 in./sec = speed of sound in air

$$\gamma_x = 2\pi f L_x / c_0 = 2\pi f_{11} L_x / c_0 = 0.198\pi$$

$$j_m^2(\omega) = \frac{2}{(m\pi)^2} \frac{1 - (-1)^m \cos \gamma_x}{[1 - (\gamma_x / m\pi)^2]^2} = 0.399 \text{ for } m = 1$$

$$j_n^2(\omega) = (2/n\pi)^2 = 0.406$$

$$H^2(f_{mn}/f) = Q^2 = 900 \text{ for } f_{mn} = f = 55.5 \text{ Hz}$$

$$\beta_n = 4.0 \text{ for rectangular plate with } n = 1$$

$$\frac{S[\ddot{U};f_{11}]}{S[P;f_{11}]} = \frac{\beta_n H^2(f_{mn}/f) \cdot j_m^2(\omega) \cdot j_n^2(\omega)}{(\mu g)^2} = 5.84 \cdot 10^6 \frac{g^2}{(\text{psi})^2}$$

= amplitude of first peak in Figure 65.

The amplitudes of all of the other modes in Figure 65 can be calculated with the above equations. A similar procedure, but with different equations for f_{mn}, $j_m^2(\omega)$ and $j_n^2(\omega)$, can be followed to calculate discrete resonant response levels for the other acceleration spectra.

For constant Q modes, an increase in frequency f leads to an increase in modal bandwidths, $\Delta f = f/Q$. When the modal density, $\mathcal{N}(f)$, is relatively high, and the frequency-separation between modes is correspondingly low, the modal bandwidths may increase to such an extent that modal bandwidths overlap. In this case, the number, N, of modes having resonance frequencies within the bandwidth Δf centered at f is:

$$N = \text{number of modes within bandwidth } \Delta f$$
$$= \Delta f \cdot \mathcal{N}(f) = f \cdot \mathcal{N}(f)/Q \tag{56}$$

If all of these N modes have approximately the same response level, then the total mean-square response is approximately N times the response of any one of the modes. Equation (55) can be simplified to reflect this condition by assuming that $H^2(f_{mn}/f) = Q^2$, and that β_n, $j_m^2(\omega)$ and $j_n^2(\omega)$ are the same for all N modes, so that:

$$\frac{S[\ddot{U};f]}{S[P;f]} = \frac{\beta_n \cdot Q^2 \cdot j_m^2(\omega) \cdot j_n^2(\omega)}{(\mu g)^2} N$$

$$= \frac{\beta_n \cdot Q \cdot f \cdot j_m^2(\omega) \cdot j_n^2(\omega) \cdot \mathcal{N}(f)}{(\mu g)^2} \tag{57}$$

Using slightly different assumptions, it is possible to develop another approximate response equation which differs by only a constant ($\pi/2$) from Equation (57). As before let β_n, $j_m^2(\omega)$ and $j_n^2(\omega)$ be the same for all modes having resonance frequencies in the neighborhood of f; however, assume that the modes are uniformly spaced about f with separation distance $\Delta f_{mn} = [\mathcal{N}(f)]^{-1}$. It follows from Equation (55) that:

$$\frac{S[\ddot{U};f]}{S[P;f]} \doteq \frac{\beta_n \cdot j_m^2(\omega) \cdot j_n^2(\omega) \cdot f \cdot \mathcal{N}(f)}{(\mu g)^2} \sum_{m,n} H^2\left(\frac{f_{mn}}{f}\right) \frac{\Delta f_{mn}}{f}$$

$$\doteq \frac{\beta_n \cdot j_m^2(\omega) \cdot j_n^2(\omega) \cdot f \cdot \mathcal{N}(f)}{(\mu g)^2} \int_0^\infty H^2(z) \cdot dz$$

$$= \frac{\pi}{2} \cdot \frac{\beta_n \cdot Q \cdot f \cdot j_m^2(\omega) \cdot j_n^2(\omega) \cdot \mathcal{N}(f)}{(\mu g)^2} \tag{58}$$

In order to apply Equation (57) or (58), it is necessary to determine values of $j_m^2(\omega)$ and $j_n^2(\omega)$ appropriate to the excitation frequency f and the particular form of excitation under consideration. Two special cases are considered below for flat plate response to progressive wave and reverberant excitation. Since a cylindrical shell has the same vibration characteristics as an equivalent flat plate above the ring frequency, the special cases discussed below are also applicable to high frequency shell vibrations.

Consider a rectangular flat plate with a plane acoustic wave field propagating along the x-axis at parallel incidence. Since the waves have a unit correlation along the y-axis, $j_n^2(\omega) = (2/n\pi)^2$. In addition assume that the excitation frequency f is less than the infinite plate coincidence frequency $f_\infty = c_0^2\,[\mu/D\,]^{\frac{1}{2}}/2\pi$, and also that there exists a mode (m,n) which is coincident along the x-axis. The coincident mode number $m = 2L_x f/c_0$, and the corresponding value of the joint acceptance $j_m^2(\omega) = 0.25$ if $m > 1$. From the equation for the resonance frequency of a flat rectangular plate, setting $f_{mn} = f$ leads to the following value of n^2:

$$n^2 = L_y^2\left[\frac{2}{\pi}\sqrt{\frac{\mu}{D}}\,f - \left(\frac{m}{L_x}\right)^2\right]$$

$$= L_y^2\left[\frac{2}{\pi}\sqrt{\frac{\mu}{D}}\,f - \left(\frac{2f}{c_0}\right)^2\right]$$

$$= L_y^2\left(\frac{2}{c_0}\right)^2\left[1 - \left(\frac{f}{f_\infty}\right)\right] f \cdot f_\infty$$

Since the structure is a flat plate, $\beta_n = 4$ and $\mathcal{N}(f) = L_x L_y\,[\mu/D\,]^{\frac{1}{2}}/2 = \pi L_x L_y f_\infty/c_0^2$. It follows that Equation (58) can be reduced to the following approximate equation for response:

$$\frac{S[\ddot{U};f]}{S[P;f]} \doteq \frac{L_x Q}{2L_y (\mu g)^2\,[1-(f/f_\infty)]}, \quad f < f_\infty \tag{59}$$

Although many assumptions are involved in the development of Equation (59), this expression provides a reasonable order-of-magnitude estimate of the response and provides an indication of the average shape of the acceleration spectrum. First it is interesting to note that at frequencies $f << f_\infty$, the acceleration spectrum is independent of frequency; and this effect can be seen in Figures 64 and 67. In Figure 64, the coincidence frequency f_∞ occurs at 15,900 Hz and is not shown on the graph, but the spectrum below 10,000 Hz is quite flat. The coincidence frequency, f_∞, in Figure 62 occurs at 322 Hz, and the increase in response at this frequency is predicted by Equation (59) as well as the relatively flat spectrum below coincidence. (Note that Equation (59) is not applicable for the low order resonances.) As listed in Table 7, the surface weights for these two flat plates are $\mu g = 0.0032, 0.0139$ lb/in.^{2}, respectively.

Substituting these values into Equation (59) along with appropriate values of L_x, L_y, Q *shown in the figure titles,* the computed average responses are:

$$\frac{S[\ddot{U};f]}{S[P;f]} \doteq \frac{2.25 \cdot 10^5}{\left[1 - \frac{f}{15900}\right]}, \qquad \text{Figure 64}$$

$$\doteq \frac{2.08 \cdot 10^4}{\left[1 - \frac{f}{326}\right]}, \qquad \text{Figure 67}$$

These approximations are close to those obtained by more complicated analyses. It is interesting to note that if Equation (59) is used to estimate the acceleration spectrum in Figure 65, the estimate is $2.19 \cdot 10^6/[1 - f/5000]$, which is much greater than the accurately computed spectrum. This is expected since this spectrum consists essentially of the responses of individual modes. Finally, it should be noted that Equation (59) is merely an extension of mass law, $S[\ddot{U},f]/S[P;f] = 1/(\mu g)^2$, in that it corrects for the plate aspect ratio, damping, and the existence of a coincidence frequency; and in a sense, it is the applicable mass law at frequencies below coincidence.

The second special case of interest concerns the response of a flat plate or cylindrical shell to reverberant excitation above coincidence. Reference 1 shows that above coincidence the joint acceptances $j_m^2(\omega)$ and $j_n^2(\omega)$ for a reverberant acoustic field are:

$$\left.\begin{aligned} j_m^2(\omega) &\doteq c_0/4\,L_x\,f \\ j_n^2(\omega) &\doteq c_0/4\,L_y\,f \end{aligned}\right\} \quad f > f_\infty$$

Using these expressions along with $\beta_n = 4$, $\mathcal{N}(f) = \pi L_x L_y f_\infty/c_0^2$, and including a factor of 2.0 to account for surface reflections, Equation (58) becomes:

$$\frac{S[\ddot{U};f]}{S[P;f]} \doteq \frac{\pi^2}{4} \frac{Q}{(\mu g)^2} \left(\frac{f_\infty}{f}\right), \quad f_\infty < f \tag{60}$$

Equation (60) predicts an f^{-1} roll-off of response for $f > f_\infty$, and this can be seen in all of the Figures 68-90 with the exceptions of Figures 80 and 81 for which f_∞ lies off the graph. In several figures, such as Figure 82, Equation (60) was used to fill in the high frequency portion of the acceleration spectrum which could not easily be obtained by the digital computer. Numerical evaluations of Equation (60) for any of the reverberant responses shows that this equation is an accurate approximation.

3.8 Statistical Energy Analysis of the Reverberant Response of Cylinders

A method which can be used to predict the response of structures to an external excitation is offered by the statistical energy analysis (References 14 and 15). This method is based on the fact that the time average power flow between two simple oscillators, linearly coupled and excited by a wide-band excitation, is proportional to the difference in their time-average total energy, the power flow being always from the oscillator of higher energy to that of lower energy. This principle can be expressed by the following equation.

$$\langle P_{12} \rangle = \Phi_{12} \left[\langle E_1 \rangle - \langle E_2 \rangle \right]$$

where

$\langle P_{12} \rangle$ = time average power flow from oscillator 1 to oscillator 2

$\langle E_1 \rangle$ = time average total energy of oscillator 1

$\langle E_2 \rangle$ = time average total energy of oscillator 2

Φ_{12} = coupling factor between the two oscillators. An expression for this factor can be found by using the admittance concept (Reference 15).

This principle can be extended to two vibrating systems, A and B, for which the time average power transferred from A to B can be written in the following form:

$$P_{AB} = \Phi_{AB} \cdot N_A \cdot N_B \left[\frac{E_A}{N_A} - \frac{E_B}{N_B} \right] \tag{61}$$

where

Φ_{AB} = average mode-to-mode coupling factor between the two subsystems

E_A = average total energy of subsystem A

E_B = average total energy of subsystem B

N_A = number of modes in subsystem A

N_B = number of modes in subsystem B.

The above expression is valid when the subsystems satisfy one of the following conditions (which in most cases are approximately satisfied): (see Reference 15)

a. The coupling factors between modes are all equal.

b. Modes within the same subsystem have the same time-average total energy.

c. The time-average total energy of a mode is independent of its coupling to any particular mode in the other subsystem.

When a multimodal system is excited in a band of frequencies, its modes can be divided into resonant and non-resonant modes within the band and each of these groups can be divided into groups of modes which satisfy one of the above mentioned conditions. Then, Equation (61) can be applied among the resonant groups. The energy transmission between nonresonant modes and between resonant and nonresonant modes cannot be predicted by the statistical energy analysis and, usually, it is calculated by using classical vibrational analysis. Equation (61) can be written in the following fashion:

$$P_{AB} = \omega\, \eta_{AB}\, n_A \left[\frac{E_A}{n_A} - \frac{E_B}{n_B}\right]$$

where

ω = center frequency of the excitation band

$\eta_{AB} \equiv \Phi_{AB} N_B/\omega$ = coupling loss factor

n_A = average modal density of system A over a band of frequency Δ; it is defined as:

$$n_A = \frac{N_A\,(f + \Delta/2) - N_A\,(f - \Delta/2)}{\Delta}$$

$N_A(f)$ = average number of modes with resonance frequencies below f

n_B = average modal density of system B.

Now, a power balance equation can be written for each vibrating system. These equations will state that the summation of the power received from other systems, the power given to other systems and the power dissipated must be equal to zero in steady state conditions. For example, the power-balance equation for the nth system of a series has the following form:

$$\omega\, \eta_{n,n+1}\, n_n \left[\frac{E_n}{n_n} - \frac{E_{n+1}}{n_{n+1}}\right] + \omega\, \eta_{n,n-1}\, n_n \left[\frac{E_n}{n_n} - \frac{E_{n-1}}{n_{n-1}}\right] + \omega\, \eta_n\, E_n + P^{NR}_{n,n-1} + P^{NR}_{n,n+1} = 0 \qquad (62)$$

where

$\omega\, \eta_n\, E_n$ = power dissipated

η_n = dissipating loss factor

$P^{NR}_{n,n-1}$ and $P^{NR}_{n,n+1}$ are the power transmitted through nonresonant modes.

If equations similar to Equation (62) are written for each vibrating system of the series, a set of linear equations is obtained. This set can be solved for the energy of the resonant modal group in terms of the coupling and dissipating loss factors, modal densities and power transmitted from nonresonant modal groups. Finally, the response of the vibrating systems can be predicted in the form of power spectral density. In fact, the PSDs of an acoustic field and of a structural system are given in term of the average energy by the following relations:

$$S_p(f) = \frac{\rho_0 c_0^2 \; E}{V \Delta} \tag{63}$$

$$S_a(f) = \frac{\omega^2 E}{M \Delta} \tag{64}$$

Equation (63) gives the sound pressure level spectral density $S_p(f)$ (which is a function of frequency, f) in terms of the average energy, E, within a band of frequency Δ, the density of the medium, ρ_0, the speed of sound, c_0, the volume, V, and the band of frequency Δ. Equation (64) gives the acceleration spectral density of a structural system $S_a(f)$, in terms of the average energy, E, the mass, M, the band center frequency, ω, and the band of frequency Δ.

In the case of a cylinder excited by a reverberant acoustic field, the following expression can be derived to predict the response:

$$\frac{S_{a2}}{S_{p1}} = \frac{\pi c_0}{A \rho_s \rho_0} \left[\frac{\eta_{2AF,1} n_{2AF}}{2\eta_{2AF,1} + \eta_{2AF}} + \frac{\eta_{2AS,1} n_{2AS}}{2\eta_{2AS,1} + \eta_{2AS}} \right] \left[1 + \frac{S_{p3}}{S_{p1}} \right] \left[\frac{1}{g^2} \right] \left(\frac{g^2}{psi^2} \right) \tag{65}$$

where

S_{a2} = acceleration spectral density

S_{p1} = sound pressure spectral density

$$\frac{S_{p1}}{S_{p3}} = \frac{\eta_{2AS,1} n_{2AS} + \eta_{1AF,1} n_{2AF} + \eta_3 n_3}{\dfrac{\eta_{2AS,1} n_{2AS}}{2\eta_{2AS,1} + \eta_{2AS}} + \dfrac{\eta^2_{2AF,1} n_{2AF}}{2\,\eta_{2AF,1} + \eta_{2AF}}} - 1 \quad \text{(= noise reduction)} \tag{66}$$

c_0 = speed of sound in air

ρ_0 = mass density of air

A = surface area of cylinder

ρ_s = surface mass density of cylinder

g = gravity acceleration

n_{2AF} = modal density of the resonant acoustically fast (AF) modal group

n_{2AS} = modal density of the resonant acoustically slow (AS) modal group

n_3 = modal density of the resonance interior space modes

$\eta_{2AF,1}$ = coupling loss factor between the acoustic field and the resonant AF mode group

$\eta_{2AS,1}$ = coupling loss factor between the acoustic field and the resonant AF mode group

η_{2AF} = dissipating loss factor of the resonant AF modal group

η_{2AS} = dissipating loss factor of the resonant AS modal group

η_3 = dissipating loss factor of the interior space modal group

Values of the above factors and modal densities are given by the following expressions:

a) Modal Densities

An expression for the total modal density of a simply supported thin cylindrical shell is given by Bolotin's formula (Reference 16)

$$n_t(\nu) = \frac{\ell\sqrt{3}}{\pi h}\int_0^{\theta_m}\left[1 - \frac{\sin^4\theta}{\nu^2}\right]^{-\frac{1}{2}} d\theta \tag{67}$$

where

$\nu = \frac{f}{f_r}$ = ratio of frequency f to the ring frequency f_r

$f_r = c_L/2\pi a$

c_L = speed of sound in the material

a = radius of cylinder

h = thickness of shell wall

$$\theta_m = \begin{cases} \sin^{-1}\sqrt{\nu} & \text{if} \quad \nu < 1 \\ \pi/2 & \text{if} \quad \nu \geq 1 \end{cases}$$

The number of AF modes below the frequency ν (for $\nu < \nu_c$), N_{2AF}, is given by (Reference 14, page 45)

$$N_{2AF}^{(\nu)} = \frac{2\ell}{\pi a\beta}\int_0^{\theta_m}\left[\frac{\nu_c}{2} - \frac{\nu_c}{2}\left(1 - \frac{4\sin^4\theta}{\nu_c^2}\right)^{\frac{1}{2}}\right] d\theta \tag{68}$$

where

$$\beta = \frac{h}{a\sqrt{12}}$$

$\nu_c = f_c/f_r$

f_c = critical frequency $\equiv$ frequency at which the free-bending wave speed in the panel is equal to the speed of sound. Therefore, the critical frequency is found from

$$c_b = \sqrt{\omega_c}\left[\frac{D}{\mu}\right]^{\frac{1}{4}} = c_0$$

or

$$f_c = \frac{c_0^2}{2\pi}\sqrt{\frac{\mu}{D}}$$

where

c_b = bending wave speed

D = flexural rigidity

μ = surface mass density

c_0 = speed of sound in air.

The modal density of the AF modal group can be obtained from Equation (68) as

$$n_{2AF}^{(\nu)} = \frac{\partial N_{2AF}^{(\nu)}}{\partial \nu} \tag{69}$$

Now, it can be seen from Equations (68) and (69) that n_{2AF} for $1 < \nu < \nu_c$ is zero as shown also in Figure 11 of Reference 14.

For frequencies above the critical frequency, all modes are acoustically fast and then

$$n_{2AF}^{(\nu)} = n_t^{(\nu)}$$

The modal density of the AS modal group is given by the difference between the total modal density and the AF modal density.

An approximate expression for the acoustic volume modal density is

$$n_3 = \frac{4\pi^2 f^2 a^2 \ell}{c_0^3}$$

b) Coupling Loss Factors

The coupling factor between the acoustic field and the acoustically fast modes is given by (Reference 14)

$$\eta_{2AF,1} = \frac{\rho_0 c_0}{2\pi f \rho_s}$$

The coupling factor for the AS group (for $f > f_r$ and when the cylinder dimensions are greater than an acoustic wavelength) is (Reference 14)

$$\eta_{2AS,1} = \frac{\rho_0 c_0^2}{2\pi f f_c \rho_s A}\left[\lambda_0\, g_1(f/f_c) + P_r\, g_2(f/f_c)\right]$$

where

λ_0 = acoustic wavelength

P_r = *radiating perimeter* $= 4\pi a$

$$g_1(f/f_c) = \begin{cases} (4/\pi^4)(1-2f/f_c)\Big/\sqrt{f/f_c\,(1-f/f_c)} & f < 0.5\,f_c \\ 0 & f \geq 0.5\,f_c \end{cases} \quad \text{(Reference 17)}$$

$$g_2(f/f_c) = \left\{(1-f/f_c)\ln\left[(1+\sqrt{f/f_c})/(1-\sqrt{f/f_c})\right] + 2\sqrt{f/f_c}\right\}\Big/4\pi^2(1-f/f_c)^{3/2} \quad \text{(Reference 17)}$$

When the cylinder dimensions are smaller than an acoustic wavelength and for $f < f_r$, the following coupling factor is used:

$$\eta_{2AS,1} = \frac{\rho_0 c_0^2}{2\pi f f_c \rho_s A}\left(\frac{4}{\pi^4} P_r \sqrt{f/f_c}\right)$$

c) Dissipating Loss Factors

The structural loss factors are given by:

$$\eta_{2AF} = \eta_{2AS} = \frac{1}{Q}$$

where Q is the dynamic magnification factor of resonance.

The loss factor of the inside acoustic volume can be expressed in terms of the average absorption coefficient α as

$$\eta_3 = \frac{c_0\,\alpha}{4\pi f a}$$

The shell structures which were analyzed by the modal method and presented in Figures 68, 72 and 82 were also analyzed using the above statistical energy method and the comparative results were included in Figures 68, 72 and 82. The results are in good agreement for the two methods in the higher frequency region above coincidence as expected. Fair agreement was obtained in the frequency region between the ring frequency and coincidence for the examples in Figures 72 and 82. However, the comparisons at the ring frequency and coincidence and in the low frequency regions are quite different. Some of this difference can be accounted for by the fact that the energy method uses a constant generalized mass for all modes, whereas the modal method uses a generalized mass which is dependent on the circumferential mode number n.

4.0 COMPARATIVE ANALYSIS OF SHELL AND PLATE RESPONSES

Acceleration response spectra of all of the shell and plate structures introduced in Section 3.1 and listed in Tables 6 and 7 are presented in this section in Figures 36 - 118. The various applied excitation fields are also listed in Tables 6 and 7 and discussed in detail in Section 3.4. Summary discussions of the primary features of these response spectra are included below.

In general, 900 modes were used for these computations, exceptions are noted. Abrupt cut-off points in several of the spectra are the result of a lack of a sufficient number of modes in the respective computations. Tables 9 - 31 and Figures 119 - 127, which contain details of the modal contributions to the total response and associated data, are included and discussed at appropriate points throughout this section.

4.1 Responses to Progressive Wave Fields

All of the shell and plate structures listed in Tables 6 and 7 were analyzed for their acceleration response to various ducted axial correlated progressive wave acoustic fields. The respective acceleration response spectra are presented in Figures 36-67.

4.1.1 SLA Responses to Axially Correlated Duct Fields

Theoretical space averaged acceleration response spectra for the SLA are presented in Figures 36-42 for N axial ducts, where N = 1, 2, 4, 8, 16, 32, and 64, respectively. The main features of the response spectra are summarized as follows:

- The acceleration spectra shown in Figures 36–42 are greater than the comparable spectra shown in References 1 and 2 due to the inclusion of the n = 1 modes and the correction factor, $(n^2+1)/n^2$, on the generalized mass of the cylindrical shell.

- The acceleration spectrum in Figure 36 includes responses of only n = 0 (m = 1, 2, 3, ...) modes, since N = 1 implies a single duct with unit correlation around the entire circumference of the shell. *Such a correlation leads to zero generalized force of all modes ($n \geq 1$) having a* non-zero integer number of full circumferential wavelengths.

- The peak response shown in Figure 36 lies within the 200-300 Hz band which is somewhat above the ring resonance frequency of 175 Hz. Within this band the overall response is controlled by the responses of individual modes which are at resonance and which nearly satisfy the condition for acoustic coincidence along the shell axis. This can be seen in Table 10 which shows that the (12, 0)-mode produces 80 percent of the total response at 248 Hz. For purposes of comparison, a comparable summary of modal responses is presented in Table 9 for 175 Hz.

- As the number of (relatively uncorrelated) ducts increases from N = 1 to N = 16, the generalized forces decrease for the n = 0, $m \geq 1$ modes and increase for the $n \geq 1$, $m \geq 1$ modes; and hence, the peak response spectrum between 200–300 Hz decreases while the spectrum below 200 Hz increases. Furthermore, the average spectrum level increases to a maximum for N = 16, and decreases for N = 32 and 64.

An experimental acceleration response spectrum was obtained from data measured with several accelerometers during the SLA acoustic qualification tests at MSC. These data were averaged to obtain an experimentally derived space average acceleration response spectrum for the N = 16 duct experimental configuration. This single response spectrum is overlayed on the several computed response spectra in Figures 36-40. Comparisons between the theoretical spectra and the experimental spectrum indicate that;

- At low frequencies, the experimental response due to sixteen uncorrelated ducts is similar to the theoretical response for two (N = 2) uncorrelated ducts as shown in Figure 37. This might be interpreted as implying that some degree of acoustic correlation exists between adjacent ducts at low frequencies.

- The frequency band over which the theoretical and experimental spectra are approximately equal moves towards higher frequencies as N increases. Thus, it appears that any acoustic cross-correlation between adjacent ducts decreases as frequency increases.

- The above implies that cross-correlation between ducts explains the difference between theoretical and experimental acceleration spectra. However, an additional phenomenon that could be partially responsible for this difference is radiation damping within the ducts. From Reference 12, the critical damping ratio, ζ_r, due to radiation damping is estimated to be $\zeta_r = 81.3/m^4$, whereas for $Q_0 = 15$, the structural damping ratio $\zeta_0 = 1/2\,Q_0 = 0.033$. The following factor for reducing the peak response values of the odd numbered axial modes of the SLA is

$$\left[\left(\frac{Q_e}{Q_0}\right)^2\right]_m = \frac{1}{[1 + 2440/m^4]^2}, \quad m = 1,3,5, \ldots$$

  This factor virtually eliminates the first four resonant response peaks predicted theoretically and the number of remaining peaks is lessened. However, the even-numbered axial modes (m = 2, 4, 6, ...) should be relatively unaffected. Since the few even modes are also diminished, there appears to be some additional phenomena present in the low frequency portion of the experimental data, which might be explained by introducing a partial correlation of the ducts, which decreases with increasing frequency.

- Figure 40 also indicates a marked difference between the experimentally measured response and the theoretically predicted response in the high frequency region above both the ring frequency (175 Hz) and the critical frequency (322 Hz). This discrepancy is probably attributable to experimental instrumentation limitations on the one hand, and the exactness of the theoretical analysis on the other. In addition, above about 170 Hz, the ducts are able to support and transmit a variety of acoustic cross modes due to the large admittance of one wall of the duct (the SLA) which would tend to make the acoustic field within the duct less correlated at these high frequencies tending toward a more reverberant acoustic field and substantially more response. An excellent discussion of this acoustic duct phenomenon is presented in Section 9.2 of Reference 13.

4.1.2 The Effect of Axial Correlation Damping on SLA Responses

Figures 43-49 contain acceleration response spectra of the SLA excited by plane progressive acoustic waves in sixteen (N = 16) uncorrelated ducts, where the axial spatial correlation has been exponentially damped. This damped spatial correlation function is expressed as

$$C(\zeta;\omega) = \exp\left[-A\,\gamma_x\,\left|\bar{\zeta}\right|\right]\cos\gamma_x\,\bar{\zeta}$$

where

$\gamma_x = L_x\,\omega/c_0$

$\bar{\zeta} = \zeta/L_x$

ζ = separation distance

c_0 = speed of sound.

A damped correlation function is a simple simulation of a boundary layer turbulence correlation pattern (note the similarity of the A = 10.0 curve of Figure 49 and the Mach 1 curve of Figure 91), a non-plane wave, a spread-out source, and other anomalies which occur in practical progressive wave fields. The primary effect of this damping is to increase high frequency response.

The various spectra of Figures 43-49 were obtained for several values of A (A = 0, 0.01, 0.05, 0.1, 0.5, 1, 5, and 10). Note that as A increases, the high frequency response region above the critical frequency (f_c = 322 Hz) increases until about A = 0.5, after which the spectrum continues to flatten; however, a drop in level also occurs.

4.1.3 Effects of Structural Variations on SLA Responses

Figures 50-53 show the changes in SLA acceleration spectra with changes in radius. General features of these spectra are:

- As the radius decreases relative to the SLA, the stiffness increases with a corresponding decrease in response level. If the radius is reduced significantly, the possibility of axial acoustic coincidence is eliminated, so that all modes are acoustically fast axially. As a result, response levels will generally decrease with increasing frequency. However, Figures 50 and 51 show a flattening of the spectrum in the neighborhood of the ring frequency. This is caused partially by the increased modal density at the ring frequency. The curves shown in Figures 30-31 indicate that the closest approach of the $[f_c]_n$ curve to the f_{mn} curves occurs in the region below the ring frequency.

- As the radius increases relative to the SLA, the stiffness decreases and the response level increases. If the radius is increased significantly, the axial acoustic coincidence frequencies separate. This separation results in the inclusion of $(AS)_m$ modes in the frequency region between the two axial coincidences, which in turn results in a decrease in level in this same region. This result is shown in Figures 52 and 53, where a "notch" is apparent in the 80-300 Hz frequency band. As the separation between the axial coincidence frequencies increases the notch deepens. Also, as seen in Table 8, the lowest $[f_c]_{m(-)}$ frequencies for these two examples approach the corresponding ring frequencies, thereby increasing the response in the region of the ring frequencies. The higher $[f_c]_{m(+)}$ frequencies approach the infinite plate coincidence frequencies $[f_c]_{\infty}$ as seen in Table 8. Thus, it is apparent that response of a uniform cylinder generally contains at least two peaks; the reinforced ring frequency and the combined $[f_c]_{m(+)}$ and $[f_c]_n$ coincidence frequencies.

The effect of stiffness changes on SLA responses are shown in Figures 54-58. Here bending stiffnesses, D, less than and greater than that of the SLA are considered; and a single variation of extensional stiffness is considered. Key features of these data are:

- Changing the bending stiffness does not alter the ring frequency but does alter coincidence frequencies.

- Decreasing bending stiffness raises coincidence frequencies and allows for the possibility of two axial coincidence conditions with the double peaked response as shown in Figure 54. The net effect is similar to that of reducing radius.

- Increasing bending stiffness and extensional stiffness reduces the coincidence frequency and leads to spectra which decrease with increasing frequency as shown in Figure 58.

Increasing the mass of the shell reduces all resonance frequencies by a common factor, whereas coincidence frequencies remain unaltered. Thus, as shown in Figures 59 and 60, the ring frequency decreases whereas the upper (flat plate) coincidence frequency remains unchanged. As a result, a double peaked acceleration spectrum is obtained.

4.1.4 Responses of Other Shells

The responses of three smaller shells to sixteen uncorrelated duct excitations are shown in Figures 61-63. Significant features of these spectra are summarized below:

- Since Q = 30, resonance peaks for these thin shells are more distinct than those of the SLA which was analyzed for Q = 15.

- Below ring resonance, the spectra are reasonably flat and are similar to plate response characteristics.

- A short rise in response occurs at the ring resonance which for the shells is essentially equal to the axial acoustic coincidence frequency.

- Above ring resonance, the responses drop off sharply since their frequency range is controlled by acoustically slow modes which are not well coupled with the sound field.

- The spectra in Figures 61 and 62 were terminated at the frequencies shown because of a lack of modes at higher frequencies. The spectrum shown in Figure 63 was constructed from the summation of several spectra with different sets of modes used for different frequency ranges. The coincidence peak in the latter graph occurs at about 12,000 Hz which agrees with the coincidence frequency listed in Table 8.

4.1.5 Responses of Flat Plates

Four different flat plates were analyzed for response to single duct excitation (N = 1), and the four acceleration spectra are shown in Figures 64-67. With N = 1, the entire plate is exposed to a plane acoustic wave field propagating along the x-axis. All plates have a Q = 30 except the equivalent SLA panel which has a Q = 15 in order to be consistent with SLA cylinder responses. Note that the SLA panel has the same surface area as the SLA cylinder. These panel responses exhibit the following characteristics:

- In all cases, the (m,n) = (1, 1) mode of the plate has the highest response level since it has the most efficient wave length coupling with the acoustic field.

- The infinite flat plate coincidence frequencies, f_{∞}, for these four panels are:

f_{∞}	15900	4750	200	300 Hz
Fig. No.	64	65	66	67

  At these frequencies, it is expected that the response should increase to relatively high levels. This is seen to be the case in Figures 65 and 67. The 15900 Hz coincidence frequency is off the graph in Figure 64 and hence the rise in response does not appear, but would be present if the frequency scale were extended to 20,000 Hz. The 200 Hz coincidence frequency for the stiffened plate occurs near the resonance frequencies of the first few modes; and hence the response levels continue to decrease beyond 200 - 300 Hz.

- The acceleration spectra shown in Figures 64 and 67 are relatively flat between the resonance frequencies of the fundamental mode and coincidence. This effect can be predicted by a simple analysis as discussed in Section 3.7.

- The acceleration spectrum in Figure 65 is controlled by the resonances of single modes throughout the frequency range shown, and could have been predicted using single degree of freedom type analyses. From the mode numbers listed in this graph, it is concluded that response at coincidence occurs for high order m-numbers along the direction of propagation and low order n-modes normal to this direction.

4.2 Responses to Reverberant Acoustic Fields

The shell and plate structures listed in Tables 6 and 7 were analyzed for their acceleration responses to a reverberant acoustic field. The respective acceleration response spectra are presented in Figures 68-90. In addition, three structures were analyzed utilizing the statistical energy method as described in Section 3.8.

4.2.1 Shell Responses

The acceleration spectrum of the SLA is shown in Figure 68, whereas, the acceleration spectra representing structural parameter variations of the SLA are presented in Figures 69-79. The acceleration spectra of the three homogeneous skin shell examples are shown in Figures 80, 81 and 82. The main features of these response spectra are summarized as follows:

- The acceleration spectrum level shown in Figure 68 is greater than the comparable spectrum presented in References 1 and 2 due to the inclusion of the $n = 1$ modes and the correction factor $(n^2 + 1)/n^2$ on the generalized mass of the cylindrical shell.

- The acceleration spectrum in Figure 68 also contains comparable values obtained from the statistical energy analysis method outlined in Section 3.8. Note the general similarity and, especially, the agreement in the high frequency region above 350 Hz. The energy method treats the acceleration response of a cylinder in three basic regions, i.e., above the critical frequency (finite plate coincidence frequency), below the ring frequency, and between the ring frequency and critical frequency. The energy method used for the examples in this report assumes that there are only AS modes in the region between the ring frequency and the critical frequency, whereas, the discussion in Section 3.5 indicates that there are also AF modes in this region and for stiffened shells like the SLA, the number of AS modes in this frequency region is very small.

- The peaks at the ring frequency and the coincidence frequency which are apparent in the energy analysis method results included in Figures 68, 72 and 82, can be partially accounted for by noting that the energy analysis assumes a constant generalized mass for the system over the entire frequency range. The actual generalized mass is twice this value for the ring modes ($n = 0$) which would decrease the value at the ring frequency by a factor of two, in fact, wherever the ring modes are dominant there is an effective decrease in response. The generalized mass is correct for the high frequency region above the coincidence frequencies, but requires the generalized mass correction factor, as discussed in Section 3.1.5, in the low and intermediate frequency regions.

- Tables 15-18 contain details of the forty most dominant modes contributing to the acceleration spectra for the SLA at four selected frequencies. Note the change in the histogram of the percentage contributions of the modes relative to resonance.

- The peak response shown in Figure 68 is at about the ring frequency of 175 Hz which is also the region of highest modal density. The response is flat to about 300 Hz after which it falls off with a slope of 1/f and is in agreement with that of an infinite plate with the same bending stiffness and mass surface density. As seen from Table 8, the region from 175 Hz to 300 Hz contains the axial coincidence frequency of 248 Hz and the circumferential coincidence frequency of 302 Hz.

- The circumferential modal response contributions are more apparent in the acceleration spectra for reverberant acoustic excitation, since there are no ducts to suppress them. All of the acceleration spectra of Figures 68-82 are seen to have a response peak at about their respective ring resonance frequencies.

- Tables 23-26 contain details of the forty most dominant modes contributing to the acceleration spectra for the SLA with a radius of 208 inches at four selected frequencies. Note the change in the histogram of the percentage contributions of the modes relative to resonance.

- Figures 69, 70, 75, 76 and 77 are seen to have markedly different acceleration spectra as compared to their axial duct counterpart shown in Figures 50, 51, 56, 57 and 58.

- The high frequency roll-off in Figures 68-79 are all equal to their respective equivalent infinite plate responses above the infinite plate coincidence frequency.

- Figure 72 also contains comparable values obtained from the statistical energy analysis outlined in Section 3.1. The comments about the comparisons follow those given for Figure 68 above.

- Figures 80, 81 and 82 contain the acceleration spectra of three uniform cylinders to reverberant acoustic excitation. Note the characteristic drop in level just after the ring frequency. Figure 82 was obtained by using a total of 8100 modes ($m = 1, 2, \ldots 90; n = 0, 1, \ldots 89$). Note the characteristic notch between the ring frequency (1304 Hz) and the coincidence frequencies (11,750 Hz) and the 1/f roll-off above the coincidence frequencies.

- Tables 27-30 contain details of the forty most dominant modes contributing to the acceleration spectra for the 24 in. radius by 48 in. by 0.040 in. uniform cylinder at four selected frequencies. Note the change in the histogram of the percentage contributions of the modes relative to the resonance.

- Figure 82 also contains comparable values obtained from the statistical energy analysis method. Comments follows those given for Figures 68 and 72.

- Since Q = 30, the resonance peaks for these thin shells are more distinct than those of the SLA which was analyzed for Q = 15.

- Within the first half-decade above the fundamental resonance frequency, the response spectra are resonably flat. In each case the lower value of the spectrum is approximately equal to $1/(\mu g)^2$ with peak values of $Q/(\mu g)^2$.

- Above this frequency range the increase in response level is approximately proportional to frequency f^2, although several response peaks in this range exceed the response level at the ring frequency.

- Within the frequency range just below ring resonance, a significant overlapping of modal bandwidths occurs, and as a result, there exists a broad frequency band in which the response is high. Most of the vibrating energy of each shell is concentrated within this band.

- The lower axial coincidence frequency is almost equal to the ring resonance.

- Above the ring resonance frequency, the response decreases sharply.

4.2.2 Flat Plate Responses

Several flat plates were analyzed for their acceleration response to reverberant acoustic fields. The detailed parameters of the plates are listed in Table 7 and their respective acceleration spectra are shown in Figures 83-90. A few features are noted as follows:

- The acceleration spectrum shown in Figure 86 is for a flat plate whose bending stiffness and surface mass density are equivalent to the SLA. The slope and level of the spectrum above 300 Hz is identical to that of the SLA shown in Figure 68.

- Figures 87-90 are flat plates whose bending stiffness and surface mass density match that of the 24 in. radius by 48 in. by 0.040 in. uniform cylinder, therefore, the acceleration response above 11,750 Hz should match that for the cylinder above 11,750 Hz as shown in Figure 82. The flat plate response in Figure 87 indicates too low a modal density. The plate was cut in half, and as shown in Figure 88, the modal density was still deficient. The plate was again cut in half and Figure 89 shows that the response is about equal to that in Figure 82 above 11,750 Hz. The plate was cut by an additional factor of four and the acceleration response in this high frequency region is about the same as for the cylinder.

4.3 Responses to Boundary Layer Turbulence

The shell and plate structures listed in Tables 6 and 7 were analyzed for their acceleration responses to boundary layer turbulence excitation. The respective response spectra are presented in Figures 91-116.

4.3.1 Shell Responses

The acceleration spectra of the SLA for boundary layer turbulence excitation at Mach 1 and 2 for a boundary layer thickness of δ_b = 12.0 inches and at Mach 1 and 2 for δ_b = 6.0 inches, are shown in Figures 91-94, respectively. Tables 19-22 contain details of the response contributions of the forty most dominant modes at four selected frequencies for the SLA at Mach 1, δ_b = 12.0 inches. The acceleration spectra for structural variations of the SLA, and other shells and flat plates are shown in Figures 95-110. The main features of these response spectra are summarized as follows:

- At Mach 1 for the SLA and variations of the SLA, the acceleration spectra rolled off at a constant slope of about $1/f^{3/2}$ to $1/f^2$ above the respective coincidence frequency as seen in Figures 91, 93, 95-105. Note that the coincidence frequencies are less due to a decreased propagation velocity of U_c = 9810 in./sec instead of C_0 = 13,440 in./sec.

- At Mach 2 for the SLA, the acceleration spectra roll off at a constant slope of $1/f^2$ above the coincidence frequency as seen in Figures 92 and 94. Note that there is a break in the curve at the coincidence frequency which increased due to an increased propagation velocity of U_c = 15,900 in./sec.

- The low frequency portion of all of the acceleration response resembles that for duct excitation in level. Generally, the spectra are flatter.

- Figure 106 was computed for the 18 in. radius by 54 in. by 0.020 in. uniform cylinder for Mach $1/\sqrt{5}$, δ_b = 20.0 inches; whereas, Figure 107 was computed for Mach 1, δ_b = 12.0 inches. Note the overall increase in level and especially in the frequency region above 400 Hz in Figure 107.

- The response spectra for the 24 in. radius by 48 in. by 0.040 in. uniform cylinder presented in Figure 109 was obtained utilizing 8100 modes.

4.3.2 Plate Responses

The acceleration spectra of several flat plates for boundary layer turbulence excitation at Mach 1 with a boundary layer thickness of δ_b = 12.0 in. are shown in Figures 110-116. The main features of these response spectra are summarized below:

- Comparison of these spectra with the acceleration response spectra obtained for reverberant acoustic excitation (Figures 83-90) show that boundary layer turbulence generally excites more modes. There is no distinct coincidence region, in fact, there is a broadened increase of response up to coincidence as compared with the reverberant response spectra.

- Comparison of Figure 109 with Figures 114-116 above 2000 Hz indicate that a small panel of the same material and stiffness as the cylinder can exhibit the same response levels at frequencies above coincidence. This result is similar to that noted in the discussion of Section 4.2.2.

4.3.3 Response to Localized Excitation

A single example of response to localized excitation is presented in Figure 117. Here, the SLA cylinder is exposed to boundary layer turbulence concentrated in a 60.0 in. (axial) by 30.0 in. (circumferential) area, the center of which is located at the midheight of the shell. In practice, such an excitation might be associated with high turbulent pressure levels in the wake of a protuberance on the shell. For purposes of comparison, the response of a 60.0 in by 30.0 in flat plate segment of the SLA to the same excitation is shown in Figure 118. Another comparison that should be made is between the acceleration spectrum shown in Figure 91 and those in Figures 117 and 118. Figure 91 shows the response of the SLA to boundary layer excitation over the entire shell. For all three analyses, $Q = 15$, $U_c = 9810$ in./sec, and $\delta_b = 12.0$ in. Results of these comparisons are summarized below:

- The response of the SLA to localized excitation is considerably lower than the response to excitation of the entire shell, although the shapes of the acceleration spectra are generally similar. This is expected since the average mean-square response level should be approximately proportional to the square of the area over which the excitation occurs. This effect is discussed in Appendices A and B wherein it is shown that the joint acceptance $j^2_{mn}(\omega)$ for the (m, n)-mode is proportional to $(A_e/A)^2$, where A_e is the excitation area and A is the total area of the structure. For the present case, $(A_e/A)^2 = 6.28 \cdot 10^{-5}$ which is approximately the ratio between responses shown in Figures 91 and 117. The average response levels in Figure 117 should be a reasonably good estimate of the response levels at a large distance from the source of excitation.

- Responses of the shell and the flat plate segment are comparable when both structures are exposed to excitations over their entire surface areas. For localized excitation, the plate response is expected to be a better estimate of the localized response of the shell than that given in Figure 117; although the plate response is conservative due to a power flow from the region of localized excitation to the remainder of the shell.

A more detailed analysis of the shell to localized excitations would require the use of a more general response equation than Equation (55a). The more general equation would involve modal cross correlations that would appear in the modal expansion of response as cross terms between distinct (m, n) and (r, s) modes. With such cross correlation effects included, it would be possible to predict the decay of vibration levels of the shell with distance from the excitation area. This is demonstrated in Section 2.0 for a damped beam exposed to a localized point excitation.

4.4 Modal Contributions to Total Response

The number of modes required to achieve various percentages of the total response versus frequency for the three types of excitation are shown in Figures 119-127 for several of the structures analyzed in this report.

Figures 119, 120 and 121 contain the contours for the number of modes required to achieve 50, 75 and 99 percent of the total response of the SLA for N = 16 duct acoustic excitation, reverberant acoustic excitation and boundary layer turbulence, respectively. Note that a 1000 Hz it requires approximately 700 modes to achieve 99 percent of total response for reverberant and boundary layer excitation, whereas, only 200 modes are required for duct excitation. Tables 11-22 contain detailed information on the 40 most dominant modal contributors of the SLA at four select frequencies for each of the three types of excitation. Tables 23-30 contain additional detailed information on the 40 most dominant model contributors of other selected shells.

The number of modes required to achieve 99 percent of the total response of three small uniform shells and three flat plates for the three excitation fields are shown in Figures 122-127. Table 31 contains detailed information on the 40 most dominant modal contributors to the response of the flat plate of Figure 115 at 3090 Hz for boundary layer excitation. Note that the response is primarily a single mode.

5.0 CONCLUSIONS

The contents of this report have extended the analyses presented in References 1 and 2, and have shown how a computer oriented modal analysis method can be efficiently employed to study the responses of plate and shell structures to various excitation fields. Such computations are of great utility in

- the development of qualification test programs for aerospace structures in which acoustic excitation is used to simulate launch and in-flight fluctuating pressure environments,
- the interpretation of experimental response measurements,
- the calculation of structural acoustic and vibration transmission loss,
- the design of structures to minimize vibration response and maximize transmission loss,
- the development of environmental test specifications for equipment.

Although the present digital computer program is designed for duct and reverberant acoustic fields and boundary layer turbulence, it can be easily extended to include structural response to other useful acoustic environments, such as, free field acoustic plane wave excitation of a cylinder including the effects of scattering, structural response to localized close-coupled noise sources and combinations of duct and reverberant fields, etc. In addition, the equations of motion could be extended to include: the effects of discrete stiffness, the effects of damping on the spatial decay of vibration levels, the effects of lumped masses, etc.

It has also been shown that this method of analysis is in agreement with high frequency results obtained by statistical energy analyses. The modal analysis method permits detailed analyses of the responses of the well separated low frequency modes of a structure as well as the responses in the transition region from low frequencies to high frequencies. At very high frequencies, statistical energy analysis provide a more efficient approach than the present method.

As a result of the use of the modal analysis method, a tentative model of the acoustic fields generated by ducts has been constructed in a manner which agrees with experimental data. This model shows that at low frequencies, some degree of acoustic coupling exists between adjacent ducts, and that the lateral extent of this coupling decreases as frequency increases.

It has not been possible to develop an adequate explanation for differences between high frequency response obtained experimentally and theoretically. This may require further laboratory experiments under very controlled conditions.

It has been demonstrated that the method of analysis set forth in this report is an efficient method for computing the mean-square space average response of uniform plates and shells, and of the uniform equivalent of stiffened plates and shells.

Many structures encountered in practice are stiffened plates and shells in which the stiffeners divide the structure into an ensemble of plate and shell components. These components may be of different sizes and may have different levels of excitation, and different response levels due either to localization of the excitation or the different dynamic properties in a given frequency band. The method presented in this report might be used to efficiently compute the energy density levels of the various individual components over a broad frequency range. These energy levels could then be used with the power flow concepts discussed in References 14 through 17 to determine the redistribution of this energy between the various components. This would constitute a refinement of present statistical approximations for estimating energy levels of complex structures.

REFERENCES

1. White, R. W.: Predicted Vibration Responses of Apollo Structure and Effects of Pressure Correlation Lengths on Response; Wyle Laboratories Research Staff Report, WR 67-4; March 1967 and Revised March 1968.

2. White, R. W.: Theoretical Study of Acoustic Simulation of In-Flight Environments; The Shock and Vibration Bulletin No. 37, Part 5; January 1968.

3. Wilby, J. F.: The Response of Simple Panels to Turbulent Boundary Layer Excitation; AFFDL-TR-67-70; October 1967.

4. Snowdon, J. C.: Vibration and Shock in Damped Mechanical Systems; John Wiley and Sons, Inc.; 1968.

5. Skudrzyk, E.: Simple and Complex Vibratory Systems; The Pennsylvania State University Press; 1968.

6. Roark, R. J.: Formulas for Stress and Strain; Third Edition, 1954; McGraw-Hill Book Co.

7. Powell, A.: On the Response of Structures to Random Pressures and to Jet Noise in Particular; Ch. 8 of Random Vibration (S. H. Crandall, Ed.); MIT Press, Cambridge, Mass.; 1958.

8. Korn, G. A. and T. M. Korn: Mathematical Handbook for Scientists and Engineers; McGraw-Hill Book Co.; 1961.

9. Crocker, M. J. and R. W. White: Reponses of Lockheed L-2000 Supersonic Transport Fuselage to Turbulence and to Reverberant Noise; Wyle Laboratories Research Staff Consulting Report No. WCR 66-11; September 1966.

10. Potter, R. (Editor): A Study of the Acoustic Qualification Testing of the Manned Oribtal Laboratory (MOL) in Simulation of Launch and Flight Environments; Wyle Laboratories Research Staff Consulting Report No. WCR 68-1; 1968.

11. Levy, R. S., et al.: First Annual Summary Report – Experimental Determination of System Parameters for Thin Walled Cylinders; Report No. RAC 1117-6, Republic Aviation Corporation, Farmingdal, L. I., N. Y.; June 1964.

12. Bozich, D. J.: Radiation Damping of Panels Mounted in Ducts; Wyle Laboratories Research Staff Report No. WR 64-6; 1964.

13. Morse, P. M. and K. U. Ingard: Theoretical Acoustics; McGraw-Hill Book Company, New York, N. Y.; 1968.

14. Manning, J. E. et al.: Transmission of Sound and Vibration to a Shroud-Enclosed Spacecraft; BBN Report 1431; October 1966.

15. Ungar, E. E.: Fundamentals of Statistical Energy Analysis of Vibrating System; Technical Report 66-52, Air Force Flight Dynamics Laboratory, Wright-Patternson Air Force Base, Ohio; May 1966.

16. Miller, D. K. and F. D. Hart: Modal Density of Thin Circular Cylinders; NASA CR-897; December 1967.

17. Maidanik, G.: Response of Ribbed Panels to Reverberant Acoustic Fields; J. Acoust. Soc. Am., No. 34; June 1962.

18. Forsberg, K.: A Review of Analytical Methods Used to Determine the Modal Characteristics of Cylindrical Shells; NASA CR-613; June 1965.

19. Weingarten, V. I.: Free Vibration of Thin Cylindrical Shells; AIAA Journal, Vol. 2, No. 4; April 1964.

20. Wenzel, A.: Surface Pressure Correlation Function for a Cylinder in a Diffuse Reverberant Sound Field; Wyle Laboratories Research Staff Report No. WR 66-14; March 1966.

APPENDIX A

JOINT ACCEPTANCES OF A PINNED-PINNED BEAM FOR LOCALIZED EXCITATION

Consider a pinned-pinned beam, such as that shown in Figure A 1, on which a distributed random pressure loading acts over the range $x_1 \leq x \leq x_2$. The center of the loading is located at x_0, and the length of the loading is Δ_x so that

$$x_0 = (x_2 + x_1)/2$$

$$\Delta_x = x_2 - x_1 \tag{A 1}$$

It is assumed that, within the range $x_1 \leq x \leq x_2$, the load is homogeneous and is characterized by a space correlation function $C(\zeta;\omega)$ which depends only upon the separation distance ζ between any two points in the range $x_1 \leq x \leq x_2$.

The general equation for the joint acceptance, $j_m^2(\omega)$, of the m-th mode is:

$$j_m^2(\omega) = \frac{1}{L_x^2} \int_{x=x_1}^{x_2} \int_{x'=x_1}^{x_2} C(\zeta;\omega) \cdot \phi_m(x) \cdot \phi_m(x') \, dx \, dx'$$

$$= \int_{\bar{x}=\bar{x}_1}^{\bar{x}_2} \int_{\bar{x}'=\bar{x}_1}^{\bar{x}_2} C(\bar{\zeta};\omega) \cdot \phi_m(\bar{x}) \cdot \phi_m(\bar{x}') \cdot d\bar{x} \cdot d\bar{x}' \tag{A 2}$$

$$\phi_m(x) = \phi_m(\bar{x}) = \sin(m\pi x/L_x) = \sin(m\pi\bar{x}) \tag{A 3}$$

$$\bar{x} = x/L_x \tag{A 4}$$

Following the procedure developed in Reference (1), the double integral in Equation (A 2) can be reduced to a single integral by introducing the following transformation of the variables of integration:

$$\left.\begin{aligned} \bar{\xi} &= \bar{x} + \bar{x}' & \qquad \bar{x} &= (\bar{\xi} + \bar{\zeta})/2 \\ \bar{\zeta} &= \bar{x} - \bar{x}' & \qquad \bar{x}' &= (\bar{\xi} - \bar{\zeta})/2 \\ d\bar{x} \cdot d\bar{x}' &= d\bar{\xi} \cdot d\bar{\zeta}/2 & & \end{aligned}\right\} \tag{A-5}$$

This transformation of the integration space is shown graphically in Figure (A 2). The product $\phi_m(\bar{x}) \cdot \phi_m(\bar{x}')$ can be written in terms of $\bar{\xi}$ and $\bar{\zeta}$ as follows:

$$\phi_m(\bar{x}) \cdot \phi_m(\bar{x}') = \frac{1}{2}\left[\cos m\pi\bar{\zeta} - \cos m\pi\bar{\xi}\right] \tag{A 6}$$

Substituting Equations (A 5,6) into Equation (A 2), performing the integration over $\bar{\xi}$, and noting that $C(\bar{\zeta};\omega)$ is an even function of $\bar{\zeta}$ leads to:

$$j_m^2(\omega) = \frac{1}{4}\int_{\bar{\zeta}=-\bar{\Delta}_x}^{\bar{\Delta}_x} C(\bar{\zeta};\omega)\int_{\bar{\xi}=2\bar{x}_1+|\bar{\zeta}|}^{2\bar{x}_2-|\bar{\zeta}|}\left[\cos m\pi\bar{\zeta} - \cos m\pi\bar{\xi}\right]\cdot d\bar{\xi}\cdot d\bar{\zeta}$$

$$= \frac{1}{2}\int_{\bar{\zeta}=-\bar{\Delta}_x}^{\bar{\Delta}_x} C(\bar{\zeta};\omega)\left[(\bar{\Delta}_x - |\bar{\zeta}|)\cos m\pi\bar{\zeta} - \frac{\cos 2m\pi\bar{x}_0}{m\pi}\sin m\pi(\bar{\Delta}_x - |\bar{\zeta}|)\right]d\bar{\zeta}$$

$$= \int_{\bar{\zeta}=0}^{\bar{\Delta}_x} C(\bar{\zeta};\omega)\left[(\bar{\Delta}_x - \bar{\zeta})\cos m\pi\bar{\zeta} - \frac{\cos 2m\pi\bar{x}_0}{m\pi}\sin m\pi(\bar{\Delta}_x - \bar{\zeta})\right]d\bar{\zeta} \qquad \text{(A 7)}$$

The integral in Equation (A 7) can be further simplified to

$$j_m^2(\omega) = \bar{\Delta}_x^2\int_{z=0}^{1} C(z;\omega)\left[(1-z)\cos \mathcal{m}\pi z - \frac{\cos 2m\pi\bar{x}_0}{\mathcal{m}\pi}\sin \mathcal{m}\pi(1-z)\right]dz$$

or

$$\frac{j_m^2(\omega)}{\bar{\Delta}_x^2} = -\int_0^1 Z\cdot C(z;\omega)\cdot\cos \mathcal{m}\pi z\cdot dz$$

$$+\left[1 - \frac{\cos 2m\pi\bar{x}_0\cdot\sin \mathcal{m}\pi}{\mathcal{m}\pi}\right]\int_0^1 C(z;\omega)\cdot\cos \mathcal{m}\pi z\cdot dz \qquad \text{(A 8)}$$

$$+\frac{\cos 2m\pi\bar{x}_0\cdot\cos \mathcal{m}\pi}{\mathcal{m}\pi}\int_0^1 C(z;\omega)\cdot\sin \mathcal{m}\pi z\cdot dz$$

where

$$\left.\begin{aligned} z &= \bar{\zeta}/\bar{\Delta}_x = \zeta/\Delta_x \\ \mathcal{m} &= m\,\bar{\Delta}_x \end{aligned}\right\} \qquad \text{(A 9)}$$

In the form given by Equation (A 8), $j_m^2(\omega)$ is proportional to $\bar{\Delta}_x^2$, which implies in general that the joint acceptance and hence the mean-square response of a structure is proportional to the square of the area over which the excitation occurs. As $\bar{\Delta}_x \to 0$, the right-hand side of Equation (A 8) approaches a finite, non-zero quality. For example, in the case of a point force applied at x_0, $C(z;\omega) = 1.0$, $\mathcal{m} = 0$, the first term in Equation (A 8) is equal to (1/2), the second term is equal to $-\cos 2m\pi\bar{x}_0$, and the third term is equal to (1/2) $\cos 2m\pi\bar{x}_0$; and hence

$$\lim_{\Delta_x \to 0}\frac{j_m^2(\omega)}{\bar{\Delta}_x^2} = \frac{1}{2}\left[1 - \cos 2m\pi\bar{x}_0\right] = \sin^2 m\pi\bar{x}_0 \qquad \text{(A 10)}$$

which is the correct result.

Boundary Layer Turbulence Parallel to Flow Axis

The space correlation function, $C(z;\omega)$, selected here for representing a localized boundary layer turbulence is:

$$C(z;\omega) = e^{-\delta_x |z|} \cdot \cos \gamma_x z \tag{A 11}$$

$$\left.\begin{aligned} \gamma_x &= \omega \Delta_x / U_c \\ \delta_x &= a\,\gamma_x + b\,\Delta_x/\delta_b \end{aligned}\right\} \tag{A 12}$$

U_c = convection velocity

δ_b = boundary layer thickness

a, b = constants dependent upon measured characteristics of boundary layer flow field.

For the analysis of the SLA in Reference (1), nominial values of the constants a, b, U_c, δ_b are:

a = 0.10

b = 0.265

U_c = 9810 in./sec (Mach 1)

= 15900 in./sec (Mach 2)

δ_b = 12.0 in.

When the boundary layer is distributed over the entire length of the beam, the $\Delta_x = L_x$ and Equations (A 12) reduce to those presented in Reference (1).

Upon substituting Equation (A 11) into Equation (A 8) and performing the integration gives:

$$\begin{aligned}
\frac{j_m^2(\omega)}{\Delta_x^2} = & \left[\frac{\delta_x [\delta_x^2 + (\gamma_x \pm m\pi)^2] + \delta_x^2 - (\gamma_x \pm m\pi)^2}{2[\delta_x^2 + (\gamma_x \pm m\pi)^2]^2} \right] e^{-\delta_x} \cos(\gamma_x \pm m\pi) \\
& - \left[\frac{\gamma_x \pm m\pi}{2} \cdot \frac{\delta_x^2 + (\gamma_x \pm m\pi)^2 + 2\delta_x}{[\delta_x^2 + (\gamma_x \pm m\pi)^2]^2} \right] e^{-\delta_x} \sin(\gamma_x \pm m\pi) \\
& - \frac{\delta_x^2 - (\gamma_x \pm m\pi)^2}{2[\delta_x^2 + (\gamma_x \pm m\pi)^2]^2} + \frac{1}{2}\left[1 - \frac{\cos 2m\pi \bar{x}_0 \cdot \sin m\pi}{m\pi}\right] \bullet \\
& \bullet \left[\frac{\delta_x}{\delta_x^2 + (\gamma_x \pm m\pi)^2} \left\{ 1 - e^{-\delta_x} \cos(\gamma_x \pm m\pi) \right\} \right. \\
& \left. + \frac{\gamma_x \pm m\pi}{\delta_x^2 + (\gamma_x \pm m\pi)^2}\, e^{-\delta_x} \sin(\gamma_x \pm m\pi) \right]
\end{aligned} \tag{A 13}$$

$$\pm \frac{\cos 2m\pi\bar{x}_0 \cdot \cos m\pi}{2m\pi} \left[\frac{(\gamma_x \pm m\pi)}{\delta_x^2 + (\gamma_x \pm m\pi)^2} \left\{ 1 - e^{-\delta_x} \cos(\gamma_x \pm m\pi) \right\} \right.$$

$$\left. - \frac{\delta_x}{\delta_x^2 + (\gamma_x \pm m\pi)^2} \, e^{-\delta_x} \sin(\gamma_x \pm m\pi) \right] \qquad \text{(A 13) Cont.}$$

Equation (A 13) contains twice as many terms as are shown; one set is associated with the (+) sign and one set is associated with the (-) sign. The total equation for $j_m^2(\omega)/\bar{\Delta}_x^2$ is obtained by algebraically adding these two sets of terms. Equation (A 13) was used to compute the acceleration spectrum shown in Figure 117.

When the boundary layer extends over the entire length of the beam, then $\bar{\Delta}_x = 1.0$, m = m = integer, and Equation (A 13) can be reduced to:

$$j_m^2(\omega) = \frac{1}{2} \left[\frac{(\gamma_x \pm m\pi)^2 - \delta_x^2}{[\delta_x^2 + (\gamma_x \pm m\pi)^2]^2} + \frac{(m\pi \pm \gamma_x)/m\pi}{\delta_x^2 + (\gamma_x \pm m\pi)^2} \right] \left\{ 1 - (-1)^m e^{-\delta_x} \cos \gamma_x \right\}$$

$$+ \left[\frac{-\delta_x(\gamma_x \pm m\pi)}{[\delta_x^2 + (\gamma_x \pm m\pi)^2]^2} \mp \frac{\delta_x/2m\pi}{\delta_x^2 + (\gamma_x \pm m\pi)^2} \right] (-1)^m e^{-\delta_x} \sin \gamma_x$$

$$+ \frac{\delta_x/2}{\delta_x^2 + (\gamma_x \pm m\pi)^2} \qquad \text{(A 14)}$$

where the ($\pm$) sign once again implies a summation of (+) terms and (-) terms. It is a straightforward exercise to show that Equation (A 14) can be rewritten in the more condensed form of Equation (4.40) in Reference (1).

Equations (A 13, 14) are applicable to a flat rectangular plate and a cylindrical shell if the flow is directed along the x-axis, which for the shell is parallel to the center line.

When $\bar{\Delta}_x = 1.0$, coincidence between the elastic waves of the m-th mode of the beam and the turbulence wavelengths occurs when $\gamma_x = m\pi$. From Equation (A 12), the corresponding coincidence frequency is:

$$f_c = \frac{\omega_c}{2\pi} = \frac{m\,U_c}{2\,L_x} = \text{coincidence frequency for m-th mode.} \qquad \text{(A 15)}$$

Setting $\gamma_x = m\pi$ in Equation (A 14) gives the following expression for the joint acceptance, $j_m^2(\omega_c)$, at coincidence:

$$j_m^2(\omega_c) = \frac{1}{2} \left[\frac{(2m\pi)^2 - \delta_x^2}{[\delta_x^2 + (2m\pi)^2]^2} + \frac{2}{\delta_x^2 + (2m\pi)^2} - \frac{1}{\delta_x^2} \right] \left\{ 1 - e^{-\delta_x} \right\}$$

$$+ \frac{\delta_x/2}{\delta_x^2 + (2m\pi)^2} + \frac{1}{2\,\delta_x} \qquad \text{(A 16)}$$

Aerodynamically slow modes, for which response levels are generally not large, are those modes for which $\gamma_x < m\pi$; while aerodynamically fast modes are defined by the condition $\gamma_x > m\pi$.

Progressive Wave Acoustic Excitation

The joint-acceptance for a correlated acoustic wave progressing along the beam at parallel incidence can be obtained from Equation (A 13) by setting $\delta_x = 0$. If the wave acts over the entire length of the beam, then $\overline{\Delta}_x = 1.0$ and $m = m$, and in this case, Equation (A 14) reduces to the following well-known equation developed by Powell in Reference (7):

$$j_m^2(\omega) = \frac{2}{(m\pi)^2} \frac{1-(-1)^m \cos\gamma_x}{[1-(\gamma_x/m\pi)^2]^2} \tag{A 17}$$

Equation (A 17) was used to compute the acceleration spectra shown in Figures 36-42 for duct excitation of the SLA. It is often convenient to refer to a graph of Equation (A 17) in order to explain trends in response data. Such a graph is shown in Reference (7); however such a graph is complicated by the rapid fluctuations of the joint acceptance curves and by the superposition of curves for different mode numbers. It is possible to rewrite Equation (A 17) in the following alternate form:

$$j_m^2(\omega) = \frac{1}{[1+(f/f_c)]^2} \left[\frac{\sin(m\pi\epsilon/2)}{(m\pi\epsilon/2)}\right]^2 \tag{A 18}$$

ϵ = deviation of excitation frequency, f, from coincidence frequency f_c

$$= \frac{\gamma_x}{m\pi} - 1 = \frac{f}{f_c} - 1 \tag{A 19}$$

$$f_c = \frac{m\,c_0}{2\,L_x} = \text{coincidence frequency for m-th mode} \tag{A 20}$$

The fluctuating part of $j_m^2(\omega)$ is controlled by $[\sin(m\pi\epsilon/2)/(m\pi\epsilon/2)]^2$ and this factor is shown graphically in Figure A3.

Reverberant Acoustic Field

The space correlation function for a localized reverberant acoustic field on beam is chosen as

$$C(z,\omega) = \frac{\sin\gamma_x z}{\gamma_x z} \tag{A 21}$$

$$\gamma_x = \omega\,\Delta_x/c_0$$

Substituting Equation (A 21) into Equation (A 8) and performing the integration gives:

$$j_m^2(\omega) = \frac{\cos(\gamma_x + m\pi) - 1}{2\gamma_x(\gamma_x + m\pi)} + \frac{\cos(\gamma_x - m\pi) - 1}{2\gamma_x(\gamma_x - m\pi)}$$

$$+ \frac{1}{2\gamma_x}\left[1 - \frac{\cos 2m\pi\bar{x}_0 \cdot \sin m\pi}{m\pi}\right] \cdot \left[Si(\gamma_x + m\pi) + Si(\gamma_x - m\pi)\right] \qquad \text{(A 22)}$$

$$+ \frac{\cos 2m\pi\bar{x}_0 \cdot \cos m\pi}{2m\pi\gamma_x}\left[Cin(\gamma_x + m\pi) - Cin\left|\gamma_x - m\pi\right|\right]$$

where

$$Si(z) = \int_0^z \frac{\sin x}{x} \cdot dx$$

$$Cin(z) = \int_0^z \frac{1 - \cos x}{x} \cdot dx \qquad \text{(A 23)}$$

Various methods for approximating the functions $Si(z)$ and $Cin(z)$ are discussed in Reference (1). Equation (A 22) is applicable for both axes of a flat rectangular plate and for the axial direction along a cylindrical shell.

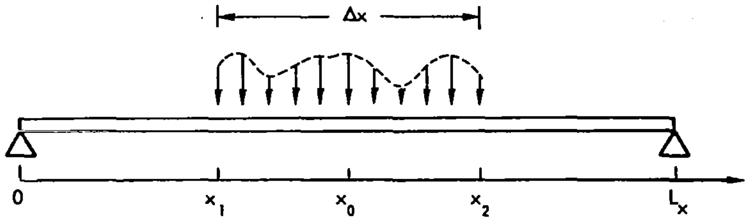

Figure A1. Pinned-Pinned Beam With Localized Excitation

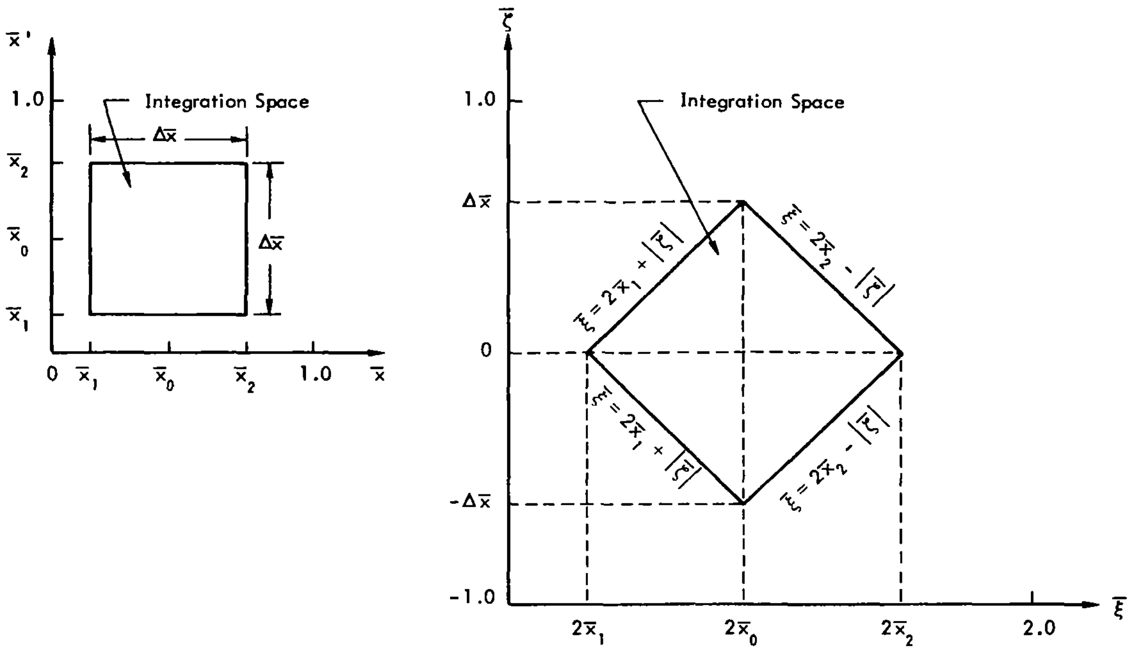

Figure A2. Transformation of Region of Integration for Joint Acceptances

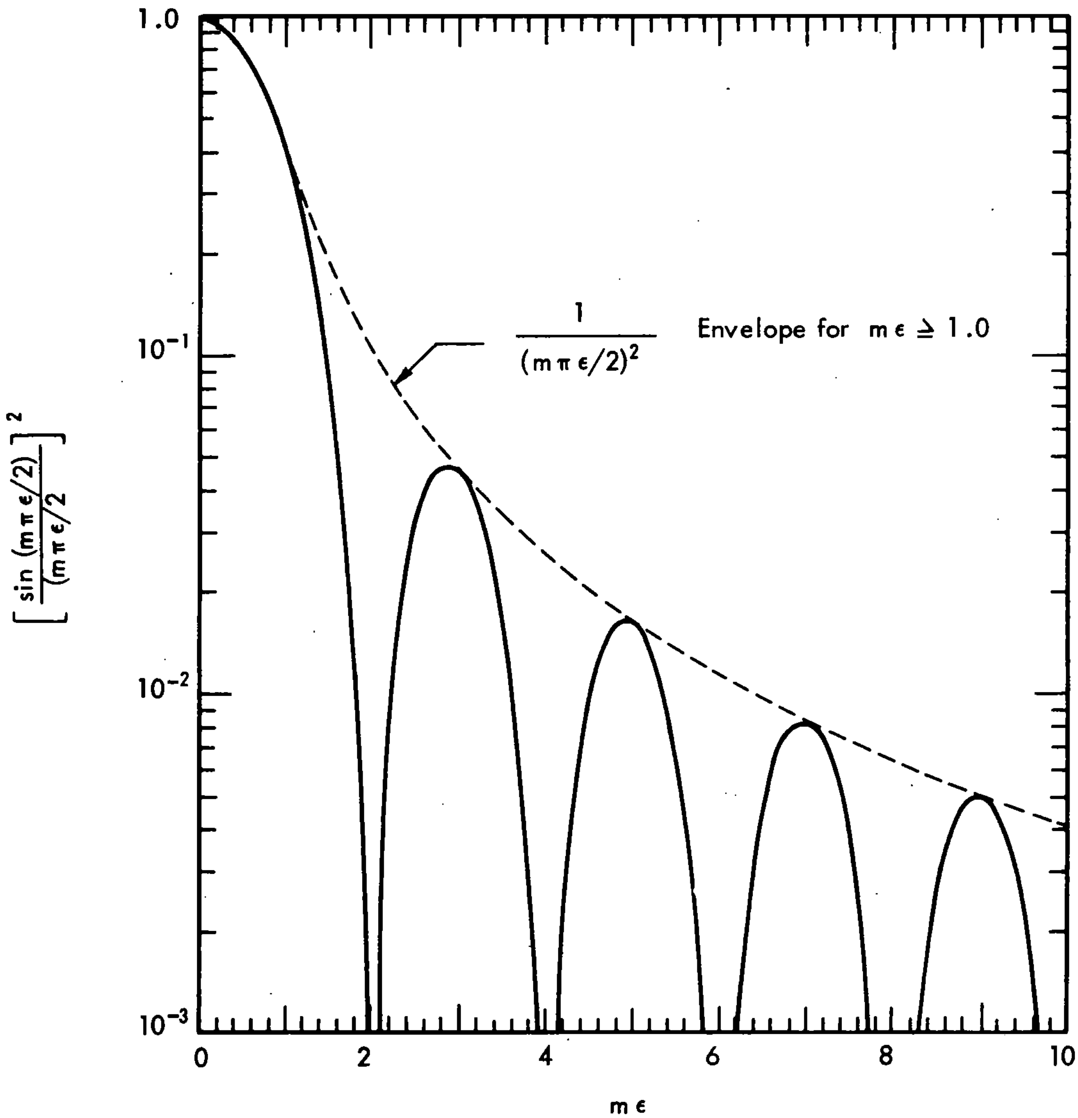

$$j_m^2(\omega) = \frac{1}{[1+(f/f_c)]^2}\left[\frac{\sin(m\pi\epsilon/2)}{m\pi\epsilon/2}\right]^2, \quad \epsilon = (f/f_c) - 1$$

$f_c = m\,c_0/2L_x$ = wave length coincidence frequency for m-th mode.

Figure A3. Joint Acceptance, $j_m^2(\omega)$, for Progressive Acoustic Wave of Frequency f on Pinned-Pinned Beam of Length L

APPENDIX B

JOINT ACCEPTANCES OF A CIRCULAR RING FOR LOCALIZED EXCITATION

Consider the circular ring shown in Figure B1 which has a distributed random pressure loading over the range $-\Delta y/2 \leq y \leq \Delta y/2$. Mode shapes of the ring modes that may respond to such an excitation are:

$$\phi_{n1}(y) = \sin(2\pi n y/L_y)$$

$$\phi_{n2}(y) = \cos(2\pi n y/L_y)$$

y = circumferential coordinates

L_y = circumferential length of ring

n = number of elastic full-waves around circumference.

Following the procedure in Reference (1), the joint acceptance $j_n^2(\omega)$ for the n-th mode of the ring can be written in the form:

$$j_n^2(\omega) = \frac{1}{L_y^2} \int_{y=-\Delta y/2}^{\Delta y/2} \int_{y'=-\Delta y/2}^{\Delta y/2} C(\eta;\omega) \cdot \left[\phi_{n2}(y) \cdot \phi_{n2}(y') + \phi_{n1}(y) \cdot \phi_{n1}(y')\right] \cdot dy \cdot dy'$$

$$= \frac{1}{L_y^2} \int_{y=-\Delta y/2}^{\Delta y/2} \int_{y'=\Delta y/2}^{\Delta y/2} C(\eta;\omega) \cdot \cos(2\pi n \eta/L_y) \cdot dy \cdot dy' \qquad \text{(B 1)}$$

$\eta = y - y'$ = separation distance around ring

$C(\eta;\omega)$ = space correlation coefficient for homogeneous pressure field.

Equation (B 1) can be reduced to a single integral by using the same procedure as that described in Appendix A and shown pictorially in Figure A 2. The resulting equation is:

$$j_n^2(\omega) = \bar{\Delta}y^2 \int_{z=0}^{1} (1-z) \cdot C(z;\omega) \cdot \cos 2\mathfrak{n}\pi z \cdot dz \qquad \text{(B 2)}$$

$\bar{\Delta}y = \Delta y/L_y$

$\mathfrak{n} = n \cdot \bar{\Delta}y$

Joint acceptance expressions are developed below for correlation functions associated with boundary layer turbulence and a reverberant acoustic field.

Boundary Layer Turbulence

For a boundary layer convected along the axis of a cylindrical shell, the space correlation coefficient around the circumference of the ring is assumed to have the form:

$$C(x;\omega) = e^{-\delta_y |z|}$$

Substituting Equation (B 3) into Equation (B 2) and integrating gives:

$$\frac{j_n^2(\omega)}{\bar{\Delta}_y^2} = \frac{(2n\pi)^2 - \delta_y^2}{[\delta_y^2 + (2n\pi)^2]^2}\left[1 - e^{-\delta_y}\cos 2n\pi\right]$$

$$- \frac{4n\pi\ \delta_y}{[\delta_y^2 + (2n\pi)^2]^2}\ e^{-\delta_y}\sin 2n\pi + \frac{\delta_y}{\delta_y^2 + (2n\pi)^2} \qquad \text{(B 3)}$$

Reverberant Acoustic Field

For a reverberant acoustic field the space correlation coefficient around the ring is approximated as follows:

$$C(z;\omega) = \frac{\sin \gamma_y z}{\gamma_y z} \qquad \text{(B 4)}$$

where

$$\gamma_y = \omega\,\Delta_y/c_0$$

Substituting Equation (B 4) into Equation (B 2) and integrating gives:

$$j_n^2(\omega) = \frac{\bar{\Delta}_y^2}{\gamma_y}\left[\mathrm{Si}\,\{(\gamma_y + 2\pi n)\} + \mathrm{Si}\,\{(\gamma_y - 2\pi n)\}\right]$$

$$+ \frac{\bar{\Delta}_y^2}{2(n\pi)^2}\ \frac{1 - \cos(4\pi n)\cos(\gamma_y) - (2\pi n/\gamma_y)\sin(4\pi n)\sin(\gamma_y)}{1 - (\gamma_y/2\pi n)^2}\ , \quad n \neq 0$$

$$= \frac{2\bar{\Delta}_y^2}{\gamma_y}\ \mathrm{Si}\,\{\gamma_y\} - \Delta_y^2\ \frac{2\,[1 - \cos(\gamma_y)]}{\gamma_y^2}\ , \quad n = 0$$

Table 1: Parameter Values Used in Numerical Example of Exact Analysis Method

Mode	First	Third
δ	1.0	1.0
ψ	$11.25°$	$11.25°$
$\sin\psi$	0.19509	0.19509
$\cos\psi$	0.98079	0.98079
λ_0	3.2032	9.6095
α	π	3π
β	0.62486	1.8747
$\cosh 2\alpha$	267.745	$7.68 \cdot 10^7$
$\cosh 2\beta$	1.88795	21.272
$\cos 2\alpha$	1.0000	1.0000
$\cos 2\beta$	0.314	-0.82107

Mode	First	Third
$\sinh 2\alpha$	267.745	$7.6777 \cdot 10^7$
$\sinh 2\beta$	1.60136	21.235
$\sin 2\alpha$	0	0
$\sin 2\beta$	0.94890	-0.57106
$\overline{\lvert\bar{U}(x)\rvert}$	1.2271	0.48151

Table 2: Values of Frequency Functions Used in Numercial Example of Modal Analysis Method for $\delta = 1.0$, $\alpha = 3\pi$ and m = 1-6.

m	$\frac{\omega}{\omega_m}$	$H\left(\frac{\omega}{\omega_m}\right)$	$\left(\frac{3}{m}\right)^3 H\left(\frac{\omega}{\omega_m}\right)$	$\theta\left(\frac{\omega}{\omega_m}\right)$
1	7.85	0.01152	0.312	$134.5°$
2	1.96	0.2185	0.738	126.4
3	0.873	1.250	1.250	72.58
4	0.490	1.250	0.526	17.50
5	0.314	1.100	0.238	6.23
6	0.218	1.050	0.131	2.86

Table 3: Numerical Values of β_{mr} for $\delta = 1.0$, $\alpha = 3\pi$, m = 1-6 and r = 1-6

m \ r	1	2	3	4	5	6
1	0.0974					
2	0.228	0.545				
3	0.184	0.545	1.560			
4	-0.0749	-0.126	0.377	0.277		
5	-0.0460	-0.0888	0.120	0.123	0.0566	
6	-0.0272	-0.0535	0.0570	0.0670	0.0312	0.0172

Table 4: Numerical Values of the Normalized Deflection Amplitude, $|U(x)|$, for $\lambda_0 = 9.6095$, Using the Exact and Modal Analyses

$\bar{x}$	Exact Analysis	Modal Analysis			
		m = 1-5	m = 1-10	m = 1-30	m = 1-30
	$\delta = 1.0$	$\delta = 1.0$	$\delta = 1.0$	$\delta = 1.0$	$2\zeta = 1.0$
0	0	0	0	0	0
0.06	0.598	0.511	0.592	0.599	0.532
0.10	0.789	0.751	0.803	0.792	0.711
0.16	0.871	0.886	0.873	0.874	0.810
0.20	0.834	0.841	0.838	0.837	0.807
0.26	0.706	0.691	0.706	0.709	0.755
0.30	0.608	0.612	0.603	0.610	0.711
0.36	0.500	0.557	0.508	0.502	0.653
0.40	0.473	0.528	0.482	0.476	0.616
0.46	0.469	0.478	0.467	0.471	0.548
0.50	0.455	0.447	0.455	0.457	0.481
0.56	0.388	0.389	0.389	0.389	0.379
0.60	0.314	0.325	0.314	0.315	0.310
0.66	0.214	0.206	0.220	0.215	0.252
0.60	0.210	0.179	0.214	0.212	0.260
0.76	0.284	0.261	0.281	0.285	0.298
0.80	0.323	0.316	0.323	0.324	0.308
0.86	0.316	0.326	0.319	0.317	0.276
0.90	0.261	0.276	0.262	0.262	0.221
0.96	0.118	0.127	0.118	0.119	0.0973
1.00	0	0	0	0	0

Table 5: Resonance Frequencies of Equivalent Cylindrical Shell

m \ n	0	1	2	3	4	5	6	7	8	9	10	11	12	13	14	15	16	17	18	19	20	21	22	23	24	25	26
1	175	82	32	20	24	35	50	68	89	113	139	169	201	236	274	314	357	403	452	504	558	616	676	739	804	873	944
2	175	136	82	52	41	44	56	73	93	117	143	173	205	240	277	318	361	407	456	508	562	619	679	742	808	876	948
3	175	156	117	85	66	61	68	82	101	124	150	179	211	246	283	324	367	413	462	514	568	625	686	748	814	882	954
4	176	165	138	111	91	82	84	95	112	134	159	188	220	255	292	333	376	422	471	522	577	634	694	757	823	891	962
5	177	171	152	131	113	104	103	112	127	147	172	200	231	266	303	344	387	433	482	533	588	645	705	768	834	902	973
6	180	176	163	147	133	125	124	131	144	163	187	215	246	280	317	358	401	447	495	547	601	659	719	781	847	916	987
7	184	182	172	161	151	145	145	151	164	182	205	232	263	297	334	374	417	463	511	563	617	675	735	797	863	931	
8	191	189	183	175	168	165	166	173	185	203	226	252	282	316	353	393	436	481	530	582	636	693	753	816	881	950	
9	200	200	195	191	187	185	188	196	209	226	248	274	304	338	374	414	457	503	551	603	657	714	774	837	902	971	
10	213	212	210	207	206	207	211	220	233	251	273	299	329	362	398	438	481	526	575	626	680	737	797	860	926	994	
11	228	228	227	227	227	230	236	246	260	278	300	326	356	389	425	464	507	552	601	652	706	763	823	886	951		
12	247	248	248	249	251	256	263	274	289	307	329	355	385	418	454	493	535	581	629	680	735	792	852	914	980		
13	270	271	271	273	277	283	292	304	319	338	361	387	416	449	485	524	567	612	660	711	766	822	882	945			
14	296	297	298	301	306	313	323	336	352	371	394	420	450	483	519	558	600	645	694	745	799	856	916	978			
15	325	326	328	331	338	346	356	370	387	406	430	456	486	519	555	594	636	681	729	781	835	891	951				
16	358	359	361	365	372	381	392	407	424	444	468	494	524	557	593	632	674	720	768	819	873	930	989				
17	393	395	397	402	409	419	431	446	463	484	508	535	565	598	634	673	715	760	808	859	913	970					
18	432	433	436	442	449	459	472	487	505	526	550	577	607	641	677	716	758	803	852	903	957						
19	474	475	478	484	492	502	515	531	549	571	595	622	653	686	722	762	804	849	897	948							
20	519	520	523	529	537	548	561	577	596	618	642	670	700	734	770	809	852	897	945	996							
21	566	567	571	577	585	596	610	626	645	667	692	720	750	784	820	860	902	947	995								
22	616	618	621	627	636	647	661	678	697	719	744	772	803	836	873	912	955	1000									
23	669	671	674	681	689	701	715	732	751	774	799	827	858	891	928	967											
24	725	726	730	736	745	757	771	788	808	830	856	884	915	949	985												
25	783	785	788	795	804	816	830	847	867	890	915	943	975														
26	844	846	850	856	865	877	892	909	929	952	977																
27	908	909	913	920	929	941	956	973	993																		
28	974	975	979	986	995																						

Table 6: Summary of Properties of Cylindrical Shells and Excitation Fields Used in Analysis

Figure No.	Structure	L_x (in.)	R (in.)	D lb-in.	K_e lb/in.	μg lb/in.^{2}	Q	Excitation Field: No. of Ducts	Excitation Field: Reverberant	Excitation Field: Boundary Layer	$\mathcal{N}^*(f)$ $f < f_0$	$\mathcal{N}(f)$ $f > f_0$
36		349	104	3.24×10^5	4.7×10^5	0.0139	15	1			0.428	0.596
37								2				
38								4				
39								8				
40								16				
41								32				
42								64				
43								16, A = 0.01				
44	Basic							16, A = 0.05				
45	SLA							16, A = 0.1				
46	Cylinder							16, A = 0.5				
47								16, A = 1				
48								16, A = 5				
49								16, A = 10				
68									✓			
91										M1, 12 in.		
92										M2, 12 in.		
93										M1, 6 in.		
94		349	104	3.24×10^5	4.7×10^5	0.0139	15			M2, 6 in.	0.428	0.596
50		349	52	3.24×10^5	4.7×10^5	0.0139	15	16				
69			52						✓		0.214	0.298
95			52							✓		
51			78					16				
70			78						✓		0.321	0.447
96			78							✓		
52			156					16				
71			156						✓		0.642	0.894
97			156							✓		
53			208					16				
72			208						✓		0.856	1.192
98			208	3.24×10^5						✓		
54			104	8.1×10^4				16				
73				8.1×10^4					✓		0.856	1.192
99	SLA			8.1×10^4						✓		
55	Cylinder			1.62×10^5				16				
74	with			1.62×10^5					✓		0.605	0.844
100	Parameter			1.62×10^5						✓		
56	Variations			6.48×10^5				16				
75				6.48×10^5					✓		0.302	0.421
101				6.48×10^5						✓		
57				1.296×10^6				16				
76				1.296×10^6					✓		0.214	0.298
102				1.296×10^6	4.7×10^5					✓		
58				1.296×10^6	1.88×10^6			16				
77				1.296×10^6	1.88×10^6				✓		0.214	0.298
103				1.296×10^6	1.88×10^6	0.0139				✓		
59				3.24×10^5	4.7×10^5	0.0278		16				
78						0.0278			✓		0.605	0.844
104						0.0278				✓		
60						0.0556		16				
79						0.0556			✓		0.856	1.192
105		349	104	3.24×10^5	4.7×10^5	0.0556	15			✓		

* $\mathcal{N}^*(f) = \mathcal{N}(f)\,[f_0/f]^{\frac{1}{2}}, \; f < f_0$

Table 6: Summary of Properties of Cylindrical Shells and Excitation Fields Used in Analysis (Continued)

Figure No.	Structure	L_x (in.)	R (in.)	D lb-in.	K_e lb/in.	μg lb/in.^{2}	Q	Excitation Field: No. of Ducts	Reverberant	Boundary Layer	$\mathcal{N}^*(f)$ $f < f_0$	$\mathcal{N}(f)$ $f > f_0$
61	Republic	54	18	7.65	2×10^5	0.002	30	16				
80	Cylinder	↕	↕	↕	↕	↕	↕		✓		0.916	1.280
106	No. 12	↕	↕	↕	↕	↕	↕			1/5 Scale		
107		54	18	7.65	2×10^5	0.002	30			✓		
62	Uniform	48	12	61.1	4×10^5	0.004	30	16				
81	Cylinder	48	12	61.1	4×10^5	0.004	30		✓		0.270	0.378
108		48	12	61.1	4×10^5	0.004	30			✓		
63	Uniform	48	24	61.1	4×10^5	0.004	30	16				
82	Cylinder	48	24	61.1	4×10^5	0.004	30		✓		0.540	0.750
109		48	24	61.1	4×10^5	0.004	30			✓		

• $\mathcal{N}^*(f) = \mathcal{N}(f)\,[f_0/f]^{\frac{1}{2}},\ f < f_0$

Table 7: Summary of Properties of Flat Panels and Excitation Fields Used in Analysis

Figure No.	Structure	L_x (in.)	L_y (in.)	D_x lb-in.	D_y lb-in.	μg lb/in.^{2}	Q	Excitation Field: Ducts	Reverberant	Boundary Layer	$\mathcal{N}(f)$
64	Thin	24	16	27.2	27.2	0.0032	30	✓			
83	Flat	24	16	27.2	27.2	0.0032	30		✓		0.101
110	Panel	24	16	27.2	27.2	0.0032	30			✓	
65	Center	24	16	956	956	0.01	30	✓			
84	Panel	24	16	956	956	0.01	30		✓		0.032
111	9-Bay	24	16	956	956	0.01	30			✓	
66	9-Bay	72.1	48.1	1.62×10^6	1.13×10^6	0.0302	30	✓			
85	Equiv.	72.1	48.1	1.62×10^6	1.13×10^6	0.0302	30		✓		0.0129*
112	Panel	72.1	48.1	1.62×10^6	1.13×10^6	0.0302	30			✓	
67	SLA	349	651	3.24×10^5	3.24×10^5	0.0139	15	✓			
86	Equiv.	349	651	3.24×10^5	3.24×10^5	0.0139	15		✓		
113	Panel	349	651	3.24×10^5	3.24×10^5	0.0139	15			✓	
87	↕	12	37.5	61.1	61.1	0.004	30		✓		
88	↕	12	19	↕	↕	↕	↕		✓		
89	Uniform	12	10	↕	↕	↕	↕		✓		
90	Cylinder	6	5	↕	↕	↕	↕		✓		
114	Equiv.	12	19	↕	↕	↕	↕			✓	
115	Panel	12	10	↕	↕	↕	↕			✓	
116	↕	6	5	61.1	61.1	0.004	30			✓	

* $D = 1.40 \times 10^6$ lb-in.

Table 8. Summary of Shell Ring Resonance and Upper Limit Parameters of Acoustic Coincidence Frequencies

Shell Structure	$\mathscr{P}$	$\mathscr{X}_0$ (-)	$\mathscr{X}_0$ (+)	$\mathscr{Y}_0$	m_c (-)	m_c (+)	n_c	$\sqrt{\beta}$	$\sqrt{\beta}\lambda_1$	f_0 (Hz)	$[f_c]_{m_-}$ (Hz)	$[f_c]_{m_+}$ (Hz)	$[f_c]_n$ (Hz)	$[f_c]_\infty$ (Hz)
SLA (Basic)	1.33	--	--	1.32	--	--	14.73	0.0894	0.836	175.0	(248)	(248)	302	322
(R = 208 in.)	0.333	0.565	1.78	1.87	4.77	14.99	29.46	0.0632	0.1183	87.5	91.6	288	302	322
(R = 156 in.)	0.593	0.685	1.46	1.61	6.69	14.24	22.09	0.073	0.1024	117.0	128.8	274	303	322
(R = 78 in.)	2.371	--	--	1.18	--	--	11.05	0.1032	0.0724	233.0	--	--	302	322
(R = 52 in.)	5.336	--	--	0.93	--	--	7.36	0.1264	0.0591	350.0	--	--	302	322
(D = 1.296 x 10^6 lb-in.)	5.336	--	--	0.93	--	--	7.36	0.1264	0.1183	175.0	--	--	151	161
(D = 6.48 x 10^5 lb-in.)	2.668	--	--	1.18	--	--	10.41	0.1063	0.0995	175.0	--	--	215	228
(D = 1.62 x 10^5 lb-in.)	0.667	0.72	1.39	1.56	10.23	19.76	20.83	0.0751	0.0703	175.0	197.0	380	429	455
(D = 8.1 x 10^4 lb-in.)	0.333	0.564	1.77	1.86	9.53	29.99	29.46	0.0632	0.0591	175.0	183.0	576	608	644
(μg = 0.0278 lb/in.^{2})	0.333	0.564	1.77	1.86	6.74	21.20	20.83	0.0894	0.0836	123.7	129.5	408	429	455
SLA (μg = 0.0556 lb/in.^{2})	0.083	0.384	2.60	2.63	4.59	31.13	29.46	0.0894	0.0836	87.5	88.5	599	608	644
Cylinder (18 in. rad. by 54 in. by 0.02 in.)	0.022	0.272	3.68	3.68	14.00	189.5	199.0	0.0185	0.0194	1740.0	1740.0	23600	23650	23750
Cylinder (12 in. rad. by 48 in. by 0.04 in.)	0.194	0.482	2.08	2.13	19.12	82.33	66.39	0.0321	0.0252	2607.0	2680.0	11500	11830	11850
Cylinder (24 in. rad. by 48 in. by 0.04 in.)	0.049	0.334	2.99	3.02	9.37	84.00	132.8	0.0227	0.0356	1304.0	1313.0	11750	11750	11850

Table 9: Forty Most Dominant Response Modes of the SLA Structure for One Correlated Duct, f = 175.580 Hz

FREQUENCY = 175.580 ACOUSTIC WAVELENGTH = 76.546

RANK	M	N	FMN/F	J2M(W).	J2N(W).	H.	BMN	RESPONSE.	CUM. RES.	PR.	PCR	SXW/AW	SYW/AW
1	9	0	1.144	0.24387	1.00000	9.821	2.000	24793.465	24793.465	41.154	41.154	1.013	9999.996
2	8	0	1.092	0.06839	1.00000	23.728	2.000	16775.992	41569.457	27.846	69.000	1.140	9999.996
3	6	0	1.029	0.00634	1.00000	122.081	2.000	8008.910	49578.367	13.294	82.293	1.520	9999.996
4	10	0	1.214	0.13764	1.00000	4.310	2.000	6150.262	55728.629	10.209	92.502	0.912	9999.996
5	4	0	1.005	0.00139	1.00000	217.048	2.000	3120.118	58848.746	5.179	97.681	2.280	9999.996
6	2	0	1.000	0.00025	1.00000	224.900	2.000	581.759	59430.504	0.966	98.647	4.559	9999.996
7	7	0	1.054	0.00056	1.00000	57.736	2.000	349.476	59779.977	0.580	99.227	1.303	9999.996
8	5	0	1.014	0.00013	1.00000	187.540	2.000	199.743	59979.719	0.332	99.558	1.824	9999.996
9	12	0	1.411	0.01522	1.00000	1.008	2.000	158.814	60138.531	0.264	99.822	0.760	9999.996
10	3	0	1.002	0.00002	1.00000	223.870	2.000	52.797	60191.328	0.088	99.909	3.040	9999.996
11	11	0	1.303	0.00118	1.00000	2.021	2.000	24.595	60215.922	0.041	99.950	0.829	9999.996
12	14	0	1.687	0.00602	1.00000	0.293	2.000	18.252	60234.172	0.030	99.981	0.651	9999.996
13	1	0	1.000	0.00000	1.00000	224.997	2.000	4.815	60238.984	0.008	99.989	9.119	9999.996
14	16	0	2.039	0.00335	1.00000	0.100	2.000	3.479	60242.461	0.006	99.994	0.570	9999.996
15	13	0	1.539	0.00032	1.00000	0.531	2.000	1.753	60244.211	0.003	99.997	0.701	9999.996
16	18	0	2.463	0.00219	1.00000	0.039	2.000	0.881	60245.090	0.001	99.999	0.507	9999.996
17	15	0	1.853	0.00016	1.00000	0.271	2.000	0.271	60245.359	0.000	99.999	0.608	9999.996
18	20	0	2.955	0.00156	1.00000	0.017	2.000	0.270	60245.629	0.000	100.000	0.456	9999.996
19	22	0	3.511	0.00118	1.00000	0.008	2.000	0.095	60245.723	0.000	100.000	0.414	9999.996
20	17	0	2.242	0.00009	1.00000	0.062	2.000	0.061	60245.781	0.000	100.000	0.536	9999.996
21	24	0	4.130	0.00093	1.00000	0.004	2.000	0.037	60245.816	0.000	100.000	0.380	9999.996
22	19	0	2.700	0.00007	1.00000	0.025	2.000	0.017	60245.832	0.000	100.000	0.480	9999.996
23	26	0	4.809	0.00075	1.00000	0.002	2.000	0.016	60245.848	0.000	100.000	0.351	9999.996
24	28	0	5.548	0.00062	1.00000	0.001	2.000	0.007	60245.852	0.000	100.000	0.326	9999.996
25	21	0	3.225	0.00005	1.00000	0.011	2.000	0.006	60245.855	0.000	100.000	0.434	9999.996
26	30	0	6.345	0.00053	1.00000	0.001	2.000	0.004	60245.855	0.000	100.000	0.304	9999.996
27	23	0	3.813	0.00004	1.00000	0.005	2.000	0.002	60245.855	0.000	100.000	0.396	9999.996
28	25	0	4.462	0.00003	1.00000	0.003	2.000	0.001	60245.855	0.000	100.000	0.365	9999.996
29	27	0	5.171	0.00002	1.00000	0.002	2.000	0.000	60245.855	0.000	100.000	0.338	9999.996
30	29	0	5.939	0.00002	1.00000	0.001	2.000	0.000	60245.855	0.000	100.000	0.314	9999.996
31	29	0	5.939	0.00002	1.00000	0.001	2.000	0.000	60245.855	0.000	100.000	0.314	9999.996
32	29	0	5.939	0.00002	1.00000	0.001	2.000	0.000	60245.855	0.000	100.000	0.314	9999.996
33	29	0	5.939	0.00002	1.00000	0.001	2.000	0.000	60245.855	0.000	100.000	0.314	9999.996
34	29	0	5.939	0.00002	1.00000	0.001	2.000	0.000	60245.855	0.000	100.000	0.314	9999.996
35	29	0	5.939	0.00002	1.00000	0.001	2.000	0.000	60245.855	0.000	100.000	0.314	9999.996
36	29	0	5.939	0.00002	1.00000	0.001	2.000	0.000	60245.855	0.000	100.000	0.314	9999.996
37	29	0	5.939	0.00002	1.00000	0.001	2.000	0.000	60245.855	0.000	100.000	0.314	9999.996
38	29	0	5.939	0.00002	1.00000	0.001	2.000	0.000	60245.855	0.000	100.000	0.314	9999.996
39	29	0	5.939	0.00002	1.00000	0.001	2.000	0.000	60245.855	0.000	100.000	0.314	9999.996
40	29	0	5.939	0.00002	1.00000	0.001	2.000	0.000	60245.855	0.000	100.000	0.314	9999.996

THE TOTAL RESPONSE OF ALL OTHER MODES AT 175.580 HZ = 0.004 100.000

TOTAL RESPONSE = 60245.859

HISTOGRAM PLOT OF PERCENTAGE RESPONSE AGAINST NORMALISED RESONANCE FREQUENCY.

```
                0                        25                        50                        75                        100
RANK   FMN/F    I                        I                         I                         I                         I
 13    1.000
  6    1.000     O
 10    1.002
  5    1.005     OOOOO
  8    1.014
  3    1.029     OOOOOOOOOOOOO
  7    1.054     O
  2    1.092     OOOOOOOOOOOOOOOOOOOOOOOOOOOO
  1    1.144     OOOOOOOOOOOOOOOOOOOOOOOOOOOOOOOOOOOOOOOOO
  4    1.214     OOOOOOOOOO
 11    1.303
  9    1.411
 15    1.539
 12    1.687
 17    1.853
 14    2.039
 20    2.242
 16    2.463
 22    2.700
 18    2.955
 25    3.225
 19    3.511
 27    3.813
 21    4.130
 28    4.462
 23    4.809
 29    5.171
 24    5.548
 30    5.939
 31    5.939
 32    5.939
 33    5.939
 34    5.939
 35    5.939
 36    5.939
 37    5.939
 38    5.939
 39    5.939
 40    5.939
 26    6.345
```

LEGEND

FMN/F	= Resonant frequency of m,n mode/frequency
J2M(W)	= Joint acceptance in x-direction, $j_m^2(\omega)$
J2N(W)	= Joint acceptance in y-direction, $j_n^2(\omega)$
H	= $H^2(\omega/\omega_{mn})$
BMN	= β_{mn}
RESPONSE	= Response of m,nth mode $(g^2/(psi)^2)$
CUM. RES.	= Cumulative Response
PR	= Percentage of total response for m,nth mode
PCR	= Cumulative response percentage of total response
SXW/AW	= Structural wavelength, x-direction/acoustic wavelength
SYW/AW	= Structural wavelength, y-direction/acoustic wavelength

Table 10: Forty Most Dominant Response Modes of the SLA Structure for One Correlated Duct, f = 247.780 Hz

FREQUENCY = 247.780 ACOUSTIC WAVELENGTH = 54.242

RANK	M	N	FMN/F	J2M(W).	J2N(W).	H.	BMN	RESPONSE.	CUM. RES.	PR	PCR	SXW/AW	SYW/AW
1	12	0	1.000	0.11985	1.00000	224.994	2.000	279199.313	279199.313	80.152	80.152	1.072	9999.996
2	13	0	1.091	0.24599	1.00000	24.263	2.000	62536.352	341735.625	17.953	98.105	0.990	9999.996
3	14	0	1.195	0.03230	1.00000	5.265	2.000	4484.898	346220.500	1.288	99.393	0.919	9999.996
4	10	0	0.861	0.00902	1.00000	14.163	2.000	1322.766	347543.250	0.380	99.773	1.287	9999.996
5	11	0	0.923	0.00104	1.00000	39.195	2.000	421.943	347965.188	0.121	99.894	1.170	9999.996
6	8	0	0.774	0.00241	1.00000	6.103	2.000	152.074	348117.250	0.044	99.937	1.609	9999.996
7	16	0	1.445	0.01216	1.00000	0.840	2.000	105.727	348222.938	0.030	99.968	0.804	9999.996
8	6	0	0.729	0.00083	1.00000	4.513	2.000	38.870	348261.750	0.011	99.979	2.145	9999.996
9	15	0	1.313	0.00109	1.00000	1.876	2.000	21.166	348282.875	0.006	99.985	0.858	9999.996
10	9	0	0.811	0.00019	1.00000	6.327	2.000	16.676	348299.500	0.005	99.990	1.430	9999.996
11	18	0	1.745	0.00501	1.00000	0.238	2.000	12.363	348311.813	0.004	99.993	0.715	9999.996
12	4	0	0.712	0.00026	1.00000	4.085	2.000	11.737	348323.500	0.003	99.996	3.217	9999.996
13	7	0	0.747	0.00006	1.00000	5.055	2.000	3.223	348326.688	0.001	99.997	1.838	9999.996
14	20	0	2.094	0.00263	1.00000	0.087	2.000	2.551	348329.188	0.001	99.998	0.643	9999.996
15	2	0	0.709	0.00006	1.00000	4.002	2.000	2.463	348331.625	0.001	99.999	6.434	9999.996
16	17	0	1.589	0.00032	1.00000	0.429	2.000	1.439	348333.063	0.000	99.999	0.757	9999.996
17	5	0	0.718	0.00002	1.00000	4.228	2.000	0.946	348334.000	0.000	99.999	2.574	9999.996
18	22	0	2.488	0.00185	1.00000	0.037	2.000	0.711	348334.688	0.000	100.000	0.585	9999.996
19	3	0	0.710	0.00001	1.00000	4.022	2.000	0.261	348334.938	0.000	100.000	4.289	9999.996
20	24	0	2.927	0.00133	1.00000	0.017	2.000	0.240	348335.125	0.000	100.000	0.536	9999.996
21	19	0	1.914	0.00016	1.00000	0.141	2.000	0.236	348335.313	0.000	100.000	0.677	9999.996
22	26	0	3.498	0.00101	1.00000	0.009	2.000	0.093	348335.375	0.000	100.000	0.495	9999.996
23	21	0	2.285	0.00013	1.00000	0.056	2.000	0.058	348335.375	0.000	100.000	0.613	9999.996
24	28	0	3.931	0.00060	1.00000	0.005	2.000	0.039	348335.375	0.000	100.000	0.460	9999.996
25	1	0	0.709	0.00000	1.00000	3.998	2.000	0.026	348335.375	0.000	100.000	12.868	9999.996
26	30	0	4.496	0.00065	1.00000	0.003	2.000	0.018	348335.375	0.000	100.000	0.429	9999.996
27	23	0	2.702	0.00007	1.00000	0.025	2.000	0.018	348335.375	0.000	100.000	0.559	9999.996
28	25	0	3.162	0.00005	1.00000	0.012	2.000	0.006	348335.375	0.000	100.000	0.515	9999.996
29	27	0	3.664	0.00004	1.00000	0.006	2.000	0.003	348335.375	0.000	100.000	0.477	9999.996
30	29	0	4.209	0.00003	1.00000	0.004	2.000	0.001	348335.375	0.000	100.000	0.444	9999.996
31	29	0	4.209	0.00003	1.00000	0.004	2.000	0.000	348335.375	0.000	100.000	0.444	9999.996
32	29	0	4.209	0.00003	1.00000	0.004	2.000	0.000	348335.375	0.000	100.000	0.444	9999.996
33	29	0	4.209	0.00003	1.00000	0.004	2.000	0.000	348335.375	0.000	100.000	0.444	9999.996
34	29	0	4.209	0.00003	1.00000	0.004	2.000	0.000	348335.375	0.000	100.000	0.444	9999.996
35	29	0	4.209	0.00003	1.00000	0.004	2.000	0.000	348335.375	0.000	100.000	0.444	9999.996
36	29	0	4.209	0.00003	1.00000	0.004	2.000	0.000	348335.375	0.000	100.000	0.444	9999.996
37	29	0	4.209	0.00003	1.00000	0.004	2.000	0.000	348335.375	0.000	100.000	0.444	9999.996
38	29	0	4.209	0.00003	1.00000	0.004	2.000	0.000	348335.375	0.000	100.000	0.444	9999.996
39	29	0	4.209	0.00003	1.00000	0.004	2.000	0.000	348335.375	0.000	100.000	0.444	9999.996
40	29	0	4.209	0.00003	1.00000	0.004	2.000	0.000	348335.375	0.000	100.000	0.444	9999.996

THE TOTAL RESPONSE OF ALL OTHER MODES AT 247.780 HZ = 0.250 100.000

TOTAL RESPONSE = 348335.625

HISTOGRAM PLOT OF PERCENTAGE RESPONSE AGAINST NORMALISED RESONANCE FREQUENCY.

```
                0                        25                        50                        75                       100
RANK   FMN/F    I                        I                         I                         I                         I
 25    0.709
 15    0.709
 19    0.710
 12    0.712
 17    0.718
  8    0.729
 13    0.747
  6    0.774
 10    0.811
  4    0.861
  5    0.923
  1    1.000    00000000000000000000000000000000000000000000000000000000000000000000000000000000
  2    1.091    000000000000000000000
  3    1.195    0
  9    1.313
  7    1.445
 16    1.589
 11    1.745
 21    1.914
 14    2.094
 23    2.285
 18    2.488
 27    2.702
 20    2.927
 28    3.162
 22    3.498
 29    3.664
 24    3.931
 30    4.209
 31    4.209
 32    4.209
 33    4.209
 34    4.209
 35    4.209
 36    4.209
 37    4.209
 38    4.209
 39    4.209
 40    4.209
 26    4.496
```

LEGEND

FMN/F	= Resonant frequency of m,n mode/frequency
J2M(W)	= Joint acceptance in x-direction, $j_m^2(\omega)$
J2N(W)	= Joint acceptance in y-direction, $j_n^2(\omega)$
H	= $H^2(\omega/\omega_{mn})$
BMN	= β_{mn}
RESPONSE	= Response of m,nth mode $(g^2/(psi)^2)$
CUM. RES.	= Cumulative Response
PR	= Percentage of total response for m,nth mode
PCR	= Cumulative response percentage of total response
SXW/AW	= Structural wavelength, x-direction/acoustic wavelength
SYW/AW	= Structural wavelength, y-direction/acoustic wavelength

Table 11: Forty Most Dominant Response Modes of the SLA Structure for Sixteen Uncorrelated Ducts, f = 89.125 Hz

FREQUENCY = 89.125 ACOUSTIC WAVELENGTH = 150.799

RANK	M	N	FMN/F	J2M(W).	J2N(W).	H.	BMN	RESPONSE.	CUM. RES.	PR	PCR	SXW/AW	SYW/AW
1	4	4	1.024	0.15352	0.00317	142.942	3.543	20387.855	20387.855	46.500	46.500	1.157	0.067
2	4	6	0.948	0.15352	0.00240	69.571	3.767	8045.941	28433.797	18.351	64.850	1.157	0.045
3	4	5	0.925	0.15352	0.00280	40.144	3.698	5288.375	33722.172	12.061	76.912	1.157	0.054
4	4	7	1.070	0.15352	0.00199	38.114	3.842	3702.627	37424.797	8.445	85.356	1.157	0.039
5	5	5	1.167	0.24043	0.00280	7.314	3.698	1508.851	38933.645	3.441	88.798	0.926	0.054
6	5	6	1.163	0.24043	0.00240	7.657	3.767	1386.752	40320.395	3.163	91.961	0.926	0.045
7	5	4	1.275	0.24043	0.00317	2.516	3.543	561.908	40882.301	1.282	93.242	0.926	0.067
8	3	3	0.950	0.00717	0.00347	73.841	3.240	493.464	41375.762	1.125	94.368	1.543	0.090
9	4	3	1.245	0.15352	0.00347	3.219	3.240	460.815	41836.574	1.051	95.419	1.157	0.090
10	5	7	1.257	0.24043	0.00199	2.921	3.842	444.327	42280.898	1.013	96.432	0.926	0.039
11	4	8	1.264	0.15352	0.00158	2.739	3.878	213.749	42494.645	0.488	96.920	1.157	0.034
12	3	7	0.922	0.00717	0.00199	36.256	3.842	173.527	42668.168	0.396	97.315	1.543	0.039
13	5	3	1.470	0.24043	0.00347	0.735	3.240	164.820	42832.984	0.376	97.691	0.926	0.090
14	5	8	1.428	0.24043	0.00158	0.918	3.878	112.155	42945.137	0.256	97.947	0.926	0.034
15	2	2	0.922	0.00372	0.00371	38.220	2.560	111.803	43056.938	0.255	98.202	2.314	0.135
16	2	8	1.054	0.00372	0.00156	57.336	3.878	108.427	43165.363	0.247	98.449	2.314	0.034
17	4	2	1.553	0.15352	0.00371	0.498	2.560	60.144	43225.504	0.137	98.586	1.157	0.135
18	5	2	1.709	0.24043	0.00371	0.270	2.560	51.031	43276.531	0.116	98.703	0.926	0.135
19	6	5	1.401	0.04764	0.00280	1.069	3.698	43.867	43320.418	0.100	98.803	0.771	0.054
20	6	6	1.391	0.04764	0.00240	1.130	3.787	40.743	43361.160	0.093	98.896	0.771	0.045
21	3	8	1.139	0.00717	0.00158	10.680	3.878	38.920	43400.078	0.089	98.985	1.543	0.034
22	4	9	1.511	0.15352	0.00120	0.605	3.903	36.117	43436.191	0.082	99.067	1.157	0.030
23	3	4	0.741	0.00717	0.00317	4.854	3.543	32.326	43468.516	0.074	99.141	1.543	0.067
24	1	8	1.009	0.00029	0.00158	207.269	3.878	31.055	43499.570	0.071	99.212	4.629	0.034
25	3	6	0.762	0.00717	0.00240	5.613	3.787	30.310	43529.879	0.069	99.281	1.543	0.045
26	5	9	1.660	0.24043	0.00120	0.324	3.903	30.273	43560.148	0.069	99.350	0.926	0.030
27	6	4	1.495	0.04764	0.00317	0.652	3.543	28.970	43589.117	0.066	99.416	0.771	0.067
28	6	7	1.469	0.04764	0.00199	0.741	3.842	22.420	43611.535	0.051	99.467	0.771	0.039
29	2	7	0.823	0.00372	0.00199	9.346	3.842	22.002	43633.535	0.050	99.517	2.314	0.039
30	3	5	0.688	0.00717	0.00280	3.576	3.698	21.997	43655.531	0.050	99.567	1.543	0.054
31	5	0	1.997	0.24043	0.00391	0.112	2.000	17.383	43672.914	0.040	99.607	0.926	9999.996
32	6	3	1.651	0.04764	0.00347	0.334	3.240	14.897	43687.809	0.034	99.641	0.771	0.090
33	4	0	1.981	0.15352	0.00391	0.117	2.000	11.604	43699.410	0.026	99.667	1.157	9999.996
34	5	1	1.914	0.24043	0.00386	0.140	1.000	10.784	43710.191	0.025	99.692	0.926	0.270
35	3	2	1.315	0.00717	0.00371	1.853	2.560	10.447	43720.637	0.024	99.716	1.543	0.135
36	6	8	1.624	0.04764	0.00158	0.372	3.878	9.049	43729.684	0.021	99.736	0.771	0.034
37	5	10	1.938	0.24043	0.00066	0.131	3.921	8.860	43738.543	0.020	99.757	0.926	0.027
38	4	10	1.799	0.15352	0.00066	0.199	3.921	8.600	43747.141	0.020	99.776	1.157	0.027
39	4	1	1.851	0.15352	0.00366	0.169	1.000	8.305	43755.445	0.019	99.795	1.157	0.270
40	2	3	0.576	0.00372	0.00347	2.251	3.240	7.805	43763.250	0.018	99.813	2.314	0.090

THE TOTAL RESPONSE OF ALL OTHER MODES AT 89.125 HZ = 82.020 100.000

TOTAL RESPONSE = 43845.270

HISTOGRAM PLOT OF PERCENTAGE RESPONSE AGAINST NORMALISED RESONANCE FREQUENCY.

```
                0                        25                        50                        75                       100
RANK   FMN/F    I                         I                         I                         I                         I
 40    0.578
 30    0.688
 23    0.741
 25    0.762
 29    0.823
 15    0.922
 12    0.922
  3    0.925    000000000000
  2    0.948    000000000000000000
  8    0.950    0
 24    1.009
  1    1.024    0000000000000000000000000000000000000000000000
 16    1.054
  4    1.070    00000000
 21    1.139
  6    1.163    000
  5    1.167    000
  9    1.245    0
 10    1.257    0
 11    1.264
  7    1.275    0
 35    1.315
 20    1.391
 19    1.401
 14    1.428
 28    1.469
 13    1.470
 27    1.495
 22    1.511
 17    1.553
 36    1.624
 32    1.651
 26    1.660
 18    1.709
 38    1.799
 39    1.851
 34    1.914
 37    1.938
 33    1.981
 31    1.997
```

LEGEND

FMN/F	= Resonant frequency of m,n mode/frequency
J2M(W)	= Joint acceptance in x-direction, $j_m^2(\omega)$
J2N(W)	= Joint acceptance in y-direction, $j_n^2(\omega)$
H	= $H^2(\omega/\omega_{mn})$
BMN	= β_{mn}
RESPONSE	= Response of m,nth mode $(g^2/(psi)^2)$
CUM. RES.	= Cumulative Response
PR	= Percentage of total response for m,nth mode
PCR	= Cumulative response percentage of total response
SXW/AW	= Structural wavelength, x-direction/acoustic wavelength
SYW/AW	= Structural wavelength, y-direction/acoustic wavelength

Table 12: Forty Most Dominant Response Modes of the SLA Structure for Sixteen Uncorrelated Ducts, f = 177.827 Hz

FREQUENCY = 177.827 ACOUSTIC WAVELENGTH = 75.579

RANK	M	N	FMN/F	J2M(W).	J2N(W).	H.	BMN	RESPONSE.	CUM. RES.	PR	PCR	SXW/AW	SYW/AW
1	9	5	1.044	0.23269	0.00280	77.567	3.698	15487.770	15487.770	16.463	16.463	1.026	0.108
2	9	4	1.051	0.23269	0.00317	63.026	3.543	13625.160	29112.930	14.483	30.946	1.026	0.135
3	8	3	0.986	0.04975	0.00347	203.939	3.240	9458.586	38571.516	10.054	41.001	1.154	0.179
4	9	6	1.060	0.23269	0.00240	49.517	3.787	8679.766	47251.281	9.226	50.227	1.026	0.090
5	9	3	1.073	0.23269	0.00347	35.453	3.240	7691.363	54942.645	8.176	58.403	1.026	0.179
6	8	7	0.974	0.04975	0.00199	145.901	3.842	4592.707	59535.352	4.882	63.285	1.154	0.077
7	8	2	1.032	0.04975	0.00371	113.173	2.560	4427.391	63962.742	4.706	67.991	1.154	0.269
8	9	2	1.100	0.23269	0.00371	20.074	2.560	3673.248	67635.938	3.905	71.896	1.026	0.269
9	8	4	0.949	0.04975	0.00317	72.318	3.543	3342.282	70978.188	3.553	75.448	1.154	0.135
10	9	7	1.103	0.23269	0.00199	18.945	3.842	2789.566	73767.750	2.965	78.413	1.026	0.077
11	8	6	0.935	0.04975	0.00240	50.757	3.787	1902.079	75669.813	2.022	80.435	1.154	0.090
12	8	8	1.045	0.04975	0.00158	74.422	3.878	1882.177	77551.938	2.001	82.436	1.154	0.067
13	8	5	0.928	0.04975	0.00280	43.544	3.698	1858.747	79410.625	1.976	84.412	1.154	0.108
14	9	0	1.130	0.23269	0.00391	12.140	2.000	1827.606	81238.188	1.943	86.354	1.026	9999.996
15	10	4	1.160	0.16289	0.00317	7.926	3.543	1199.444	82437.625	1.275	87.629	0.924	0.135
16	10	3	1.169	0.16289	0.00347	7.161	3.240	1087.422	83525.000	1.156	88.785	0.924	0.179
17	10	5	1.166	0.16289	0.00280	7.397	3.698	1033.906	84558.875	1.099	89.884	0.924	0.108
18	9	1	1.122	0.23269	0.00386	13.799	1.000	1025.366	85584.188	1.090	90.974	1.026	0.538
19	8	0	1.078	0.04975	0.00391	31.830	2.000	1024.421	86608.563	1.089	92.063	1.154	9999.996
20	10	2	1.182	0.16289	0.00371	6.074	2.560	778.098	87386.625	0.827	92.890	0.924	0.269
21	9	8	1.176	0.23269	0.00158	6.551	3.878	774.931	88161.500	0.824	93.714	1.026	0.067
22	8	1	1.065	0.04975	0.00386	43.561	1.000	684.077	88845.563	0.727	94.441	1.154	0.538
23	10	6	1.191	0.16289	0.00240	5.491	3.787	673.783	89519.313	0.716	95.157	0.924	0.090
24	6	0	1.016	0.00522	0.00391	177.284	2.000	598.834	90118.125	0.637	95.794	1.539	9999.996
25	10	0	1.199	0.16289	0.00391	5.050	2.000	532.122	90650.188	0.566	96.359	0.924	9999.996
26	10	7	1.241	0.16289	0.00199	3.355	3.842	345.809	90995.938	0.368	96.727	0.924	0.077
27	6	1	0.988	0.00522	0.00386	205.096	1.000	341.959	91337.875	0.363	97.090	1.539	0.538
28	10	1	1.194	0.16289	0.00386	5.311	1.000	276.241	91614.063	0.294	97.384	0.924	0.538
29	9	9	1.276	0.23269	0.00120	2.488	3.903	225.178	91839.188	0.239	97.623	1.026	0.060
30	7	2	0.972	0.00197	0.00371	138.625	2.560	214.599	92053.750	0.228	97.851	1.319	0.269
31	8	9	1.146	0.04975	0.00120	9.569	3.903	185.139	92238.875	0.197	98.048	1.154	0.060
32	4	0	0.993	0.00117	0.00391	217.677	2.000	165.371	92404.188	0.176	98.224	2.309	9999.996
33	10	8	1.316	0.16289	0.00158	1.840	3.878	152.389	92556.563	0.162	98.386	0.924	0.067
34	6	2	0.917	0.00522	0.00371	34.194	2.560	140.398	92696.938	0.149	98.535	1.539	0.269
35	7	0	1.041	0.00197	0.00391	85.002	2.000	108.255	92805.188	0.115	98.650	1.319	9999.996
36	7	9	1.028	0.00197	0.00120	125.380	3.903	95.989	92901.125	0.102	98.752	1.319	0.060
37	7	1	1.022	0.00197	0.00386	151.102	1.000	94.988	92996.063	0.101	98.853	1.319	0.538
38	6	9	0.923	0.00522	0.00120	38.715	3.903	78.612	93074.625	0.084	98.936	1.539	0.060
39	6	10	1.058	0.00522	0.00086	52.533	3.921	77.024	93151.625	0.082	99.018	1.539	0.054
40	9	10	1.402	0.23269	0.00086	1.065	3.921	69.614	93221.188	0.074	99.092	1.026	0.054

THE TOTAL RESPONSE OF ALL OTHER MODES AT 177.827 HZ = 854.125 100.000

TOTAL RESPONSE = 94075.313

HISTOGRAM PLOT OF PERCENTAGE RESPONSE AGAINST NORMALISED RESONANCE FREQUENCY.

```
                0                        25                        50                        75                        100
RANK   FMN/F    I                        I                         I                         I                         I
 34    0.917
 38    0.923
 13    0.928    00
 11    0.935    00
  9    0.949    0000
 30    0.972
  6    0.974    00000
  3    0.988    0000000000
 27    0.988
 32    0.993
 24    1.016    0
 37    1.022
 36    1.028
  7    1.032    00000
 35    1.041
  1    1.044    0000000000000000
 12    1.045    00
  2    1.051    00000000000000
 39    1.058
  4    1.060    000000000
 22    1.065    0
  5    1.073    00000000
 19    1.078    0
  8    1.100    0000
 10    1.103    000
 18    1.122    0
 14    1.130    00
 31    1.146
 15    1.160    0
 17    1.166    0
 16    1.169    0
 21    1.176    0
 20    1.182    0
 23    1.191    0
 28    1.194
 25    1.199    0
 26    1.241
 29    1.276
 33    1.316
 40    1.402
```

LEGEND

FMN/F	= Resonant frequency of m,n mode/frequency
J2M(W)	= Joint acceptance in x-direction, $j_m^2(\omega)$
J2N(W)	= Joint acceptance in y-direction, $j_n^2(\omega)$
H	= $H^2(\omega/\omega_{mn})$
BMN	= β_{mn}
RESPONSE	= Response of m,nth mode $(g^2/(psi)^2)$
CUM. RES.	= Cumulative Response
PR	= Percentage of total response for m,nth mode
PCR	= Cumulative response percentage of total response
SXW/AW	= Structural wavelength, x-direction/acoustic wavelength
SYW/AW	= Structural wavelength, y-direction/acoustic wavelength

Table 13: Forty Most Dominant Response Modes of the SLA Structure for Sixteen Uncorrelated Ducts, f = 223.871 Hz

FREQUENCY = 223.871 ACOUSTIC WAVELENGTH = 60.035

RANK	M	N	FMN/F	J2M(W).	J2N(W).	H.	BMN	RESPONSE.	CUM. RES.	PR	PCR	SXW/AW	SYW/AW
1	11	3	1.014	0.16922	0.00347	185.378	3.240	29247.020	29247.020	18.717	18.717	1.057	0.226
2	11	4	1.017	0.16922	0.00317	172.310	3.543	27089.809	56336.828	17.337	36.054	1.057	0.169
3	11	2	1.017	0.16922	0.00371	174.291	2.560	23194.090	79530.875	14.844	50.898	1.057	0.339
4	11	5	1.030	0.16922	0.00280	117.518	3.698	17064.484	96595.313	10.921	61.819	1.057	0.136
5	11	0	1.022	0.16922	0.00391	151.118	2.000	16544.355	113139.625	10.588	72.406	1.057	9999.996
6	11	1	1.020	0.16922	0.00366	158.112	1.000	8544.348	121683.938	5.468	77.875	1.057	0.678
7	11	6	1.058	0.16922	0.00240	52.558	3.787	6699.996	128383.875	4.288	82.162	1.057	0.113
8	12	3	1.112	0.22972	0.00347	16.231	3.240	3476.228	131860.063	2.225	84.387	0.969	0.226
9	12	2	1.108	0.22972	0.00371	17.485	2.560	3158.753	135018.813	2.022	86.409	0.969	0.339
10	12	4	1.123	0.22972	0.00317	13.587	3.543	2899.714	137918.500	1.856	88.264	0.969	0.169
11	12	0	1.107	0.22972	0.00391	17.830	2.000	2649.849	140568.313	1.696	89.960	0.969	9999.996
12	11	7	1.102	0.16922	0.00199	19.513	3.842	2089.441	142657.750	1.337	91.297	1.057	0.097
13	12	5	1.143	0.22972	0.00280	9.964	3.698	1964.152	144621.875	1.257	92.554	0.969	0.136
14	12	1	1.107	0.22972	0.00366	17.608	1.000	1306.377	145928.250	0.836	93.390	0.969	0.678
15	10	7	0.966	0.01003	0.00199	194.829	3.842	1236.655	147164.875	0.791	94.182	1.163	0.097
16	12	6	1.177	0.22972	0.00240	6.457	3.787	1117.299	148282.125	0.715	94.897	0.969	0.113
17	11	8	1.165	0.16922	0.00158	7.528	3.878	647.612	148929.688	0.414	95.311	1.057	0.085
18	9	9	1.014	0.00776	0.00120	186.216	3.903	567.906	149497.563	0.363	95.675	1.292	0.075
19	12	7	1.226	0.22972	0.00199	3.842	3.842	558.436	150055.938	0.357	96.032	0.969	0.097
20	10	0	0.952	0.01003	0.00391	79.063	2.000	513.092	150569.000	0.328	96.360	1.163	9999.996
21	10	6	0.946	0.01003	0.00240	67.125	3.787	507.226	151076.188	0.325	96.685	1.163	0.113
22	10	2	0.939	0.01003	0.00371	56.103	2.560	442.562	151518.688	0.283	96.968	1.163	0.339
23	10	3	0.928	0.01003	0.00347	43.493	3.240	406.752	151925.438	0.260	97.228	1.163	0.226
24	10	8	1.045	0.01003	0.00158	74.275	3.878	378.779	152304.188	0.242	97.471	1.163	0.085
25	10	5	0.926	0.01003	0.00280	41.563	3.698	357.751	152661.938	0.229	97.700	1.163	0.136
26	10	4	0.922	0.01003	0.00317	37.924	3.543	353.424	153015.313	0.226	97.926	1.163	0.169
27	12	8	1.292	0.22972	0.00158	2.195	3.878	256.364	153271.625	0.164	98.090	0.969	0.085
28	10	1	0.949	0.01003	0.00366	71.534	1.000	229.148	153500.750	0.147	98.237	1.163	0.678
29	11	9	1.246	0.16922	0.00120	3.209	3.903	211.166	153711.875	0.135	98.372	1.057	0.075
30	9	8	0.934	0.00776	0.00158	49.648	3.878	195.823	153907.688	0.125	98.497	1.292	0.085
31	13	3	1.223	0.04154	0.00347	3.969	3.240	153.707	154061.375	0.098	98.595	0.894	0.226
32	13	2	1.213	0.04154	0.00371	4.364	2.560	142.552	154203.875	0.091	98.687	0.894	0.339
33	13	4	1.240	0.04154	0.00317	3.387	3.543	130.711	154334.563	0.084	98.770	0.894	0.169
34	13	0	1.207	0.04154	0.00391	4.640	2.000	124.699	154459.250	0.080	98.850	0.894	9999.996
35	9	0	0.898	0.00776	0.00391	24.192	2.000	121.429	154580.625	0.078	98.928	1.292	9999.996
36	12	9	1.375	0.22972	0.00120	1.246	3.903	111.333	154691.938	0.071	98.999	0.969	0.075
37	9	2	0.874	0.00776	0.00371	16.918	2.560	103.218	154795.125	0.066	99.065	1.292	0.339
38	13	5	1.267	0.04154	0.00280	2.685	3.698	95.692	154890.813	0.061	99.126	0.894	0.136
39	9	3	0.853	0.00776	0.00347	12.845	3.240	92.908	154983.688	0.059	99.186	1.292	0.226
40	8	10	1.012	0.00157	0.00086	195.732	3.921	86.197	155069.875	0.055	99.241	1.453	0.068

THE TOTAL RESPONSE OF ALL OTHER MODES AT 223.871 HZ = 1186.375 100.000

TOTAL RESPONSE = 156256.250

HISTOGRAM PLOT OF PERCENTAGE RESPONSE AGAINST NORMALISED RESONANCE FREQUENCY.

RANK	FMN/F	0 I . . . 25 I . . . 50 I . . . 75 I . . . 100 I
39	0.853	
37	0.874	
35	0.898	
26	0.922	
25	0.926	
23	0.928	
30	0.934	
22	0.939	
21	0.946	
28	0.949	
20	0.952	
15	0.966	0
40	1.012	
18	1.014	
1	1.014	0000000000000000000
3	1.017	000000000000000
2	1.017	00000000000000000
6	1.020	00000
5	1.022	00000000000
4	1.030	00000000000
24	1.045	
7	1.058	0000
12	1.102	0
11	1.107	00
14	1.107	0
9	1.108	00
8	1.112	00
10	1.123	00
13	1.143	0
17	1.165	
16	1.177	0
34	1.207	
32	1.213	
31	1.223	
19	1.226	
33	1.240	
29	1.246	
38	1.267	
27	1.292	
36	1.375	

LEGEND

FMN/F	= Resonant frequency of m,n mode/frequency
J2M(W)	= Joint acceptance in x-direction, $j_m^2(\omega)$
J2N(W)	= Joint acceptance in y-direction, $j_n^2(\omega)$
H	= $H^2(\omega/\omega_{mn})$
BMN	= β_{mn}
RESPONSE	= Response of m,nth mode $(g^2/(psi)^2)$
CUM. RES.	= Cumulative Response
PR	= Percentage of total response for m,nth mode
PCR	= Cumulative response percentage of total response
SXW/AW	= Structural wavelength, x-direction/acoustic wavelength
SYW/AW	= Structural wavelength, y-direction/acoustic wavelength

Table 14: Forty Most Dominant Response Modes of the SLA Structure for Sixteen Uncorrelated Ducts, f = 398.105 Hz

FREQUENCY = 398.105 ACOUSTIC WAVELENGTH = 33.760

RANK	M	N	FMN/F	J2M(W).	J2N(W).	H.	BMN	RESPONSE.	CUM. RES.	PR	PCR	SXW/AW	SYW/AW
1	16	6	0.987	0.00269	0.00240	199.012	3.787	402.995	402.995	6.181	6.181	1.292	0.201
2	17	3	1.011	0.00146	0.00347	199.421	3.240	270.566	673.560	4.150	10.331	1.216	0.402
3	17	2	0.998	0.00146	0.00371	225.206	2.560	257.727	931.287	3.953	14.284	1.216	0.603
4	20	3	1.329	0.16363	0.00347	1.676	3.240	255.626	1186.914	3.921	18.205	1.034	0.402
5	16	7	1.023	0.00269	0.00199	147.996	3.842	251.735	1438.648	3.861	22.066	1.292	0.172
6	20	2	1.315	0.16363	0.00371	1.857	2.560	238.964	1677.612	3.665	25.731	1.034	0.603
7	20	4	1.350	0.16363	0.00317	1.458	3.543	221.660	1899.272	3.400	29.131	1.034	0.301
8	20	0	1.303	0.16363	0.00391	2.021	2.000	213.915	2113.187	3.281	32.412	1.034	9999.996
9	16	5	0.958	0.00269	0.00280	91.702	3.698	211.521	2324.708	3.244	35.656	1.292	0.241
10	17	0	0.989	0.00146	0.00391	206.435	2.000	194.355	2519.063	2.981	38.637	1.216	9999.996
11	21	3	1.450	0.23266	0.00347	0.818	3.240	177.467	2696.530	2.722	41.359	0.985	0.402
12	20	5	1.377	0.16363	0.00280	1.229	3.698	172.552	2869.082	2.647	44.005	1.034	0.241
13	17	4	1.029	0.00146	0.00317	123.305	3.543	166.707	3035.789	2.557	46.562	1.216	0.301
14	21	2	1.434	0.23266	0.00371	0.887	2.560	162.264	3198.053	2.489	49.051	0.985	0.603
15	18	0	1.086	0.00934	0.00391	26.646	2.000	161.062	3359.115	2.470	51.521	1.149	9999.996
16	18	2	1.097	0.00934	0.00371	21.567	2.560	158.459	3517.573	2.430	53.952	1.149	0.603
17	21	4	1.471	0.23266	0.00317	0.733	3.543	158.414	3675.987	2.430	56.381	0.985	0.301
18	18	3	1.110	0.00934	0.00347	16.565	3.240	146.907	3822.894	2.253	58.635	1.149	0.402
19	21	0	1.422	0.23266	0.00391	0.947	2.000	142.573	3965.466	2.187	60.821	0.985	9999.996
20	16	4	0.935	0.00269	0.00317	51.244	3.543	127.975	4093.441	1.963	62.784	1.292	0.301
21	21	5	1.499	0.23266	0.00280	0.639	3.698	127.605	4221.043	1.957	64.741	0.985	0.241
22	20	6	1.411	0.16363	0.00240	1.008	3.787	124.258	4345.301	1.906	66.647	1.034	0.201
23	18	4	1.129	0.00934	0.00317	12.318	3.543	106.923	4452.223	1.640	68.287	1.149	0.301
24	20	1	1.306	0.16363	0.00386	1.978	1.000	103.365	4555.586	1.585	69.873	1.034	1.205
25	17	1	0.991	0.00146	0.00386	213.649	1.000	99.380	4654.965	1.524	71.397	1.216	1.205
26	21	6	1.533	0.23266	0.00240	0.544	3.787	95.413	4750.375	1.463	72.860	0.985	0.201
27	16	3	0.919	0.00269	0.00347	35.771	3.240	89.649	4840.023	1.375	74.235	1.292	0.402
28	20	7	1.452	0.16363	0.00199	0.809	3.842	83.742	4923.762	1.284	75.520	1.034	0.172
29	18	1	1.089	0.00934	0.00386	25.240	1.000	75.308	4999.066	1.155	76.675	1.149	1.205
30	17	5	1.053	0.00146	0.00280	60.079	3.698	75.022	5074.086	1.151	77.825	1.216	0.241
31	21	1	1.425	0.23266	0.00386	0.932	1.000	69.219	5143.301	1.062	78.887	0.985	1.205
32	18	5	1.154	0.00934	0.00280	8.586	3.698	68.835	5212.133	1.056	79.943	1.149	0.241
33	14	10	0.992	0.00113	0.00086	216.618	3.921	68.703	5280.836	1.054	80.996	1.477	0.121
34	21	7	1.575	0.23266	0.00199	0.454	3.842	66.884	5347.719	1.026	82.022	0.985	0.172
35	16	2	0.908	0.00269	0.00371	28.853	2.560	60.992	5408.707	0.935	82.958	1.292	0.603
36	16	8	1.066	0.00269	0.00158	42.052	3.878	57.469	5466.176	0.881	83.839	1.292	0.151
37	20	8	1.499	0.16363	0.00158	0.638	3.878	53.052	5519.227	0.814	84.653	1.034	0.151
38	21	8	1.623	0.23266	0.00158	0.373	3.878	44.088	5563.313	0.676	85.329	0.985	0.151
39	16	0	0.899	0.00269	0.00391	24.810	2.000	43.146	5606.457	0.662	85.991	1.292	9999.996
40	18	6	1.186	0.00934	0.00240	5.821	3.787	40.967	5647.422	0.628	86.619	1.149	0.201

THE TOTAL RESPONSE OF ALL OTHER MODES AT 398.105 HZ = 872.426 100.000

TOTAL RESPONSE = 6519.848

HISTOGRAM PLOT OF PERCENTAGE RESPONSE AGAINST NORMALISED RESONANCE FREQUENCY.

```
                 0                        25                        50                        75                        100
RANK    FMN/F    I                         I                         I                         I                         I
 39     0.899    O
 35     0.908    O
 27     0.919    O
 20     0.935    OO
  9     0.958    OOO
  1     0.987    OOOOOO
 10     0.989    OOO
 25     0.991    OO
 33     0.992    O
  3     0.998    OOOO
  2     1.011    OOOO
  5     1.023    OOOO
 13     1.029    OOO
 30     1.053    O
 36     1.066    O
 15     1.086    OO
 29     1.089    O
 16     1.097    OO
 18     1.110    OO
 23     1.129    OO
 32     1.154    O
 40     1.186    O
  8     1.303    OOO
 24     1.306    OO
  6     1.315    OOOO
  4     1.329    OOOO
  7     1.350    OOO
 12     1.377    OOO
 22     1.411    OO
 19     1.422    OO
 31     1.425    O
 14     1.434    OO
 11     1.450    OOO
 28     1.452    O
 17     1.471    OO
 21     1.499    OO
 37     1.499    O
 26     1.533    O
 34     1.575    O
 38     1.623    O
```

LEGEND

FMN/F	= Resonant frequency of m,n mode/frequency
J2M(W)	= Joint acceptance in x-direction, $j_m^2(\omega)$
J2N(W)	= Joint acceptance in y-direction, $j_n^2(\omega)$
H	= $H^2(\omega/\omega_{mn})$
BMN	= β_{mn}
RESPONSE	= Response of m,nth mode $(g^2/(psi)^2)$
CUM. RES.	= Cumulative Response
PR	= Percentage of total response for m,nth mode
PCR	= Cumulative response percentage of total response
SXW/AW	= Structural wavelength, x-direction/acoustic wavelength
SYW/AW	= Structural wavelength, y-direction/acoustic wavelength

Table 15: Forty Most Dominant Response Modes of the SLA Structure for Reverberant Acoustic Field, f = 89.125 Hz

FREQUENCY = 89.125 ACOUSTIC WAVELENGTH = 150.799

RANK	M	N	FMN/F	J2M(W).	J2N(W).	H.	BMN	RESPONSE.	CUM. RES.	PR	PCR	SXW/AW	SYW/AW
1	4	4	1.024	0.09149	0.09017	142.942	3.543	21625.215	21625.215	43.420	43.420	1.157	1.079
2	3	3	0.950	0.10621	0.11004	73.641	3.240	14473.285	36098.500	29.060	72.480	1.543	1.439
3	2	2	0.922	0.10710	0.11217	38.220	2.560	6083.953	42182.453	12.216	84.695	2.314	2.158
4	1	1	0.917	0.10790	0.11264	34.132	1.000	2150.806	44333.258	4.318	89.014	4.629	4.317
5	3	4	0.741	0.10621	0.09017	4.654	3.543	852.560	45185.816	1.712	90.725	1.543	1.079
6	4	3	1.245	0.09149	0.11004	3.219	3.240	543.569	45729.383	1.091	91.817	1.157	1.439
7	4	5	0.925	0.09149	0.00673	40.144	3.698	473.100	46202.480	0.950	92.767	1.157	0.863
8	1	6	1.009	0.10790	0.00105	207.269	3.878	471.884	46674.363	0.947	93.714	4.629	0.540
9	2	3	0.578	0.10710	0.11004	2.251	3.240	444.823	47119.184	0.893	94.607	2.314	1.439
10	4	6	0.948	0.09149	0.00265	69.571	3.787	330.063	47449.246	0.663	95.270	1.157	0.719
11	3	2	1.316	0.10621	0.11217	1.853	2.560	292.589	47741.832	0.587	95.858	1.543	2.158
12	2	4	0.457	0.10710	0.09017	1.596	3.543	282.580	48024.410	0.567	96.425	2.314	1.079
13	1	3	0.223	0.10790	0.11004	1.107	3.240	220.455	48244.863	0.443	96.868	4.629	1.439
14	1	2	0.357	0.10790	0.11217	1.313	2.560	210.535	48455.398	0.423	97.290	4.629	2.158
15	1	4	0.270	0.10790	0.09017	1.163	3.543	207.582	48662.980	0.417	97.707	4.629	1.079
16	5	4	1.275	0.04166	0.09017	2.516	3.543	173.382	48836.359	0.348	98.055	0.926	1.079
17	2	6	1.054	0.10710	0.00105	57.336	3.878	129.569	48965.926	0.260	98.315	2.314	0.540
18	3	7	0.922	0.10621	0.00155	36.258	3.842	125.370	49091.293	0.252	98.567	1.543	0.617
19	4	7	1.070	0.09149	0.00155	36.114	3.842	107.585	49198.875	0.216	98.783	1.157	0.617
20	4	2	1.553	0.09149	0.11217	0.498	2.560	67.743	49266.617	0.136	98.919	1.157	2.158
21	5	3	1.470	0.04166	0.11004	0.735	3.240	56.557	49323.172	0.114	99.033	0.926	1.439
22	3	5	0.688	0.10621	0.00673	3.576	3.698	48.930	49372.102	0.098	99.131	1.543	0.863
23	5	5	1.167	0.04166	0.00673	7.314	3.698	39.267	49411.367	0.079	99.210	0.926	0.863
24	2	1	1.531	0.10710	0.11264	0.550	1.000	34.393	49445.758	0.069	99.279	2.314	4.317
25	3	6	0.762	0.10621	0.00265	5.613	3.787	30.917	49476.672	0.062	99.341	1.543	0.719
26	2	7	0.823	0.10710	0.00155	9.348	3.842	30.886	49507.555	0.062	99.403	2.314	0.617
27	2	5	0.496	0.10710	0.00673	1.756	3.698	24.228	49531.781	0.049	99.451	2.314	0.863
28	3	6	1.139	0.10621	0.00105	10.680	3.878	23.936	49555.715	0.048	99.500	1.543	0.540
29	1	7	0.772	0.10790	0.00155	6.041	3.842	20.110	49575.824	0.040	99.540	4.629	0.617
30	1	5	0.398	0.10790	0.00673	1.411	3.698	19.610	49595.434	0.039	99.579	4.629	0.863
31	5	2	1.709	0.04166	0.11217	0.270	2.560	16.721	49612.152	0.034	99.613	0.926	2.158
32	5	6	1.163	0.04166	0.00265	7.657	3.787	16.549	49628.699	0.033	99.646	0.926	0.719
33	2	6	0.632	0.10710	0.00265	2.757	3.787	15.309	49644.008	0.031	99.677	2.314	0.719
34	1	0	1.970	0.10790	0.11301	0.120	2.000	15.174	49659.180	0.030	99.707	4.629	9999.996
35	2	0	1.970	0.10710	0.11301	0.120	2.000	15.046	49674.223	0.030	99.737	2.314	9999.996
36	3	0	1.973	0.10621	0.11301	0.119	2.000	14.818	49689.039	0.030	99.767	1.543	9999.996
37	3	1	1.751	0.10621	0.11264	0.233	1.000	14.473	49703.512	0.029	99.796	1.543	4.317
38	4	0	1.961	0.09149	0.11301	0.117	2.000	12.504	49716.012	0.025	99.821	1.157	9999.996
39	1	6	0.568	0.10790	0.00265	2.174	3.787	12.163	49728.172	0.024	99.846	4.629	0.719
40	6	4	1.495	0.00913	0.09017	0.652	3.543	9.836	49738.004	0.020	99.866	0.771	1.079

THE TOTAL RESPONSE OF ALL OTHER MODES AT 89.125 HZ = 66.965 100.000

TOTAL RESPONSE = 49804.969

HISTOGRAM PLOT OF PERCENTAGE RESPONSE AGAINST NORMALISED RESONANCE FREQUENCY.

```
                0                        25                        50                        75                       100
RANK   FMN/F    I                        I                         I                         I                         I
 13    0.223
 15    0.270
 14    0.357
 30    0.398
 12    0.457    0
 27    0.496
 39    0.568
  9    0.578    0
 33    0.632
 22    0.688
  5    0.741    00
 25    0.762
 29    0.772
 26    0.823
  4    0.917    0000
  3    0.922    000000000000
 18    0.922
  7    0.925    0
 10    0.948    0
  2    0.950    00000000000000000000000000000
  8    1.009    0
  1    1.024    0000000000000000000000000000000000000000000
 17    1.054
 19    1.070
 28    1.139
 32    1.163
 23    1.167
  6    1.245    0
 16    1.275
 11    1.315    0
 21    1.470
 40    1.495
 24    1.531
 20    1.553
 31    1.709
 37    1.751
 34    1.970
 35    1.970
 36    1.973
 38    1.961
```

LEGEND

FMN/F	= Resonant frequency of m,n mode/frequency
J2M(W)	= Joint acceptance in x-direction, $j_m^2(\omega)$
J2N(W)	= Joint acceptance in y-direction, $j_n^2(\omega)$
H	= $H^2(\omega/\omega_{mn})$
BMN	= β_{mn}
RESPONSE	= Response of m,nth mode $(g^2/(psi)^2)$
CUM. RES.	= Cumulative Response
PR	= Percentage of total response for m,nth mode
PCR	= Cumulative response percentage of total response
SXW/AW	= Structural wavelength, x-direction/acoustic wavelength
SYW/AW	= Structural wavelength, y-direction/acoustic wavelength

Table 16: Forty Most Dominant Response Modes of the SLA Structure for Reverberant Acoustic Field, f = 177.827 Hz

FREQUENCY = 177.827 ACOUSTIC WAVELENGTH = 75.579

RANK	M	N	FMN/F	J2M(W).	J2N(W).	H.	BMN	RESPONSE.	CUM. RES.	PR	PCR	SXW/AW	SYW/AW
1	8	3	0.988	0.05144	0.05728	203.939	3.240	10077.074	10077.074	8.255	8.255	1.154	2.871
2	8	7	0.974	0.05144	0.05613	145.901	3.842	8375.355	18452.430	6.861	15.116	1.154	1.230
3	5	0	1.001	0.05376	0.05737	224.413	2.000	7165.664	25618.094	5.870	20.986	1.847	9999.996
4	4	0	0.993	0.05396	0.05737	217.677	2.000	6976.070	32594.164	5.715	26.701	2.309	9999.996
5	3	0	0.989	0.05404	0.05737	206.709	2.000	6633.961	39228.125	5.434	32.135	3.078	9999.996
6	2	0	0.988	0.05410	0.05737	202.212	2.000	6497.352	45725.477	5.323	37.458	4.618	9999.996
7	1	0	0.987	0.05413	0.05737	201.503	2.000	6477.801	52203.277	5.307	42.764	9.235	9999.996
8	6	0	1.016	0.05355	0.05737	177.284	2.000	5638.172	57841.449	4.619	47.383	1.539	9999.996
9	7	2	0.972	0.05280	0.05734	138.625	2.560	5560.152	63401.602	4.555	51.938	1.319	4.307
10	8	2	1.032	0.05144	0.05734	113.173	2.560	4422.590	67824.188	3.623	55.561	1.154	4.307
11	8	8	1.045	0.05144	0.05340	74.422	3.878	4102.957	71927.125	3.361	58.922	1.154	1.077
12	8	4	0.949	0.05144	0.05719	72.318	3.543	3901.724	75828.813	3.196	62.118	1.154	2.153
13	6	1	0.988	0.05355	0.05736	205.096	1.000	3260.823	79089.625	2.671	64.789	1.539	8.613
14	9	5	1.044	0.03577	0.05704	77.567	3.698	3029.458	82119.063	2.482	67.271	1.026	1.723
15	8	6	0.935	0.05144	0.05676	50.757	3.787	2904.515	85023.563	2.379	69.650	1.154	1.436
16	7	0	1.041	0.05280	0.05737	85.002	2.000	2665.320	87688.875	2.183	71.834	1.319	9999.996
17	8	5	0.928	0.05144	0.05704	43.544	3.698	2445.549	90134.375	2.003	73.837	1.154	1.723
18	7	1	1.022	0.05280	0.05736	151.102	1.000	2368.600	92502.938	1.940	75.777	1.319	8.613
19	9	4	1.051	0.03577	0.05719	63.026	3.543	2364.696	94867.625	1.937	77.715	1.026	2.153
20	7	8	0.924	0.05280	0.05340	39.927	3.878	2259.282	97126.875	1.851	79.565	1.319	1.077
21	9	6	1.060	0.03577	0.05676	49.517	3.787	1970.486	99097.313	1.614	81.180	1.026	1.436
22	5	1	0.960	0.05376	0.05736	96.298	1.000	1537.184	100634.438	1.259	82.439	1.847	8.613
23	7	3	0.908	0.05280	0.05728	29.174	3.240	1479.596	102114.000	1.212	83.651	1.319	2.871
24	6	2	0.917	0.05355	0.05734	34.194	2.560	1391.070	103505.063	1.140	84.790	1.539	4.307
25	7	9	1.028	0.05280	0.00970	125.380	3.903	1296.466	104801.500	1.062	85.852	1.319	0.957
26	9	3	1.073	0.03577	0.05728	35.453	3.240	1218.237	106019.688	0.998	86.850	1.026	2.871
27	8	0	1.076	0.05144	0.05737	31.830	2.000	972.413	106992.063	0.797	87.647	1.154	9999.996
28	9	7	1.103	0.03577	0.05613	18.945	3.842	756.295	107748.313	0.620	88.266	1.026	1.230
29	7	7	0.852	0.05280	0.05613	12.694	3.842	747.908	108496.188	0.613	88.879	1.319	1.230
30	7	4	0.850	0.05280	0.05719	12.530	3.543	693.845	109190.000	0.568	89.447	1.319	2.153
31	4	1	0.928	0.05396	0.05736	43.052	1.000	669.751	109879.750	0.565	90.012	2.309	8.613
32	8	1	1.065	0.05144	0.05736	43.061	1.000	657.654	110537.375	0.539	90.551	1.154	8.613
33	5	2	0.857	0.05376	0.05734	13.496	2.560	551.226	111088.563	0.452	91.003	1.847	4.307
34	9	2	1.100	0.03577	0.05734	20.074	2.560	545.506	111634.063	0.447	91.449	1.026	4.307
35	7	6	0.815	0.05280	0.05676	8.619	3.787	506.222	112140.250	0.415	91.864	1.319	1.436
36	6	3	0.828	0.05355	0.05728	9.777	3.240	502.906	112643.125	0.412	92.276	1.539	2.871
37	7	5	0.816	0.05280	0.05704	8.692	3.698	501.032	113144.125	0.410	92.687	1.319	1.723
38	6	8	0.814	0.05355	0.05340	8.539	3.878	490.090	113634.188	0.401	93.088	1.539	1.077
39	6	9	0.923	0.05355	0.00970	38.715	3.903	406.029	114040.188	0.333	93.421	1.539	0.957
40	5	10	0.972	0.05376	0.00215	136.123	3.921	319.354	114359.500	0.262	93.682	1.847	0.861

THE TOTAL RESPONSE OF ALL OTHER MODES AT 177.827 HZ = 7712.313 100.000

TOTAL RESPONSE = 122071.813

HISTOGRAM PLOT OF PERCENTAGE RESPONSE AGAINST NORMALISED RESONANCE FREQUENCY.

RANK	FMN/F	0 I ... 25 I ... 50 I ... 75 I ... 100 I
38	0.814	
35	0.815	
37	0.816	
36	0.828	
30	0.850	O
29	0.852	O
33	0.857	
23	0.908	O
24	0.917	O
39	0.923	
20	0.924	OO
31	0.928	O
17	0.928	OO
15	0.935	OO
12	0.949	OOO
22	0.960	O
40	0.972	
9	0.972	OOOOO
2	0.974	OOOOOOO
7	0.987	OOOOO
6	0.988	OOOOO
1	0.988	OOOOOOOO
13	0.988	OOO
5	0.989	OOOOO
4	0.993	OOOOOO
3	1.001	OOOOOO
8	1.016	OOOOO
18	1.022	OO
25	1.028	O
10	1.032	OOOO
16	1.041	OO
14	1.044	OO
11	1.045	OOO
19	1.051	OO
21	1.060	OO
32	1.065	O
26	1.073	O
27	1.078	O
34	1.100	
28	1.103	O

LEGEND

- FMN/F = Resonant frequency of m,n mode/frequency
- J2M(W) = Joint acceptance in x-direction, $j_m^2(\omega)$
- J2N(W) = Joint acceptance in y-direction, $j_n^2(\omega)$
- H = $H^2(\omega/\omega_{mn})$
- BMN = β_{mn}
- RESPONSE = Response of m,nth mode $(g^2/(psi)^2)$
- CUM. RES. = Cumulative Response
- PR = Percentage of total response for m,nth mode
- PCR = Cumulative response percentage of total response
- SXW/AW = Structural wavelength, x-direction/acoustic wavelength
- SYW/AW = Structural wavelength, y-direction/acoustic wavelength

Table 17: Forty Most Dominant Response Modes of the SLA Structure for Reverberant Acoustic Field, f = 223.871 Hz

FREQUENCY = 223.871   ACOUSTIC WAVELENGTH = 60.035

RANK	M	N	FMN/F	J2M(W).	J2N(W).	H.	BMN	RESPONSE.	CUM. RES.	PR	PCR	SXW/AW	SYW/AW
1	8	10	1.012	0.04257	0.04369	195.732	3.921	7386.957	7386.957	8.939	8.939	1.453	1.084
2	10	7	0.986	0.04165	0.04539	194.829	3.842	7324.352	14711.309	8.863	17.802	1.163	1.549
3	9	9	1.014	0.04199	0.04482	188.216	3.903	7155.871	21867.180	8.659	26.461	1.292	1.205
4	11	4	1.017	0.03502	0.04562	172.310	3.543	5048.797	26915.977	6.110	32.571	1.057	2.711
5	11	3	1.014	0.03502	0.04565	185.378	3.240	4970.164	31886.141	6.014	38.585	1.057	3.615
6	11	2	1.017	0.03502	0.04567	174.291	2.560	3693.771	35579.910	4.470	43.055	1.057	5.422
7	11	5	1.030	0.03502	0.04557	117.518	3.698	3590.322	39170.230	4.345	47.400	1.057	2.169
8	10	8	1.045	0.04165	0.04521	74.275	3.878	2806.929	41977.156	3.397	50.796	1.163	1.355
9	11	0	1.022	0.03502	0.04568	151.118	2.000	2502.880	44480.035	3.029	53.825	1.057	9999.996
10	10	6	0.946	0.04165	0.04550	67.125	3.787	2493.411	46973.445	3.017	56.842	1.163	1.807
11	9	8	0.934	0.04199	0.04521	49.646	3.878	1891.408	48864.852	2.289	59.131	1.292	1.355
12	11	6	1.058	0.03502	0.04550	52.558	3.787	1641.634	50506.484	1.987	61.118	1.057	1.807
13	10	0	0.952	0.04165	0.04568	79.063	2.000	1557.313	52063.797	1.885	63.002	1.163	9999.996
14	6	11	0.965	0.04283	0.01593	111.403	3.935	1548.276	53612.070	1.874	64.876	1.938	0.986
15	10	5	0.926	0.04165	0.04557	41.563	3.698	1510.121	55122.191	1.827	66.703	1.163	2.169
16	10	2	0.939	0.04165	0.04567	56.103	2.560	1414.025	56536.215	1.711	68.414	1.163	5.422
17	7	10	0.920	0.04266	0.04369	36.868	3.921	1395.213	57931.426	1.688	70.103	1.661	1.084
18	10	3	0.928	0.04165	0.04565	43.493	3.240	1386.785	59318.211	1.678	71.781	1.163	3.615
19	10	4	0.922	0.04165	0.04562	37.924	3.543	1321.507	60639.715	1.599	73.380	1.163	2.711
20	11	1	1.020	0.03502	0.04568	158.112	1.000	1309.255	61948.969	1.584	74.964	1.057	10.844
21	8	9	0.911	0.04257	0.04482	30.416	3.903	1172.316	63121.285	1.419	76.383	1.453	1.205
22	7	11	1.042	0.04266	0.01593	81.354	3.935	1126.165	64247.449	1.363	77.746	1.661	0.986
23	10	1	0.949	0.04165	0.04568	71.534	1.000	704.452	64951.898	0.852	78.598	1.163	10.844
24	9	7	0.877	0.04199	0.04539	17.511	3.842	663.636	65615.500	0.803	79.401	1.292	1.549
25	11	7	1.102	0.03502	0.04539	19.513	3.842	616.822	66232.313	0.746	80.148	1.057	1.549
26	9	10	1.113	0.04199	0.04369	15.917	3.921	592.533	66824.813	0.717	80.865	1.292	1.084
27	10	9	1.125	0.04165	0.04482	13.056	3.903	492.403	67317.188	0.596	81.460	1.163	1.205
28	9	0	0.898	0.04199	0.04568	24.192	2.000	480.373	67797.500	0.581	82.042	1.292	9999.996
29	9	2	0.874	0.04199	0.04567	16.918	2.560	429.846	68227.313	0.520	82.562	1.292	5.422
30	9	6	0.842	0.04199	0.04550	11.367	3.787	425.654	68652.938	0.515	83.077	1.292	1.807
31	6	10	0.840	0.04283	0.04369	11.148	3.921	423.351	69076.250	0.512	83.589	1.938	1.084
32	9	3	0.853	0.04199	0.04565	12.845	3.240	412.867	69489.063	0.500	84.089	1.292	3.615
33	8	8	0.830	0.04257	0.04521	10.047	3.878	388.024	69877.063	0.470	84.558	1.453	1.355
34	4	12	0.989	0.04294	0.00209	206.009	3.945	378.206	70255.250	0.458	85.016	2.907	0.904
35	9	4	0.835	0.04199	0.04562	10.537	3.543	370.139	70625.375	0.448	85.464	1.292	2.711
36	9	5	0.829	0.04199	0.04557	9.933	3.698	363.829	70989.188	0.440	85.904	1.292	2.169
37	5	11	0.899	0.04288	0.01593	24.703	3.935	343.671	71332.813	0.416	86.320	2.325	0.986
38	7	9	0.817	0.04266	0.04482	8.787	3.903	339.428	71672.188	0.411	86.730	1.661	1.205
39	8	0	0.856	0.04257	0.04568	13.432	2.000	270.390	71942.563	0.327	87.058	1.453	9999.996
40	11	8	1.165	0.03502	0.04521	7.528	3.878	239.205	72181.750	0.289	87.347	1.057	1.355

THE TOTAL RESPONSE OF ALL OTHER MODES AT 223.871 HZ = 10456.125 100.000

TOTAL RESPONSE = 82637.875

HISTOGRAM PLOT OF PERCENTAGE RESPONSE AGAINST NORMALISED RESONANCE FREQUENCY.

```
                 0                        25                        50                        75                        100
RANK    FMN/F    I                         I                         I                         I                         I
 38     0.817
 36     0.829
 33     0.830
 35     0.835
 31     0.840    0
 30     0.842    0
 32     0.853
 39     0.856
 29     0.874    0
 24     0.877    0
 28     0.898    0
 37     0.899
 21     0.911    0
 17     0.920    00
 19     0.922    00
 15     0.926    00
 18     0.928    00
 11     0.934    00
 16     0.939    00
 10     0.946    000
 23     0.949    0
 13     0.952    00
 14     0.965    00
  2     0.986    0000000000
 34     0.989
  1     1.012    0000000000
  3     1.014    0000000000
  5     1.014    000000
  6     1.017    0000
  4     1.017    000000
 20     1.020    00
  9     1.022    000
  7     1.030    0000
 22     1.042    0
  8     1.045    000
 12     1.058    00
 25     1.102    0
 26     1.113    0
 27     1.125    0
 40     1.165
```

LEGEND

- FMN/F = Resonant frequency of m,n mode/frequency
- J2M(W) = Joint acceptance in x-direction, $j_m^2(\omega)$
- J2N(W) = Joint acceptance in y-direction, $j_n^2(\omega)$
- H = $H^2(\omega/\omega_{mn})$
- BMN = β_{mn}
- RESPONSE = Response of m,nth mode $(g^2/(psi)^2)$
- CUM. RES. = Cumulative Response
- PR = Percentage of total response for m,nth mode
- PCR = Cumulative response percentage of total response
- SXW/AW = Structural wavelength, x-direction/acoustic wavelength
- SYW/AW = Structural wavelength, y-direction/acoustic wavelength

Table 18: Forty Most Dominant Response Modes of the SLA Structure for Reverberant Acoustic Field, f = 398.105 Hz

FREQUENCY = 398.105   ACOUSTIC WAVELENGTH = 33.760

RANK	M	N	FMN/F	J2M(W).	J2N(W).	H.	BMN	RESPONSE.	CUM. RES.	PR	PCR	SXW/AW	SYW/AW
1	8	15	0.992	0.02415	0.02557	216.858	3.965	2748.583	2748.583	4.112	4.112	2.584	1.286
2	10	14	1.006	0.02413	0.02563	215.908	3.959	2736.814	5485.395	4.094	8.207	2.068	1.377
3	14	10	0.992	0.02402	0.02574	216.616	3.921	2718.540	8203.934	4.067	12.274	1.477	1.928
4	6	16	1.013	0.02417	0.02547	190.374	3.969	2407.487	10611.418	3.602	15.876	3.446	1.205
5	16	6	0.987	0.02386	0.02578	199.012	3.787	2401.254	13012.672	3.592	19.468	1.292	3.214
6	11	13	0.980	0.02412	0.02567	173.399	3.953	2197.014	15209.684	3.287	22.755	1.880	1.483
7	5	16	0.979	0.02417	0.02547	165.608	3.969	2097.336	17307.016	3.138	25.893	4.135	1.205
8	17	3	1.011	0.02383	0.02579	199.421	3.240	2055.082	19362.098	3.075	28.967	1.216	6.428
9	1	17	1.021	0.02414	0.02528	155.620	3.972	1955.926	21318.023	2.926	31.893	20.675	1.134
10	13	11	0.974	0.02406	0.02572	146.783	3.935	1851.397	23169.418	2.770	34.663	1.590	1.753
11	17	2	0.996	0.02383	0.02579	225.206	2.560	1833.854	25003.270	2.744	37.407	1.216	9.642
12	15	5	1.023	0.02400	0.02575	145.919	3.903	1821.774	26825.043	2.726	40.132	1.378	2.143
13	16	7	1.023	0.02388	0.02577	147.996	3.842	1811.147	28636.188	2.710	42.842	1.292	2.755
14	15	8	0.973	0.02400	0.02576	141.619	3.878	1757.373	30393.559	2.629	45.471	1.378	2.410
15	12	12	0.970	0.02409	0.02570	130.519	3.945	1650.214	32043.770	2.469	47.940	1.723	1.607
16	2	17	1.030	0.02415	0.02528	118.021	3.972	1483.291	33527.059	2.219	50.159	10.338	1.134
17	17	4	1.029	0.02383	0.02579	123.305	3.543	1369.470	34916.527	2.079	52.238	1.216	4.821
18	17	0	0.989	0.02383	0.02579	206.435	2.000	1313.365	36229.891	1.965	54.203	1.216	9999.996
19	16	5	0.958	0.02388	0.02578	91.702	3.698	1080.815	37310.703	1.617	55.820	1.292	3.857
20	4	16	0.951	0.02410	0.02547	75.401	3.969	953.882	38264.582	1.427	57.247	5.169	1.205
21	3	17	1.046	0.02415	0.02528	73.722	3.972	926.468	39191.047	1.386	58.633	6.892	1.134
22	9	15	1.046	0.02415	0.02557	72.870	3.965	923.352	40114.398	1.381	60.014	2.297	1.286
23	13	12	1.049	0.02406	0.02570	66.976	3.945	846.297	40960.691	1.266	61.281	1.590	1.607
24	9	14	0.945	0.02415	0.02563	65.607	3.959	832.198	41792.887	1.245	62.526	2.297	1.377
25	7	15	0.945	0.02416	0.02557	64.784	3.965	821.448	42614.332	1.229	63.755	2.954	1.286
26	12	13	1.059	0.02409	0.02567	59.066	3.953	747.741	43362.070	1.119	64.873	1.723	1.483
27	7	16	1.054	0.02416	0.02547	58.374	3.969	738.055	44100.129	1.104	65.977	2.954	1.205
28	17	5	1.053	0.02383	0.02578	60.079	3.698	706.506	44806.633	1.057	67.034	1.216	3.857
29	17	1	0.991	0.02383	0.02579	213.849	1.000	680.255	45486.887	1.018	68.052	1.216	19.283
30	14	11	1.059	0.02402	0.02572	51.194	3.935	644.286	46131.172	0.964	69.016	1.477	1.753
31	14	9	0.934	0.02402	0.02575	50.093	3.903	626.055	46757.227	0.937	69.953	1.477	2.143
32	16	4	0.935	0.02385	0.02579	51.244	3.543	578.745	47335.969	0.866	70.818	1.292	4.821
33	15	7	0.931	0.02400	0.02577	46.076	3.842	566.615	47902.582	0.848	71.666	1.378	2.755
34	3	16	0.929	0.02416	0.02547	44.266	3.969	560.106	48462.688	0.838	72.504	6.892	1.205
35	16	8	1.066	0.02386	0.02576	42.052	3.878	519.328	48982.016	0.777	73.281	1.292	2.410
36	4	17	1.067	0.02415	0.02528	40.991	3.972	515.064	49497.078	0.771	74.052	5.169	1.134
37	11	14	1.072	0.02412	0.02563	36.273	3.959	459.615	49956.691	0.688	74.739	1.880	1.377
38	10	13	0.914	0.02413	0.02567	32.195	3.953	408.081	50364.770	0.611	75.350	2.068	1.483
39	2	16	0.914	0.02416	0.02547	32.188	3.969	407.290	50772.059	0.609	75.959	10.338	1.205
40	16	3	0.919	0.02386	0.02579	35.771	3.240	369.462	51141.520	0.553	76.512	1.292	6.428

THE TOTAL RESPONSE OF ALL OTHER MODES AT 398.105 HZ = 15699.730 100.000

TOTAL RESPONSE = 66841.250

HISTOGRAM PLOT OF PERCENTAGE RESPONSE AGAINST NORMALISED RESONANCE FREQUENCY.

RANK	FMN/F	0 I ... 25 I ... 50 I ... 75 I ... 100 I
39	0.914	0
38	0.914	0
40	0.919	0
34	0.929	0
33	0.931	0
31	0.934	0
32	0.935	0
25	0.945	0
24	0.945	0
20	0.951	0
19	0.958	00
15	0.970	00
14	0.973	000
10	0.974	000
7	0.979	000
6	0.980	000
5	0.987	0000
18	0.989	00
29	0.991	0
3	0.992	0000
1	0.992	0000
11	0.998	000
2	1.006	0000
8	1.011	000
4	1.013	0000
9	1.021	000
13	1.023	000
12	1.023	000
17	1.029	00
16	1.030	00
21	1.046	0
22	1.046	0
23	1.049	0
28	1.053	0
26	1.053	0
27	1.054	0
30	1.059	0
35	1.066	0
36	1.067	0
37	1.072	0

LEGEND

FMN/F	= Resonant frequency of m,n mode/frequency
J2M(W)	= Joint acceptance in x-direction, $j_m^2(\omega)$
J2N(W)	= Joint acceptance in y-direction, $j_n^2(\omega)$
H	= $H^2(\omega/\omega_{mn})$
BMN	= β_{mn}
RESPONSE	= Response of m,nth mode $(g^2/(psi)^2)$
CUM. RES.	= Cumulative Response
PR	= Percentage of total response for m,nth mode
PCR	= Cumulative response percentage of total response
SXW/AW	= Structural wavelength, x-direction/acoustic wavelength
SYW/AW	= Structural wavelength, y-direction/acoustic wavelength

Table 19: Forty Most Dominant Response Modes of the SLA Structure for Boundary Layer Turbulence (U_c = 9810 in./sec; δ_b = 12.0 in.), f = 89.125 Hz

FREQUENCY = 89.125 ACOUSTIC WAVELENGTH = 110.070

RANK	M	N	FMN/F	J2M(W).	J2N(W).	H.	BMN	RESPONSE.	CUM. RES.	PR	PCR	SXW/AW	SYW/AW
1	4	4	1.024	0.03555	0.01068	142.942	3.543	995.247	995.247	21.472	21.472	1.585	1.479
2	1	8	1.009	0.02063	0.01012	207.269	3.878	868.946	1864.193	18.747	40.219	6.341	0.739
3	4	6	0.948	0.03555	0.01044	69.571	3.787	506.070	2370.263	10.918	51.137	1.585	0.986
4	3	3	0.950	0.02833	0.01077	73.841	3.240	377.754	2748.017	8.150	59.287	2.114	1.971
5	4	5	0.925	0.03555	0.01057	40.144	3.698	288.749	3036.766	6.230	65.517	1.585	1.183
6	4	7	1.070	0.03555	0.01029	38.114	3.842	277.227	3313.993	5.981	71.498	1.585	0.845
7	2	8	1.054	0.02339	0.01012	57.336	3.878	272.509	3586.502	5.879	77.377	3.171	0.739
8	3	7	0.922	0.02833	0.01029	38.258	3.842	221.806	3808.308	4.785	82.163	2.114	0.845
9	2	2	0.922	0.02339	0.01083	38.220	2.560	128.287	3936.595	2.768	84.930	3.171	2.957
10	5	6	1.163	0.04362	0.01044	7.657	3.787	68.652	4005.247	1.481	86.411	1.268	0.986
11	5	5	1.167	0.04362	0.01057	7.314	3.698	64.843	4070.090	1.399	87.810	1.268	1.183
12	3	8	1.139	0.02833	0.01012	10.680	3.878	61.485	4131.574	1.327	89.137	2.114	0.739
13	2	7	0.823	0.02339	0.01029	9.348	3.842	44.741	4176.313	0.965	90.102	3.171	0.845
14	1	1	0.917	0.02063	0.01087	34.132	1.000	39.612	4215.922	0.855	90.957	6.341	5.914
15	3	6	0.762	0.02833	0.01044	5.613	3.787	32.547	4248.465	0.702	91.659	2.114	0.986
16	3	4	0.741	0.02833	0.01068	4.854	3.543	26.940	4275.402	0.581	92.240	2.114	1.479
17	5	7	1.257	0.04382	0.01029	2.921	3.842	26.185	4301.586	0.565	92.805	1.268	0.845
18	1	7	0.772	0.02063	0.01029	6.041	3.842	25.505	4327.090	0.550	93.355	6.341	0.845
19	5	4	1.275	0.04382	0.01068	2.516	3.543	21.590	4348.676	0.466	93.821	1.268	1.479
20	4	3	1.245	0.03555	0.01077	3.219	3.240	20.663	4369.336	0.446	94.266	1.585	1.971
21	3	5	0.688	0.02833	0.01057	3.576	3.698	20.504	4389.840	0.442	94.709	2.114	1.183
22	4	8	1.264	0.03555	0.01012	2.739	3.878	19.780	4409.617	0.427	95.136	1.585	0.739
23	2	6	0.632	0.02339	0.01044	2.757	3.787	13.195	4422.809	0.285	95.420	3.171	0.986
24	6	6	1.391	0.04946	0.01044	1.130	3.787	11.441	4434.246	0.247	95.667	1.057	0.986
25	6	5	1.401	0.04946	0.01057	1.069	3.698	10.698	4444.941	0.231	95.898	1.057	1.183
26	1	9	1.277	0.02063	0.00994	2.471	3.903	10.239	4455.180	0.221	96.118	6.341	0.657
27	2	3	0.578	0.02339	0.01077	2.251	3.240	9.506	4464.684	0.205	96.324	3.171	1.971
28	1	6	0.568	0.02063	0.01044	2.174	3.787	9.179	4473.859	0.198	96.522	6.341	0.986
29	2	9	1.320	0.02339	0.00994	1.784	3.903	8.381	4482.238	0.181	96.702	3.171	0.657
30	2	5	0.496	0.02339	0.01057	1.756	3.698	8.313	4490.551	0.179	96.882	3.171	1.183
31	5	8	1.428	0.04362	0.01012	0.916	3.878	8.169	4498.719	0.176	97.058	1.268	0.739
32	3	2	1.315	0.02833	0.01083	1.853	2.560	7.535	4506.254	0.163	97.220	2.114	2.957
33	6	7	1.469	0.04946	0.01029	0.741	3.842	7.495	4513.746	0.162	97.382	1.057	0.845
34	2	4	0.457	0.02339	0.01068	1.596	3.543	7.311	4521.056	0.158	97.540	3.171	1.479
35	6	4	1.495	0.04946	0.01068	0.652	3.543	6.314	4527.367	0.136	97.676	1.057	1.479
36	3	9	1.397	0.02833	0.00994	1.091	3.903	6.209	4533.574	0.134	97.810	2.114	0.657
37	1	5	0.398	0.02063	0.01057	1.411	3.698	5.891	4539.465	0.127	97.937	6.341	1.183
38	5	3	1.470	0.04382	0.01077	0.735	3.240	5.817	4545.281	0.126	98.062	1.268	1.971
39	1	4	0.270	0.02063	0.01068	1.163	3.543	4.702	4549.980	0.101	98.164	6.341	1.479
40	4	9	1.511	0.03555	0.00994	0.605	3.903	4.318	4554.297	0.093	98.257	1.585	0.657

THE TOTAL RESPONSE OF ALL OTHER MODES AT 89.125 HZ = 80.793 100.000

TOTAL RESPONSE = 4635.090

HISTOGRAM PLOT OF PERCENTAGE RESPONSE AGAINST NORMALISED RESONANCE FREQUENCY.

```
                  0                         25                        50                        75                        100
RANK    FMN/F     I                         I                         I                         I                         I
 39     0.270
 37     0.398
 34     0.457
 30     0.496
 28     0.568
 27     0.578
 23     0.632
 21     0.688
 16     0.741     0
 15     0.762     0
 18     0.772     0
 13     0.823     0
 14     0.917     0
  9     0.922     000
  8     0.922     00000
  5     0.925     000000
  3     0.948     00000000000
  4     0.950     00000000
  2     1.009     0000000000000000000
  1     1.024     000000000000000000000
  7     1.054     000000
  6     1.070     000000
 12     1.139     0
 10     1.163     0
 11     1.167     0
 20     1.245
 17     1.257     0
 22     1.264
 19     1.275
 26     1.277
 32     1.315
 29     1.320
 24     1.391
 36     1.397
 25     1.401
 31     1.428
 33     1.469
 38     1.470
 35     1.495
 40     1.511
```

LEGEND

- FMN/F = Resonant frequency of m,n mode/frequency
- J2M(W) = Joint acceptance in x-direction, $j_m^2(\omega)$
- J2N(W) = Joint acceptance in y-direction, $j_n^2(\omega)$
- H = $H^2(\omega/\omega_{mn})$
- BMN = β_{mn}
- RESPONSE = Response of m,nth mode $(g^2/(psi)^2)$
- CUM. RES. = Cumulative Response
- PR = Percentage of total response for m,nth mode
- PCR = Cumulative response percentage of total response
- SXW/AW = Structural wavelength, x-direction/acoustic wavelength
- SYW/AW = Structural wavelength, y-direction/acoustic wavelength

Table 20: Forty Most Dominant Response Modes of the SLA · Structure for Boundary Layer Turbulence (U_c = 9810 in./sec; δ_b = 12.0 in.), f = 177.827 Hz

FREQUENCY = 177.827 ACOUSTIC WAVELENGTH = 55.166

RANK	M	N	FMN/F	J2M(W).	J2N(W).	H.	BMN	RESPONSE.	CUM. RES.	PR	PCR	SXW/AW	SYW/AW
1	8	3	0.988	0.01792	0.00772	203.939	3.240	472.809	472.809	7.543	7.543	1.582	3.934
2	8	7	0.974	0.01792	0.00754	145.901	3.842	391.802	864.610	6.250	13.793	1.582	1.686
3	7	9	1.028	0.01442	0.00740	175.380	3.903	270.425	1135.035	4.314	18.107	1.808	1.311
4	9	5	1.044	0.02257	0.00764	77.567	3.698	256.165	1391.200	4.087	22.193	1.406	2.360
5	3	11	1.013	0.00764	0.00724	189.809	3.935	219.374	1610.574	3.500	25.693	4.218	1.073
6	8	2	1.032	0.01792	0.00774	113.173	2.560	207.926	1818.500	3.317	29.010	1.582	5.900
7	7	2	0.972	0.01442	0.00774	138.625	2.560	205.058	2023.558	3.271	32.281	1.808	5.900
8	5	10	0.972	0.01005	0.00732	136.123	3.921	203.261	2226.819	3.243	35.524	2.531	1.180
9	9	4	1.051	0.02257	0.00769	63.026	3.543	200.479	2427.298	3.198	38.722	1.406	2.950
10	8	6	1.045	0.01792	0.00747	74.422	3.878	200.008	2627.306	3.191	41.913	1.582	1.475
11	8	4	0.949	0.01792	0.00769	72.318	3.543	182.598	2809.904	2.913	44.825	1.582	2.950
12	5	0	1.001	0.01005	0.00776	224.413	2.000	181.069	2990.973	2.889	47.714	2.531	9999.996
13	2	11	0.977	0.00725	0.00724	160.167	3.935	171.143	3162.115	2.730	50.444	6.326	1.073
14	6	0	1.016	0.01188	0.00776	177.284	2.000	169.126	3331.242	2.698	53.142	2.109	9999.996
15	9	6	1.060	0.02257	0.00760	49.517	3.767	166.371	3497.613	2.654	55.796	1.406	1.967
16	4	0	0.993	0.00874	0.00776	217.677	2.000	152.864	3650.477	2.439	58.235	3.163	9999.996
17	8	6	0.935	0.01792	0.00760	50.757	3.767	135.370	3785.846	2.160	60.394	1.582	1.967
18	3	0	0.989	0.00764	0.00776	206.709	2.000	130.164	3916.010	2.076	62.471	4.218	9999.996
19	2	0	0.988	0.00725	0.00776	202.712	2.000	117.721	4033.731	1.878	64.349	6.326	9999.996
20	8	5	0.928	0.01792	0.00764	43.544	3.698	114.150	4147.879	1.821	66.170	1.582	2.360
21	1	0	0.987	0.00691	0.00776	201.503	2.000	111.886	4259.762	1.785	67.955	12.653	9999.996
22	9	3	1.073	0.02257	0.00772	35.453	3.240	103.547	4363.309	1.652	69.606	1.406	3.934
23	7	0	1.041	0.01442	0.00776	85.002	2.000	98.466	4461.773	1.571	71.177	1.808	9999.996
24	6	1	0.988	0.01188	0.00775	205.096	1.000	97.771	4559.543	1.560	72.737	2.109	11.801
25	6	10	1.058	0.01188	0.00732	52.533	3.921	92.747	4652.289	1.480	74.216	2.109	1.180
26	1	11	0.956	0.00691	0.00724	88.138	3.935	89.825	4742.113	1.433	75.649	12.653	1.073
27	7	1	1.022	0.01442	0.00775	151.102	1.000	87.466	4829.578	1.395	77.045	1.808	11.801
28	7	6	0.924	0.01442	0.00747	39.927	3.878	86.393	4915.969	1.378	78.423	1.808	1.475
29	6	9	0.923	0.01188	0.00740	38.715	3.903	68.767	4984.734	1.097	79.520	2.109	1.311
30	9	7	1.103	0.02257	0.00754	16.945	3.842	64.093	5048.824	1.022	80.542	1.406	1.686
31	4	11	1.064	0.00874	0.00724	43.941	3.935	56.637	5105.461	0.904	81.446	3.163	1.073
32	7	3	0.908	0.01442	0.00772	29.174	3.240	54.457	5159.914	0.869	82.314	1.808	3.934
33	9	2	1.100	0.02257	0.00774	20.074	2.560	46.461	5206.371	0.741	83.056	1.406	5.900
34	8	0	1.078	0.01792	0.00776	31.830	2.000	45.796	5252.164	0.731	83.786	1.582	9999.996
35	6	2	0.917	0.01188	0.00774	34.194	2.560	41.656	5293.816	0.665	84.451	2.109	5.900
36	5	1	0.960	0.01005	0.00775	96.298	1.000	38.826	5332.641	0.619	85.070	2.531	11.801
37	4	10	0.902	0.00874	0.00732	25.866	3.921	33.616	5366.254	0.536	85.606	3.163	1.180
38	10	4	1.160	0.02836	0.00769	7.926	3.543	31.683	5397.934	0.505	86.111	1.265	2.950
39	8	1	1.065	0.01792	0.00775	43.061	1.000	30.959	5428.891	0.494	86.605	1.582	11.801
40	10	5	1.166	0.02836	0.00764	7.397	3.698	30.699	5459.586	0.490	87.095	1.265	2.360

THE TOTAL RESPONSE OF ALL OTHER MODES AT 177.827 HZ = 808.957 100.000

TOTAL RESPONSE = 6268.543

HISTOGRAM PLOT OF PERCENTAGE RESPONSE AGAINST NORMALISED RESONANCE FREQUENCY.

```
               0                        25                        50                        75                        100
RANK   FMN/F   I                        I                         I                         I                         I
 37    0.902   O
 32    0.908   O
 35    0.917   O
 29    0.923   O
 28    0.924   O
 20    0.928   OO
 17    0.935   OO
 11    0.949   OOO
 26    0.956   O
 36    0.960   O
  8    0.972   OOO
  7    0.972   OOO
  2    0.974   OOOOOO
 13    0.977   OOO
 21    0.987   OO
 19    0.988   OO
  1    0.988   OOOOOOOO
 24    0.988   OO
 18    0.989   OO
 16    0.993   OO
 12    1.001   OOO
  5    1.013   OOO
 14    1.016   OOO
 27    1.022   O
  3    1.028   OOOO
  6    1.032   OOO
 23    1.041   OO
  4    1.044   OOOO
 10    1.045   OOO
  9    1.051   OOO
 25    1.058   O
 15    1.060   OOO
 31    1.064   O
 39    1.065
 22    1.073   OO
 34    1.078   O
 33    1.100   O
 30    1.103   O
 38    1.160   O
 40    1.166
```

LEGEND

FMN/F	= Resonant frequency of m,n mode/frequency
J2M(W)	= Joint acceptance in x-direction, $j_m^2(\omega)$
J2N(W)	= Joint acceptance in y-direction, $j_n^2(\omega)$
H	= $H^2(\omega/\omega_{mn})$
BMN	= β_{mn}
RESPONSE	= Response of m,nth mode $(g^2/(psi)^2)$
CUM. RES.	= Cumulative Response
PR	= Percentage of total response for m,nth mode
PCR	= Cumulative response percentage of total response
SXW/AW	= Structural wavelength, x-direction/acoustic wavelength
SYW/AW	= Structural wavelength, y-direction/acoustic wavelength

Table 21: Forty Most Dominant Response Modes of the SLA Structure for Boundary Layer Turbulence (U_c = 9810 in./sec; δ_b = 12.0 in.), f = 223.871 Hz

FREQUENCY = 223.871 ACOUSTIC WAVELENGTH = 43.820

RANK	M	N	FMN/F	J2M(W).	J2N(W).	H.	BMN	RESPONSE.	CUM. RES.	PR	PCR	SXW/AW	SYW/AW
1	11	4	1.017	0.01662	0.00670	172.310	3.543	352.119	352.119	7.413	7.413	1.448	3.714
2	11	3	1.014	0.01662	0.00673	185.378	3.240	347.489	699.608	7.316	14.729	1.448	4.952
3	10	7	0.986	0.01347	0.00661	194.229	3.842	344.737	1044.345	7.258	21.986	1.593	2.122
4	9	9	1.014	0.01109	0.00651	188.216	3.903	274.667	1319.011	5.782	27.769	1.770	1.651
5,	11	2	1.017	0.01662	0.00674	174.291	2.560	258.718	1577.730	5.447	33.215	1.448	7.428
6	11	5	1.030	0.01662	0.00668	117.518	3.698	243.650	1827.380	5.256	38.471	1.448	2.971
7	8	10	1.012	0.00935	0.00646	195.732	3.921	238.720	2066.100	5.026	43.497	1.991	1.486
8	11	0	1.022	0.01662	0.00675	151.118	2.000	175.566	2241.666	3.696	47.193	1.448	9999.996
9	4	12	0.989	0.00564	0.00634	206.009	3.945	150.447	2392.113	3.167	50.360	3.982	1.238
10	10	8	1.045	0.01347	0.00656	74.275	3.878	131.795	2523.907	2.775	53.135	1.593	1.857
11	10	6	0.946	0.01347	0.00664	67.125	3.767	117.749	2641.657	2.479	55.614	1.593	2.476
12	11	6	1.058	0.01662	0.00664	52.558	3.787	113.767	2755.424	2.395	58.009	1.448	2.476
13	6	11	0.965	0.00695	0.00640	111.403	3.935	100.976	2856.400	2.126	60.135	2.655	1.351
14	11	1	1.020	0.01662	0.00675	158.112	1.000	91.804	2948.204	1.933	62.068	1.448	14.856
15	7	11	1.042	0.00796	0.00640	81.354	3.935	84.432	3032.636	1.778	63.845	2.276	1.351
16	10	0	0.952	0.01347	0.00675	79.063	2.000	74.439	3107.074	1.567	65.412	1.593	9999.996
17	9	8	0.934	0.01109	0.00656	49.646	3.878	72.519	3179.594	1.527	66.939	1.770	1.857
18	10	5	0.926	0.01347	0.00668	41.563	3.698	71.554	3251.147	1.506	68.445	1.593	2.971
19	5	12	1.041	0.00623	0.00634	85.831	3.945	68.367	3320.015	1.450	69.895	3.186	1.238
20	10	2	0.939	0.01347	0.00674	56.103	2.560	67.490	3387.504	1.421	71.316	1.593	7.428
21	10	3	0.928	0.01347	0.00673	43.493	3.240	66.070	3453.574	1.391	72.707	1.593	4.952
22	10	4	0.922	0.01347	0.00670	37.924	3.543	62.805	3516.379	1.322	74.029	1.593	3.714
23	3	12	0.949	0.00524	0.00634	71.680	3.945	48.646	3565.024	1.024	75.053	5.310	1.238
24	11	7	1.102	0.01662	0.00661	19.513	3.842	42.605	3607.629	0.897	75.950	1.448	2.122
25	7	10	0.920	0.00796	0.00646	36.888	3.921	38.497	3646.125	0.810	76.761	2.276	1.486
26	12	3	1.112	0.02070	0.00673	16.231	3.240	37.882	3684.007	0.798	77.558	1.327	4.952
27	8	9	0.911	0.00933	0.00651	30.416	3.903	37.229	3721.236	0.784	78.342	1.991	1.651
28	12	4	1.123	0.02070	0.00670	13.587	3.543	34.570	3755.806	0.728	79.070	1.327	3.714
29	10	1	0.949	0.01347	0.00675	71.534	1.000	33.660	3789.466	0.709	79.778	1.593	14.856
30	12	2	1.108	0.02070	0.00674	17.465	2.560	32.317	3821.782	0.680	80.459	1.327	7.428
31	1	13	1.061	0.00482	0.00628	47.622	3.953	29.463	3851.245	0.620	81.079	15.929	1.143
32	12	5	1.143	0.02070	0.00668	9.964	3.698	26.356	3877.601	0.555	81.634	1.327	2.971
33	12	0	1.107	0.02073	0.00675	17.830	2.000	25.791	3903.392	0.543	82.177	1.327	9999.996
34	9	7	0.877	0.01109	0.00661	17.511	3.842	25.507	3928.898	0.537	82.714	1.770	2.122
35	2	12	0.921	0.00497	0.00634	37.163	3.945	23.931	3952.829	0.504	83.218	7.964	1.238
36	10	9	1.125	0.01347	0.00651	13.056	3.903	23.145	3975.974	0.487	83.705	1.593	1.651
37	9	10	1.113	0.01109	0.00646	15.917	3.921	23.144	3999.118	0.487	84.192	1.770	1.486
38	2	13	1.078	0.00497	0.00626	31.912	3.953	20.376	4019.494	0.429	84.621	7.964	1.143
39	5	11	0.899	0.00623	0.00640	24.703	3.935	19.962	4039.456	0.420	85.041	3.186	1.351
40	9	0	0.898	0.01109	0.00675	24.192	2.000	18.750	4058.206	0.395	85.436	1.770	9999.996

THE TOTAL RESPONSE OF ALL OTHER MODES AT 223.871 HZ = 691.782 100.000

TOTAL RESPONSE = 4749.988

HISTOGRAM PLOT OF PERCENTAGE RESPONSE AGAINST NORMALISED RESONANCE FREQUENCY.

```
                 0                             25                             50                             75                             100
RANK    FMN/F    I                              I                              I                              I                              I
 34     0.877    O
 40     0.898
 39     0.899
 27     0.911    O
 25     0.920    O
 35     0.921    O
 22     0.922    O
 18     0.926    OO
 21     0.928    O
 17     0.934    OO
 20     0.939    O
 11     0.946    OO
 29     0.949    O
 23     0.949    O
 16     0.952    OO
 13     0.965    OO
  3     0.986    OOOOOOO
  9     0.989    OOO
  7     1.012    OOOOO
  4     1.014    OOOOOO
  2     1.014    OOOOOOO
  5     1.017    OOOOO
  1     1.017    OOOOOOO
 14     1.020    OO
  8     1.022    OOOO
  6     1.030    OOOOO
 19     1.041    O
 15     1.042    OO
 10.    1.045    OOO
 12     1.058    OO
 31     1.061    O
 38     1.078
 24     1.102    O
 33     1.107    O
 30     1.108    O
 26     1.112    O
 37     1.113
 28     1.123    O
 36     1.125
 32     1.143    O
```

LEGEND

FMN/F	= Resonant frequency of m,n mode/frequency
J2M(W)	= Joint acceptance in x-direction, $j_m^2(\omega)$
J2N(W)	= Joint acceptance in y-direction, $j_n^2(\omega)$
H	= $H^2(\omega/\omega_{mn})$
BMN	= β_{mn}
RESPONSE	= Response of m,nth mode $(g^2/(psi)^2)$
CUM. RES.	= Cumulative Response
PR	= Percentage of total response for m,nth mode
PCR	= Cumulative response percentage of total response
SXW/AW	= Structural wavelength, x-direction/acoustic wavelength
SYW/AW	= Structural wavelength, y-direction/acoustic wavelength

Table 22: Forty Most Dominant Response Modes of the SLA Structure for Boundary Layer Turbulence (U_c = 9810 in./sec; δ_b = 12.0 in.), f = 398.105 Hz

FREQUENCY = 398.105 ACOUSTIC WAVELENGTH = 24.642

RANK	M	N	FMN/F	J2M(W).	J2N(W).	H.	BMN	RESPONSE.	CUM. RES.	PR	PCR	SXW/AW	SYW/AW
1	16	6	0.987	0.00517	0.00450	199.012	3.787	90.718	90.718	4.953	4.953	1.770	4.403
2	17	3	1.011	0.00587	0.00452	199.421	3.240	88.766	179.484	4.846	9.799	1.666	8.806
3	14	10	0.992	0.00412	0.00444	216.618	3.921	80.508	259.992	4.395	14.194	2.023	2.642
4	17	2	0.998	0.00587	0.00453	225.206	2.560	79.285	339.276	4.329	18.523	1.666	13.209
5	16	7	1.023	0.00517	0.00449	147.996	3.842	68.262	407.538	3.727	22.249	1.770	3.774
6	15	9	1.023	0.00460	0.00446	145.919	3.903	60.409	467.947	3.298	25.548	1.888	2.935
7	17	4	1.029	0.00587	0.00452	123.305	3.543	59.938	527.884	3.272	28.820	1.666	6.605
8	15	8	0.973	0.00460	0.00447	141.619	3.878	58.449	586.333	3.191	32.011	1.888	3.302
9	17	0	0.989	0.00587	0.00453	206.435	2.000	56.824	643.157	3.102	35.113	1.666	9999.996
10	10	14	1.006	0.00290	0.00436	215.908	3.959	55.901	699.058	3.052	38.165	2.833	1.887
11	13	11	0.974	0.00373	0.00442	146.783	3.935	49.316	748.374	2.692	40.857	2.179	2.402
12	8	15	0.992	0.00255	0.00433	216.858	3.965	49.103	797.477	2.681	43.538	3.541	1.761
13	11	13	0.980	0.00313	0.00438	173.399	3.953	48.626	846.103	2.655	46.193	2.575	2.032
14	16	5	0.958	0.00517	0.00451	91.702	3.698	40.915	887.018	2.234	48.427	1.770	5.284
15	12	12	0.970	0.00340	0.00440	130.519	3.945	39.922	926.940	2.180	50.606	2.360	2.202
16	6	16	1.013	0.00230	0.00431	190.374	3.969	38.803	965.743	2.118	52.725	4.721	1.651
17	5	16	0.979	0.00222	0.00431	165.808	3.969	32.495	998.238	1.774	54.499	5.665	1.651
18	17	5	1.053	0.00587	0.00451	60.079	3.698	30.426	1028.664	1.661	56.160	1.666	5.284
19	17	1	0.991	0.00587	0.00453	213.849	1.000	29.427	1058.090	1.607	57.766	1.666	26.419
20	1	17	1.021	0.00203	0.00428	155.620	3.972	27.847	1085.937	1.520	59.287	28.326	1.554
21	13	12	1.049	0.00373	0.00440	66.976	3.945	22.459	1108.396	1.226	60.513	2.179	2.202
22	16	4	0.935	0.00517	0.00452	51.244	3.543	21.945	1130.342	1.198	61.711	1.770	6.605
23	2	17	1.030	0.00206	0.00428	118.021	3.972	21.346	1151.687	1.165	62.876	14.163	1.554
24	16	8	1.066	0.00517	0.00447	42.052	3.878	19.521	1171.208	1.066	63.942	1.770	3.302
25	14	11	1.059	0.00412	0.00442	51.194	3.935	19.013	1190.220	1.038	64.980	2.023	2.402
26	15	7	0.931	0.00460	0.00449	46.078	3.842	18.896	1209.116	1.032	66.012	1.888	3.774
27	14	9	0.934	0.00412	0.00446	50.093	3.903	18.601	1227.718	1.016	67.027	2.023	2.935
28	12	13	1.053	0.00340	0.00438	59.086	3.953	18.021	1245.739	0.984	68.011	2.360	2.032
29	9	15	1.046	0.00271	0.00433	72.370	3.965	17.540	1263.279	0.958	68.969	3.147	1.761
30	9	14	0.945	0.00271	0.00436	65.607	3.959	15.860	1279.139	0.866	69.834	3.147	1.887
31	17	6	1.083	0.00587	0.00450	28.353	3.787	14.670	1293.808	0.801	70.635	1.666	4.403
32	4	16	0.951	0.00215	0.00431	75.401	3.969	14.310	1308.119	0.781	71.417	7.081	1.651
33	16	3	0.919	0.00517	0.00452	35.771	3.240	14.028	1322.146	0.766	72.182	1.770	8.806
34	7	15	0.945	0.00241	0.00433	64.784	3.965	13.901	1336.048	0.759	72.941	4.047	1.761
35	3	17	1.046	0.00209	0.00428	73.722	3.972	13.573	1349.620	0.741	73.682	9.442	1.554
36	7	16	1.054	0.00241	0.00431	58.374	3.969	12.464	1362.084	0.680	74.363	4.047	1.651
37	15	10	1.082	0.00460	0.00444	29.270	3.921	12.128	1374.212	0.662	75.025	1.888	2.642
38	11	14	1.072	0.00313	0.00436	36.273	3.959	10.135	1384.347	0.553	75.578	2.575	1.887
39	13	10	0.908	0.00373	0.00444	29.122	3.921	9.791	1394.138	0.535	76.113	2.179	2.642
40	15	6	0.896	0.00460	0.00450	23.750	3.787	9.625	1403.764	0.525	76.638	1.888	4.403

THE TOTAL RESPONSE OF ALL OTHER MODES AT 398.105 HZ = 427.910 100.000

TOTAL RESPONSE = 1831.673

HISTOGRAM PLOT OF PERCENTAGE RESPONSE AGAINST NORMALISED RESONANCE FREQUENCY.

RANK	FMN/F	0 I ... 25 I ... 50 I ... 75 I ... 100 I
40	0.896	0
39	0.908	0
33	0.919	0
26	0.931	0
27	0.934	0
22	0.935	0
34	0.945	0
30	0.945	0
32	0.951	0
14	0.958	00
15	0.970	00
8	0.973	000
11	0.974	000
17	0.979	00
13	0.980	000
1	0.987	00000
9	0.989	000
19	0.991	00
3	0.992	0000
12	0.992	000
4	0.998	0000
10	1.006	000
2	1.011	00000
16	1.013	00
20	1.021	00
5	1.023	0000
6	1.023	000
7	1.029	000
23	1.030	0
35	1.046	0
29	1.046	0
21	1.049	0
18	1.053	00
28	1.053	0
36	1.054	0
25	1.059	0
24	1.066	0
38	1.072	0
37	1.082	0
31	1.083	0

LEGEND

- FMN/F = Resonant frequency of m,n mode/frequency
- J2M(W) = Joint acceptance in x-direction, $j_m^2(\omega)$
- J2N(W) = Joint acceptance in y-direction, $j_n^2(\omega)$
- H = $H^2(\omega/\omega_{mn})$
- BMN = β_{mn}
- RESPONSE = Response of m,nth mode $(g^2/(psi)^2)$
- CUM. RES. = Cumulative Response
- PR = Percentage of total response for m,nth mode
- PCR = Cumulative response percentage of total response
- SXW/AW = Structural wavelength, x-direction/acoustic wavelength
- SYW/AW = Structural wavelength, y-direction/acoustic wavelength

Table 23: Forty Most Dominant Modes of the SLA Structure with Radius Increased to 208 In., for a Reverberant Acoustic Field, f = 89.125 Hz

FREQUENCY = 89.125 ACOUSTIC WAVELENGTH = 150.799

RANK	M	N	FMN/F	J2M(W).	J2N(W).	H.	BMN	RESPONSE.	CUM. RES.	PR	PCR	SXW/AW	SYW/AW
1	3	0	0.992	0.10621	0.05724	216.768	2.000	13642.121	13642.121	12.831	12.831	1.543	9999.996
2	2	0	0.986	0.10710	0.05724	197.655	2.000	12542.624	26184.945	11.797	24.628	2.314	9999.996
3	1	0	0.985	0.10795	0.05724	192.665	2.000	12317.566	38502.512	11.585	36.214	4.629	9999.996
4	4	0	1.008	0.09149	0.05724	208.210	2.000	11287.168	49789.680	10.616	46.830	1.157	9999.996
5	5	2	1.006	0.04168	0.05720	214.107	2.560	6764.020	56553.699	6.362	53.192	0.926	4.317
6	4	1	0.992	0.09149	0.05723	216.795	1.000	5875.367	62429.066	5.526	58.718	1.157	8.634
7	5	3	0.968	0.04168	0.05715	123.688	3.240	4940.918	67369.938	4.647	63.365	0.926	2.878
8	4	2	0.948	0.09149	0.05720	69.640	2.560	4829.172	72199.063	4.542	67.907	1.157	4.317
9	3	1	0.963	0.10621	0.05723	104.939	1.000	3301.595	75500.625	3.105	71.013	1.543	8.634
10	6	6	0.993	0.00913	0.05664	217.844	3.787	2207.156	77707.750	2.076	73.089	0.771	1.439
11	5	0	1.042	0.04168	0.05724	82.464	2.000	2036.630	79744.375	1.916	75.004	0.926	9999.996
12	6	8	0.988	0.00913	0.05354	205.451	3.878	2014.876	81759.250	1.895	76.899	0.771	1.079
13	6	5	1.011	0.00913	0.05691	200.277	3.698	1991.260	83750.500	1.873	78.772	0.771	1.727
14	6	7	0.984	0.00913	0.05603	189.716	3.842	1929.050	85679.500	1.814	80.586	0.771	1.233
15	5	4	0.924	0.04168	0.05706	39.929	3.543	1741.637	87421.125	1.638	82.224	0.926	2.158
16	4	3	0.884	0.09149	0.05715	19.635	3.240	1721.666	89142.750	1.619	83.844	1.157	2.878
17	3	2	0.864	0.10621	0.05720	19.488	2.560	1568.831	90711.563	1.476	85.319	1.543	4.317
18	5	1	1.033	0.04168	0.05723	109.610	1.000	1353.320	92064.875	1.273	86.592	0.926	8.634
19	2	1	0.921	0.10710	0.05723	37.037	1.000	1174.956	93239.813	1.105	87.697	2.314	8.634
20	6	4	1.034	0.00913	0.05706	104.544	3.543	998.479	94238.250	0.939	88.636	0.771	2.158
21	5	5	0.882	0.04168	0.05691	18.850	3.698	855.939	95094.188	0.805	89.441	0.926	1.727
22	4	4	0.814	0.09149	0.05706	8.593	3.543	822.760	95916.938	0.774	90.215	1.157	2.158
23	3	3	0.781	0.10621	0.05715	6.443	3.240	655.889	96572.813	0.617	90.832	1.543	2.878
24	5	6	0.847	0.04168	0.05664	12.023	3.787	556.316	97129.125	0.523	91.355	0.926	1.439
25	4	5	0.749	0.09149	0.05691	5.122	3.698	510.475	97639.563	0.480	91.835	1.157	1.727
26	2	2	0.768	0.10710	0.05720	5.854	2.560	475.205	98114.750	0.447	92.282	2.314	4.317
27	6	3	1.059	0.00913	0.05715	50.846	3.240	444.749	98559.438	0.418	92.701	0.771	2.878
28	5	7	0.825	0.04168	0.05603	9.534	3.842	442.754	99002.188	0.416	93.117	0.926	1.233
29	6	9	1.007	0.00913	0.01040	212.459	3.903	407.365	99409.500	0.383	93.500	0.771	0.959
30	5	8	0.820	0.04168	0.05354	9.069	3.878	406.188	99815.688	0.382	93.882	0.926	1.079
31	4	6	0.697	0.09149	0.05664	3.753	3.787	381.183	100196.813	0.359	94.241	1.157	1.439
32	3	4	0.677	0.10621	0.05706	3.386	3.543	376.352	100573.125	0.354	94.595	1.543	2.158
33	4	7	0.665	0.09149	0.05603	3.190	3.842	325.192	100898.313	0.306	94.901	1.157	1.233
34	4	8	0.655	0.09149	0.05354	3.05[illegible]	3.878	300.141	101198.438	0.282	95.183	1.157	1.079
35	3	5	0.590	0.10621	0.05691	2.342	3.698	270.944	101469.375	0.255	95.438	1.543	1.727
36	2	3	0.604	0.10710	0.05715	2.473	3.240	253.791	101723.125	0.239	95.676	2.314	2.878
37	3	6	0.528	0.10621	0.05664	1.916	3.787	225.960	101949.063	0.213	95.889	1.543	1.439
38	6	2	1.060	0.00913	0.05720	30.108	2.560	208.268	102157.313	0.196	96.085	0.771	4.317
39	3	7	0.495	0.10621	0.05603	1.753	3.842	207.470	102364.750	0.195	96.280	1.543	1.233
40	3	8	0.493	0.10621	0.05354	1.743	3.878	198.946	102563.688	0.187	96.467	1.543	1.079

THE TOTAL RESPONSE OF ALL OTHER MODES AT 89.125 HZ = 3756.375 100.000

TOTAL RESPONSE = 106320.063

HISTOGRAM PLOT OF PERCENTAGE RESPONSE AGAINST NORMALISED RESONANCE FREQUENCY.

```
                  0                         25                        50                        75                        100
RANK    FMN/F     I                         I                         I                         I                         I
 40     0.493
 39     0.495
 37     0.528
 35     0.590
 36     0.604
 34     0.655
 33     0.665
 32     0.677
 31     0.697
 25     0.749
 26     0.768
 23     0.781     0
 22     0.814     0
 30     0.820
 28     0.825
 24     0.847     0
 21     0.882     0
 17     0.864     0
 16     0.884     00
 19     0.921     0
 15     0.924     00
  8     0.948     00000
  9     0.963     000
  7     0.968     00000
 14     0.984     00
  3     0.985     000000000000
  2     0.986     000000000000
 12     0.988     00
  1     0.992     0000000000000
  6     0.992     000000
 10     0.993     00
  5     1.006     000000
 29     1.007
  4     1.008     00000000000
 13     1.011     00
 18     1.033     0
 20     1.034     0
 11     1.042     00
 27     1.059
 38     1.060
```

LEGEND

FMN/F	=	Resonant frequency of m,n mode/frequency
J2M(W)	=	Joint acceptance in x-direction, $j_m^2(\omega)$
J2N(W)	=	Joint acceptance in y-direction, $j_n^2(\omega)$
H	=	$H^2(\omega/\omega_{mn})$
BMN	=	β_{mn}
RESPONSE	=	Response of m,nth mode $(g^2/(psi)^2)$
CUM. RES.	=	Cumulative Response
PR	=	Percentage of total response for m,nth mode
PCR	=	Cumulative response percentage of total response
SXW/AW	=	Structural wavelength, x-direction/acoustic wavelength
SYW/AW	=	Structural wavelength, y-direction/acoustic wavelength

Table 24: Forty Most Dominant Modes of the SLA Structure, with Radius Increased to 208 in., for a Reverberant Acoustic Field, f = 177.827 Hz

FREQUENCY = 177.827 ACOUSTIC WAVELENGTH = 75.579

RANK	M	N	FMN/F	J2M(W).	J2N(W).	H.	BMN	RESPONSE.	CUM. RES.	PR	PCR	SXW/AW	SYW/AW
1	9	14	0.987	0.03577	0.02850	200.650	3.959	4192.047	4192.047	11.756	11.756	1.026	1.230
2	8	16	0.972	0.05144	0.02764	139.580	3.969	4077.332	8269.379	11.435	23.191	1.154	1.077
3	8	17	1.033	0.05144	0.02070	108.957	3.972	2385.288	10654.664	6.689	29.880	1.154	1.013
4	9	15	1.038	0.03577	0.02827	93.978	3.965	1950.416	12605.078	5.470	35.350	1.026	1.148
5	10	11	0.995	0.01100	0.02873	222.923	3.935	1434.643	14039.719	4.023	39.373	0.924	1.566
6	9	13	0.942	0.03577	0.02861	59.847	3.953	1253.367	15293.082	3.515	42.888	1.026	1.325
7	8	15	0.917	0.05144	0.02827	34.465	3.965	1028.581	16321.660	2.885	45.773	1.154	1.148
8	7	17	0.925	0.05280	0.02070	40.790	3.972	916.543	17238.203	2.570	48.343	1.319	1.013
9	10	12	1.032	0.01100	0.02868	111.613	3.945	719.030	17957.230	2.016	50.360	0.924	1.436
10	10	10	0.964	0.01100	0.02876	108.515	3.921	696.740	18653.969	1.954	52.314	0.924	1.723
11	9	12	0.902	0.03577	0.02868	25.909	3.945	542.806	19196.773	1.522	53.836	1.026	1.436
12	9	16	1.093	0.03577	0.02764	23.168	3.969	470.636	19667.406	1.320	55.156	1.026	1.077
13	8	14	0.867	0.05144	0.02850	15.372	3.959	461.810	20129.215	1.295	56.451	1.154	1.230
14	7	16	0.864	0.05280	0.02764	14.890	3.969	446.436	20575.648	1.252	57.703	1.319	1.077
15	11	5	0.996	0.00353	0.02884	223.596	3.698	436.207	21011.852	1.223	58.926	0.840	3.445
16	11	6	1.010	0.00353	0.02883	201.765	3.787	402.961	21414.809	1.130	60.056	0.840	2.871
17	11	4	0.985	0.00353	0.02884	192.018	3.543	358.980	21773.785	1.007	61.063	0.840	4.307
18	7	18	0.991	0.05280	0.00152	213.114	3.975	351.251	22125.035	0.985	62.048	1.319	0.957
19	10	9	0.936	0.01100	0.02879	52.520	3.903	335.933	22460.965	0.942	62.990	0.924	1.914
20	9	11	0.867	0.03577	0.02873	15.317	3.935	320.570	22781.531	0.899	63.889	1.026	1.566
21	8	13	0.822	0.05144	0.02861	9.261	3.953	278.911	23060.441	0.782	64.671	1.154	1.325
22	11	3	0.977	0.00353	0.02885	156.678	3.240	268.227	23328.668	0.752	65.424	0.840	5.742
23	11	7	1.028	0.00353	0.02882	127.221	3.842	257.646	23586.313	0.723	66.146	0.840	2.461
24	7	15	0.809	0.05280	0.02827	8.165	3.965	250.114	23836.426	0.701	66.847	1.319	1.148
25	6	17	0.831	0.05355	0.02070	10.117	3.972	230.569	24066.992	0.647	67.494	1.539	1.013
26	10	13	1.073	0.01100	0.02861	35.432	3.953	228.173	24295.164	0.640	68.134	0.924	1.325
27	9	10	0.837	0.03577	0.02876	10.759	3.921	224.653	24519.816	0.630	68.764	1.026	1.723
28	10	8	0.914	0.01100	0.02880	32.207	3.878	204.802	24724.617	0.574	69.338	0.924	2.153
29	8	12	0.783	0.05144	0.02868	6.562	3.945	197.690	24922.305	0.554	69.893	1.154	1.436
30	11	2	0.971	0.00353	0.02885	133.678	2.560	180.610	25102.914	0.507	70.399	0.840	8.613
31	6	16	0.769	0.05355	0.02764	5.916	3.969	179.915	25282.828	0.505	70.904	1.539	1.077
32	9	9	0.812	0.03577	0.02879	8.405	3.903	174.824	25457.652	0.490	71.394	1.026	1.914
33	7	14	0.759	0.05280	0.02850	5.470	3.959	168.677	25626.328	0.473	71.867	1.319	1.230
34	8	11	0.750	0.05144	0.02873	5.141	3.935	154.732	25781.059	0.434	72.301	1.154	1.566
35	9	8	0.792	0.03577	0.02880	7.052	3.878	145.827	25926.883	0.409	72.710	1.026	2.153
36	10	7	0.895	0.01100	0.02882	23.103	3.842	145.602	26072.484	0.408	73.118	0.924	2.461
37	11	8	1.049	0.00353	0.02880	66.895	3.878	136.690	26209.172	0.383	73.502	0.840	2.153
38	9	17	1.153	0.03577	0.02070	8.713	3.972	132.644	26341.813	0.372	73.874	1.026	1.013
39	8	10	0.722	0.05144	0.02876	4.314	3.921	129.545	26471.355	0.363	74.237	1.154	1.723
40	9	7	0.776	0.03577	0.02882	6.225	3.842	127.590	26598.941	0.358	74.595	1.026	2.461

THE TOTAL RESPONSE OF ALL OTHER MODES AT 177.827 HZ = 9058.965 100.000

TOTAL RESPONSE = 35657.906

HISTOGRAM PLOT OF PERCENTAGE RESPONSE AGAINST NORMALISED RESONANCE FREQUENCY.

```
                 0                        25                        50                        75                        100
RANK    FMN/F    I                        I                         I                         I                         I
 39     0.722
 34     0.750
 33     0.759
 31     0.769    0
 40     0.776
 29     0.783    0
 35     0.792
 24     0.809    0
 32     0.812
 21     0.822    0
 25     0.831    0
 27     0.837    0
 14     0.864    0
 20     0.867    0
 13     0.867    0
 36     0.895
 11     0.902    00
 28     0.914    0
  7     0.917    000
  8     0.925    000
 19     0.936    0
  6     0.942    0000
 10     0.964    00
 30     0.971    0
  2     0.972    00000000000
 22     0.977    0
 17     0.985    0
  1     0.987    000000000000
 18     0.991    0
  5     0.995    0000
 15     0.996    0
 16     1.010    0
 23     1.028    0
  9     1.032    00
  3     1.033    0000000
  4     1.038    00000
 37     1.049
 26     1.073    0
 12     1.093    0
 38     1.153
```

LEGEND

FMN/F	= Resonant frequency of m,n mode/frequency
J2M(W)	= Joint acceptance in x-direction, $j_m^2(\omega)$
J2N(W)	= Joint acceptance in y-direction, $j_n^2(\omega)$
H	= $H^2(\omega/\omega_{mn})$
BMN	= β_{mn}
RESPONSE	= Response of m,nth mode $(g^2/(psi)^2)$
CUM. RES.	= Cumulative Response
PR	= Percentage of total response for m,nth mode
PCR	= Cumulative response percentage of total response
SXW/AW	= Structural wavelength, x-direction/acoustic wavelength
SYW/AW	= Structural wavelength, y-direction/acoustic wavelength

Table 25: Forty Most Dominant Modes of the SLA Structure, with Radius Increased to 208 in., for a Reverberant Acoustic Field, f = 223.871 Hz

FREQUENCY = 223.871 ACOUSTIC WAVELENGTH = 60.035

RANK	M	N	FMN/F	J2M(W).	J2N(W).	H.	BMN	RESPONSE.	CUM. RES.	PR	PCR	SXW/AW	SYW/AW
1	8	20	0.987	0.04257	0.02239	199.501	3.960	3916.491	3916.491	7.361	7.361	1.453	1.084
2	11	14	1.004	0.03502	0.02267	219.627	3.959	3605.605	7522.094	6.777	14.137	1.057	1.549
3	10	17	1.022	0.04165	0.02278	151.350	3.972	2952.985	10475.078	5.550	19.687	1.163	1.276
4	9	19	1.023	0.04199	0.02261	146.584	3.978	2865.639	13340.715	5.386	25.073	1.292	1.141
5	10	16	0.974	0.04165	0.02282	145.725	3.969	2845.776	16186.488	5.349	30.422	1.163	1.355
6	9	18	0.968	0.04199	0.02272	121.909	3.975	2393.026	18579.512	4.498	34.919	1.292	1.205
7	7	21	0.965	0.04266	0.02158	114.217	3.962	2166.687	20746.195	4.072	38.991	1.661	1.033
8	11	13	0.967	0.03502	0.02269	119.003	3.953	1951.868	22698.063	3.668	42.660	1.057	1.668
9	12	10	0.998	0.01525	0.02292	225.043	3.921	1596.419	24294.480	3.000	45.660	0.969	2.169
10	8	21	1.050	0.04257	0.02158	65.809	3.962	1245.647	25540.125	2.341	48.001	1.453	1.033
11	11	15	1.045	0.03502	0.02285	74.623	3.965	1225.563	26765.688	2.303	50.305	1.057	1.446
12	12	9	0.973	0.01525	0.02293	143.413	3.903	1012.928	27778.613	1.904	52.209	0.969	2.410
13	12	11	1.026	0.01525	0.02291	135.574	3.935	964.718	28743.328	1.813	54.022	0.969	1.972
14	10	15	0.930	0.04165	0.02265	44.938	3.965	877.724	29621.051	1.650	55.671	1.163	1.446
15	8	19	0.928	0.04257	0.02261	42.995	3.978	852.115	30473.164	1.602	57.273	1.453	1.141
16	11	12	0.933	0.03502	0.02290	48.594	3.945	795.833	31268.996	1.496	58.769	1.057	1.807
17	10	18	1.074	0.04165	0.02272	35.197	3.975	685.365	31954.359	1.288	60.057	1.163	1.205
18	9	17	0.916	0.04199	0.02278	33.777	3.972	664.344	32618.703	1.249	61.305	1.292	1.276
19	9	20	1.082	0.04199	0.02239	29.132	3.960	564.137	33182.840	1.060	62.366	1.292	1.084
20	12	8	0.952	0.01525	0.02293	78.131	3.878	548.406	33731.246	1.031	63.396	0.969	2.711
21	7	20	0.902	0.04266	0.02239	26.275	3.960	516.960	34248.203	0.972	64.368	1.661	1.084
22	7	22	1.032	0.04266	0.00501	112.056	3.964	493.881	34742.082	0.928	65.296	1.661	0.986
23	11	11	0.903	0.03502	0.02291	26.522	3.935	433.414	35175.492	0.815	66.111	1.057	1.972
24	6	21	0.892	0.04283	0.02158	22.217	3.962	423.142	35598.633	0.795	66.906	1.938	1.033
25	6	22	0.959	0.04283	0.00501	95.212	3.964	421.319	36019.949	0.792	67.698	1.938	0.986
26	10	14	0.889	0.04165	0.02267	21.132	3.959	412.587	36432.535	0.775	68.473	1.163	1.549
27	11	16	1.090	0.03502	0.02282	24.686	3.969	405.360	36837.895	0.762	69.235	1.057	1.355
28	12	12	1.057	0.01525	0.02290	53.737	3.945	383.221	37221.113	0.720	69.955	0.969	1.807
29	12	7	0.934	0.01525	0.02294	49.244	3.842	342.483	37563.594	0.644	70.599	0.969	3.098
30	8	18	0.872	0.04257	0.02272	16.484	3.975	328.024	37891.617	0.617	71.215	1.453	1.205
31	9	16	0.868	0.04199	0.02282	15.624	3.969	307.574	38199.188	0.578	71.794	1.292	1.355
32	11	10	0.876	0.03502	0.02292	17.473	3.921	284.653	38483.840	0.535	72.329	1.057	2.169
33	13	3	1.013	0.00344	0.02295	190.541	3.240	251.931	38735.770	0.473	72.802	0.894	7.229
34	10	13	0.853	0.04165	0.02269	12.848	3.953	250.607	38986.375	0.471	73.273	1.163	1.668
35	12	6	0.918	0.01525	0.02294	35.309	3.767	242.092	39228.465	0.455	73.728	0.969	3.615
36	10	19	1.129	0.04165	0.02261	12.354	3.978	239.583	39468.047	0.450	74.178	1.163	1.141
37	7	19	0.843	0.04266	0.02261	11.506	3.978	228.542	39696.586	0.430	74.608	1.661	1.141
38	13	2	1.007	0.00344	0.02295	212.510	2.560	222.018	39918.602	0.417	75.025	0.894	10.844
39	13	4	1.022	0.00344	0.02294	153.139	3.543	221.414	40140.012	0.416	75.441	0.894	5.422
40	11	9	0.853	0.03502	0.02293	12.938	3.903	209.855	40349.863	0.394	75.836	1.057	2.410

THE TOTAL RESPONSE OF ALL OTHER MODES AT 223.871 HZ = 12857.102 100.000

TOTAL RESPONSE = 53206.965

HISTOGRAM PLOT OF PERCENTAGE RESPONSE AGAINST NORMALISED RESONANCE FREQUENCY.

```
                 0                        25                        50                        75                        100
RANK    FMN/F    I                        I                         I                         I                         I
 37     0.843
 34     0.853
 40     0.853
 31     0.868    0
 30     0.872    0
 32     0.876    0
 26     0.889    0
 24     0.892    0
 21     0.902    0
 23     0.903    0
 18     0.916    0
 35     0.918
 15     0.928    00
 14     0.930    00
 16     0.933    0
 29     0.934    0
 20     0.952    0
 25     0.959    0
  7     0.965    0000
  8     0.967    0000
  6     0.968    0000
 12     0.973    00
  5     0.974    00000
  1     0.987    0000000
  9     0.998    000
  2     1.004    0000000
 38     1.007
 33     1.013
 39     1.022
  3     1.022    000000
  4     1.023    00000
 13     1.026    00
 22     1.032    0
 11     1.045    00
 10     1.050    00
 28     1.057    0
 17     1.074    0
 19     1.082    0
 27     1.090    0
 36     1.129
```

LEGEND

FMN/F	= Resonant frequency of m,n mode/frequency
J2M(W)	= Joint acceptance in x-direction, $j_m^2(\omega)$
J2N(W)	= Joint acceptance in y-direction, $j_n^2(\omega)$
H	= $H^2(\omega/\omega_{mn})$
BMN	= β_{mn}
RESPONSE	= Response of m,nth mode $(g^2/(psi)^2)$
CUM. RES.	= Cumulative Response
PR	= Percentage of total response for m,nth mode
PCR	= Cumulative response percentage of total response
SXW/AW	= Structural wavelength, x-direction/acoustic wavelength
SYW/AW	= Structural wavelength, y-direction/acoustic wavelength

Table 26: Forty Most Dominant Modes of the SLA Structure, with Radius Increased to 208 in., for a Reverberant Acoustic Field, f = 398.105 Hz

FREQUENCY = 398.105   ACOUSTIC WAVELENGTH = 33.760

RANK	M	N	FMN/F	J2M(W).	J2N(W).	H.	BMN	RESPONSE.	CUM. RES.	PR	PCR	SXW/AW	SYW/AW
1	12	25	0.999	0.02409	0.01291	225.250	3.987	1445.339	1445.339	3.035	3.035	1.723	1.543
2	10	28	1.002	0.02413	0.01289	223.799	3.990	1437.774	2883.114	3.019	6.054	2.068	1.377
3	14	21	1.000	0.02402	0.01292	224.818	3.962	1437.720	4320.832	3.019	9.072	1.477	1.836
4	16	15	1.001	0.02388	0.01292	224.682	3.965	1423.176	5744.008	2.988	12.061	1.292	2.571
5	9	29	0.993	0.02415	0.01289	217.960	3.991	1400.791	7144.797	2.941	15.002	2.297	1.330
6	17	10	0.996	0.02383	0.01293	223.967	3.921	1400.315	8545.109	2.940	17.942	1.216	3.857
7	13	23	0.993	0.02408	0.01291	218.263	3.965	1399.473	9944.582	2.938	20.880	1.590	1.677
8	15	18	0.989	0.02400	0.01292	208.638	3.975	1332.448	11277.027	2.798	23.678	1.378	2.143
9	17	11	1.014	0.02383	0.01293	187.219	3.935	1174.540	12451.566	2.466	26.144	1.216	3.506
10	17	9	0.981	0.02383	0.01293	174.107	3.903	1083.579	13535.145	2.275	28.420	1.216	4.285
11	11	27	1.018	0.02412	0.01290	166.784	3.989	1071.285	14606.430	2.249	30.669	1.880	1.428
12	15	19	1.021	0.02400	0.01292	155.276	3.978	991.226	15597.652	2.081	32.750	1.378	2.030
13	16	14	0.976	0.02388	0.01293	155.144	3.959	981.493	16579.145	2.061	34.811	1.292	2.755
14	11	26	0.972	0.02412	0.01290	138.369	3.968	888.878	17468.020	1.866	36.677	1.880	1.483
15	16	16	1.027	0.02388	0.01292	131.212	3.969	831.945	18299.961	1.747	38.424	1.292	2.410
16	17	8	0.967	0.02383	0.01293	118.275	3.878	731.376	19031.336	1.536	39.960	1.216	4.821
17	14	20	0.965	0.02402	0.01292	113.344	3.980	724.605	19755.941	1.521	41.481	1.477	1.928
18	17	12	1.033	0.02383	0.01293	108.152	3.945	680.252	20436.191	1.428	42.910	1.216	3.214
19	13	24	1.034	0.02408	0.01291	106.058	3.966	680.097	21116.285	1.428	44.338	1.590	1.607
20	18	3	1.027	0.02348	0.01293	131.204	3.240	668.063	21784.348	1.403	45.740	1.149	12.855
21	15	17	0.960	0.02400	0.01292	97.101	3.972	619.131	22403.477	1.300	47.040	1.378	2.269
22	18	4	1.032	0.02348	0.01293	109.879	3.543	611.836	23015.313	1.285	48.325	1.149	9.642
23	14	22	1.037	0.02402	0.01291	94.468	3.984	604.273	23619.582	1.269	49.594	1.477	1.753
24	18	2	1.023	0.02348	0.01293	148.306	2.560	596.660	24216.242	1.253	50.846	1.149	19.283
25	12	24	0.956	0.02409	0.01291	87.880	3.986	563.872	24780.113	1.184	52.030	1.723	1.607
26	13	22	0.954	0.02408	0.01291	82.553	3.984	529.233	25309.344	1.111	53.142	1.590	1.753
27	10	27	0.953	0.02413	0.01290	81.004	3.989	520.511	25829.852	1.093	54.235	2.068	1.428
28	16	13	0.954	0.02388	0.01293	81.715	3.953	516.149	26346.000	1.084	55.318	1.292	2.967
29	18	0	1.019	0.02348	0.01293	162.754	2.000	511.555	26857.555	1.074	56.392	1.149	9999.996
30	17	7	0.954	0.02383	0.01293	83.290	3.842	510.236	27367.789	1.071	57.464	1.216	5.509
31	18	5	1.040	0.02348	0.01293	87.430	3.698	508.118	27875.906	1.067	58.531	1.149	7.713
32	12	26	1.043	0.02409	0.01290	78.837	3.968	505.843	28381.746	1.062	59.593	1.723	1.483
33	10	29	1.052	0.02413	0.01289	61.994	3.991	398.146	28779.891	0.836	60.429	2.068	1.330
34	18	6	1.049	0.02348	0.01293	66.771	3.787	397.333	29177.223	0.834	61.263	1.149	6.428
35	9	28	0.943	0.02415	0.01289	61.144	3.990	393.085	29570.305	0.825	62.088	2.297	1.377
36	17	6	0.944	0.02383	0.01293	62.829	3.767	379.401	29949.703	0.797	62.885	1.216	6.428
37	8	29	0.940	0.02415	0.01289	57.356	3.991	368.717	30318.418	0.774	63.659	2.584	1.330
38	15	20	1.054	0.02400	0.01292	57.329	3.980	366.118	30684.535	0.769	64.428	1.378	1.928
39	17	13	1.054	0.02383	0.01293	58.046	3.953	365.821	31050.355	0.768	65.196	1.216	2.967
40	16	17	1.055	0.02388	0.01292	56.850	3.972	360.748	31411.102	0.757	65.953	1.292	2.269

THE TOTAL RESPONSE OF ALL OTHER MODES AT 398.105 HZ = 16215.113 100.000

TOTAL RESPONSE = 47626.215

HISTOGRAM PLOT OF PERCENTAGE RESPONSE AGAINST NORMALISED RESONANCE FREQUENCY.

```
RANK  FMN/F  0          25          50          75          100
             I          I           I           I           I
 37   0.940  0
 35   0.943  0
 36   0.944  0
 27   0.953  0
 28   0.954  0
 26   0.954  0
 30   0.954  0
 25   0.956  0
 21   0.960  0
 17   0.965  00
 16   0.967  00
 14   0.972  00
 13   0.976  00
 10   0.981  00
  8   0.989  000
  5   0.993  000
  7   0.993  000
  6   0.996  000
  1   0.999  000
  3   1.000  000
  4   1.001  000
  2   1.002  000
  9   1.014  00
 11   1.018  00
 29   1.019  0
 12   1.021  00
 24   1.023  0
 15   1.027  00
 20   1.027  0
 22   1.032  0
 18   1.033  0
 19   1.034  0
 23   1.037  0
 31   1.040  0
 32   1.043  0
 34   1.049  0
 33   1.052  0
 39   1.054  0
 38   1.054  0
 40   1.055  0
```

LEGEND

FMN/F	= Resonant frequency of m,n mode/frequency
J2M(W)	= Joint acceptance in x-direction, $j_m^2(\omega)$
J2N(W)	= Joint acceptance in y-direction, $j_n^2(\omega)$
H	= $H^2(\omega/\omega_{mn})$
BMN	= β_{mn}
RESPONSE	= Response of m,nth mode $(g^2/(psi)^2)$
CUM. RES.	= Cumulative Response
PR	= Percentage of total response for m,nth mode
PCR	= Cumulative response percentage of total response
SXW/AW	= Structural wavelength, x-direction/acoustic wavelength
SYW/AW	= Structural wavelength, y-direction/acoustic wavelength

Table 27: *Forty Most Dominant Modes of Republic Cylinder No. 12 (18 in. Radius by 54 in. Length by 0.020 in.) for a Reverberant Acoustic Field, f = 891.248 Hz*

FREQUENCY = 891.248   ACOUSTIC WAVELENGTH = 15.080

RANK	M	N	FMN/F	J2M(W).	J2N(W).	H.	BMN	RESPONSE.	CUM. RES.	PR	PCR	SXW/AW	SYW/AW
1	5	5	1.021	0.06835	0.06503	346.261	3.698	1422954.000	1422954.000	17.403	17.403	1.432	1.500
2	4	4	1.020	0.06920	0.06540	353.552	3.543	1417510.000	2840464.000	17.336	34.739	1.790	1.875
3	6	6	1.021	0.06611	0.06412	333.404	3.787	1337858.000	4178322.000	16.362	51.102	1.194	1.250
4	3	3	1.020	0.06951	0.06559	357.000	3.240	1318435.000	5496757.000	16.125	67.226	2.387	2.500
5	2	2	1.020	0.06571	0.06570	358.262	2.560	1050005.000	6546762.000	12.842	80.068	3.581	3.750
6	7	7	1.022	0.04435	0.05889	313.314	3.842	785973.688	7332735.000	9.613	89.681	1.023	1.071
7	1	1	1.020	0.06979	0.06575	358.513	1.000	411252.313	7743987.000	5.030	94.710	7.162	7.500
8	6	7	0.872	0.06611	0.05889	17.192	3.842	64279.168	7808266.000	0.786	95.497	1.194	1.071
9	5	6	0.844	0.06835	0.06412	11.986	3.787	49726.242	7857992.000	0.608	96.105	1.432	1.250
10	4	5	0.805	0.06920	0.06503	6.005	3.698	33310.375	7891302.000	0.407	96.512	1.790	1.500
11	8	8	1.024	0.01269	0.00733	285.290	3.878	26113.129	7917415.000	0.319	96.832	0.895	0.938
12	6	5	1.195	0.06611	0.06503	5.425	3.698	21564.488	7938979.000	0.264	97.095	1.194	1.500
13	3	4	0.744	0.06951	0.06540	5.008	3.543	20167.488	7959146.000	0.247	97.342	2.387	1.875
14	7	6	1.169	0.04435	0.06412	7.333	3.787	19741.805	7978887.000	0.241	97.583	1.023	1.250
15	5	7	0.701	0.06835	0.05889	3.868	3.842	14951.328	7993838.000	0.183	97.766	1.432	1.071
16	5	4	1.232	0.06835	0.06540	3.714	3.543	14705.879	8008543.000	0.180	97.946	1.432	1.875
17	4	6	0.640	0.06920	0.06412	2.865	3.787	12035.230	8020578.000	0.147	98.093	1.790	1.250
18	2	3	0.639	0.06971	0.06559	2.854	3.240	10568.941	8031146.000	0.129	98.222	3.581	2.500
19	3	5	0.552	0.06951	0.06503	2.070	3.698	8651.738	8039797.000	0.106	98.328	2.387	1.500
20	4	3	1.289	0.06920	0.06559	2.274	3.240	8361.254	8048158.000	0.102	98.431	1.790	2.500
21	7	8	0.893	0.04435	0.00733	24.060	3.878	7578.852	8055736.000	0.093	98.523	1.023	0.938
22	4	7	0.516	0.06920	0.05889	1.857	3.842	7267.316	8063003.000	0.089	98.612	1.790	1.071
23	8	7	1.151	0.01289	0.05889	9.335	3.842	6804.570	8069807.000	0.083	98.695	0.895	1.071
24	3	6	0.421	0.06951	0.06412	1.476	3.787	6227.199	8076034.000	0.076	98.771	2.387	1.250
25	2	4	0.420	0.06971	0.06540	1.473	3.543	5949.684	8081983.000	0.073	98.844	3.581	1.875
26	2	5	0.292	0.06971	0.06503	1.195	3.698	5006.758	8086989.000	0.061	98.905	3.581	1.500
27	3	7	0.329	0.06951	0.05889	1.258	3.842	4944.695	8091933.000	0.060	98.966	2.387	1.071
28	2	6	0.213	0.06971	0.06412	1.098	3.787	4644.547	8096577.000	0.057	99.023	3.581	1.250
29	6	4	1.388	0.06611	0.06540	1.161	3.543	4445.172	8101022.000	0.054	99.077	1.194	1.875
30	7	5	1.332	0.04435	0.06503	1.664	3.698	4436.520	8105458.000	0.054	99.131	1.023	1.500
31	1	2	0.420	0.06979	0.06570	1.473	2.560	4321.148	8109779.000	0.053	99.184	7.162	3.750
32	1	6	0.063	0.06979	0.06412	1.008	3.787	4269.395	8114048.000	0.052	99.236	7.162	1.250
33	1	5	0.084	0.06979	0.06503	1.014	3.698	4255.516	8118303.000	0.052	99.288	7.162	1.500
34	1	4	0.126	0.06979	0.06540	1.032	3.543	4173.637	8122476.000	0.051	99.339	7.162	1.875
35	2	7	0.164	0.06971	0.05889	1.056	3.842	4163.367	8126639.000	0.051	99.390	3.581	1.071
36	1	3	0.212	0.06979	0.06559	1.096	3.240	4064.387	8130703.000	0.050	99.440	7.162	2.500
37	1	7	0.054	0.06979	0.05889	1.006	3.842	3970.041	8134673.000	0.049	99.489	7.162	1.071
38	3	2	1.388	0.06951	0.06570	1.164	2.560	3401.310	8138074.000	0.042	99.530	2.387	3.750
39	5	3	1.468	0.06835	0.06559	0.747	3.240	2712.189	8140786.000	0.033	99.563	1.432	2.500
40	6	8	0.747	0.06611	0.00733	5.109	3.878	2396.409	8143184.000	0.029	99.593	1.194	0.938

THE TOTAL RESPONSE OF ALL OTHER MODES AT 891.248 HZ = 33298.000 100.000

TOTAL RESPONSE = 8176482.000

HISTOGRAM PLOT OF PERCENTAGE RESPONSE AGAINST NORMALISED RESONANCE FREQUENCY.

```
                 0                         25                        50                        75                        100
RANK   FMN/F     I                         I                         I                         I                         I
 37    0.054
 32    0.063
 33    0.084
 34    0.126
 35    0.164
 36    0.212
 28    0.213
 26    0.292
 27    0.329
 31    0.420
 25    0.420
 24    0.421
 22    0.516
 19    0.552
 18    0.639
 17    0.640
 15    0.701
 13    0.744
 40    0.747
 10    0.805
  9    0.844     0
  8    0.872     0
 21    0.893
  7    1.020     00000
  5    1.020     00000000000000
  4    1.020     00000000000000000
  2    1.020     000000000000000000
  1    1.021     000000000000000000
  3    1.021     00000000000000000
  6    1.022     0000000000
 11    1.024
 23    1.151
 14    1.169
 12    1.195
 16    1.232
 20    1.289
 30    1.332
 38    1.388
 29    1.388
 39    1.468
```

LEGEND

FMN/F	= Resonant frequency of m,n mode/frequency
J2M(W)	= Joint acceptance in x-direction, $j_m^2(\omega)$
J2N(W)	= Joint acceptance in y-direction, $j_n^2(\omega)$
H	= $H^2(\omega/\omega_{mn})$
BMN	= β_{mn}
RESPONSE	= Response of m,nth mode $(g^2/(psi)^2)$
CUM. RES.	= Cumulative Response
PR	= Percentage of total response for m,nth mode
PCR	= Cumulative response percentage of total response
SXW/AW	= Structural wavelength, x-direction/acoustic wavelength
SYW/AW	= Structural wavelength, y-direction/acoustic wavelength

Table 28: Forty Most Dominant Modes of Republic Cylinder No. 12 (18 in. Radius by 54 in. Length by 0.020 in.) for a Reverberant Acoustic Field, f = 1258.924 Hz

FREQUENCY = 1258.924 ACOUSTIC WAVELENGTH = 10.676

RANK	M	N	FMN/F	J2M(W).	J2N(W).	H.	BMN	RESPONSE.	CUM. RES.	PR	PCR	SXW/AW	SYW/AW
1	9	6	0.984	0.04617	0.04654	484.914	3.787	986416.063	986416.063	17.784	17.784	1.124	1.766
2	6	4	0.983	0.04903	0.04668	446.125	3.543	904331.188	1890747.000	16.304	34.089	1.686	2.649
3	8	5	1.019	0.04811	0.04662	382.057	3.698	792289.688	2683036.000	14.284	48.373	1.265	2.119
4	3	2	0.982	0.04936	0.04673	437.747	2.560	646260.625	3329296.000	11.652	60.024	3.372	5.297
5	5	3	1.040	0.04921	0.04671	129.986	3.240	241993.063	3571289.000	4.363	64.387	2.023	3.531
6	11	7	1.012	0.00820	0.04641	584.812	3.842	213628.063	3784917.000	3.852	68.239	0.920	1.513
7	10	7	0.957	0.02967	0.04641	124.160	3.842	164212.313	3949129.000	2.961	71.199	1.012	1.513
8	7	5	0.943	0.04876	0.04662	75.302	3.698	158264.438	4107393.000	2.853	74.053	1.446	2.119
9	10	6	1.042	0.02967	0.04654	118.612	3.787	155070.500	4262463.000	2.796	76.848	1.012	1.766
10	7	4	1.064	0.04876	0.04668	52.951	3.543	106746.500	4369209.000	1.925	78.773	1.445	2.649
11	12	8	0.988	0.00317	0.04617	604.474	3.878	85757.438	4454966.000	1.546	80.319	0.843	1.324
12	8	6	0.914	0.04811	0.04654	35.595	3.787	75449.188	4530415.000	1.360	81.679	1.265	1.766
13	9	5	1.079	0.04617	0.04662	35.656	3.698	70960.688	4601375.000	1.279	82.959	1.124	2.119
14	4	3	0.913	0.04930	0.04671	34.639	3.240	64605.563	4665980.000	1.165	84.124	2.529	3.531
15	15	10	0.996	0.00142	0.04321	857.982	3.921	51436.836	4717416.000	0.927	85.051	0.674	1.059
16	9	7	0.892	0.04617	0.04641	23.503	3.842	48366.004	4765782.000	0.872	85.923	1.124	1.513
17	14	9	1.012	0.00167	0.04563	567.014	3.903	42122.641	4807904.000	0.759	86.682	0.723	1.177
18	5	4	0.872	0.04921	0.04668	17.171	3.543	34933.230	4842837.000	0.630	87.312	2.023	2.649
19	8	4	1.125	0.04811	0.04668	13.897	3.543	27642.402	4870479.000	0.498	87.810	1.265	2.649
20	6	3	1.124	0.04903	0.04671	14.013	3.240	25994.156	4896473.000	0.469	88.279	1.686	3.531
21	6	5	0.846	0.04903	0.04662	12.229	3.698	25843.832	4922316.000	0.466	88.745	1.686	2.119
22	10	8	0.876	0.02967	0.04617	18.095	3.878	24034.176	4946350.000	0.433	89.178	1.012	1.324
23	13	9	0.969	0.00244	0.04563	208.741	3.903	22706.438	4969056.000	0.409	89.588	0.778	1.177
24	11	8	0.936	0.00820	0.04617	61.218	3.878	22457.945	4991513.000	0.405	89.993	0.920	1.324
25	7	6	0.828	0.04876	0.04654	10.016	3.787	21517.668	5013030.000	0.388	90.380	1.445	1.766
26	4	2	1.124	0.04930	0.04673	14.056	2.560	20723.914	5033753.000	0.374	90.754	2.529	5.297
27	13	8	1.033	0.00244	0.04617	176.392	3.878	19289.617	5053042.000	0.348	91.102	0.778	1.324
28	8	7	0.815	0.04811	0.04641	8.805	3.842	18880.699	5071922.000	0.340	91.442	1.265	1.513
29	10	5	1.126	0.02967	0.04662	13.655	3.698	17464.922	5089386.000	0.315	91.757	1.012	2.119
30	9	8	0.806	0.04617	0.04617	8.073	3.878	16684.758	5106070.000	0.301	92.058	1.124	1.324
31	9	4	1.171	0.04617	0.04668	7.187	3.543	13718.688	5119788.000	0.247	92.305	1.124	2.649
32	7	3	1.183	0.04876	0.04671	6.215	3.240	11464.789	5131252.000	0.207	92.512	1.445	3.531
33	11	6	1.089	0.00820	0.04654	27.956	3.787	10094.656	5141346.000	0.182	92.694	0.920	1.766
34	10	9	0.799	0.02967	0.04563	7.617	3.903	10062.918	5151408.000	0.181	92.875	1.012	1.177
35	7	7	0.724	0.04876	0.04641	4.398	3.842	9557.953	5160965.000	0.172	93.048	1.445	1.513
36	8	8	0.725	0.04811	0.04617	4.429	3.878	9537.074	5170502.000	0.172	93.220	1.265	1.324
37	6	6	0.723	0.04903	0.04654	4.378	3.787	9457.391	5179959.000	0.171	93.390	1.686	1.766
38	5	5	0.723	0.04921	0.04662	4.366	3.698	9260.738	5189219.000	0.167	93.557	2.023	2.119
39	9	9	0.727	0.04617	0.04563	4.474	3.903	9197.418	5198416.000	0.166	93.723	1.124	1.177
40	12	7	1.058	0.00317	0.04641	64.225	3.842	9072.996	5207488.000	0.164	93.886	0.843	1.513

THE TOTAL RESPONSE OF ALL OTHER MODES AT 1258.924 HZ = 339093.000 100.000

TOTAL RESPONSE = 5546581.000

HISTOGRAM PLOT OF PERCENTAGE RESPONSE AGAINST NORMALISED RESONANCE FREQUENCY.

```
                0                        25                        50                        75                        100
RANK   FMN/F    I                        I                         I                         I                         I
 38    0.723
 37    0.723
 35    0.724
 36    0.725
 39    0.727
 34    0.799
 30    0.806
 28    0.815
 25    0.828
 21    0.846
 18    0.872    0
 22    0.876
 16    0.892    0
 14    0.913    0
 12    0.914    0
 24    0.936
  8    0.943    000
  7    0.957    000
 23    0.969
  4    0.982    000000000000
  2    0.983    0000000000000000
  1    0.984    000000000000000000
 11    0.988    00
 15    0.996    0
  6    1.012    0000
 17    1.012    0
  3    1.019    00000000000000
 27    1.033
  5    1.040    0000
  9    1.042    000
 40    1.058
 10    1.064    00
 13    1.079    0
 33    1.089
 26    1.124
 20    1.124
 19    1.125
 29    1.126
 31    1.171
 32    1.183
```

LEGEND

FMN/F	=	Resonant frequency of m,n mode/frequency
J2M(W)	=	Joint acceptance in x-direction, $j_m^2(\omega)$
J2N(W)	=	Joint acceptance in y-direction, $j_n^2(\omega)$
H	=	$H^2(\omega/\omega_{mn})$
BMN	=	β_{mn}
RESPONSE	=	Response of m,nth mode $(g^2/(psi)^2)$
CUM. RES.	=	Cumulative Response
PR	=	Percentage of total response for m,nth mode
PCR	=	Cumulative response percentage of total response
SXW/AW	=	Structural wavelength, x-direction/acoustic wavelength
SYW/AW	=	Structural wavelength, y-direction/acoustic wavelength

Table 29: Forty Most Dominant Modes of Republic Cylinder No. 12 (18 in. Radius by 54 in. Length by 0.020 in.) for a Reverberant Acoustic Field, f = 1778.278 Hz

FREQUENCY = 1778.278 ACOUSTIC WAVELENGTH = 7.558

RANK	M	N	FMN/F	J2M(W).	J2N(W).	H.	BMN	RESPONSE.	CUM. RES.	PR	PCR	SXW/AW	SYW/AW
1	13	0	0.979	0.03320	0.03319	364.862	2.000	200981.250	200981.250	3.870	3.870	1.099	9999.996
2	12	0	0.979	0.03393	0.03319	353.712	2.000	199133.438	400114.688	3.834	7.704	1.191	9999.996
3	11	0	0.978	0.03448	0.03319	345.333	2.000	197571.313	597686.000	3.804	11.508	1.299	9999.996
4	10	0	0.978	0.03461	0.03319	339.116	2.000	194724.563	792410.563	3.749	15.257	1.429	9999.996
5	9	0	0.978	0.03477	0.03319	334.600	2.000	193036.813	985447.375	3.717	18.974	1.588	9999.996
6	8	0	0.978	0.03482	0.03319	331.409	2.000	191470.188	1176917.000	3.687	22.660	1.786	9999.996
7	7	0	0.978	0.03489	0.03319	329.248	2.000	190596.813	1367513.000	3.670	26.330	2.041	9999.996
8	6	0	0.977	0.03491	0.03319	327.859	2.000	189933.750	1557446.000	3.657	29.987	2.382	9999.996
9	5	0	0.977	0.03495	0.03319	327.025	2.000	189628.750	1747074.000	3.651	33.638	2.858	9999.996
10	4	0	0.977	0.03496	0.03319	326.569	2.000	189444.188	1936518.000	3.648	37.286	3.572	9999.996
11	1	0	0.977	0.03499	0.03319	326.286	2.000	189434.625	2125952.000	3.647	40.933	14.290	9999.996
12	2	0	0.977	0.03498	0.03319	326.299	2.000	189412.750	2315364.000	3.647	44.580	7.145	9999.996
13	3	0	0.977	0.03498	0.03319	326.362	2.000	189407.875	2504771.000	3.647	48.227	4.763	9999.996
14	14	0	0.980	0.02355	0.03319	379.493	2.000	148309.813	2653080.000	2.856	51.082	1.021	9999.996
15	13	2	0.959	0.03320	0.03318	132.750	2.560	93587.125	2746667.000	1.802	52.884	1.099	7.482
16	12	2	0.955	0.03393	0.03318	113.164	2.560	81537.313	2828204.000	1.570	54.454	1.191	7.482
17	14	2	0.962	0.02355	0.03318	153.772	2.560	76913.063	2905117.000	1.481	55.935	1.021	7.482
18	13	1	0.974	0.03320	0.03319	272.730	1.000	75113.250	2980230.000	1.446	57.381	1.099	14.965
19	12	1	0.973	0.03393	0.03319	252.536	1.000	71084.438	3051314.000	1.369	58.750	1.191	14.965
20	11	2	0.950	0.03448	0.03318	94.684	2.560	69329.563	3120643.000	1.335	60.085	1.299	7.482
21	11	1	0.971	0.03448	0.03319	232.672	1.000	66555.875	3187198.000	1.281	61.366	1.299	14.965
22	10	1	0.969	0.03461	0.03319	212.105	1.000	60894.891	3248092.000	1.172	62.539	1.429	14.965
23	14	1	0.976	0.02355	0.03319	294.325	1.000	57510.910	3305602.000	1.107	63.646	1.021	14.965
24	10	2	0.944	0.03461	0.03318	77.203	2.560	56736.930	3362338.000	1.092	64.738	1.429	7.482
25	9	1	0.967	0.03477	0.03319	189.686	1.000	54772.730	3417110.000	1.055	65.793	1.588	14.965
26	13	3	0.934	0.03320	0.03318	58.506	3.240	52194.188	3469304.000	1.005	66.798	1.099	4.988
27	15	0	0.981	0.00747	0.03319	398.552	2.000	49430.531	3518734.000	0.952	67.749	0.953	9999.996
28	8	1	0.964	0.03482	0.03319	165.219	1.000	47725.883	3566459.000	0.919	68.668	1.786	14.965
29	14	3	0.941	0.02355	0.03318	71.077	3.240	44987.016	3611446.000	0.866	69.535	1.021	4.988
30	9	2	0.936	0.03477	0.03318	60.837	2.560	44919.531	3656365.000	0.865	70.399	1.588	7.482
31	12	3	0.926	0.03393	0.03318	47.426	3.240	43241.688	3699606.000	0.833	71.232	1.191	4.988
32	7	1	0.960	0.03489	0.03319	137.604	1.000	39827.102	3739433.000	0.767	71.999	2.041	14.965
33	11	3	0.917	0.03448	0.03318	37.680	3.240	34912.922	3774345.000	0.672	72.671	1.299	4.988
34	8	2	0.925	0.03482	0.03318	45.675	2.560	33920.758	3808265.000	0.653	73.324	1.786	7.482
35	6	1	0.953	0.03491	0.03319	107.220	1.000	31056.141	3839321.000	0.598	73.922	2.382	14.965
36	15	2	0.965	0.00747	0.03318	176.863	2.560	28073.898	3867394.000	0.541	74.463	0.953	7.482
37	13	4	0.902	0.03320	0.03317	28.162	3.543	27466.195	3894862.000	0.529	74.991	1.099	3.741
38	10	3	0.904	0.03461	0.03318	29.197	3.240	27151.723	3922013.000	0.523	75.514	1.429	4.988
39	7	2	0.910	0.03489	0.03318	32.720	2.560	24241.824	3946254.000	0.467	75.981	2.041	7.482
40	14	4	0.913	0.02355	0.03317	34.878	3.543	24135.578	3970389.000	0.465	76.446	1.021	3.741

THE TOTAL RESPONSE OF ALL OTHER MODES AT 1778.278 HZ = 1223353.000 100.000

TOTAL RESPONSE = 5193742.000

HISTOGRAM PLOT OF PERCENTAGE RESPONSE AGAINST NORMALISED RESONANCE FREQUENCY.

RANK	FMN/F	0 I ... 25 I ... 50 I ... 75 I ... 100 I
37	0.902	O
38	0.904	O
39	0.910	
40	0.913	
33	0.917	O
34	0.925	O
31	0.926	O
26	0.934	O
30	0.936	O
29	0.941	O
24	0.944	O
20	0.950	O
35	0.953	O
16	0.955	OO
15	0.959	OO
32	0.960	O
17	0.962	O
28	0.964	O
36	0.965	O
25	0.967	O
22	0.969	O
21	0.971	O
19	0.973	O
18	0.974	O
23	0.976	O
11	0.977	OOOO
12	0.977	OOOO
13	0.977	OOOO
10	0.977	OOOO
9	0.977	OOOO
8	0.977	OOOO
7	0.978	OOOO
6	0.978	OOOO
5	0.978	OOOO
4	0.978	OOOO
3	0.978	OOOO
2	0.979	OOOO
1	0.979	OOOO
14	0.980	OOO
27	0.981	O

LEGEND

- FMN/F = Resonant frequency of m,n mode/frequency
- J2M(W) = Joint acceptance in x-direction, $j_m^2(\omega)$
- J2N(W) = Joint acceptance in y-direction, $j_n^2(\omega)$
- H = $H^2(\omega/\omega_{mn})$
- BMN = β_{mn}
- RESPONSE = Response of m,nth mode $(g^2/(psi)^2)$
- CUM. RES. = Cumulative Response
- PR = Percentage of total response for m,nth mode
- PCR = Cumulative response percentage of total response
- SXW/AW = Structural wavelength, x-direction/acoustic wavelength
- SYW/AW = Structural wavelength, y-direction/acoustic wavelength

Table 30: Forty Most Dominant Modes of Republic Cylinder No. 12 (18 in. Radius by 54 in. Length by 0.020 in.) for a Reverberant Acoustic Field, f = 3981.065 Hz

FREQUENCY = 3981.065   ACOUSTIC WAVELENGTH = 3.376

RANK	M	N	FMN/F	J2M(W).	J2N(W).	H.	BMN	RESPONSE.	CUM. RES.	PR	PCR	SXW/AW	SYW/AW
1	29	7	0.439	0.01523	0.01488	1.535	3.842	334.001	334.001	0.145	0.145	1.103	4.786
2	28	7	0.435	0.01536	0.01488	1.520	3.842	333.792	667.794	0.144	0.289	1.143	4.786
3	29	8	0.434	0.01523	0.01488	1.518	3.878	333.392	1001.186	0.144	0.433	1.103	4.188
4	28	8	0.429	0.01536	0.01488	1.502	3.878	332.916	1334.102	0.144	0.577	1.143	4.188
5	30	7	0.444	0.01502	0.01488	1.551	3.842	332.899	1667.000	0.144	0.721	1.066	4.786
6	28	6	0.440	0.01536	0.01488	1.537	3.787	332.681	1999.681	0.144	0.865	1.143	5.584
7	29	6	0.444	0.01523	0.01488	1.551	3.787	332.634	2332.315	0.144	1.00[illegible]	1.103	5.584
8	30	8	0.439	0.01502	0.01488	1.535	3.878	332.543	2664.858	0.144	1.153	1.066	4.188
9	27	7	0.431	0.01543	0.01488	1.506	3.842	332.071	2996.929	0.144	1.297	1.185	4.786
10	29	9	0.429	0.01523	0.01488	1.500	3.903	331.575	3328.504	0.144	1.441	1.103	3.722
11	30	6	0.448	0.01502	0.01488	1.566	3.787	331.298	3659.802	0.143	1.584	1.066	5.584
12	27	6	0.436	0.01543	0.01488	1.524	3.787	331.239	3991.041	0.143	1.727	1.185	5.584
13	30	9	0.434	0.01502	0.01488	1.518	3.903	330.987	4322.027	0.143	1.871	1.066	3.722
14	27	8	0.424	0.01543	0.01488	1.487	3.878	330.916	4652.941	0.143	2.014	1.185	4.188
15	28	9	0.423	0.01536	0.01488	1.483	3.903	330.831	4983.770	0.143	2.157	1.143	3.722
16	26	7	0.426	0.01548	0.01488	1.493	3.842	330.179	5313.945	0.143	2.300	1.230	4.786
17	26	6	0.432	0.01548	0.01488	1.512	3.787	329.644	5643.586	0.143	2.443	1.230	5.584
18	29	10	0.423	0.01523	0.01488	1.462	3.921	329.004	5972.590	0.142	2.585	1.103	3.350
19	26	8	0.420	0.01548	0.01488	1.473	3.878	328.730	6301.316	0.142	2.727	1.230	4.188
20	30	10	0.429	0.01502	0.01488	1.500	3.921	328.675	6629.988	0.142	2.870	1.066	3.350
21	27	9	0.418	0.01543	0.01488	1.467	3.903	328.560	6958.547	0.142	3.012	1.185	3.722
22	28	5	0.444	0.01536	0.01488	1.552	3.698	328.123	7286.668	0.142	3.154	1.143	6.700
23	28	10	0.417	0.01536	0.01488	1.464	3.921	328.001	7614.668	0.142	3.296	1.143	3.350
24	25	7	0.422	0.01551	0.01488	1.480	3.842	327.917	7942.582	0.142	3.438	1.280	4.786
25	29	5	0.448	0.01523	0.01488	1.565	3.698	327.845	8270.426	0.142	3.580	1.103	6.700
26	25	6	0.429	0.01551	0.01488	1.500	3.787	327.699	8598.121	0.142	3.721	1.280	5.584
27	27	5	0.441	0.01543	0.01488	1.541	3.698	326.950	8925.070	0.142	3.863	1.185	6.700
28	30	5	0.452	0.01502	0.01488	1.579	3.698	326.315	9251.383	0.141	4.004	1.066	6.700
29	25	8	0.415	0.01551	0.01488	1.458	3.878	326.160	9577.539	0.141	4.145	1.280	4.188
30	26	9	0.412	0.01548	0.01488	1.451	3.903	326.095	9903.633	0.141	4.286	1.230	3.722
31	29	11	0.416	0.01523	0.01487	1.463	3.935	325.973	10229.605	0.141	4.427	1.103	3.046
32	30	11	0.423	0.01502	0.01487	1.482	3.935	325.893	10555.496	0.141	4.569	1.066	3.046
33	24	6	0.425	0.01553	0.01488	1.489	3.787	325.730	10881.223	0.141	4.710	1.333	5.584
34	26	5	0.438	0.01548	0.01488	1.529	3.698	325.647	11206.867	0.141	4.850	1.230	6.700
35	24	7	0.418	0.01553	0.01488	1.467	3.842	325.610	11532.477	0.141	4.991	1.333	4.786
36	27	10	0.411	0.01543	0.01488	1.447	3.921	325.476	11857.949	0.141	5.132	1.185	3.350
37	28	11	0.410	0.01536	0.01487	1.444	3.935	324.725	12182.672	0.141	5.273	1.143	3.046
38	25	5	0.434	0.01551	0.01488	1.519	3.698	324.017	12506.688	0.140	5.413	1.280	6.700
39	23	6	0.421	0.01555	0.01488	1.478	3.787	323.619	12830.305	0.140	5.553	1.391	5.584
40	24	8	0.410	0.01553	0.01488	1.444	3.878	323.529	13153.832	0.140	5.693	1.333	4.188

THE TOTAL RESPONSE OF ALL OTHER MODES AT 3981.065 HZ = 217894.375 100.000

TOTAL RESPONSE = 231046.250

HISTOGRAM PLOT OF PERCENTAGE RESPONSE AGAINST NORMALISED RESONANCE FREQUENCY.

RANK	FMN/F	0 I	25 I	50 I	75 I	100 I
40	0.410					
37	0.410					
36	0.411					
30	0.412					
29	0.415					
31	0.416					
23	0.417					
35	0.418					
21	0.418					
19	0.420					
39	0.421					
24	0.422					
18	0.423					
32	0.423					
15	0.423					
14	0.424					
33	0.425					
16	0.426					
10	0.429					
20	0.429					
26	0.429					
4	0.429					
9	0.431					
17	0.432					
13	0.434					
3	0.434					
38	0.434					
2	0.435					
12	0.436					
34	0.438					
8	0.439					
1	0.439					
6	0.440					
27	0.441					
5	0.444					
7	0.444					
22	0.444					
25	0.448					
11	0.448					
28	0.452					

LEGEND

FMN/F	= Resonant frequency of m,n mode/frequency
J2M(W)	= Joint acceptance in x-direction, $j_m^2(\omega)$
J2N(W)	= Joint acceptance in y-direction, $j_n^2(\omega)$
H	= $H^2(\omega/\omega_{mn})$
BMN	= β_{mn}
RESPONSE	= Response of m,nth mode $(g^2/(psi)^2)$
CUM. RES.	= Cumulative Response
PR	= Percentage of total response for m,nth mode
PCR	= Cumulative response percentage of total response
SXW/AW	= Structural wavelength, x-direction/acoustic wavelength
SYW/AW	= Structural wavelength, y-direction/acoustic wavelength

Table 31: Forty Most Dominant Response Modes of Flat Plate (10 in. by 12 in. by 0.040 in) for Boundary Layer Turbulence (U_c = 9810 in./sec; δ_b = 12.0 in.), f = 3069.877 Hz

FREQUENCY = 3069.877 ACOUSTIC WAVELENGTH = 3.196

RANK	M	N	FMN/F	J2M(W).	J2N(W).	H.	BMN	RESPONSE.	CUM. RES.	PR	PCR	SXW/AW	SYW/AW
1	6	8	1.000	0.13066	0.01626	899.566	4.000	478004.875	478004.875	45.021	45.021	1.043	0.469
2	5	9	1.010	0.06462	0.01544	649.649	4.000	161984.750	639989.625	15.257	60.278	1.252	0.417
3	8	5	1.011	0.04612	0.01852	601.450	4.000	128404.438	768394.063	12.094	72.372	0.782	0.751
4	7	7	1.032	0.11516	0.01706	183.676	4.000	88651.563	857045.625	8.350	80.722	0.894	0.536
5	9	1	1.016	0.02274	0.02025	469.969	4.000	54115.441	911161.063	5.097	85.819	0.695	3.755
6	7	6	0.920	0.11516	0.01782	40.665	4.000	20502.344	931663.375	1.931	87.750	0.894	0.626
7	3	10	0.975	0.01307	0.01461	288.481	4.000	13776.074	945439.438	1.298	89.047	2.086	0.376
8	9	2	1.041	0.02274	0.02002	119.567	4.000	13608.672	959048.063	1.282	90.329	0.695	1.878
9	8	4	0.934	0.04612	0.01913	57.469	4.000	12675.949	971724.000	1.194	91.523	0.782	0.939
10	6	7	0.871	0.13066	0.01706	16.806	4.000	9366.051	981090.000	0.882	92.405	1.043	0.536
11	7	5	0.825	0.11516	0.01852	9.726	4.000	5095.766	986185.750	0.480	92.885	0.894	0.751
12	4	10	1.062	0.02435	0.01461	56.543	4.000	5027.895	991213.625	0.474	93.358	1.565	0.376
13	6	9	1.147	0.13066	0.01544	9.928	4.000	5006.418	996220.000	0.472	93.830	1.043	0.417
14	5	8	0.863	0.06462	0.01626	15.212	4.000	3994.996	1000214.938	0.376	94.206	1.252	0.469
15	8	6	1.106	0.04612	0.01782	19.396	4.000	3984.930	1004199.813	0.375	94.582	0.782	0.626
16	8	3	0.873	0.04612	0.01964	17.463	4.000	3958.350	1008158.125	0.373	94.954	0.782	1.252
17	7	8	1.162	0.11516	0.01626	8.095	4.000	3723.394	1011881.500	0.351	95.305	0.894	0.469
18	9	3	1.085	0.02274	0.01964	30.650	4.000	3444.840	1015326.313	0.324	95.630	0.695	1.252
19	6	6	0.758	0.13066	0.01782	5.517	4.000	3211.806	1018538.063	0.303	95.932	1.043	0.626
20	7	4	0.747	0.11516	0.01913	5.111	4.000	2766.750	1021304.813	0.261	96.193	0.894	0.939
21	4	9	0.896	0.02435	0.01544	26.126	4.000	2454.388	1023759.188	0.231	96.424	1.565	0.417
22	8	2	0.830	0.04612	0.02002	10.264	4.000	2368.608	1026127.750	0.223	96.647	0.782	1.878
23	7	3	0.667	0.11516	0.01964	3.576	4.000	1987.250	1028115.000	0.187	96.834	0.894	1.252
24	6	5	0.663	0.13066	0.01852	3.164	4.000	1926.270	1030041.250	0.181	97.015	1.043	0.751
25	8	1	0.804	0.04612	0.02025	7.969	4.000	1860.428	1031901.625	0.175	97.191	0.782	3.755
26	7	2	0.644	0.11516	0.02002	2.911	4.000	1648.694	1033550.313	0.155	97.346	0.894	1.878
27	5	10	1.174	0.06462	0.01461	6.911	4.000	1631.023	1035181.313	0.154	97.500	1.252	0.376
28	7	1	0.618	0.11516	0.02025	2.612	4.000	1496.746	1036678.000	0.141	97.641	0.894	3.755
29	6	4	0.586	0.13066	0.01913	2.314	4.000	1446.662	1038124.625	0.136	97.777	1.043	0.939
30	1	11	1.057	0.00716	0.01379	66.753	4.000	1417.437	1039542.000	0.134	97.910	6.259	0.341
31	5	7	0.734	0.06462	0.01706	4.681	4.000	1289.779	1040831.750	0.121	98.032	1.252	0.536
32	6	3	0.525	0.13066	0.01964	1.906	4.000	1222.770	1042054.500	0.115	98.147	1.043	1.252
33	6	2	0.482	0.13066	0.02002	1.698	4.000	1109.309	1043163.750	0.104	98.251	1.043	1.878
34	9	4	1.145	0.02274	0.01913	10.179	4.000	1107.286	1044271.000	0.104	98.356	0.695	0.939
35	6	1	0.456	0.13066	0.02025	1.594	4.000	1054.545	1045325.500	0.099	98.455	1.043	3.755
36	2	10	0.913	0.00205	0.01461	34.927	4.000	1027.463	1046352.938	0.097	98.552	3.129	0.376
37	6	10	1.311	0.13066	0.01461	1.932	4.000	922.069	1047275.000	0.087	98.639	1.043	0.376
38	7	9	1.308	0.11516	0.01544	1.968	4.000	858.708	1048133.688	0.081	98.719	0.894	0.417
39	8	7	1.219	0.04612	0.01706	4.222	4.000	830.388	1048964.000	0.078	98.798	0.782	0.536
40	5	6	0.622	0.06462	0.01782	2.652	4.000	763.479	1049727.000	0.072	98.870	1.252	0.626

THE TOTAL RESPONSE OF ALL OTHER MODES AT 3069.877 HZ = 12002.000 100.000

HISTOGRAM PLOT OF PERCENTAGE RESPONSE AGAINST NORMALISED RESONANCE FREQUENCY.

```
                 0                        25                        50                        75                        100
RANK   FMN/F     I                         I                         I                         I                         I
 35    0.456
 33    0.482
 32    0.525
 29    0.586
 28    0.618
 40    0.622
 26    0.644
 24    0.663
 23    0.667
 31    0.734
 20    0.747
 19    0.758
 25    0.804
 11    0.825
 22    0.830
 14    0.863
 10    0.871     0
 16    0.873
 21    0.898
 36    0.913
  6    0.920     00
  9    0.934     0
  7    0.975     0
  1    1.000     000000000000000000000000000000000000000000000
  2    1.010     000000000000000
  3    1.011     000000000000
  5    1.016     00000
  4    1.032     00000000
  8    1.041     0
 30    1.057
 12    1.062
 18    1.085
 15    1.106
 34    1.145
 13    1.147
 17    1.162
 27    1.174
 39    1.219
 38    1.308
 37    1.311
```

LEGEND

FMN/F	= Resonant frequency of m,n mode/frequency
J2M(W)	= Joint acceptance in x-direction, $j_m^2(\omega)$
J2N(W)	= Joint acceptance in y-direction, $j_n^2(\omega)$
H	= $H^2(\omega/\omega_{mn})$
BMN	= β_{mn}
RESPONSE	= Response of m,nth mode $(g^2/(psi)^2)$
CUM. RES.	= Cumulative Response
PR	= Percentage of total response for m,nth mode
PCR	= Cumulative response percentage of total response
SXW/AW	= Structural wavelength, x-direction/acoustic wavelength
SYW/AW	= Structural wavelength, y-direction/acoustic wavelength

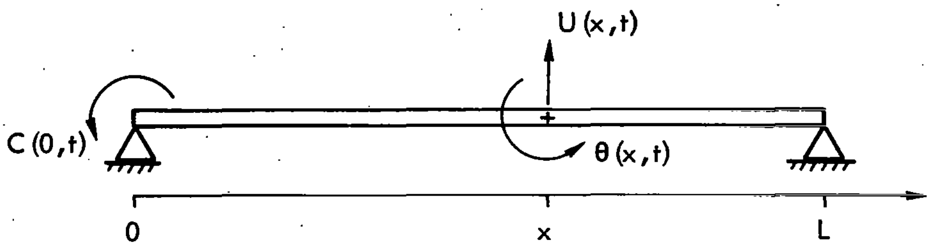

Figure 1. Pinned-Pinned Beam with End Couple, $C(0,t)$; Orientations of Deflection $U(x,t)$, and Slope $\theta(x,t)$.

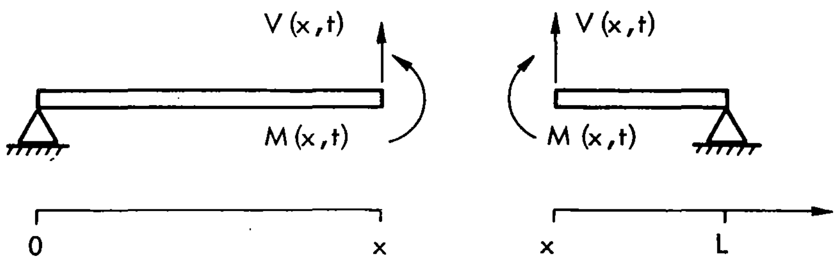

Figure 2. Orientations of Internal Beam Bending Moment $M(x,t)$, and Shear Force $V(x,t)$.

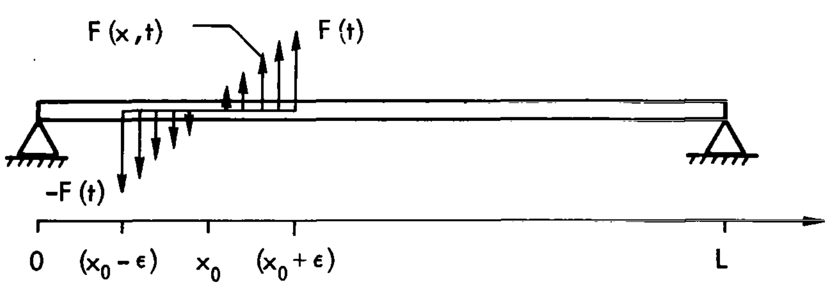

Figure 3. Distribution of Applied Force Per Unit Length, $F(x,t)$, Equivalent to a Point Couple $C(x_0,t)$ at x_0.

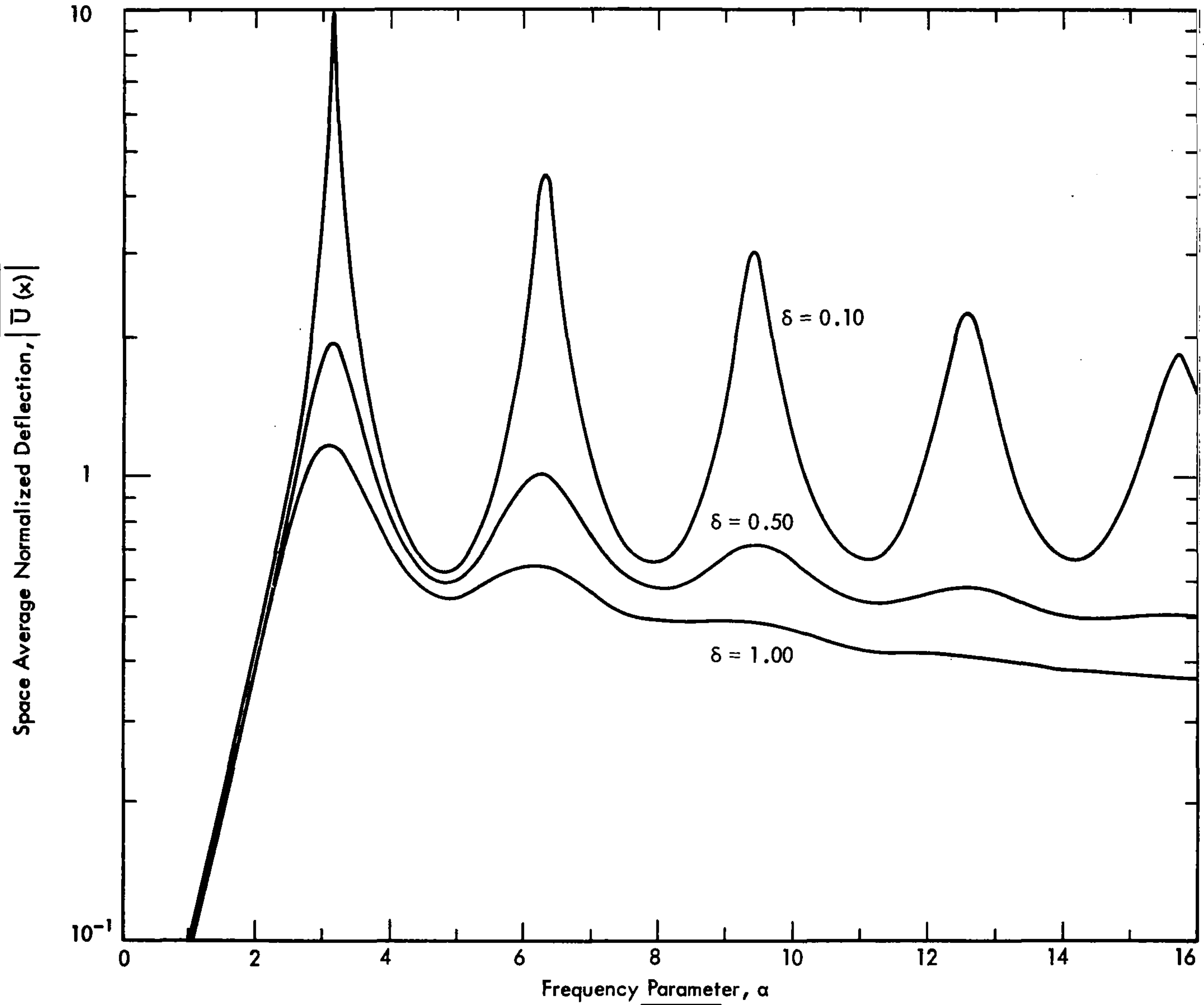

Figure 4. Space-Average Normalized Deflection, $\overline{|\overline{U}(x)|}$, as a Function of the Frequency Parameter α for δ = 0.10, 0.50, and 1.00.

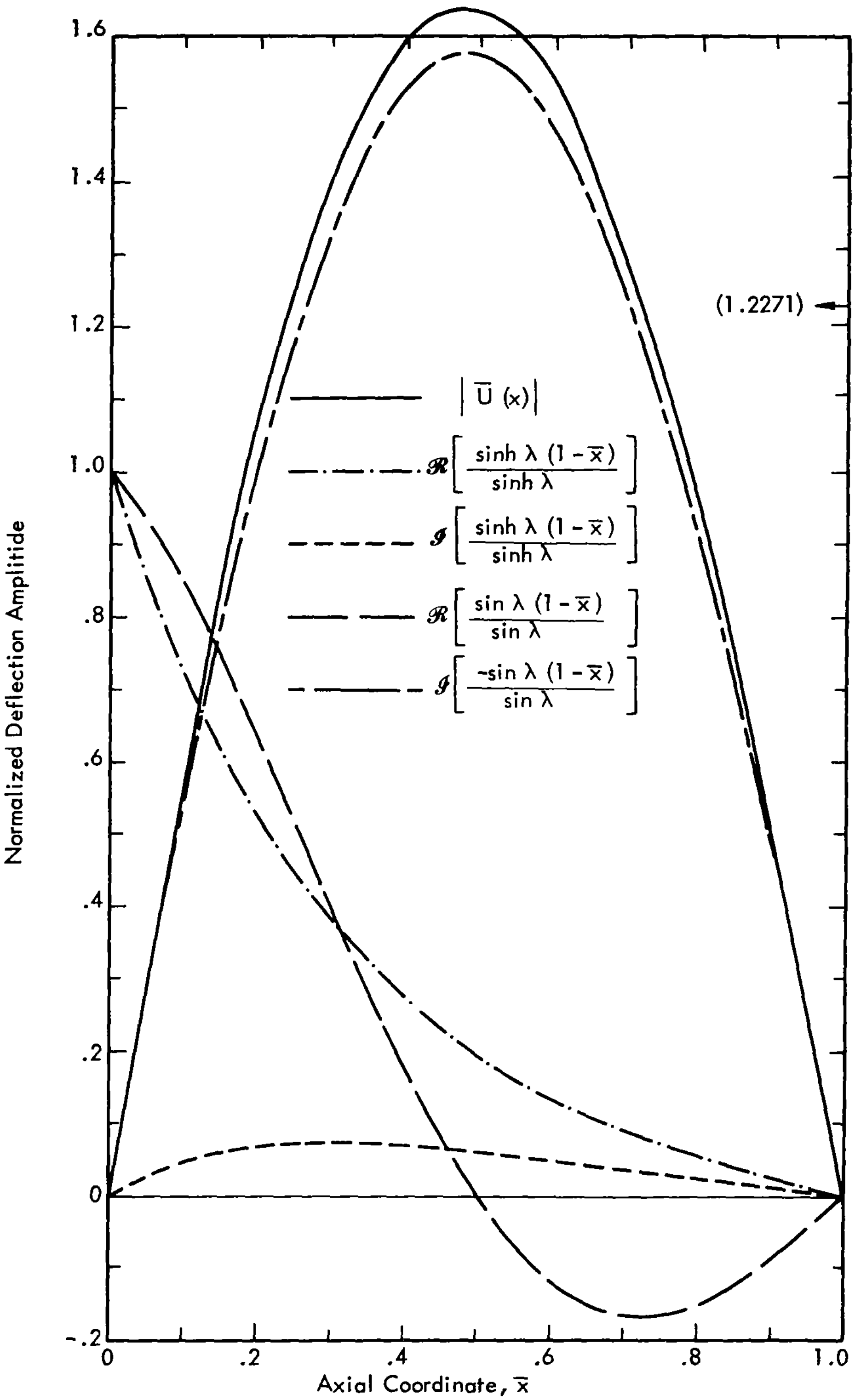

Figure 5. Spanwise Distributions of Real, Imaginary and Absolute Values of Normalized Deflection Amplitude for $\alpha = \pi$ (Fundamental Mode) and $\delta = 1.0$.

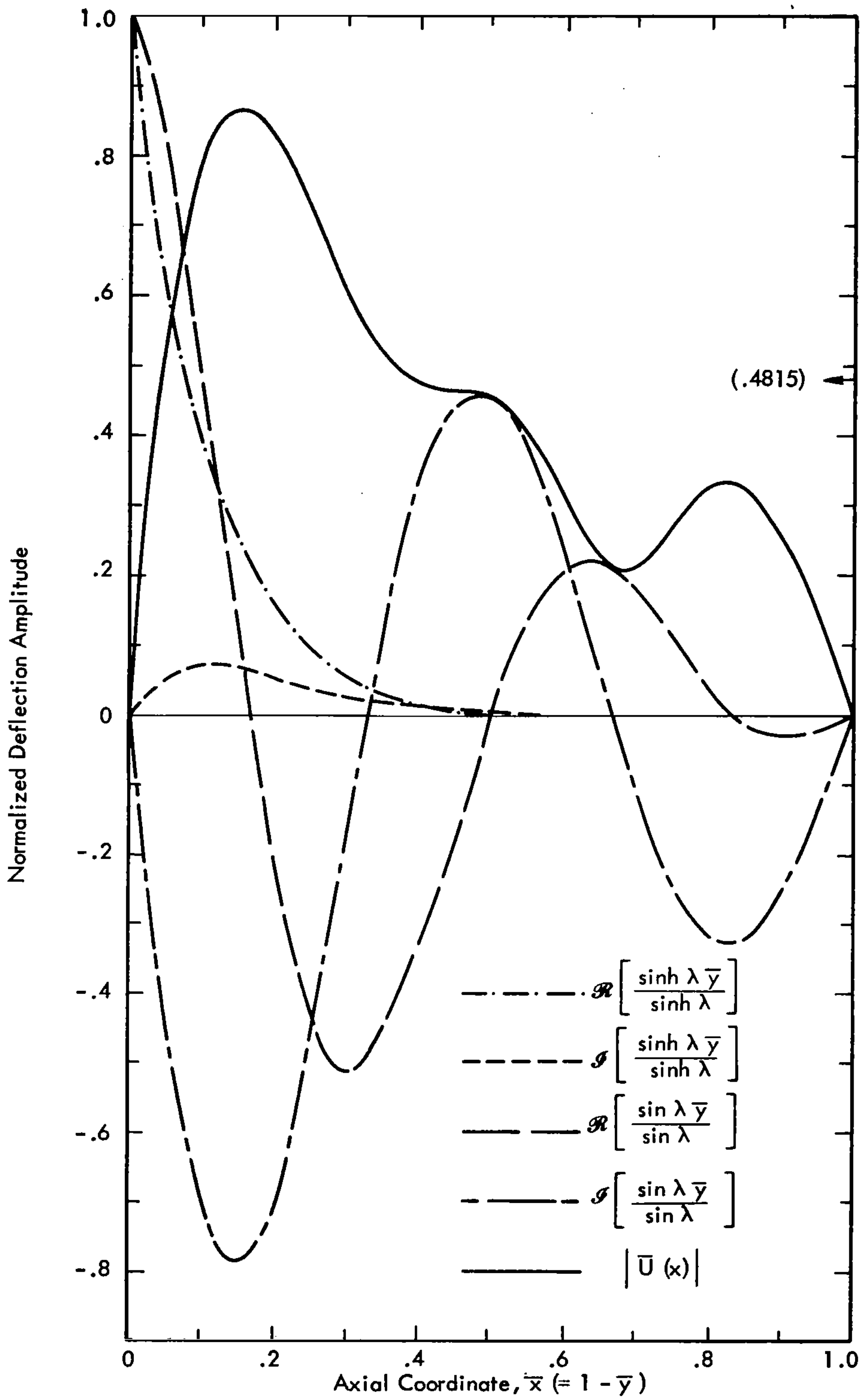

Figure 6. Spanwise Distributions of Real, Imaginary and Absolute Values of Normalized Deflection Amplitude for $\alpha = 3\pi$ (Third Mode) and $\delta = 1.0$.

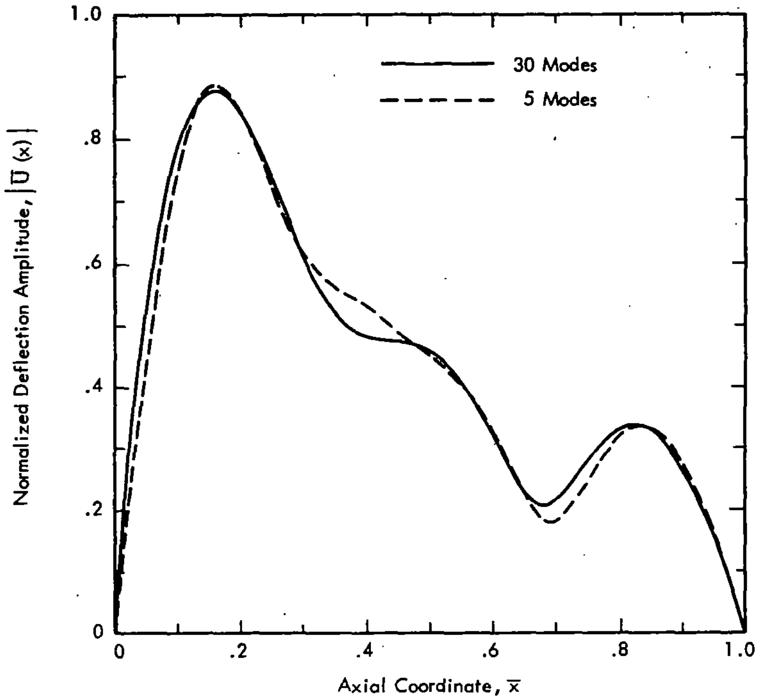

Figure 7. Comparison of Normalized Deflection Amplitude, $|\overline{U}(x)|$, Determined by Modal Analysis Method for 5 and 30 Modes and for $\delta = 1.0$, $\lambda_0 = 9.6095$.

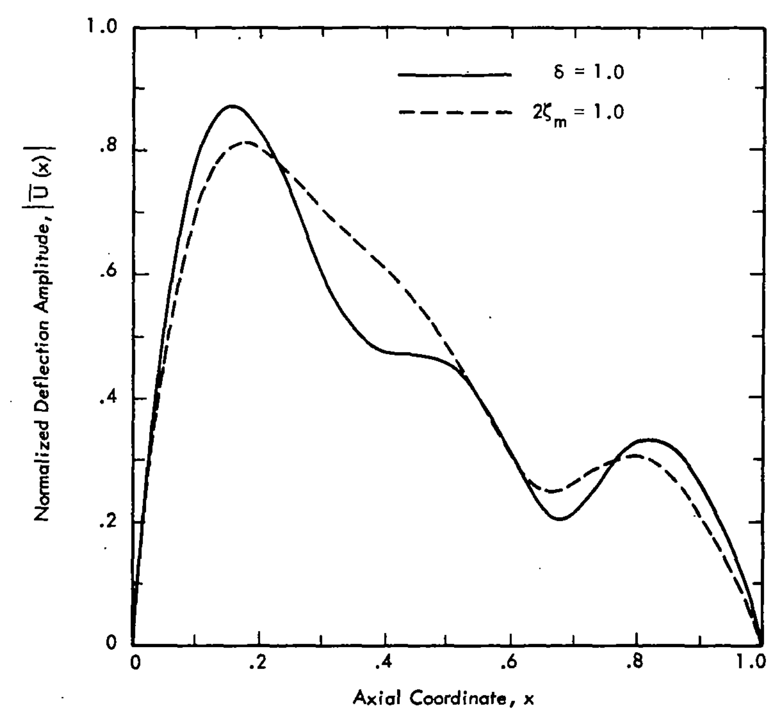

Figure 8. Comparison of Normalized Deflection Amplitude, $|\overline{U}(x)|$, Determined by Modal Analyses, Using 30 Modes, for $\lambda_0 = 9.6095$ and for $\delta = 1.0$ and $2\zeta_m = 1.0$.

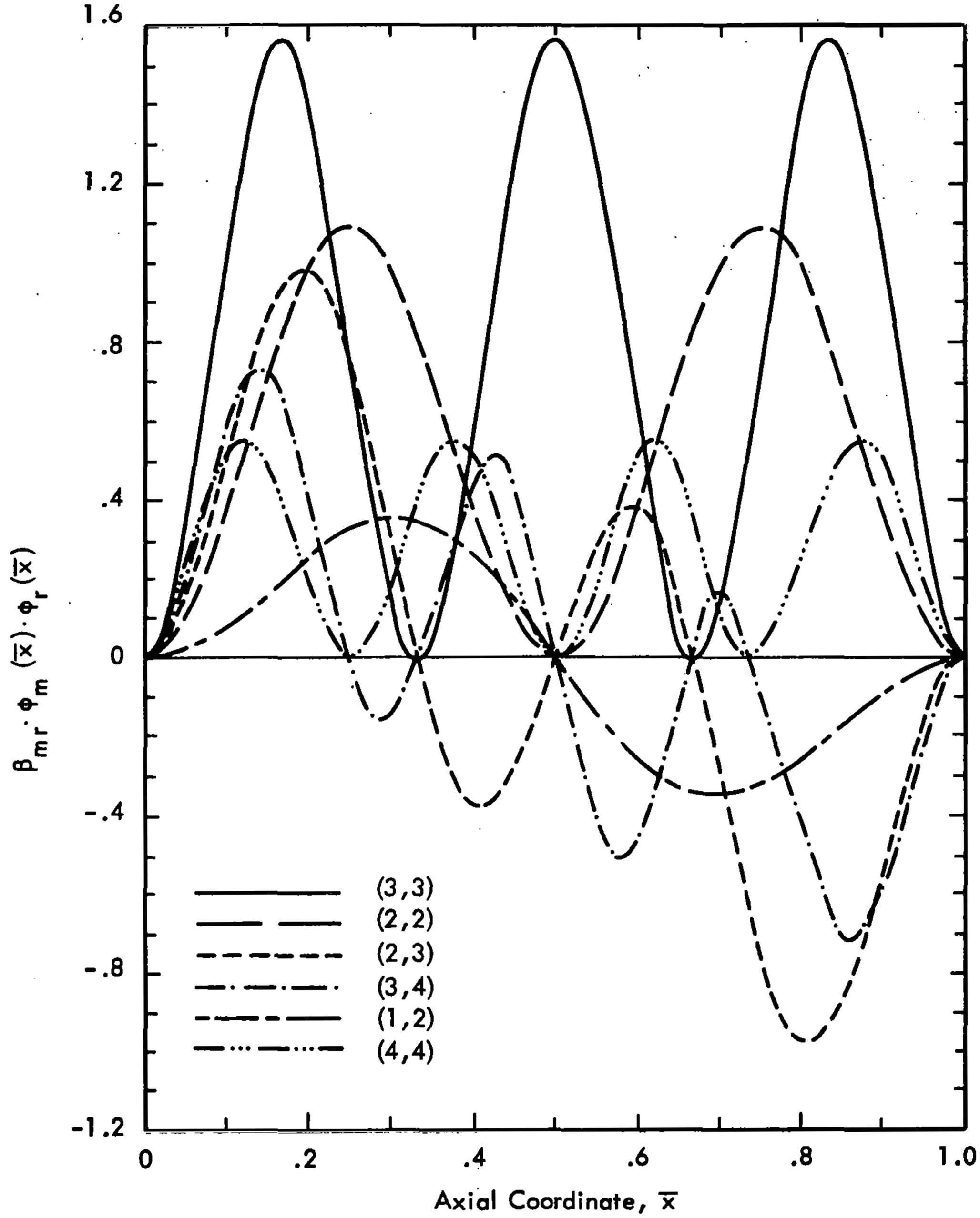

Figure 9. Contributions of Various Modal Components to the Mean-Square Deflection for $\delta = 1.0$ and $\lambda_0 = 9.6095$.

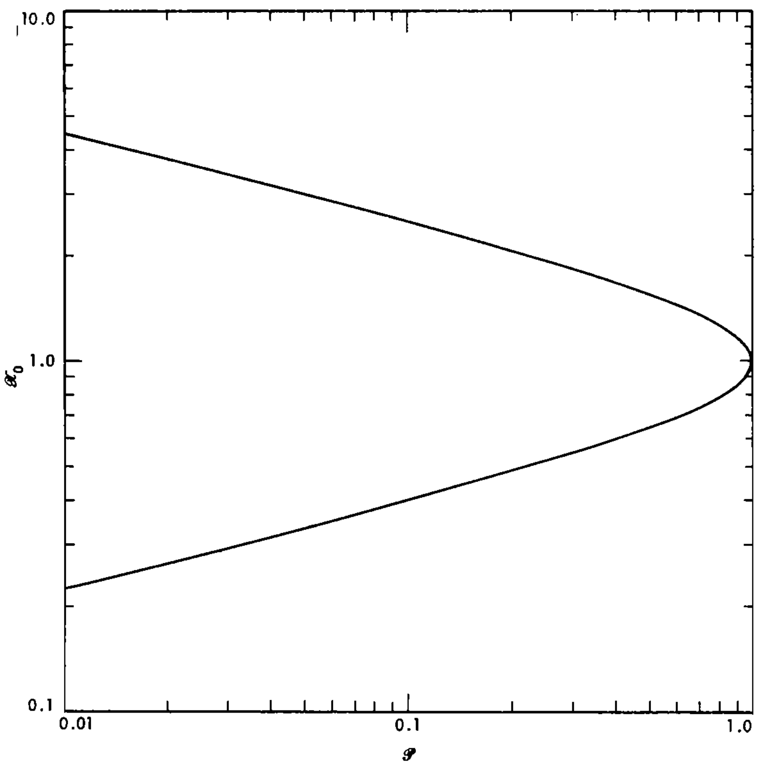

Figure 10. Relationship Between Parameters $\mathscr{K}_0$ and $\mathscr{P}$ for Axial Coincidence of Shell Modes.

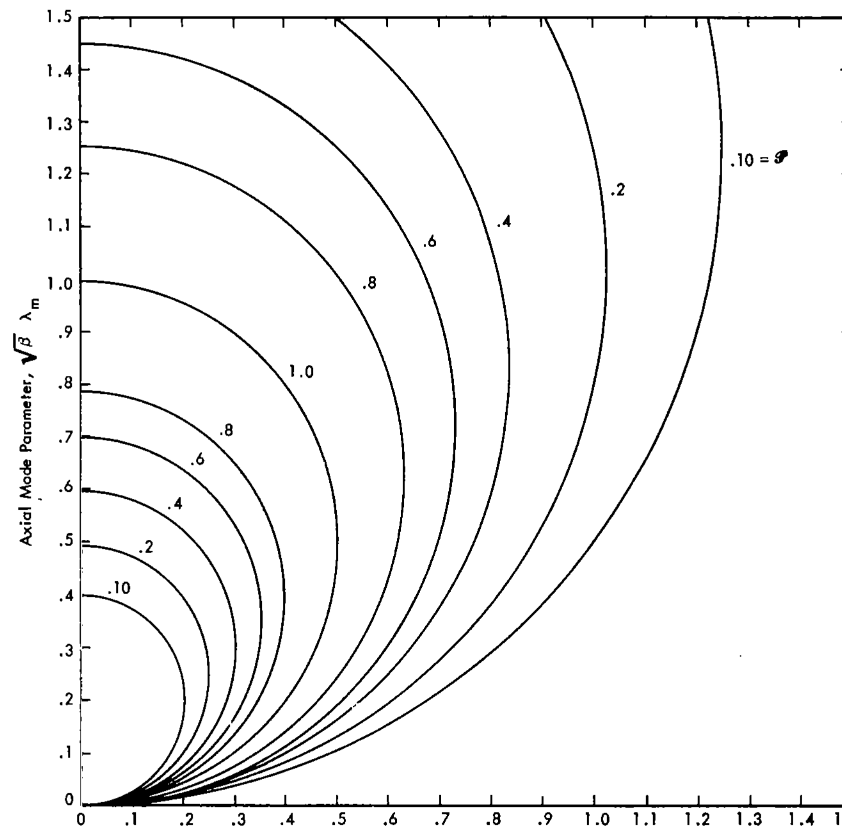

Figure 11. Contours for Axial Coincidence Conditions of Cylindrical Shell for Several Values of Parameter $\mathscr{P}$.

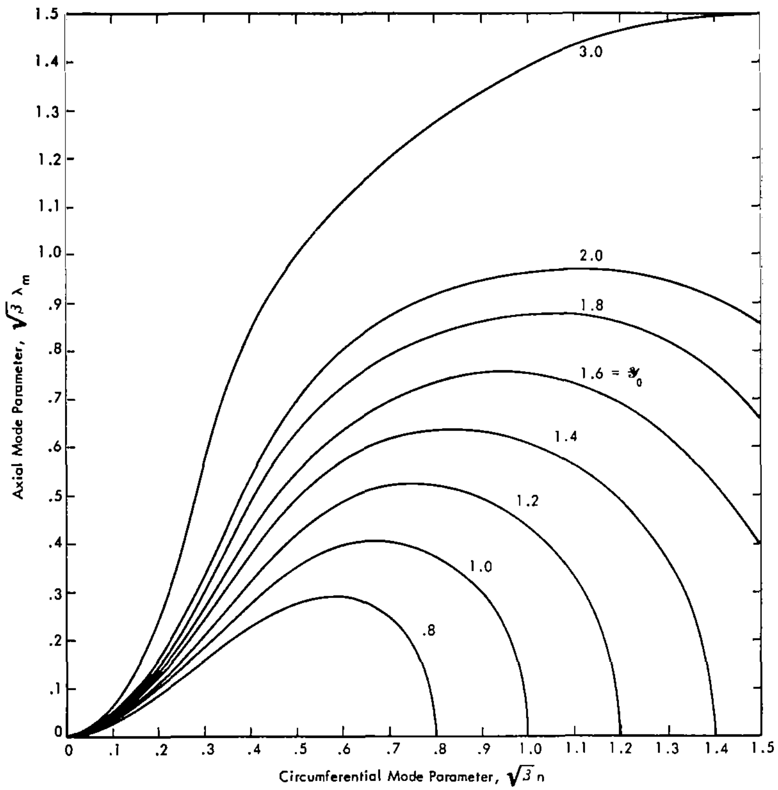

Figure 12. Contours for Circumferential Coincidence Conditions of Cylindrical Shell for Several Values of Parameter $\mathscr{Y}_0$

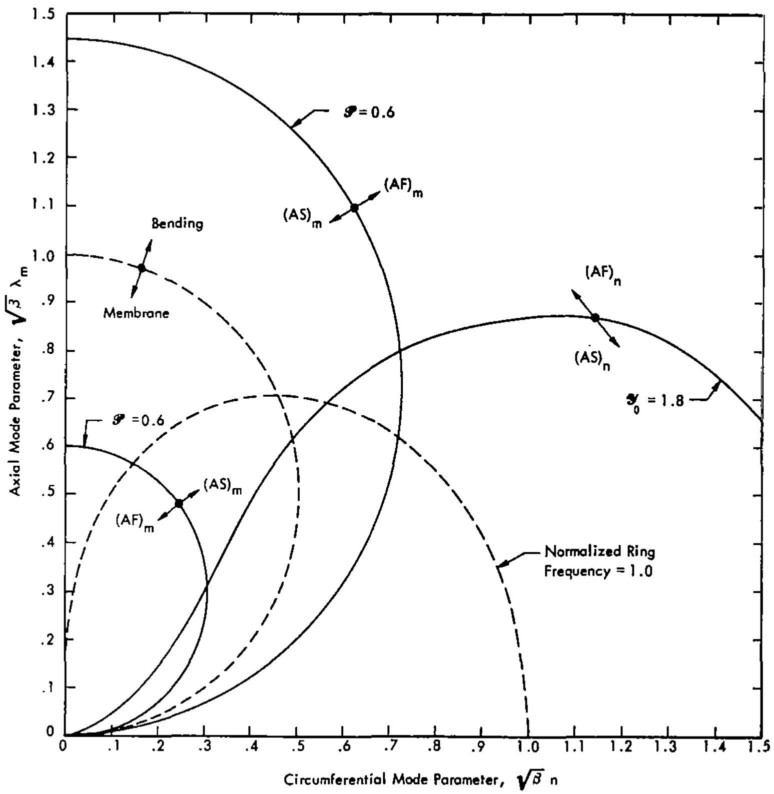

Figure 13. Typical Contours for Axial and Circumferential Coincidence Conditions Showing Regions of Acoustically Fast and Slow Modes of Shell.

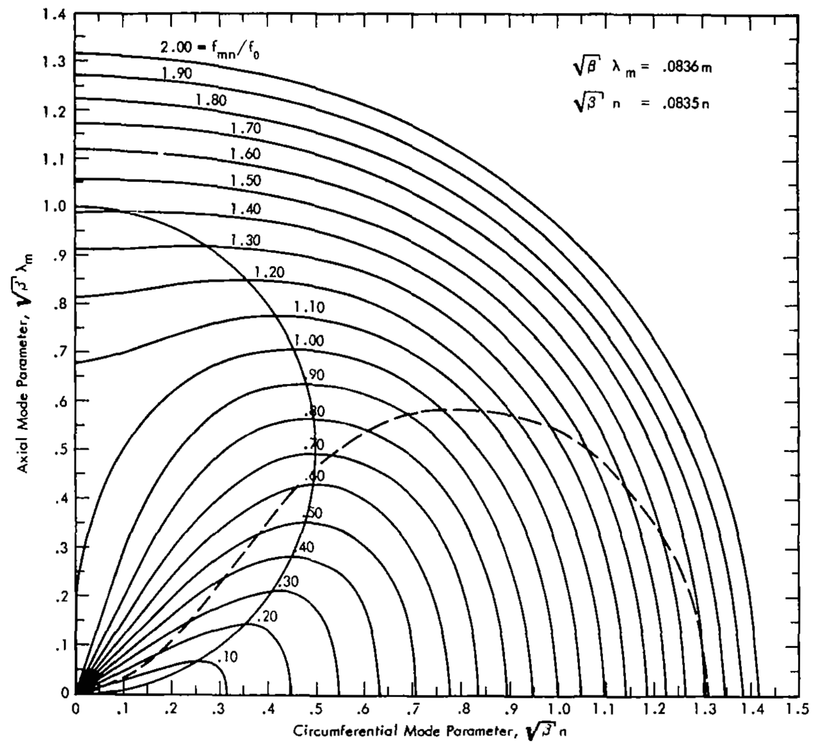

Figure 14. Contour Plots for Shell Resonance Frequencies and Acoustic Coincidences; SLA Structure

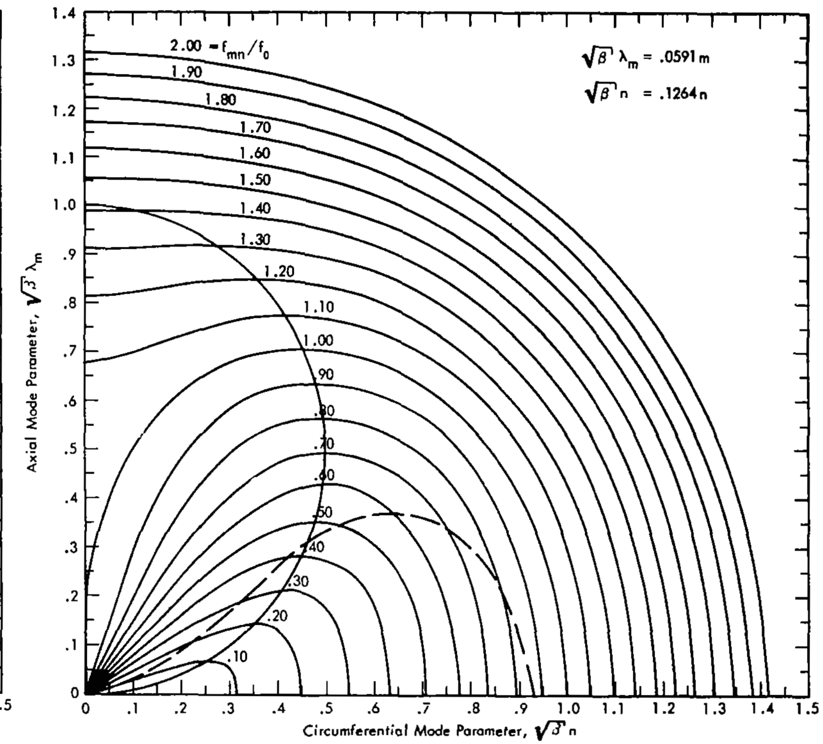

Figure 15. Contour Plots for Shell Resonance Frequencies and Acoustic Coincidences; SLA Structure, Radius = 52 in.

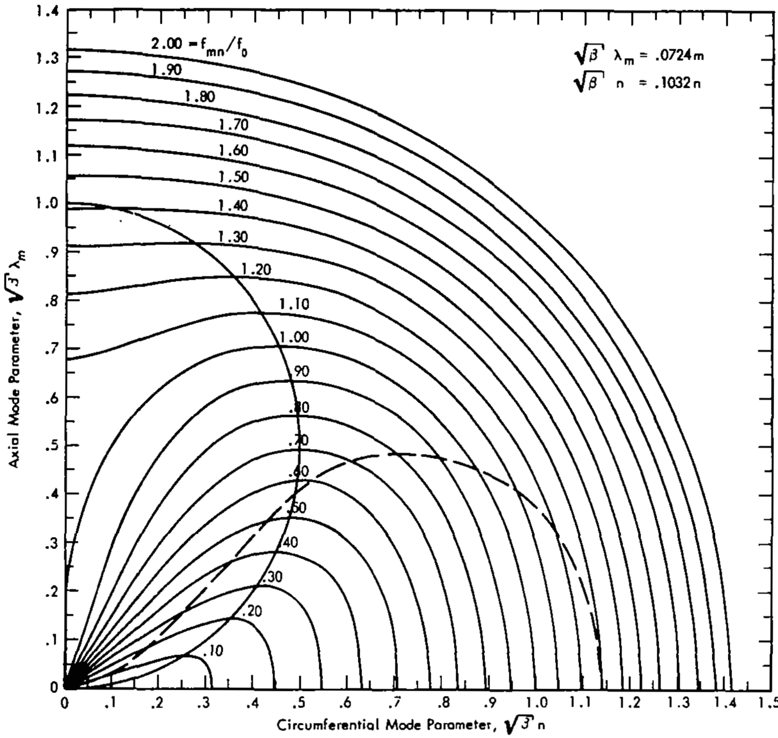

Figure 16. Contour Plots for Shell Resonance Frequencies and Acoustic Coincidences; SLA Structure, Radius = 78 in.

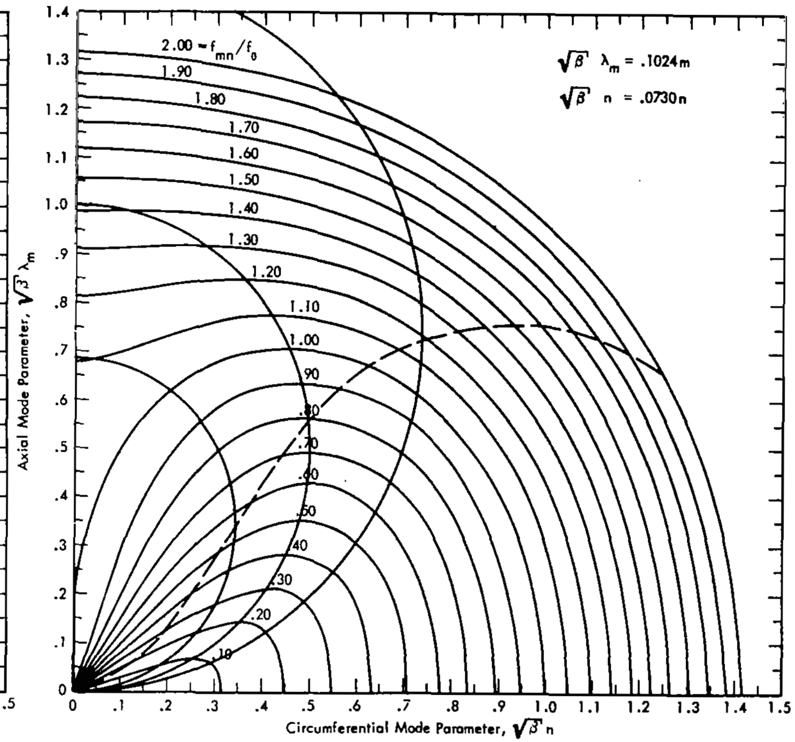

Figure 17. Contour Plots for Shell Resonance Frequencies and Acoustic Coincidences; SLA Structure, Radius = 156 in.

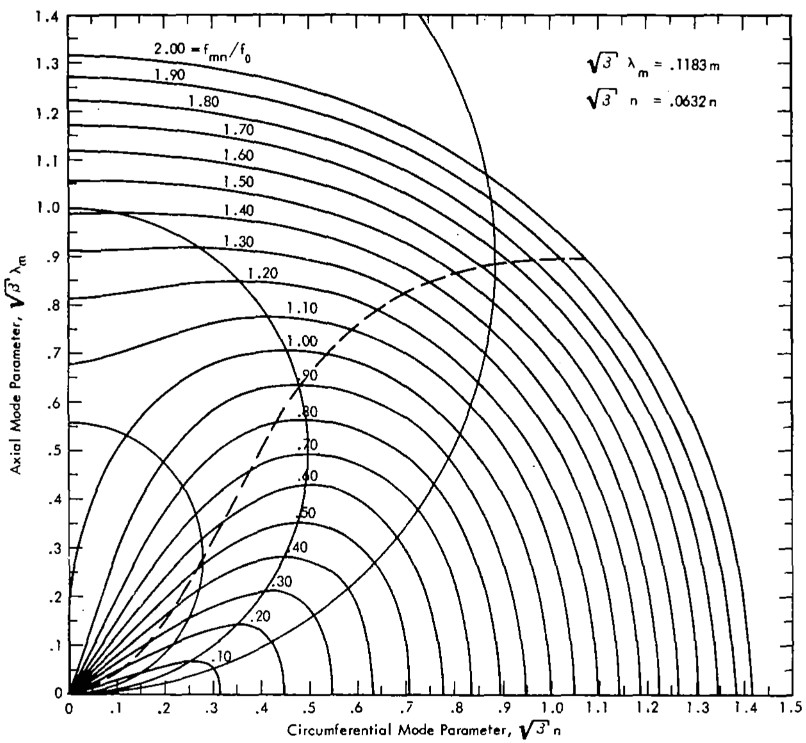

Figure 18. Contour Plots for Shell Resonance Frequencies and Acoustic Coincidences; SLA Structure, Radius = 208 in.

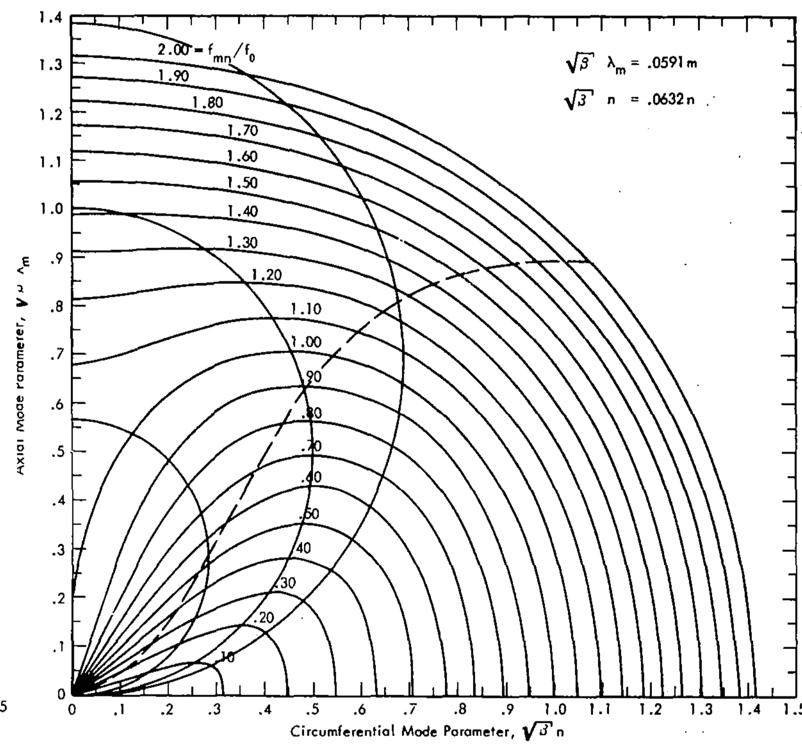

Figure 19. Contour Plots for Shell Resonance Frequencies and Acoustic Coincidences; SLA Structure, $D = 8.1 \times 10^4$ lb/in.

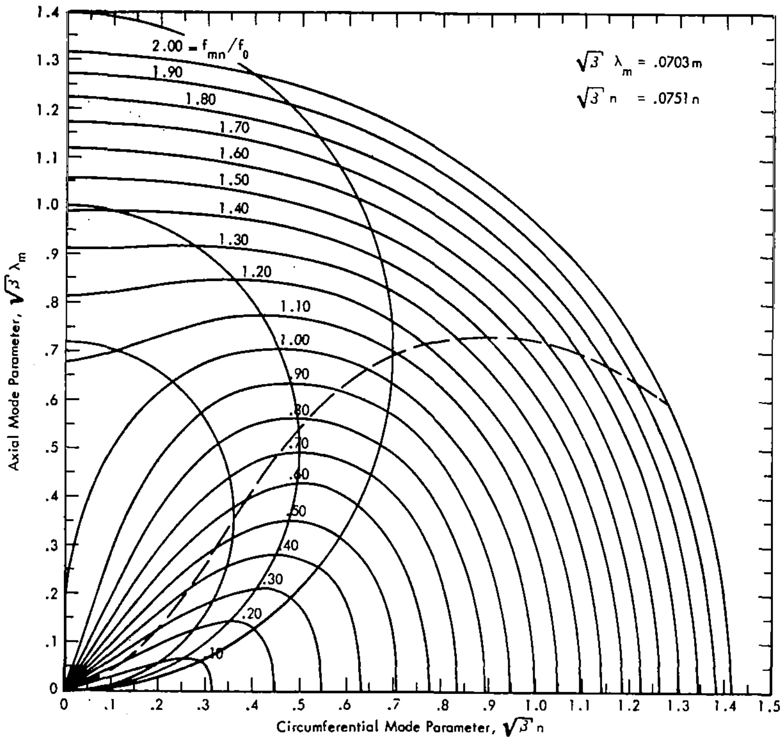

Figure 20. Contour Plots for Shell Resonance Frequencies and Acoustic Coincidences; SLA Structure, D = 1.62 x 10^5 lb/in.

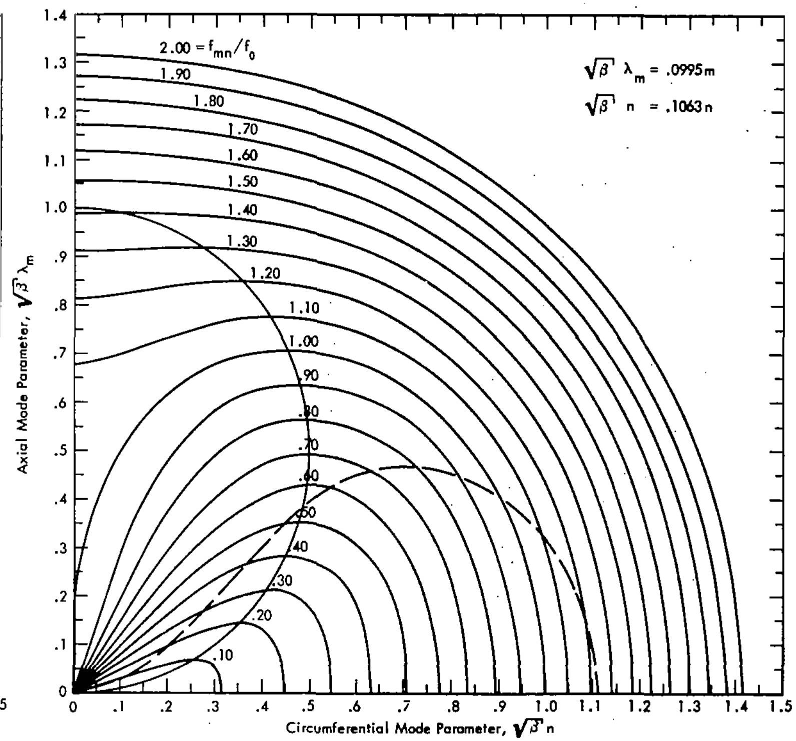

Figure 21. Contour Plots for Shell Resonance Frequencies and Acoustic Coincidences; SLA Structure, D = 6.48 x 10^5 lb/in.

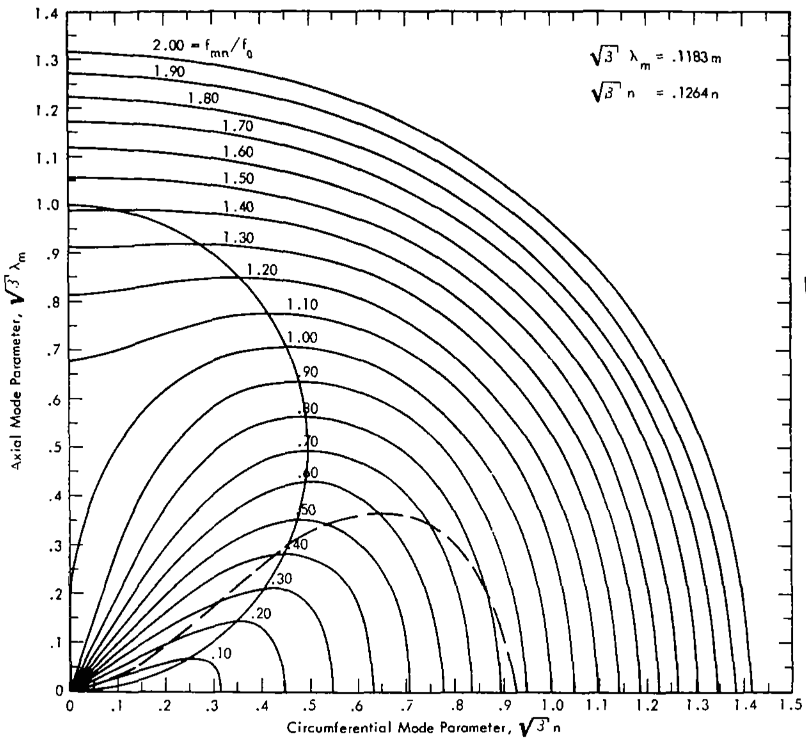

Figure 22. Contour Plots for Shell Resonance Frequencies and Acoustic Coincidences; SLA Structure, $D = 1.296 \times 10^6$ lb/in.

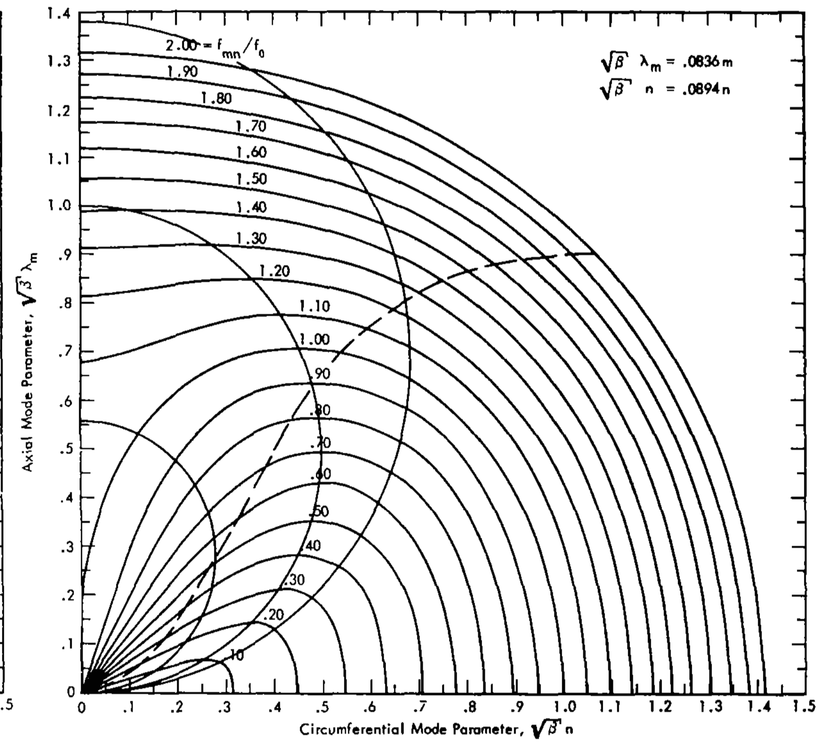

Figure 23. Contour Plots for Shell Resonance Frequencies and Acoustic Coincidences; SLA Structure, $\mu g = 0.0278$ lb/in.^{2}

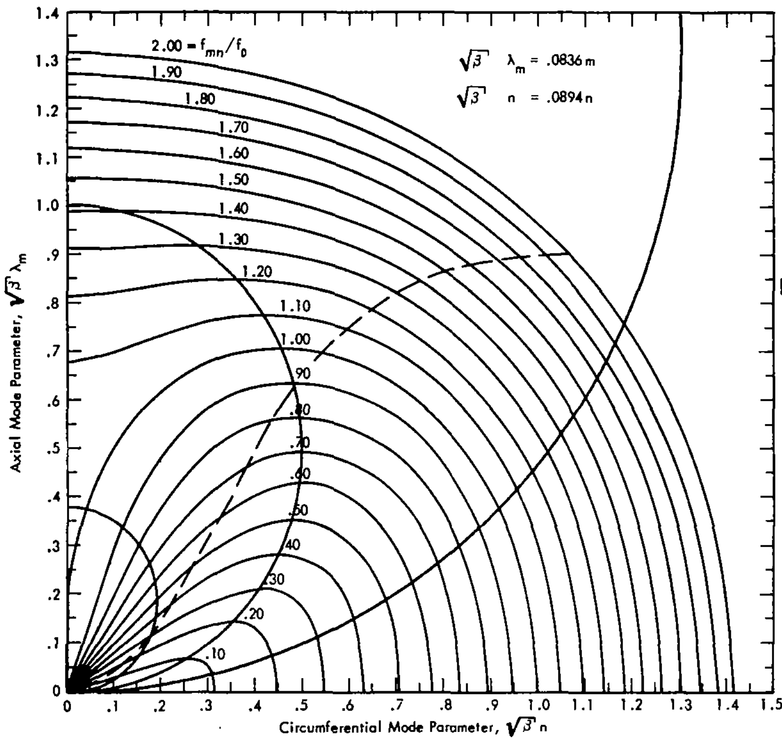

Figure 24. Contour Plots for Shell Resonance Frequencies and Acoustic Coincidences; SLA Structure, $\mu g = 0.0556\ lb/in^2$

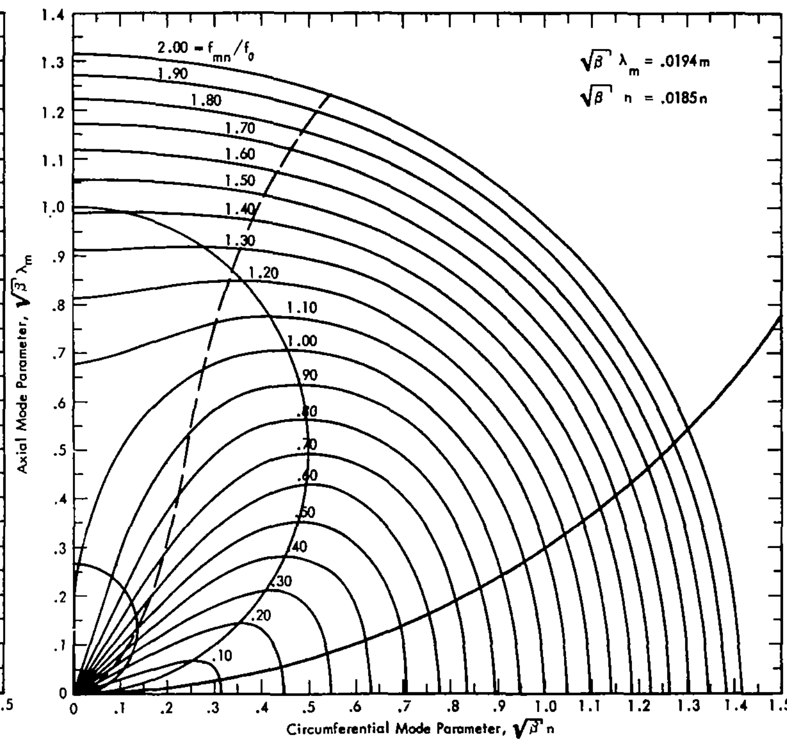

Figure 25. Contour Plots for Shell Resonance Frequencies and Acoustic Coincidences; Republic Cylinder No. 12, (18" Radius x 54" x .020")

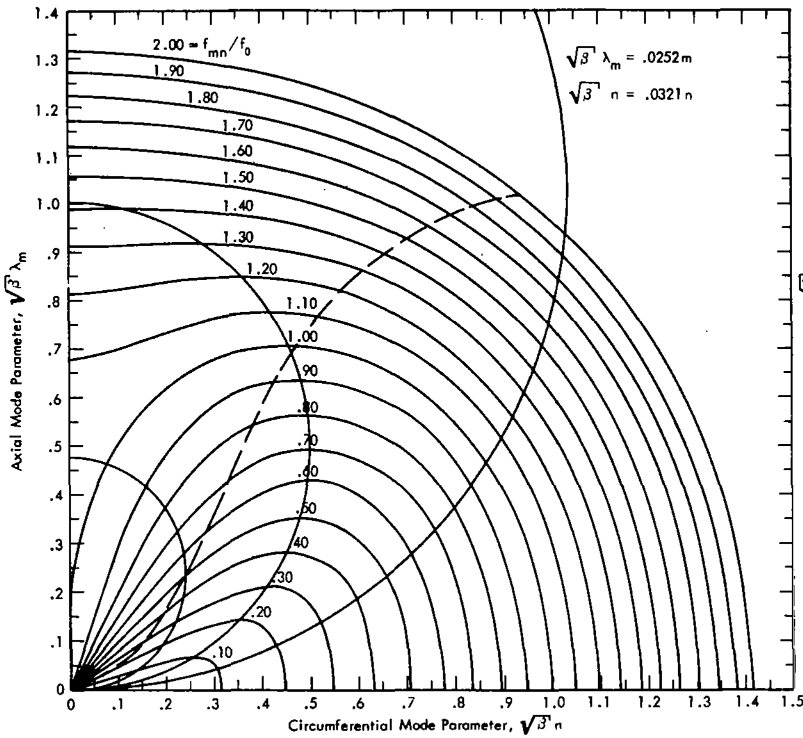

Figure 26. Contour Plots for Shell Resonance Frequencies and Acoustic Coincidences; Uniform Cylinder, (12" Radius x 48" x .040")

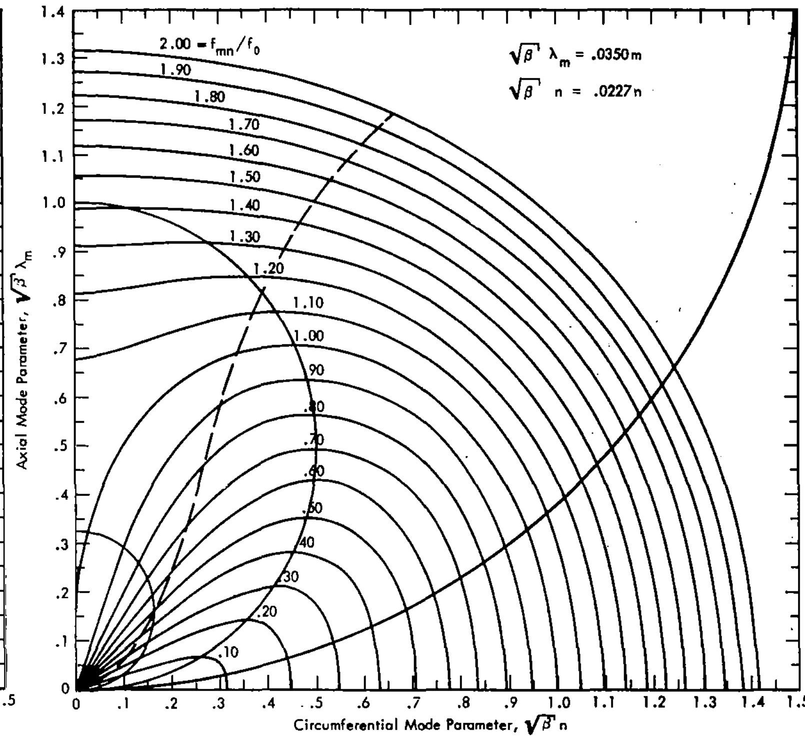

Figure 27. Contour Plots for Shell Resonance Frequencies and Acoustic Coincidences; Uniform Cylinder, (24" Radius x 48" x .040")

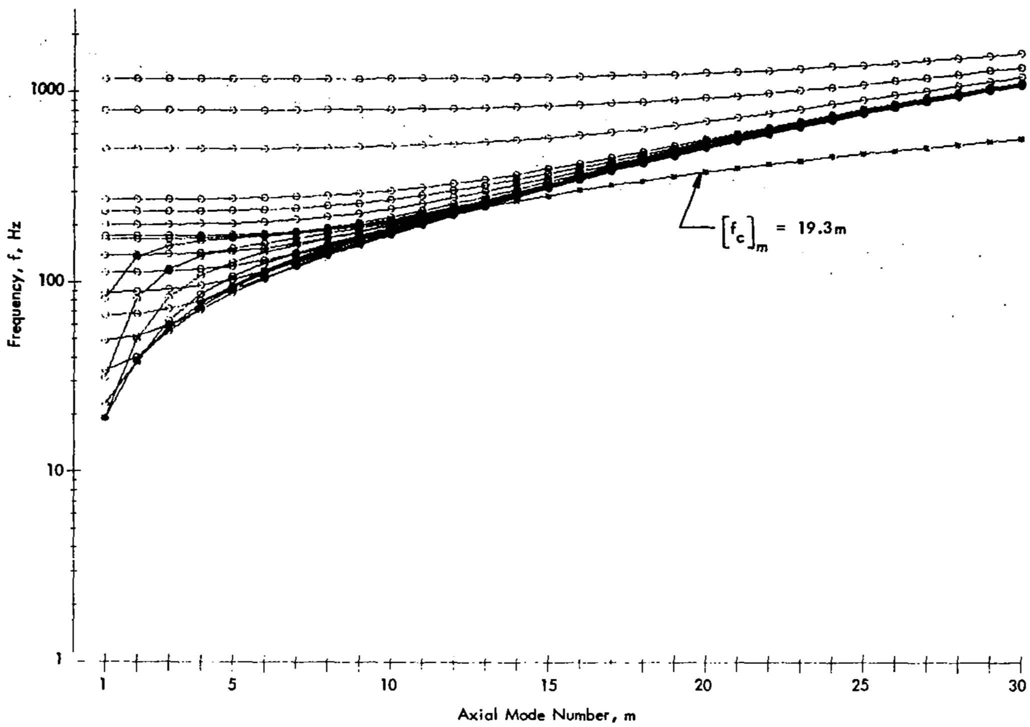

Figure 28. Distribution of Shell Resonance Frequencies versus Axial Mode Number m; SLA Structure

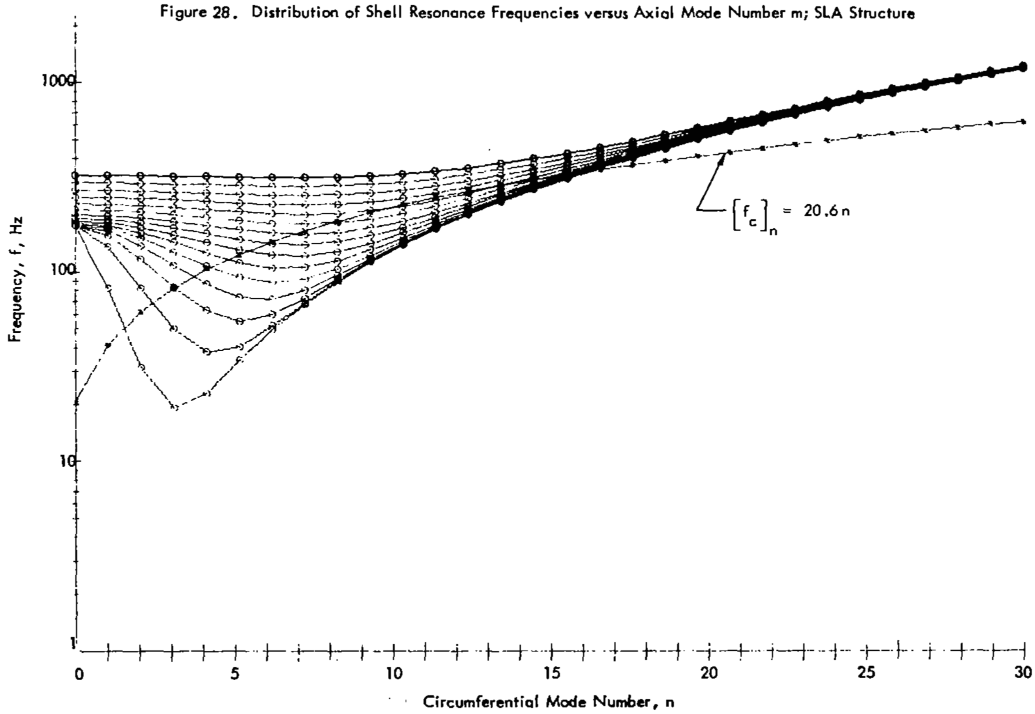

Figure 29. Distribution of Shell Resonance Frequencies versus Circumferential Mode Number n; SLA Structure

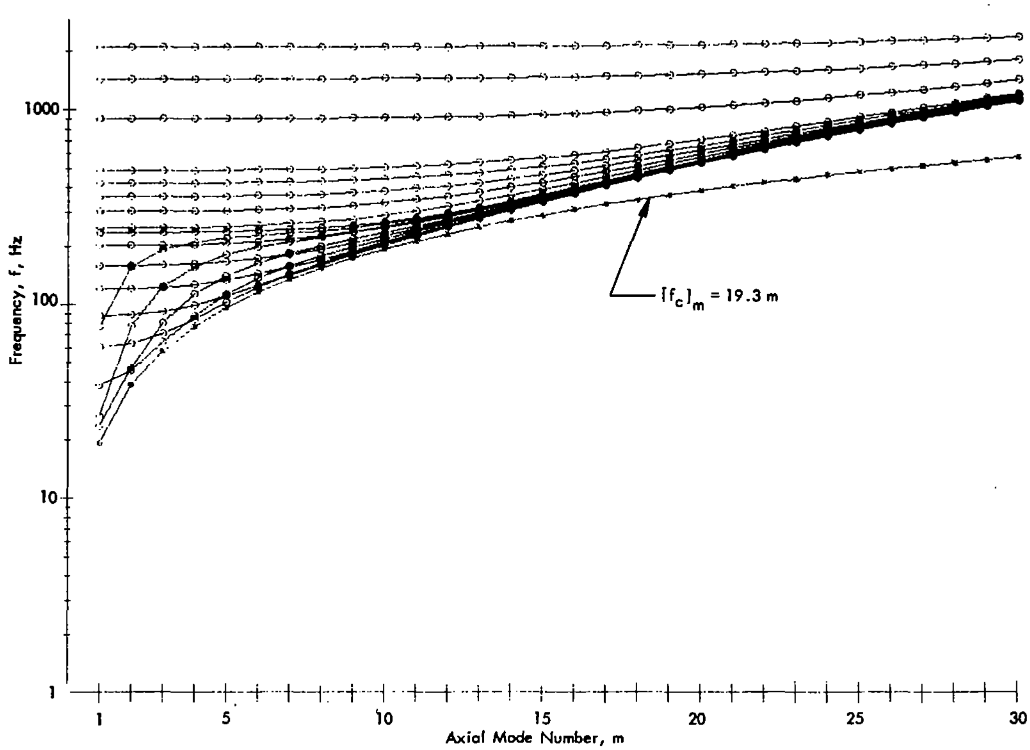

Figure 30. Distribution of Shell Resonance Frequencies versus Axial Mode Number m; SLA Structure, Radius = 78 in.

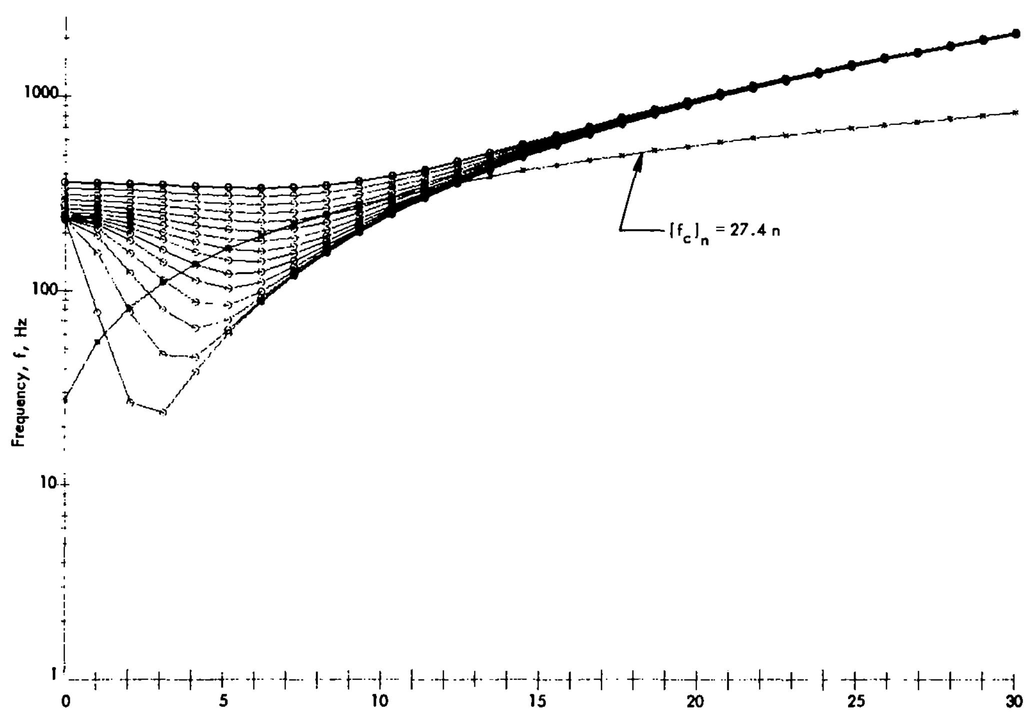

Figure 31. Distribution of Shell Resonance Frequencies versus Circumferential Mode Number n; SLA Structure, Radius = 78 in.

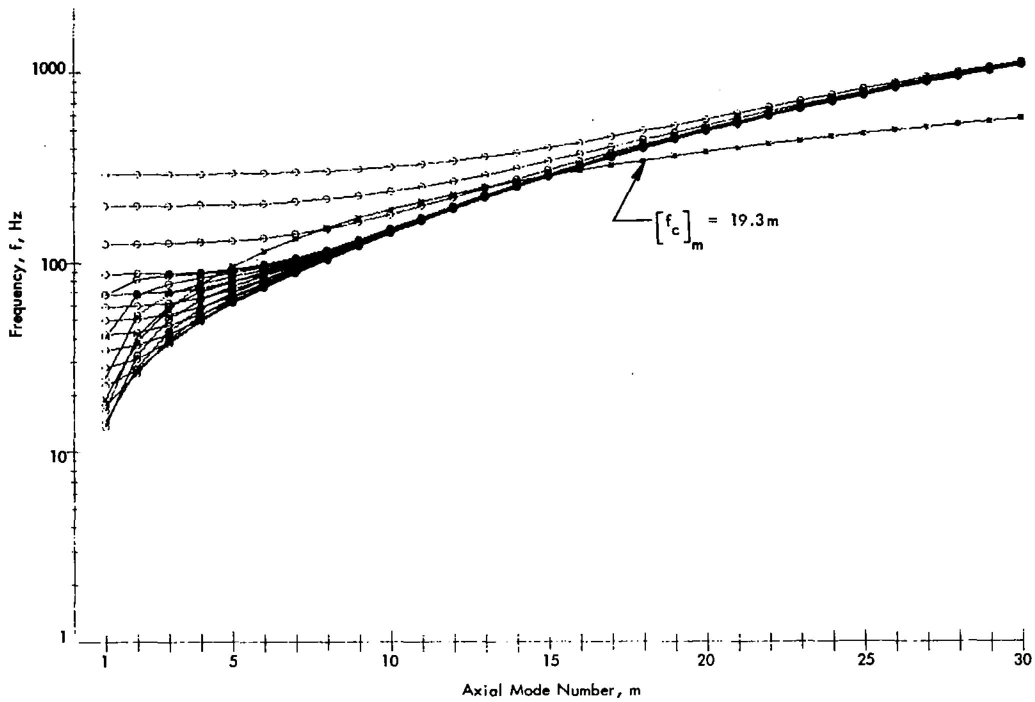

Figure 32. Distribution of Shell Resonance Frequencies versus Axial Mode Number m; SLA Structure, Radius = 208 in.

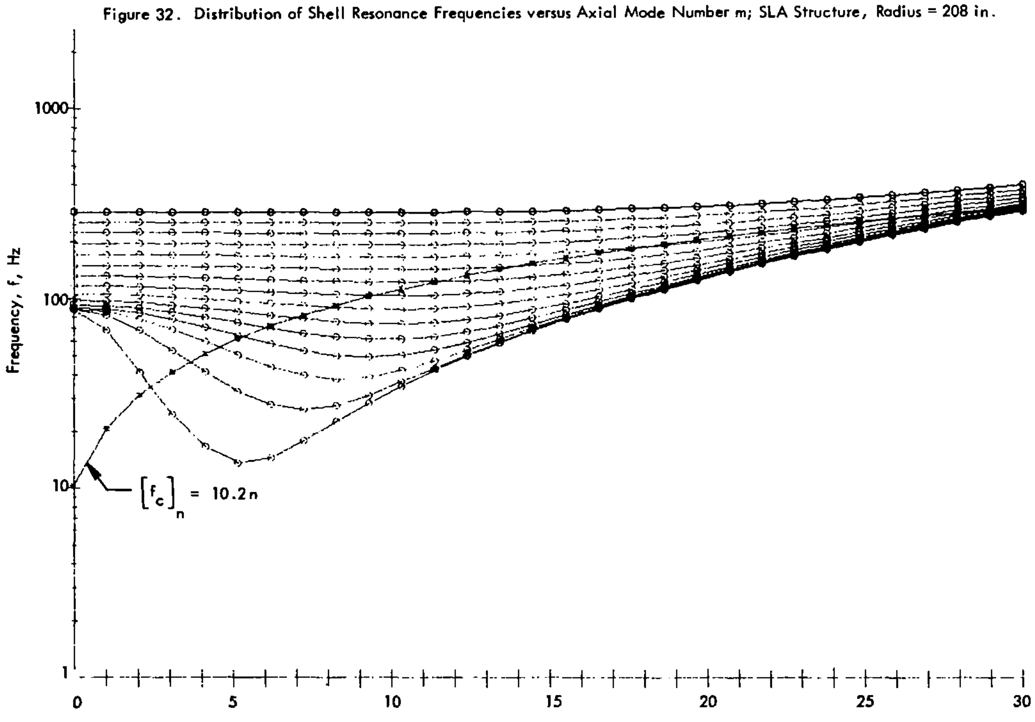

Figure 33. Distribution of Shell Resonance Frequencies versus Circumferential Mode Number n; SLA Structure, Radius = 208 in.

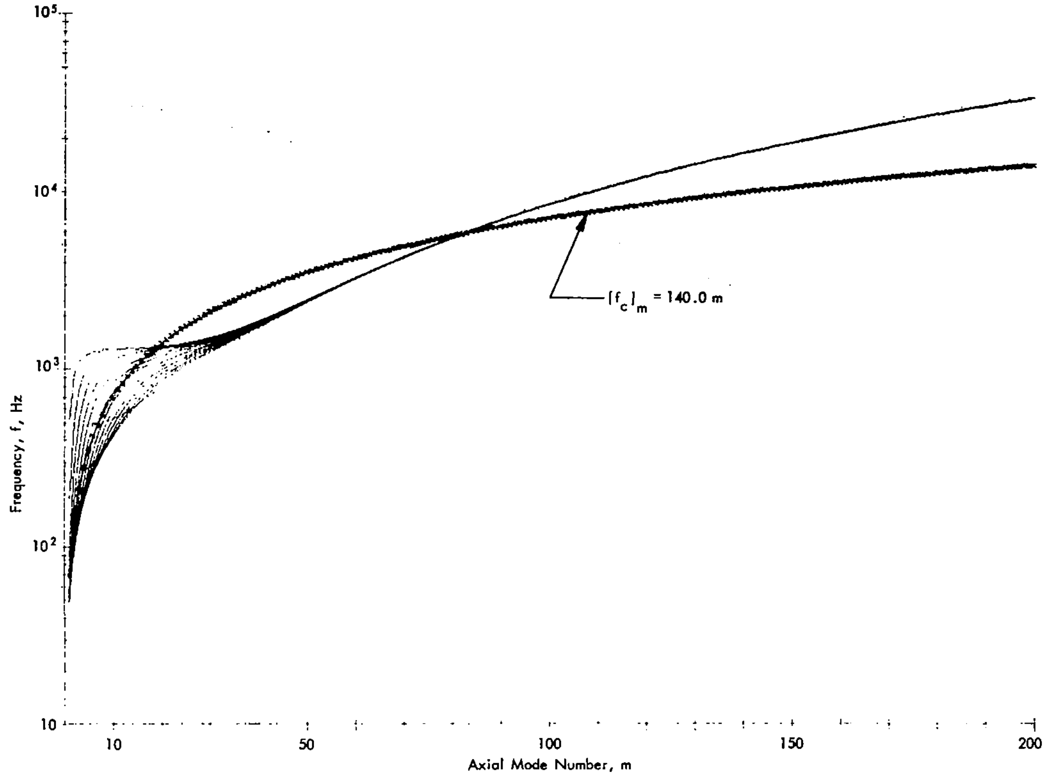

Figure 34. Distribution of Shell Resonance Frequencies versus Axial Mode Number m: Uniform Cylinder, 24 in. Radius by 48 in. by 0.040 in.

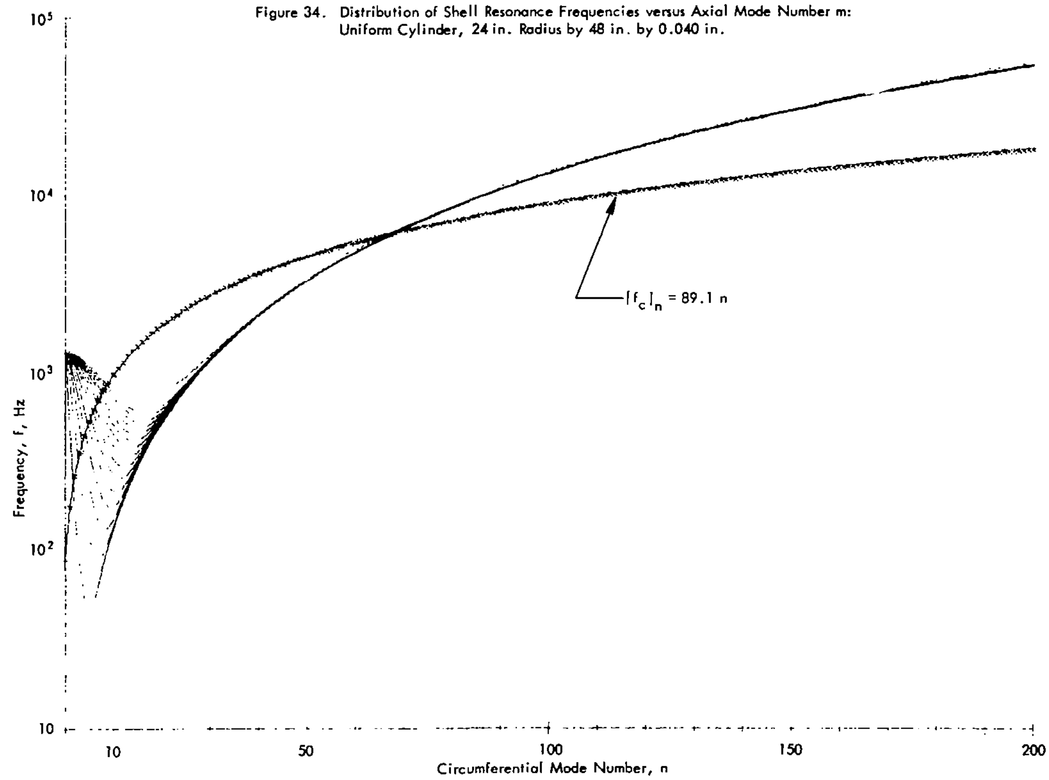

Figure 35. Distribution of Shell Resonance Frequencies versus Circumferential Mode Number n; Uniform Cylinder, 24 in. Radius by 48 in. by 0.040 in.

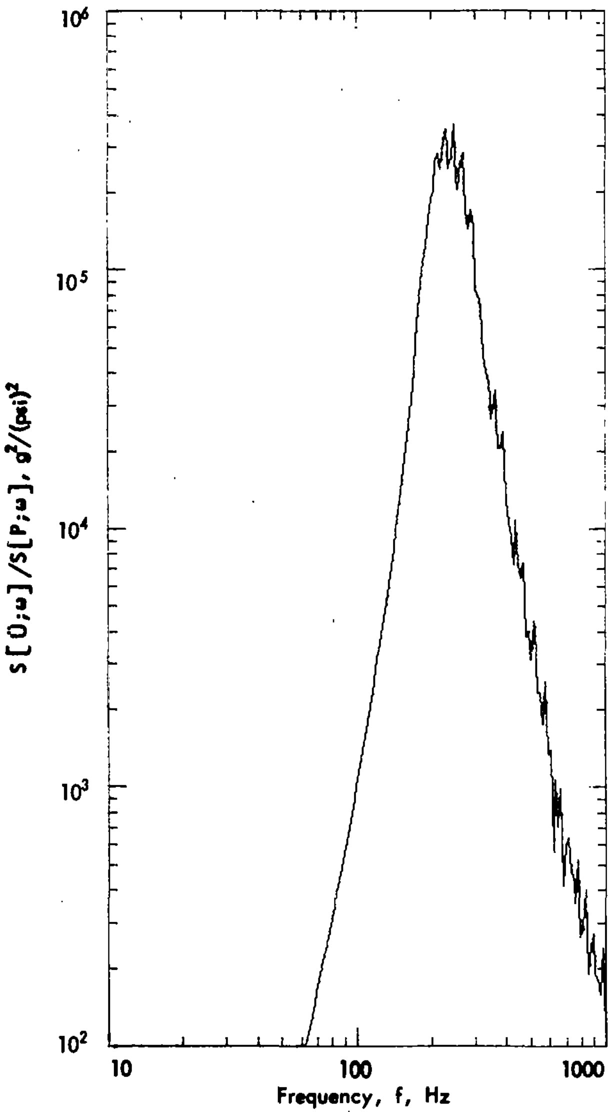

Figure 36. Acceleration Spectrum of SLA for Duct Excitation; N = 1, Q = 15

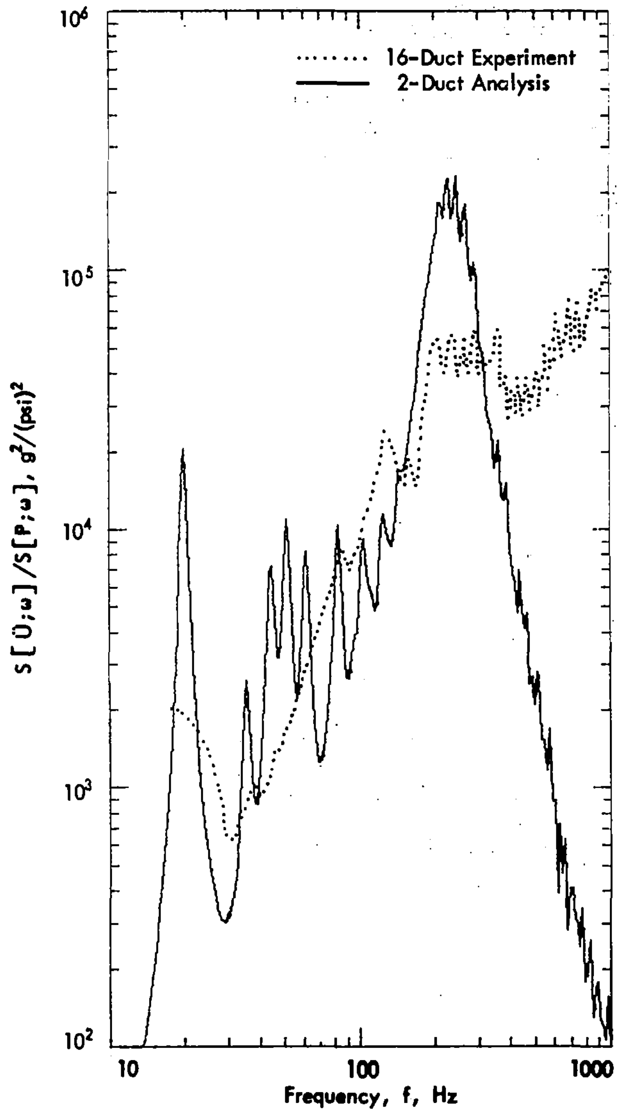

Figure 37. Theoretical and Experimental Acceleration Spectrum of SLA for Duct Excitation; N = 2, Q = 15

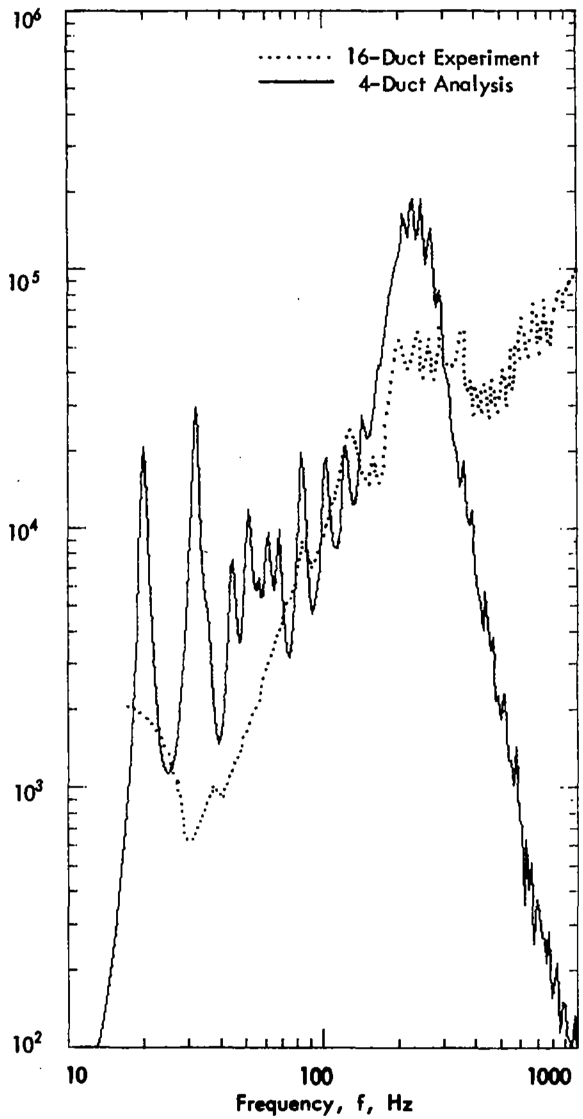

Figure 38. Theoretical and Experimental Acceleration Spectrum of SLA for Duct Excitation; N = 4, Q = 15

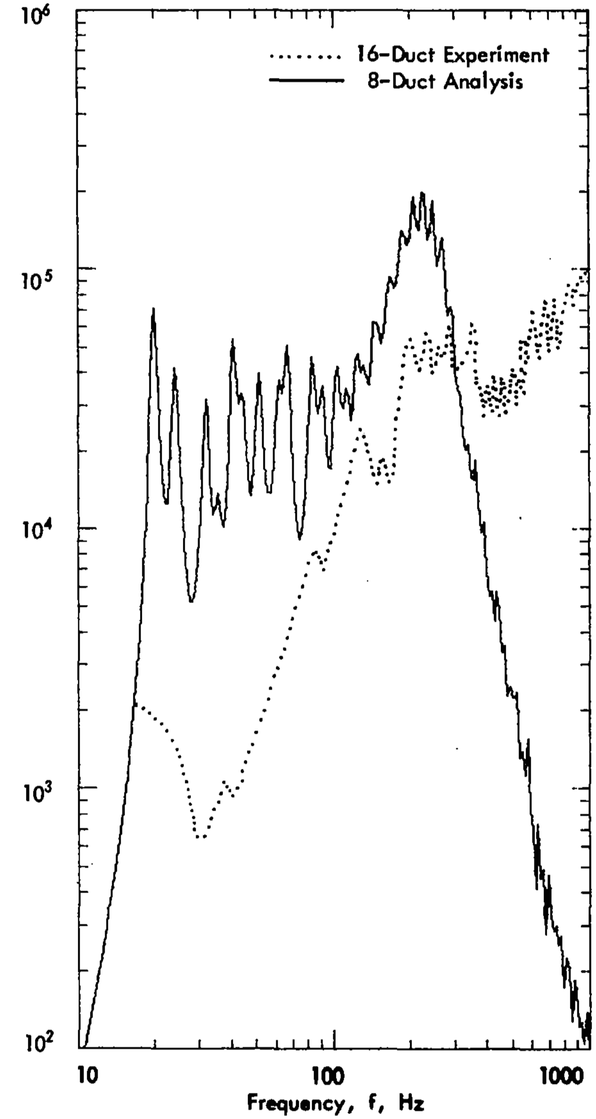

Figure 39. Theoretical and Experimental Acceleration Spectrum of SLA for Duct Excitation; N = 8, Q = 15

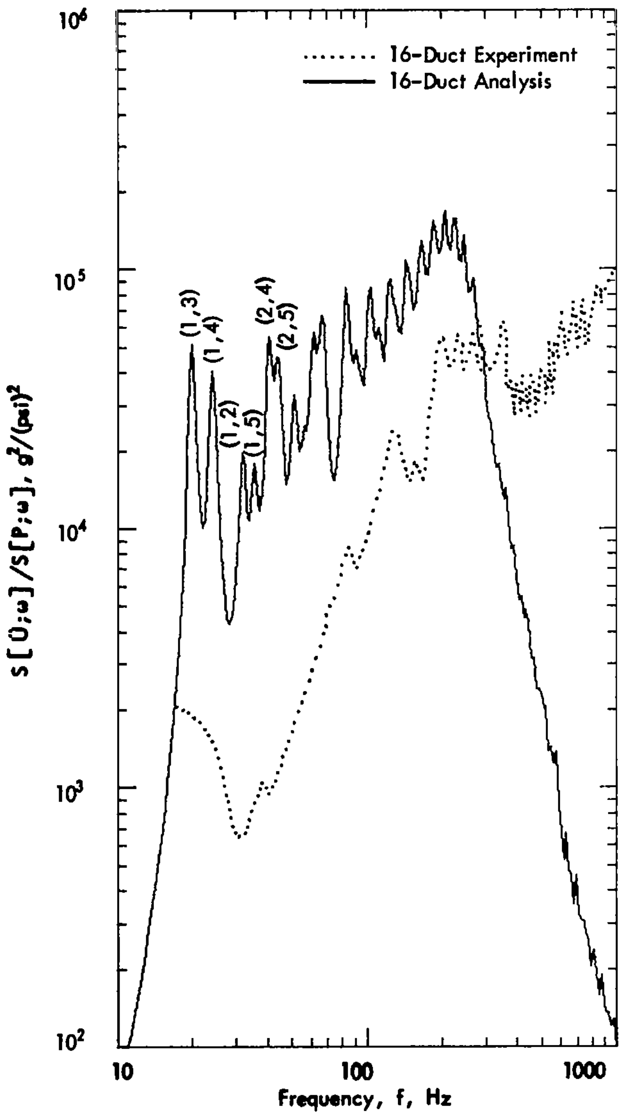

Figure 40. Theoretical and Experimental Acceleration Spectrum of SLA for Duct Excitation; N = 16, Q = 15

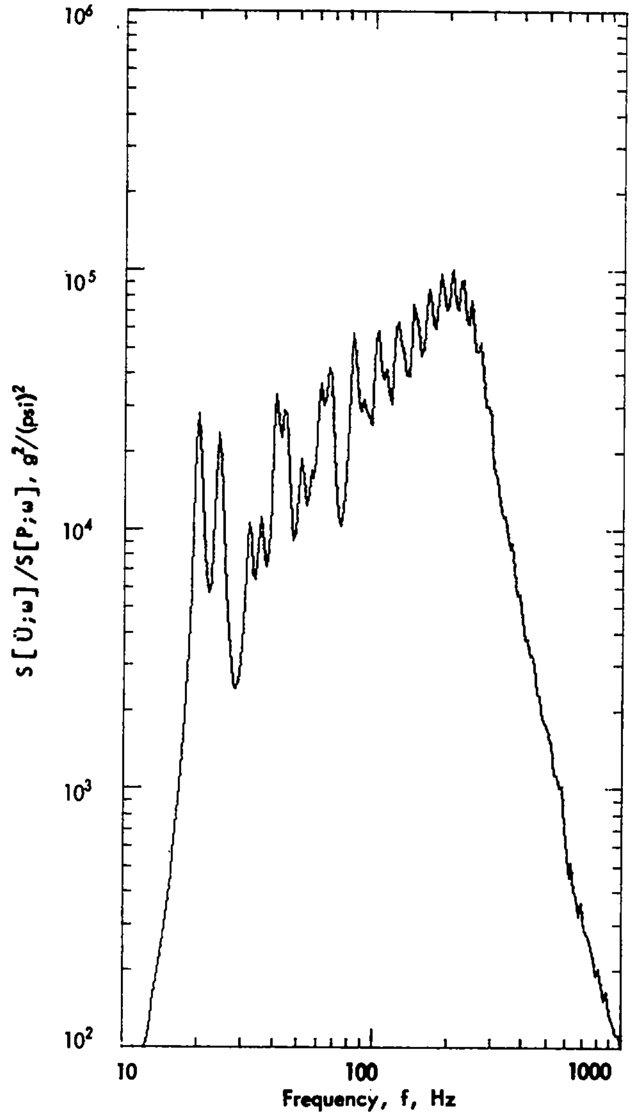

Figure 41. Acceleration Spectrum of SLA for Duct Excitation; N = 32, Q = 15

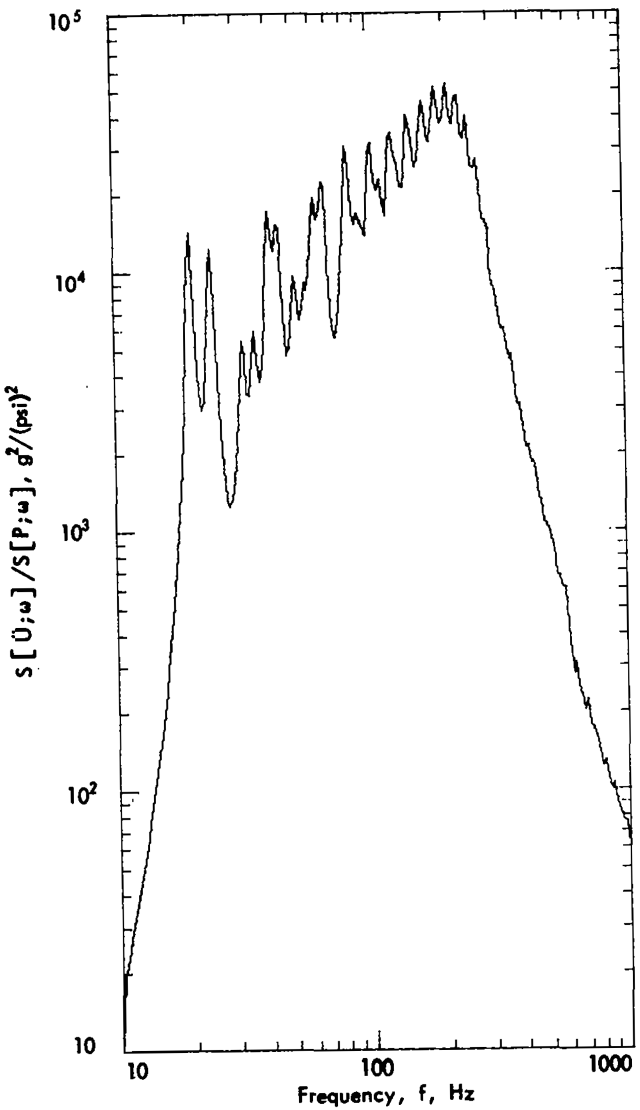

Figure 42. Acceleration Spectrum of SLA for Duct Excitation; N = 64, Q = 15

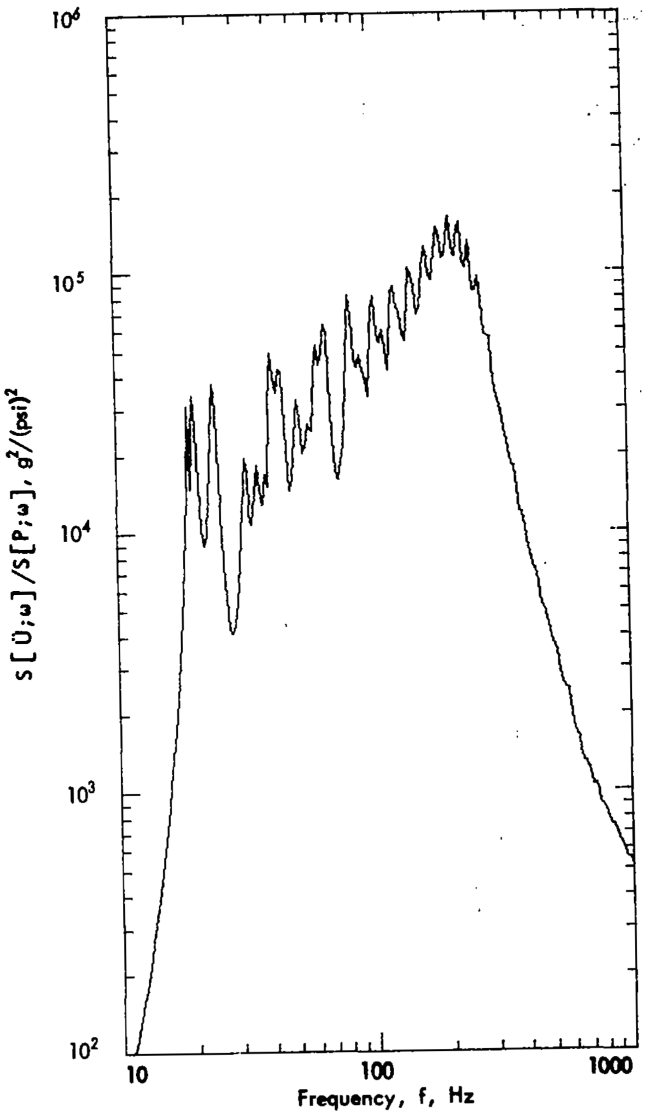

Figure 43. Acceleration Spectrum of SLA for Duct Excitation with Decaying Axial Correlation; N = 16, Q = 15, A = 0.01

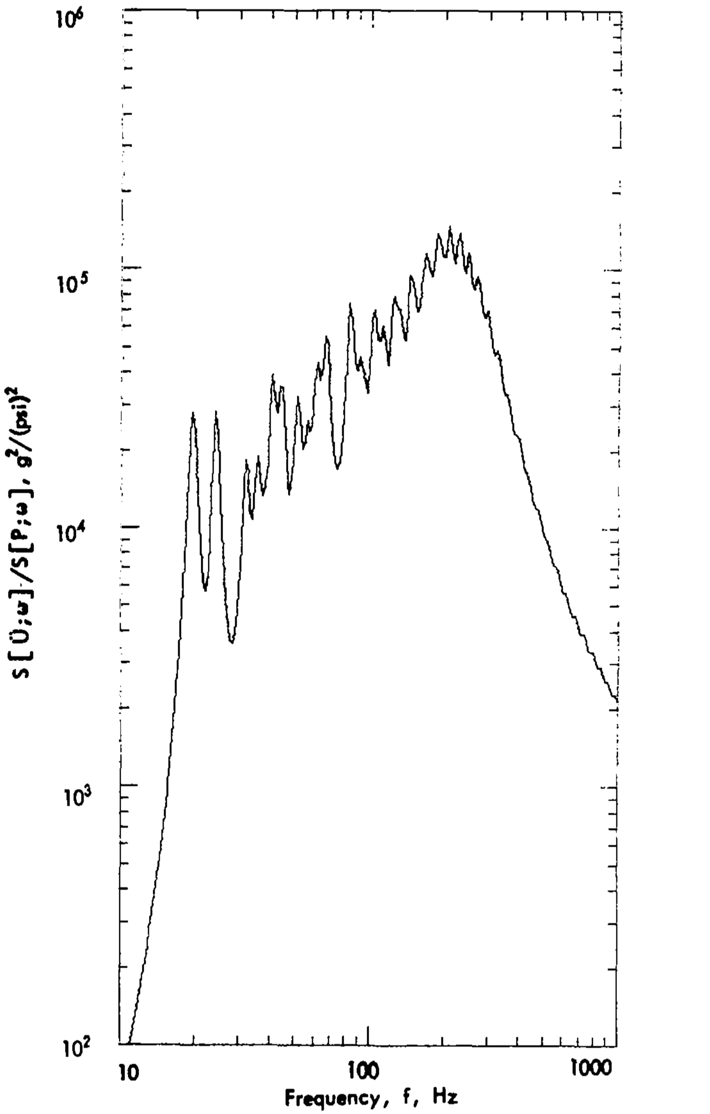

Figure 44. Acceleration Spectrum of SLA for Duct Excitation with Decaying Axial Correlation; N = 16, Q = 15, A = 0.05

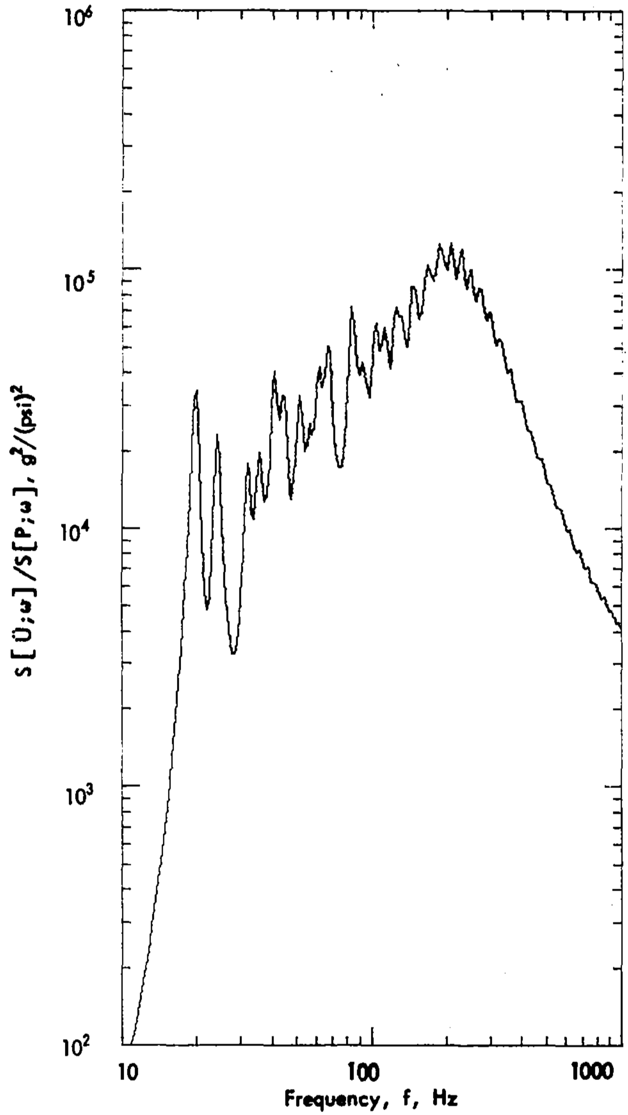

Figure 45. Acceleration Spectrum of SLA for Duct Excitation with Decaying Axial Correlation; N = 16, Q = 15, A = 0.10

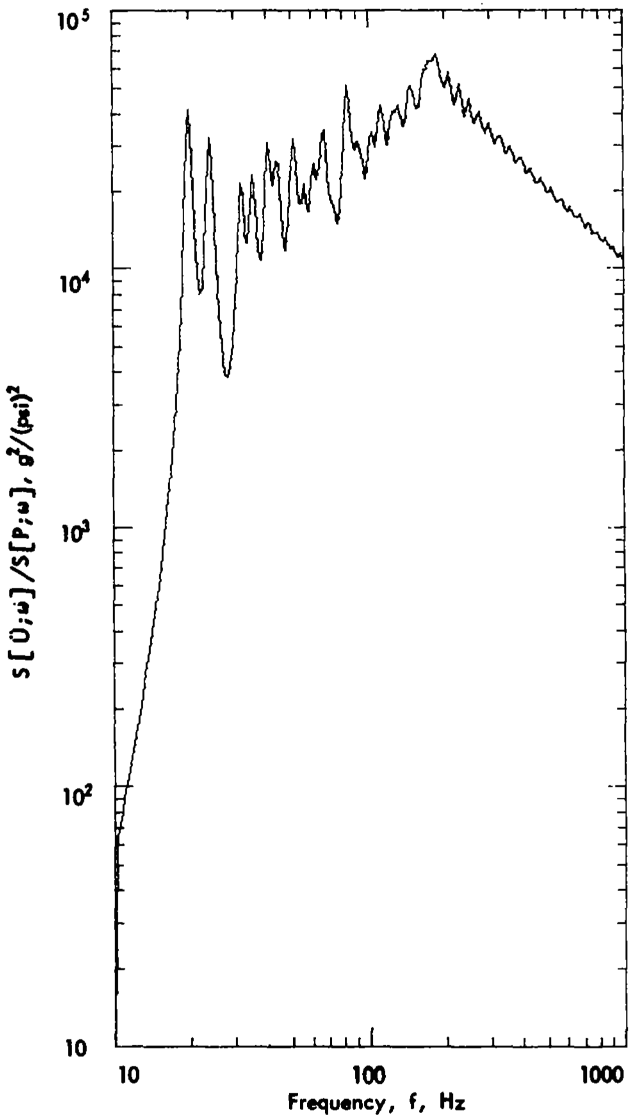

Figure 46. Acceleration Spectrum of SLA for Duct Excitation with Decaying Axial Correlation; N = 16, Q = 15, A = 0.50

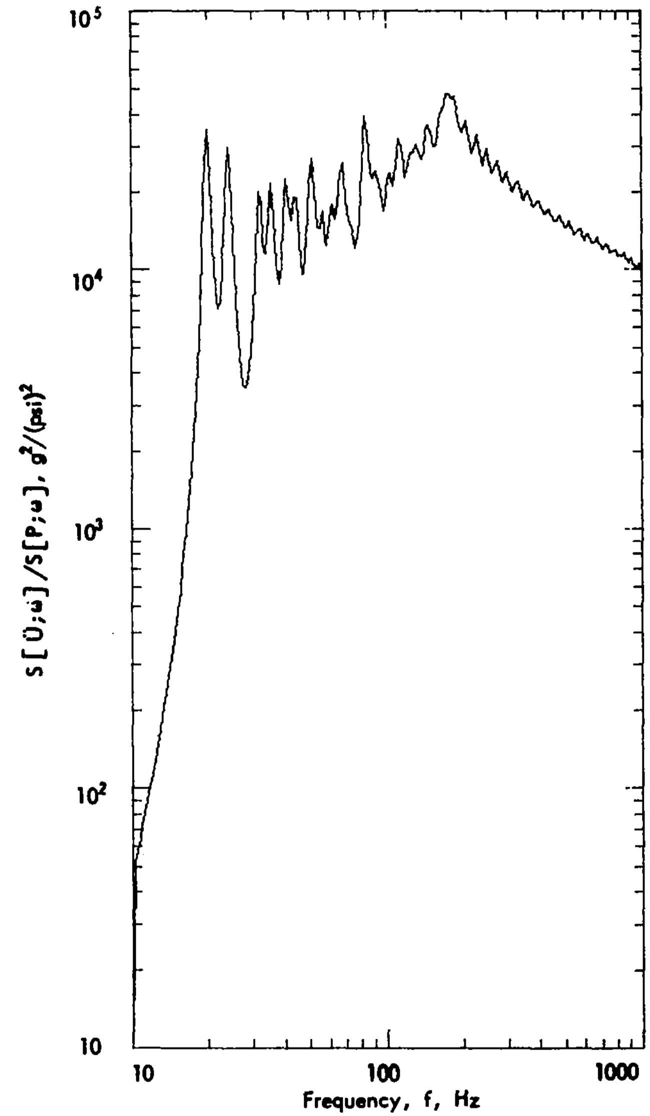

Figure 47. Acceleration Spectrum of SLA for Duct Excitation with Decaying Axial Correlation; N = 16, Q = 15, A = 1.0

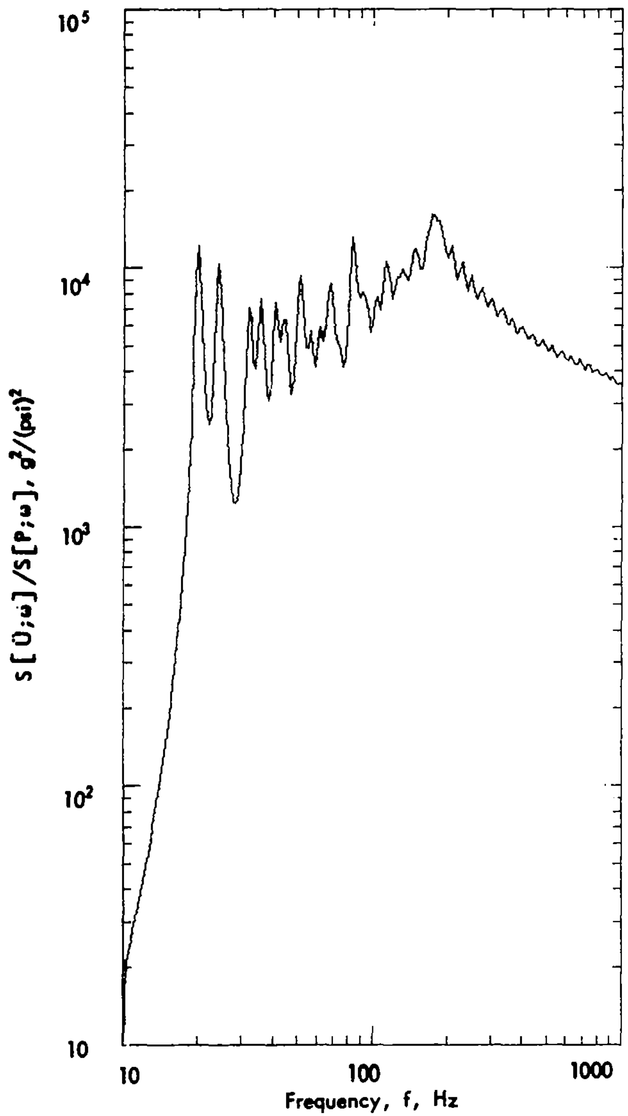

Figure 48. Acceleration Spectrum of SLA for Duct Excitation with Decaying Axial Correlation; N = 16, Q = 15, A = 5.0

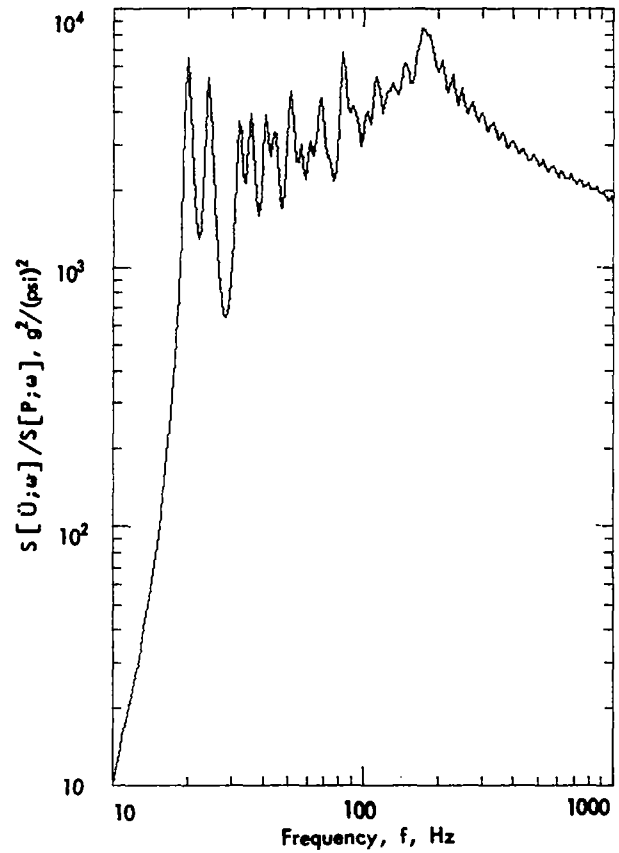

Figure 49. Acceleration Spectrum of SLA for Duct Excitation with Decaying Axial Correlation; N = 16, Q = 15, A = 10.0

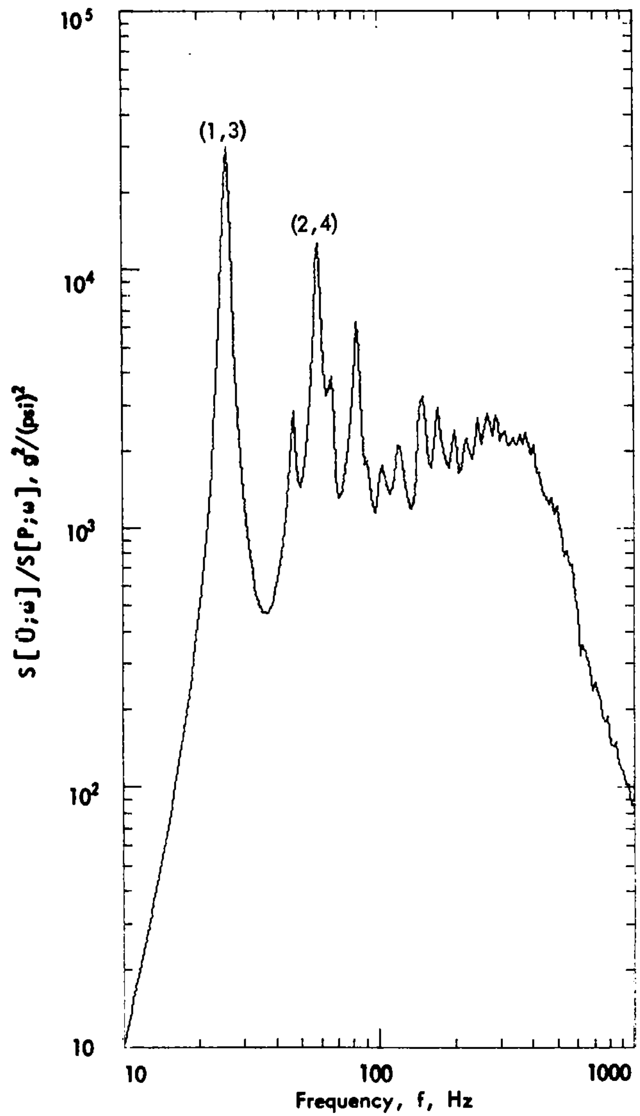

Figure 50. Effect of Radius Change on Acceleration Spectrum of SLA for Duct Excitation; N = 16, Q = 15, R = 52.0 in.

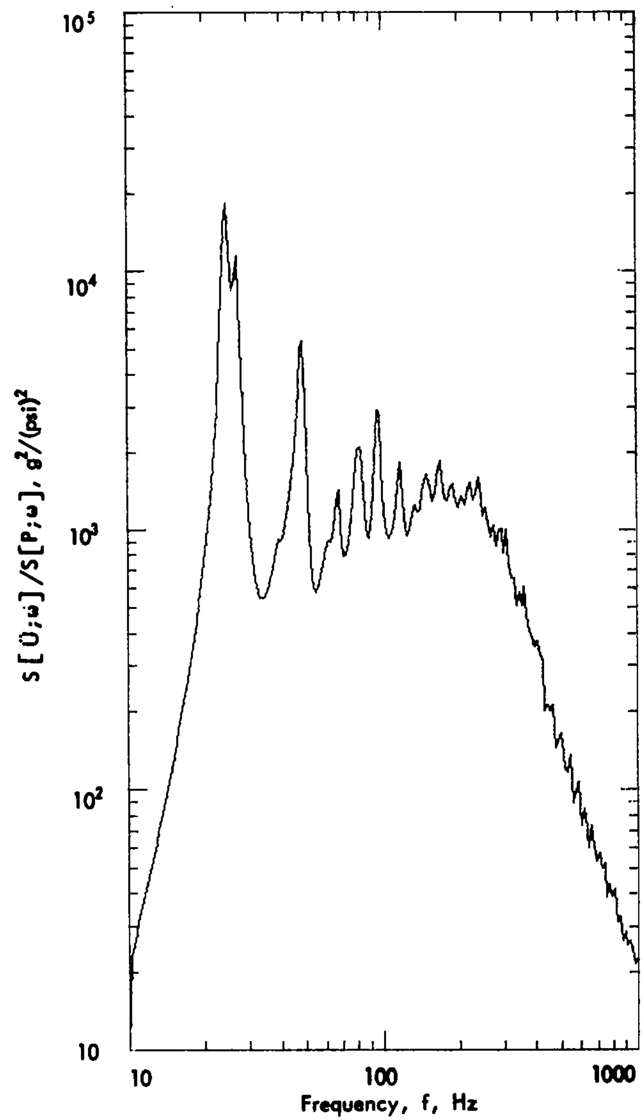

Figure 51. Effect of Radius Change on Acceleration Spectrum of SLA for Duct Excitation; N = 16, Q = 15, R = 78.0 in.

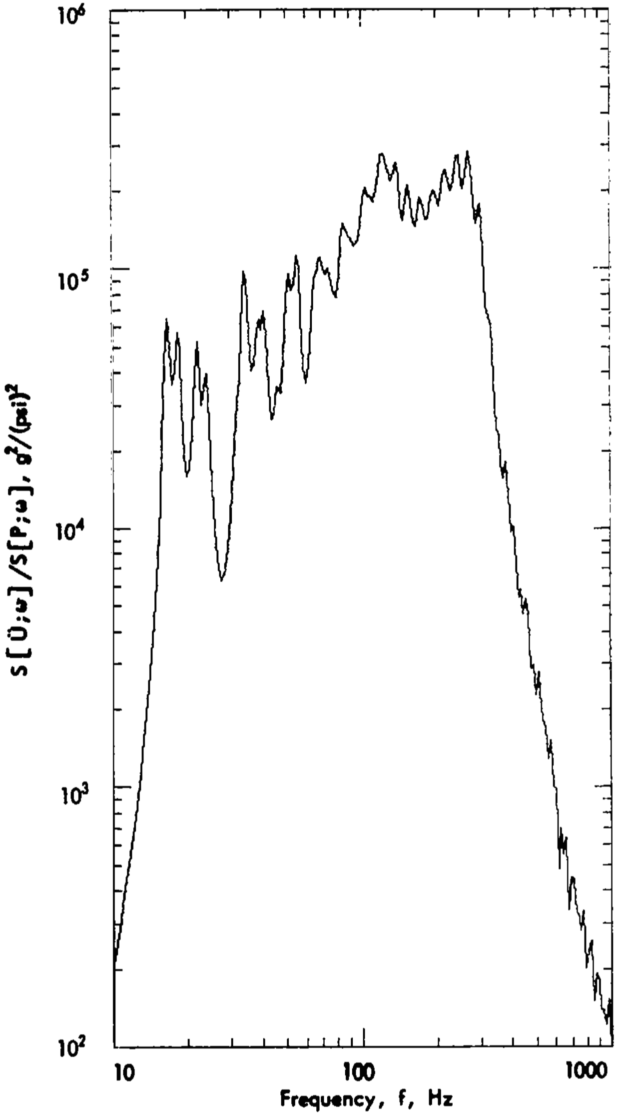

Figure 52. Effect of Radius Change on Acceleration Spectrum of SLA for Duct Excitation; N = 16, Q = 15, R = 156.0 in.

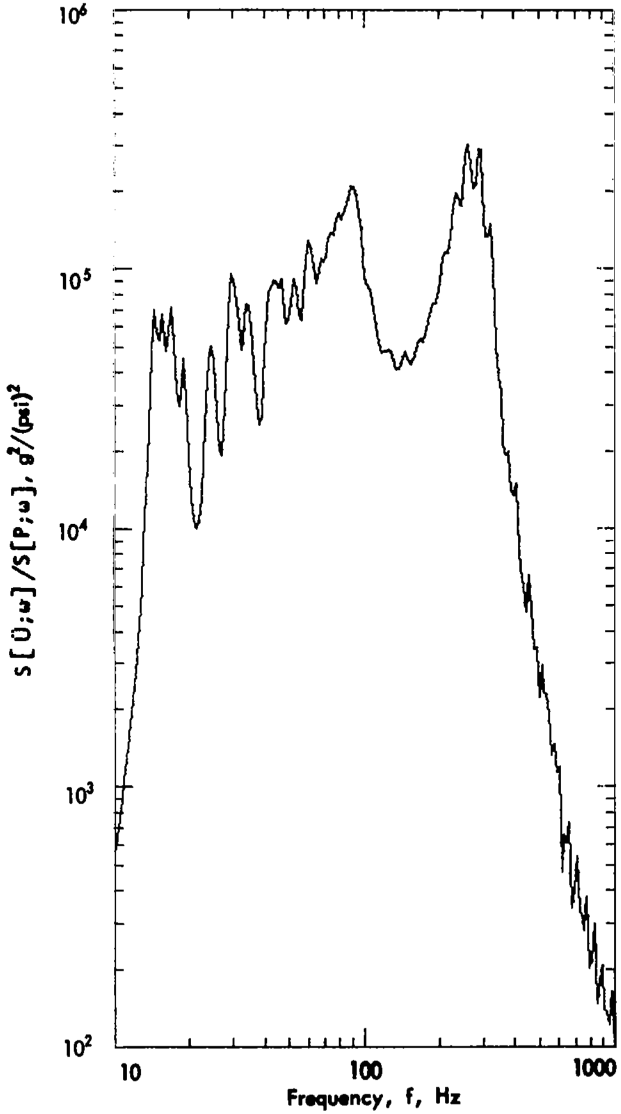

Figure 53. Effect of Radius Change on Acceleration Spectrum of SLA for Duct Excitation; N = 16, Q = 15, R = 208.0 in.

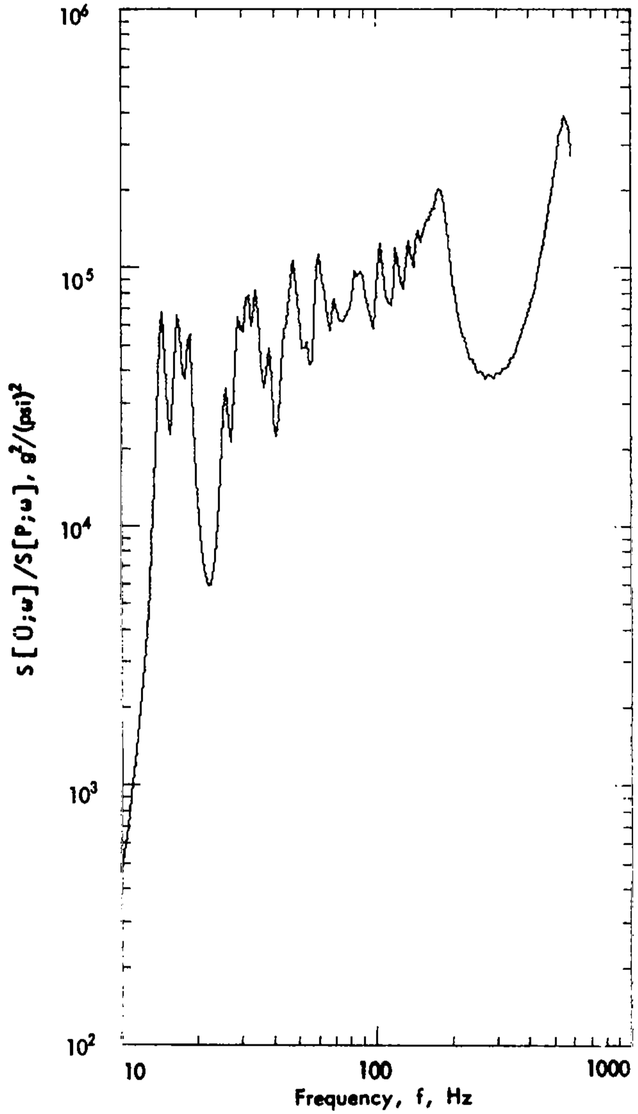

Figure 54. Effect of Stiffness Change on Acceleration Spectrum of SLA for Duct Excitation; N = 16, Q = 15, $D = 8.10 \cdot 10^4$ lb-in.

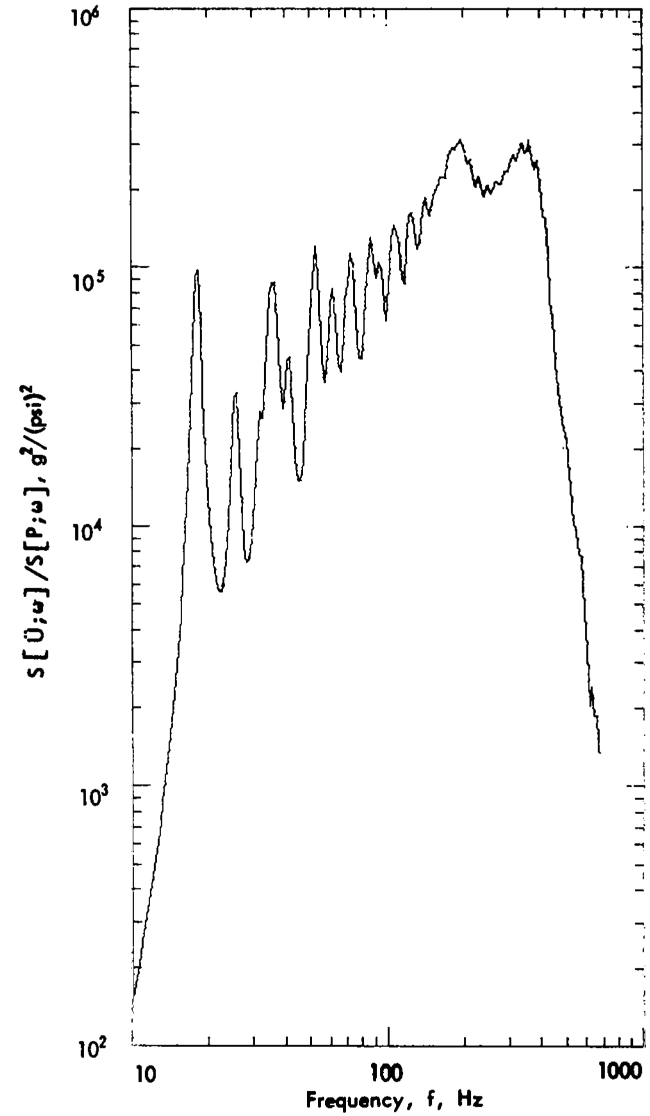

Figure 55. Effect of Stiffness Change on Acceleration Spectrum of SLA for Duct Excitation; N = 16, Q = 15, $D = 1.62 \cdot 10^5$ lb-in.

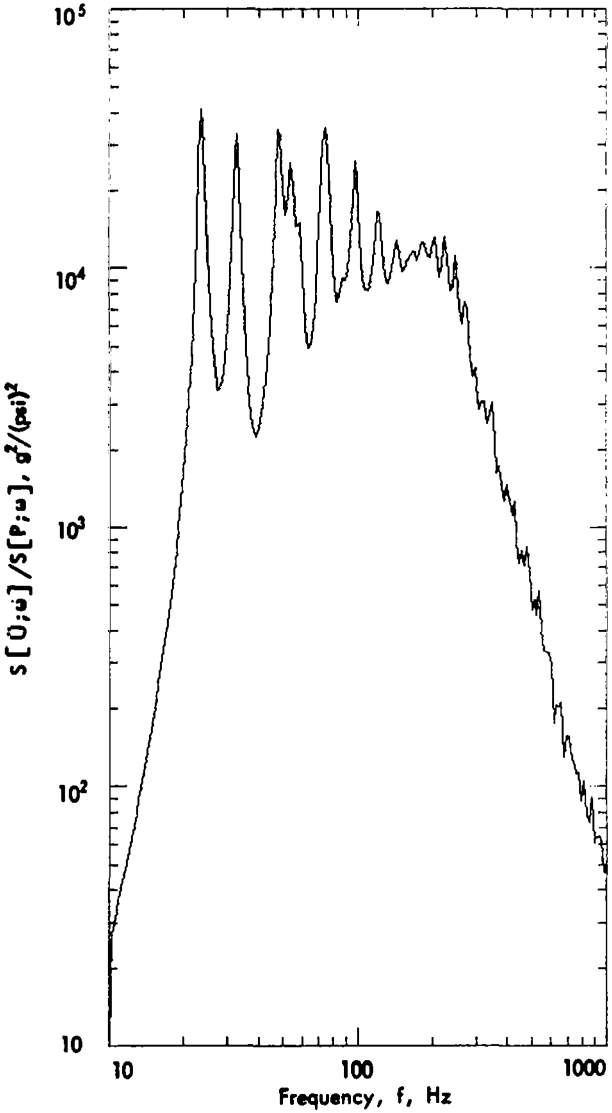

Figure 56. Effect of Sitffness Change on Acceleration, Spectrum of SLA for Duct Excitation; N = 16, Q = 15, D = 6.48 · 10^5 lb-in.

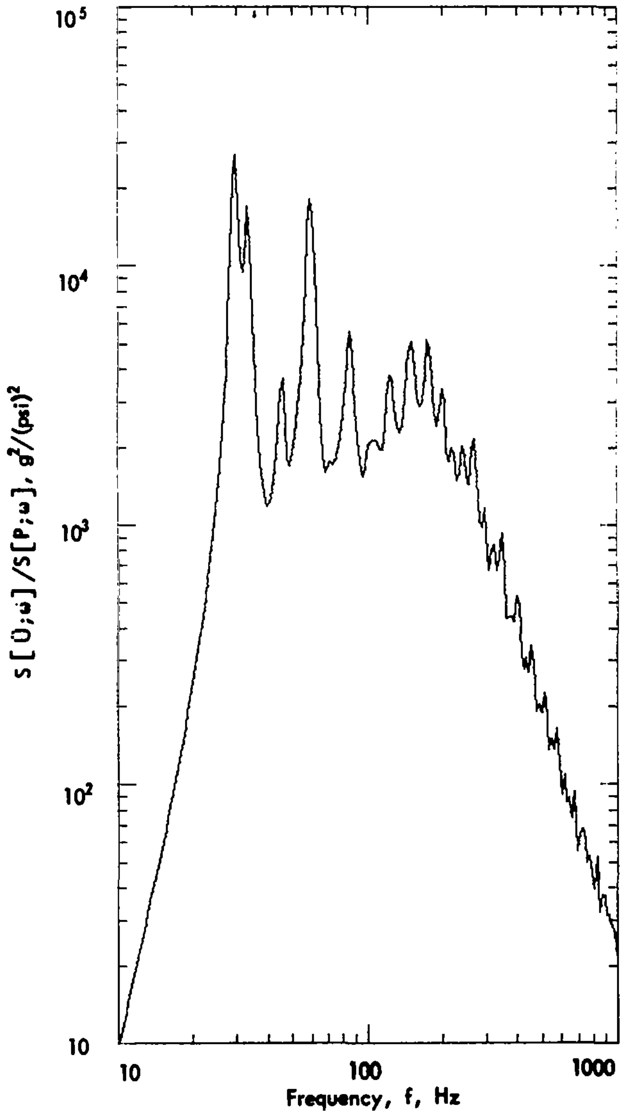

Figure 57. Effect of Stiffness Change on Acceleration, Spectrum of SLA for Duct Excitation; N = 16, Q = 15, D = 1.296 · 10^6 lb-in.

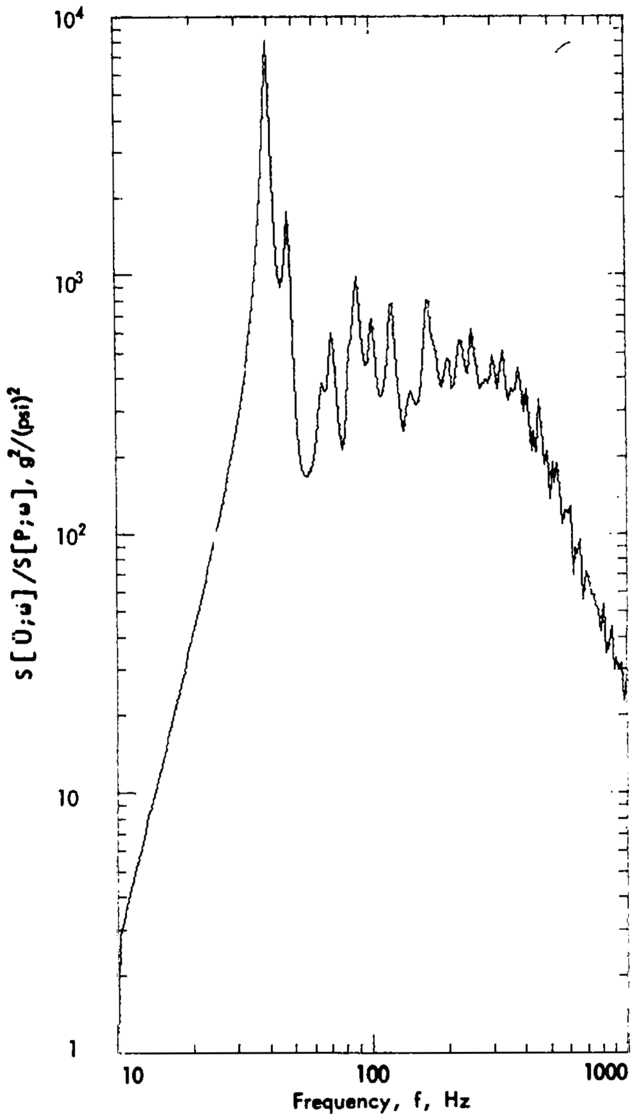

Figure 58. Effect of Stiffness Change on Acceleration Spectrum of SLA for Duct Excitation; N = 16, Q = 15, $D = 1.296 \cdot 10^6$ lb-in., $K_a = 1.88 \cdot 10^6$ lb/in.

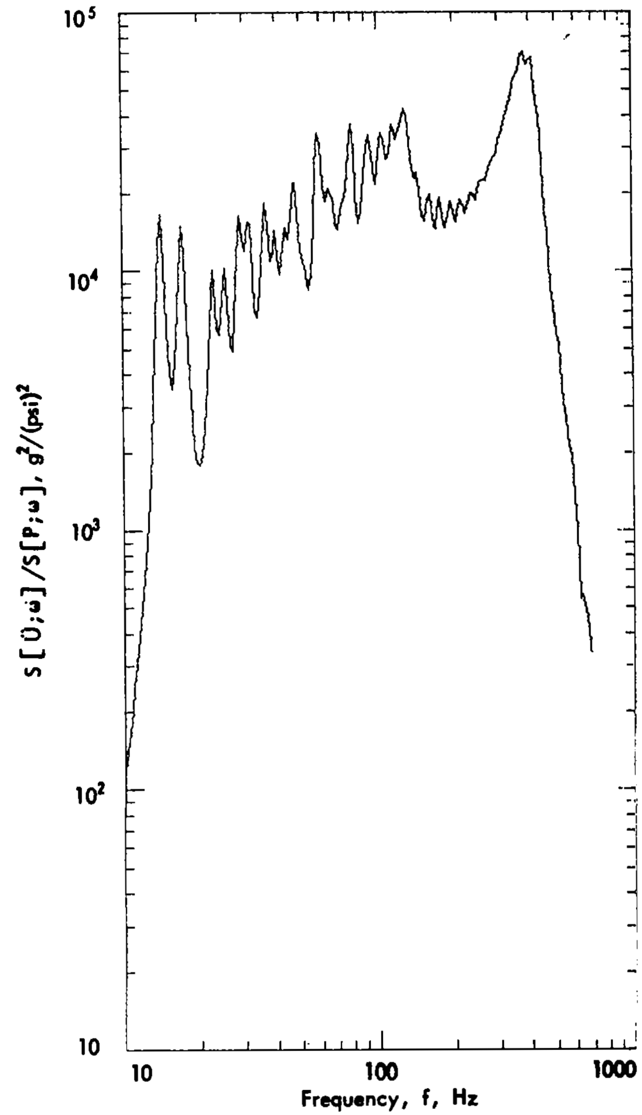

Figure 59. Effect of Surface Mass Change on Acceleration Spectrum of SLA for Duct Excitation; N = 16, Q = 15, $\mu g = 0.0278$ lb/in.^{2}

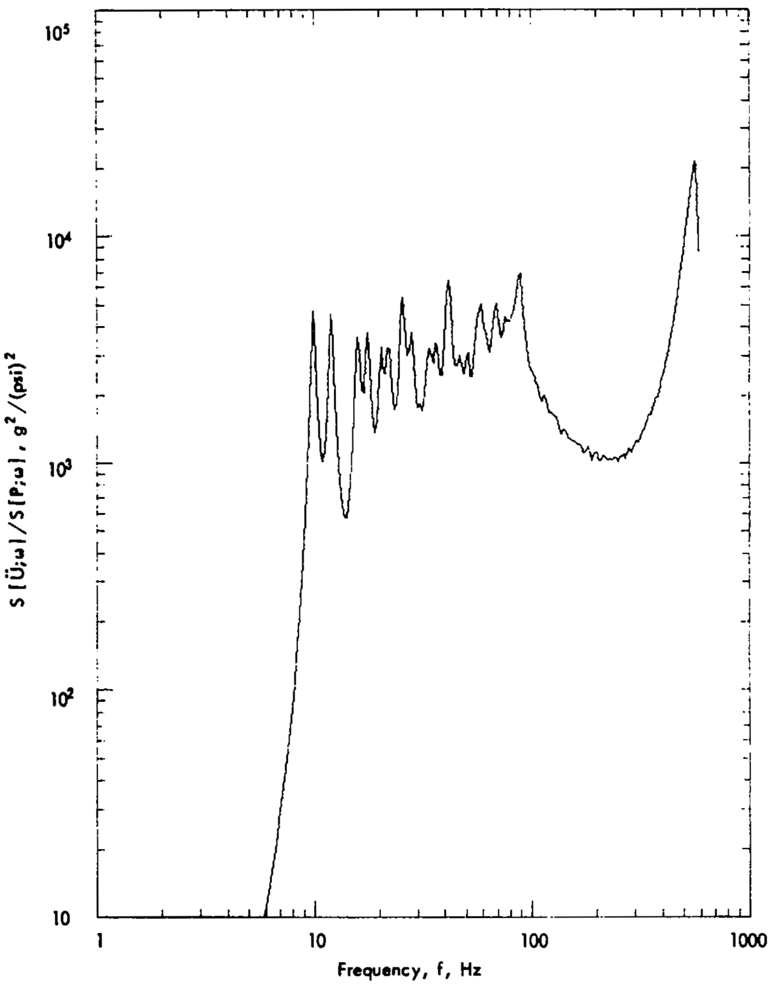

Figure 60. Effect of Surface Mass Change on Acceleration Spectrum of SLA for Duct Excitation; N = 16, Q = 15, $\mu g = 0.0556$ lb/in.^{2}

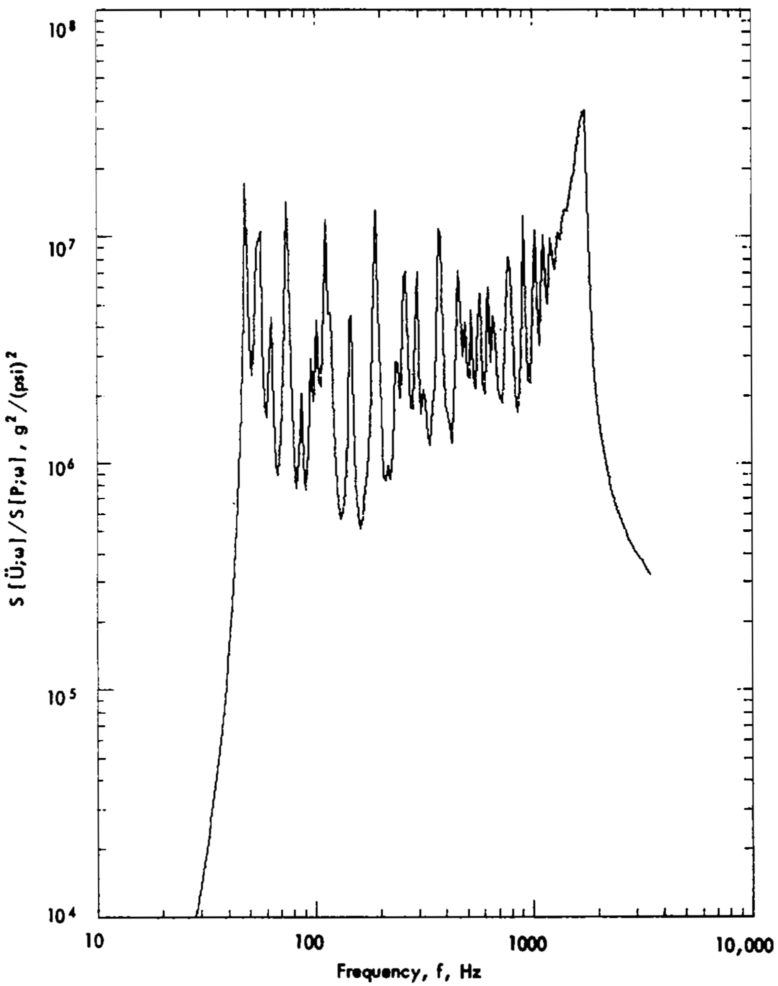

Figure 61. Acceleration Spectrum of 18 in. (Radius) by 54 in. by 0.02 in. Cylindrical Shell for Duct Excitation; N = 16, Q = 30

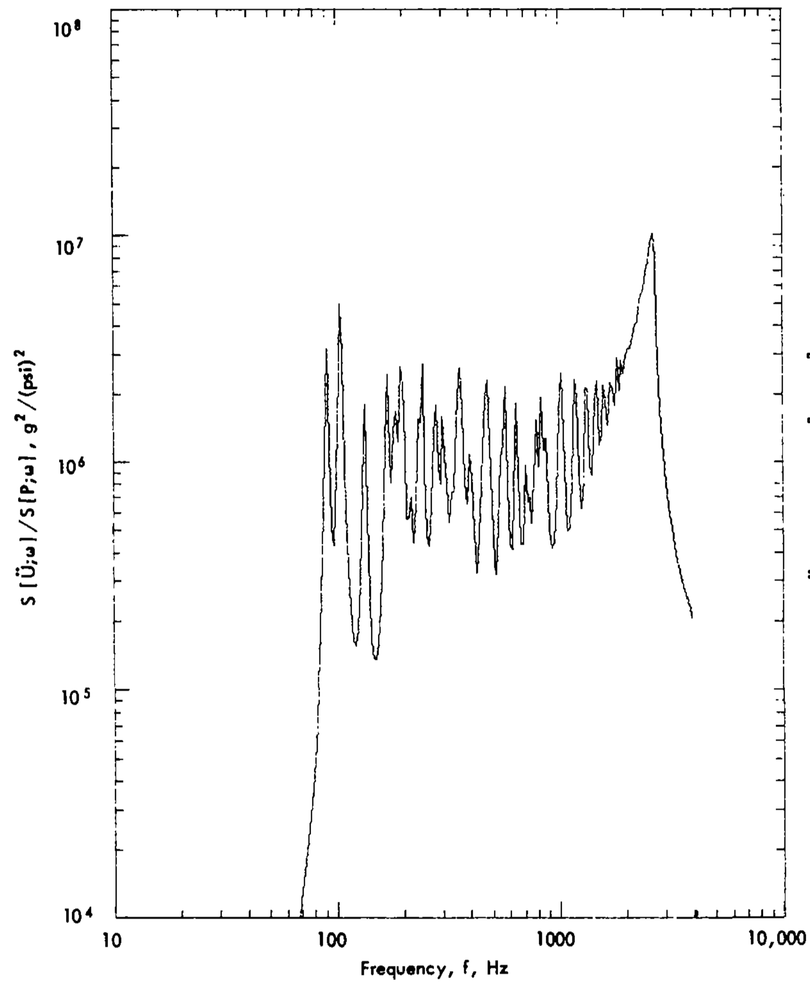

Figure 62. Acceleration Spectrum of 12 in. (Radius) by 48 in. by 0.04 in. Cylindrical Shell for Duct Excitation; N = 16, Q = 30

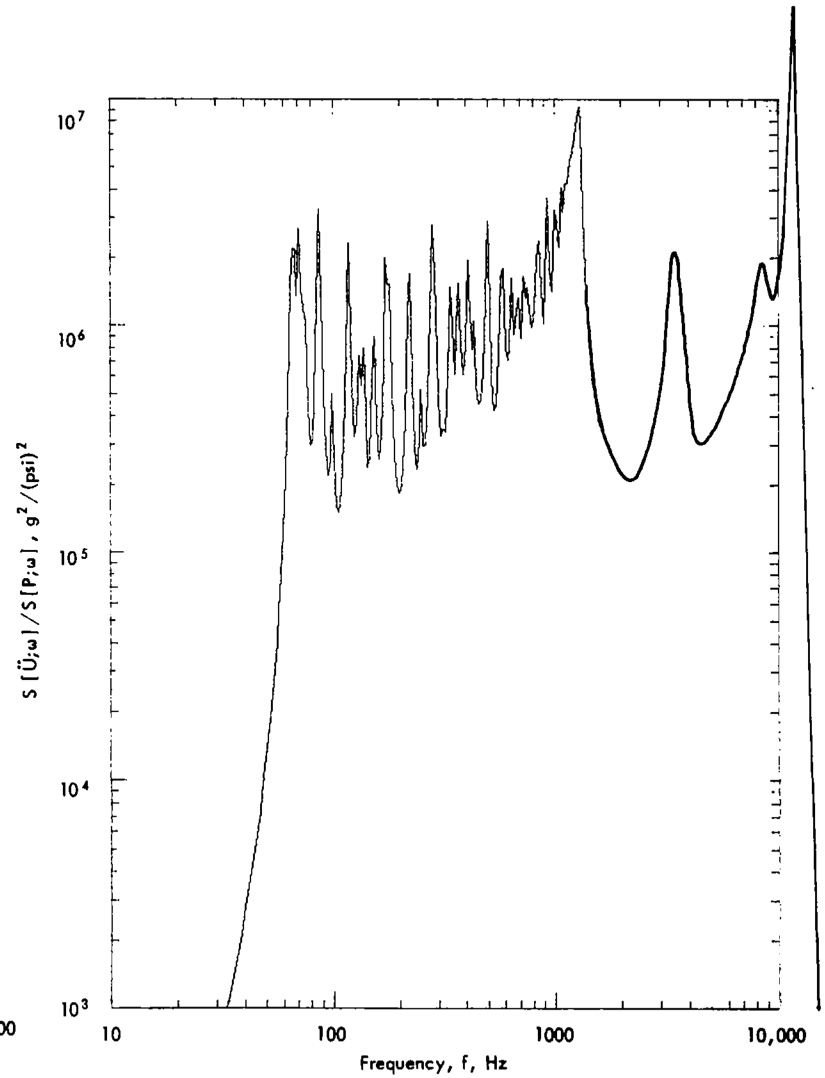

Figure 63. Acceleration Spectrum of 24 in. (Radius) by 48 in. by 0.04 in. Cylindrical Shell for Duct Excitation; N = 16, Q = 30

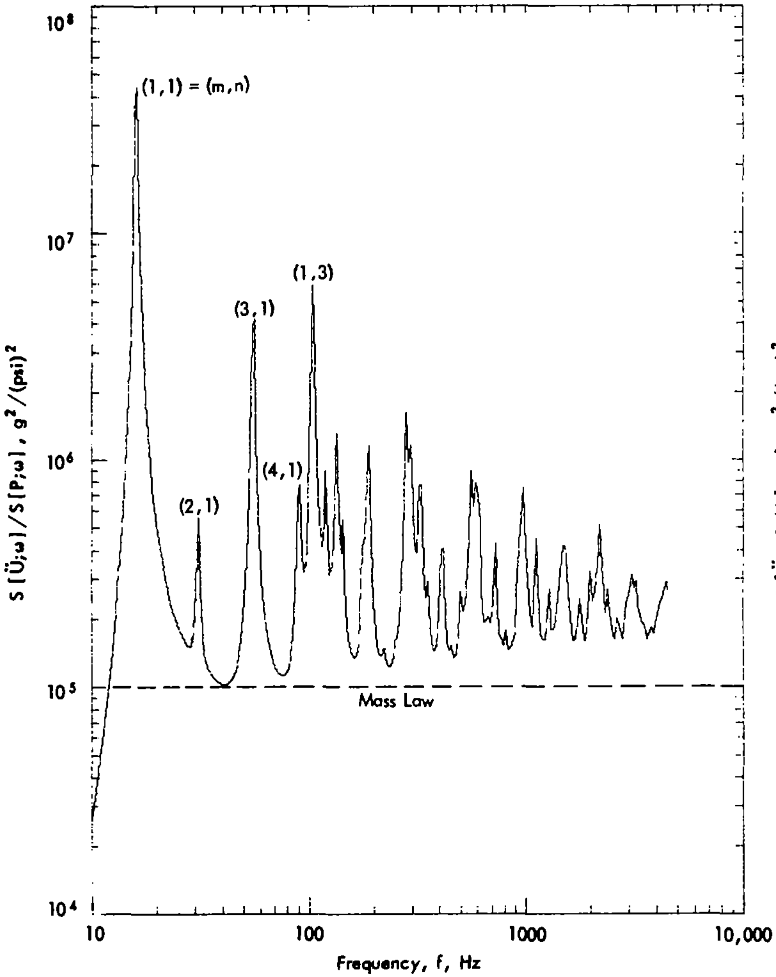

Figure 64. Acceleration Spectrum of 24 in. by 16 in. by 0.032 in. Flat Plate for Duct Excitation; N = 1, Q = 30

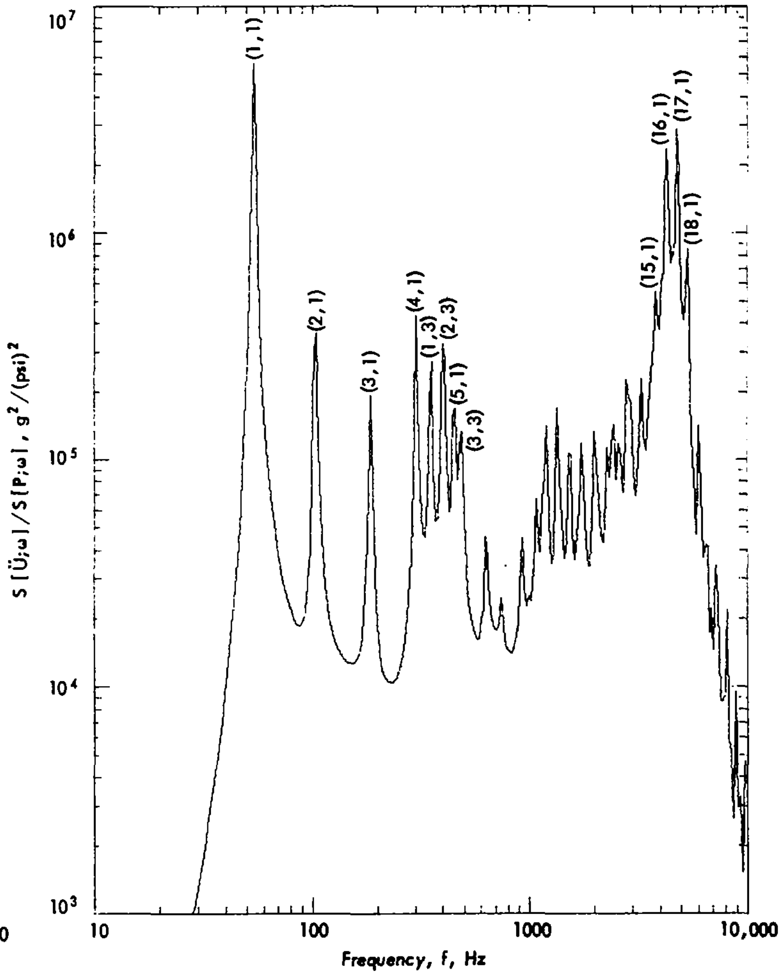

Figure 65. Acceleration Spectrum of 24 in. by 16 in. by 0.10 in. Flat Plate for Duct Excitation; N = 1, Q = 30

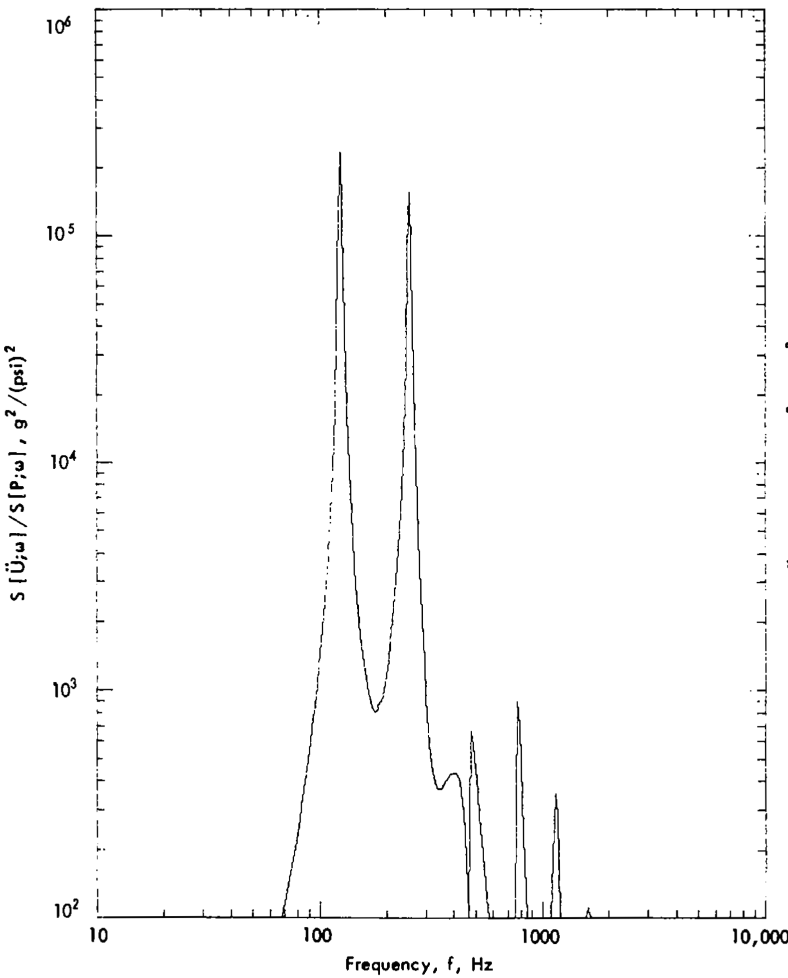

Figure 66. Acceleration Spectrum of Stiffened Flat Panel for Duct Excitation; N = 1, Q = 30

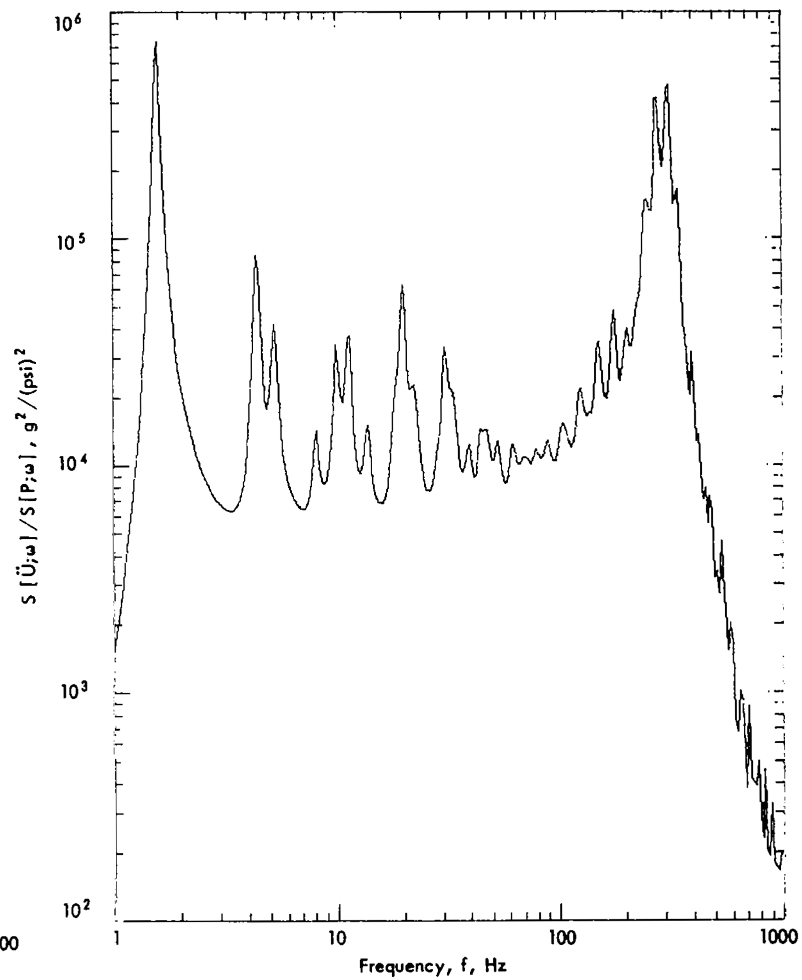

Figure 67. Acceleration Spectrum of Equivalent SLA Panel for Duct Excitation; N = 1, Q = 15

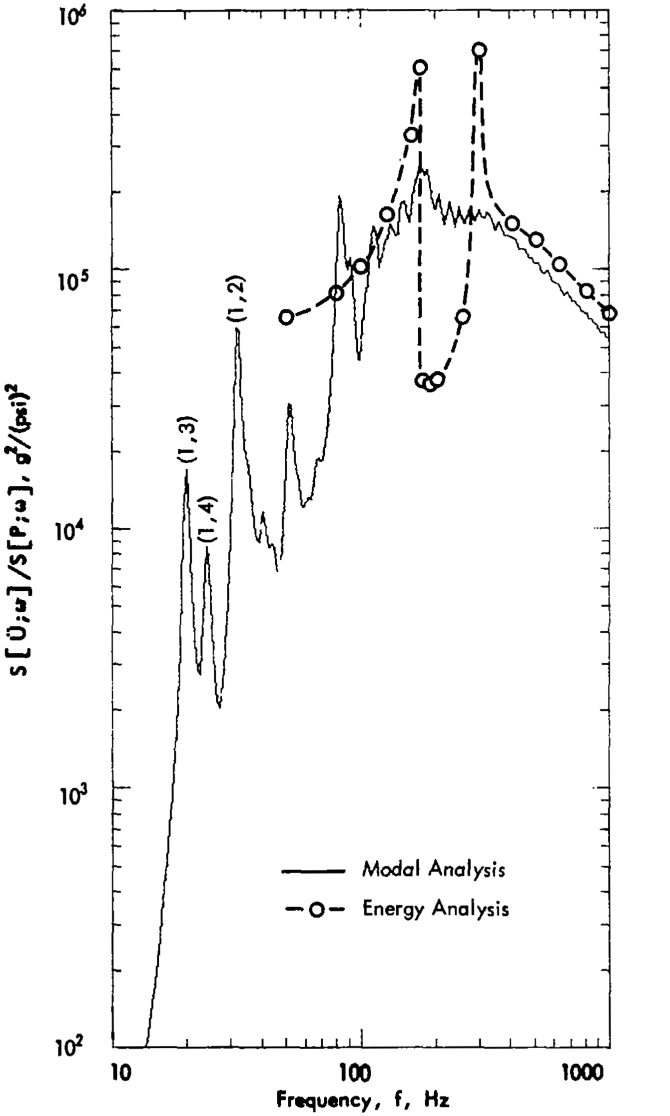

Figure 68. Acceleration Spectrum of SLA for Reverberant Field Excitation; Q = 15

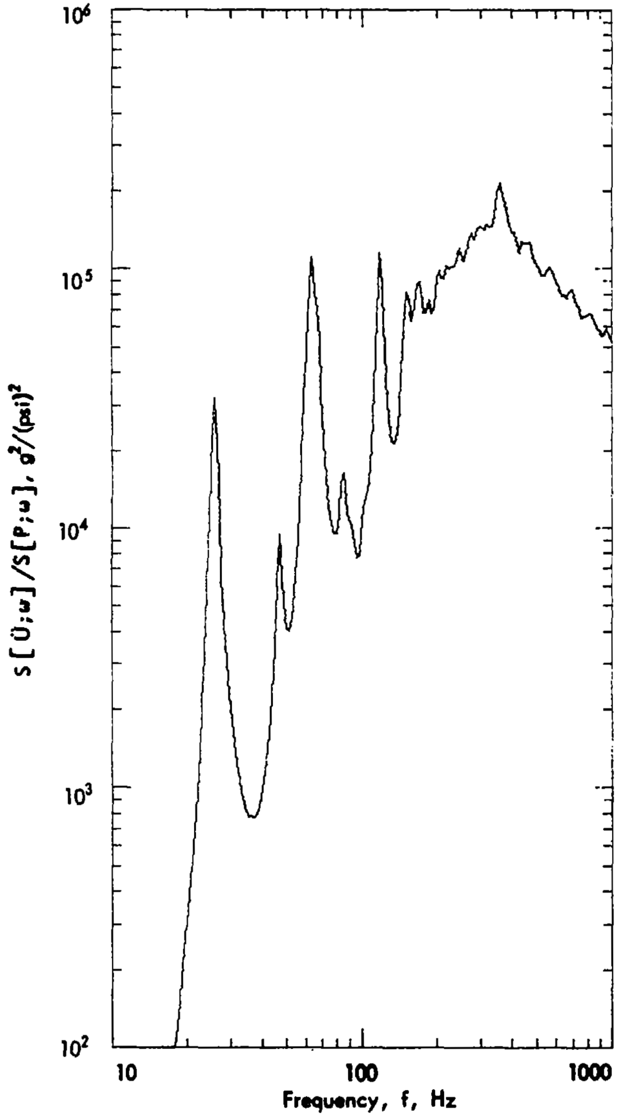

Figure 69. Effect of Radius Change on Acceleration Spectrum of SLA for Reverberant Field Excitation; Q = 15, R = 52.0 in.

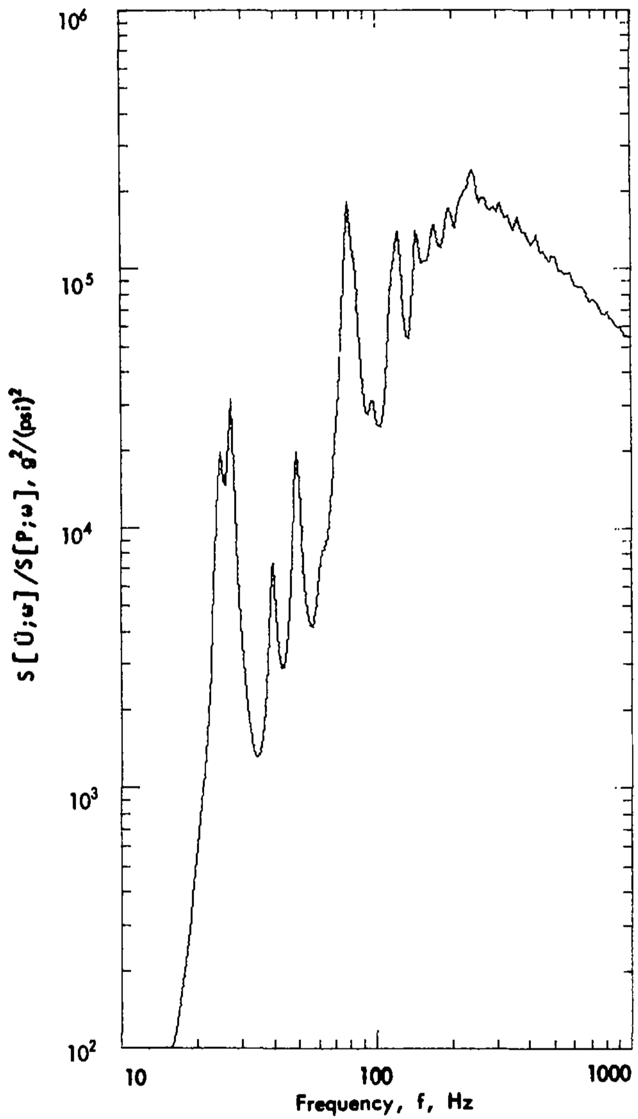

Figure 70. Effect of Radius Change on Acceleration Spectrum of SLA for Reverberant Field Excitation; Q = 15, R = 78.0 in.

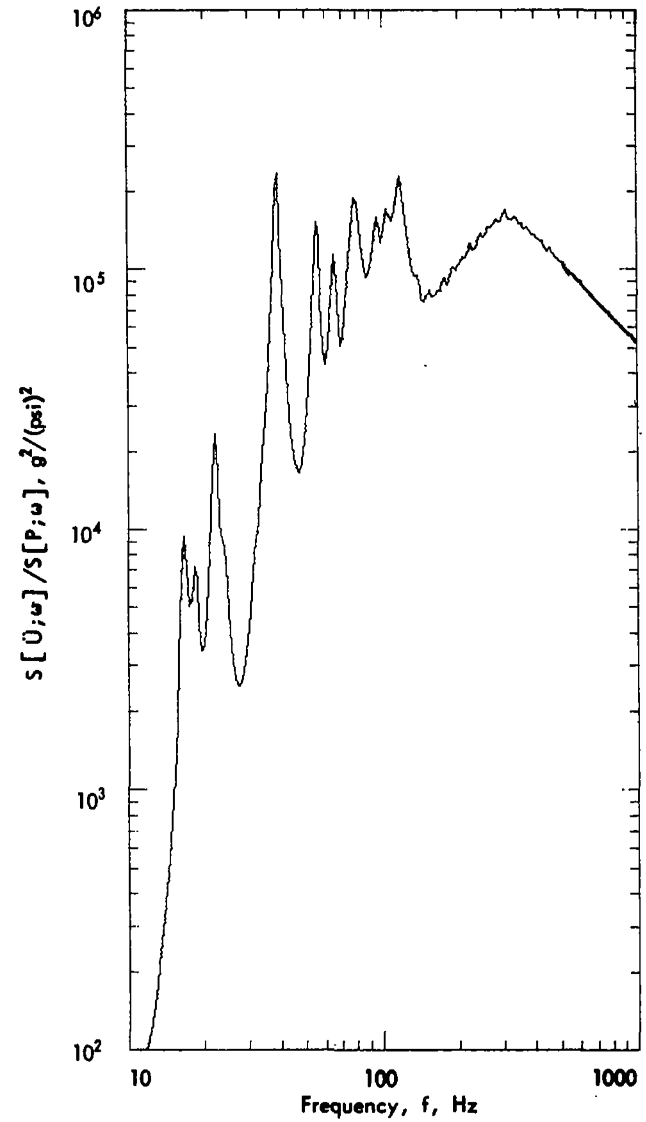

Figure 71. Effect of Radius Change on Acceleration Spectrum of SLA for Reverberant Field Excitation; Q = 15, R = 156.0 in.

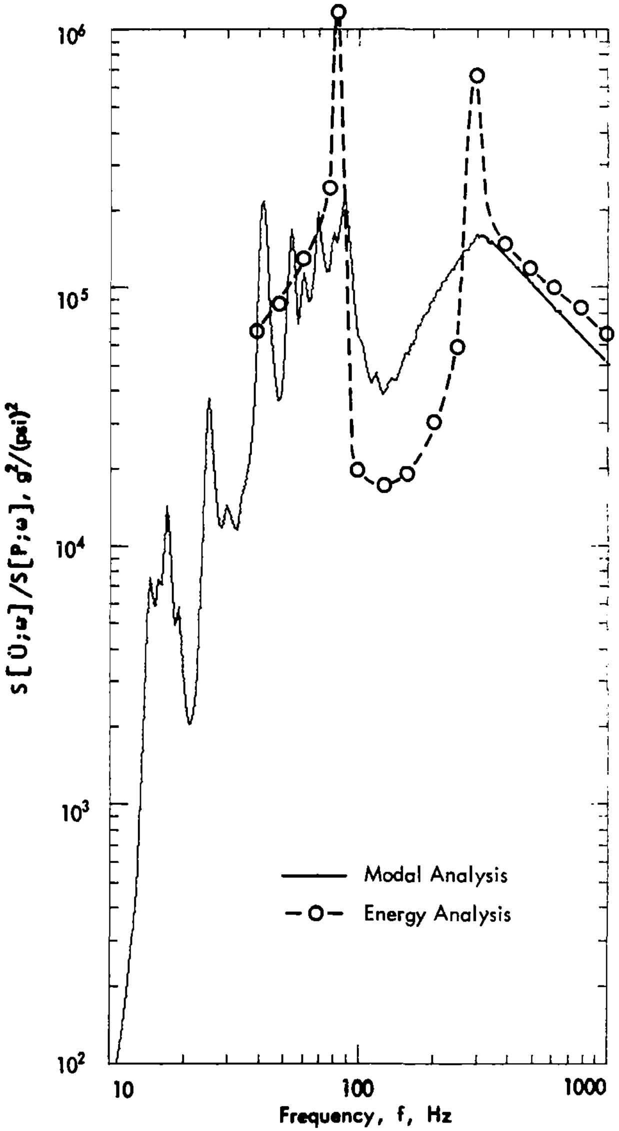

Figure 72. Effect of Radius Change on Acceleration Spectrum of SLA for Reverberant Field Excitation; Q = 15, R = 208.0 in.

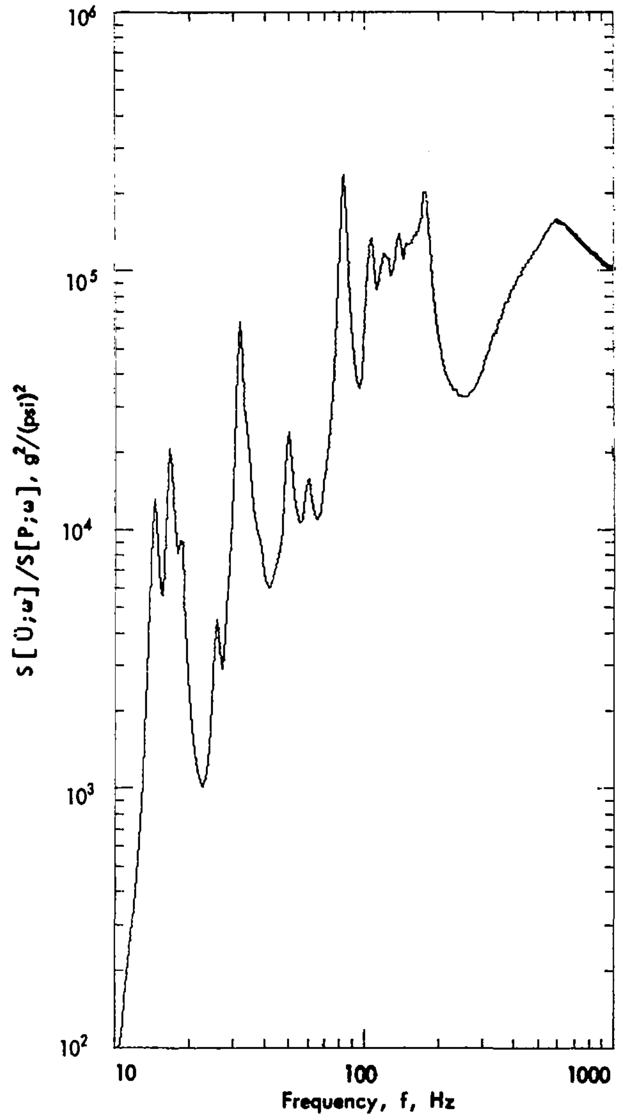

Figure 73. Effect of Stiffness Change on Acceleration Spectrum of SLA for Reverberant Field Excitation; Q = 15, D = $8.10 \cdot 10^4$ lb-in.

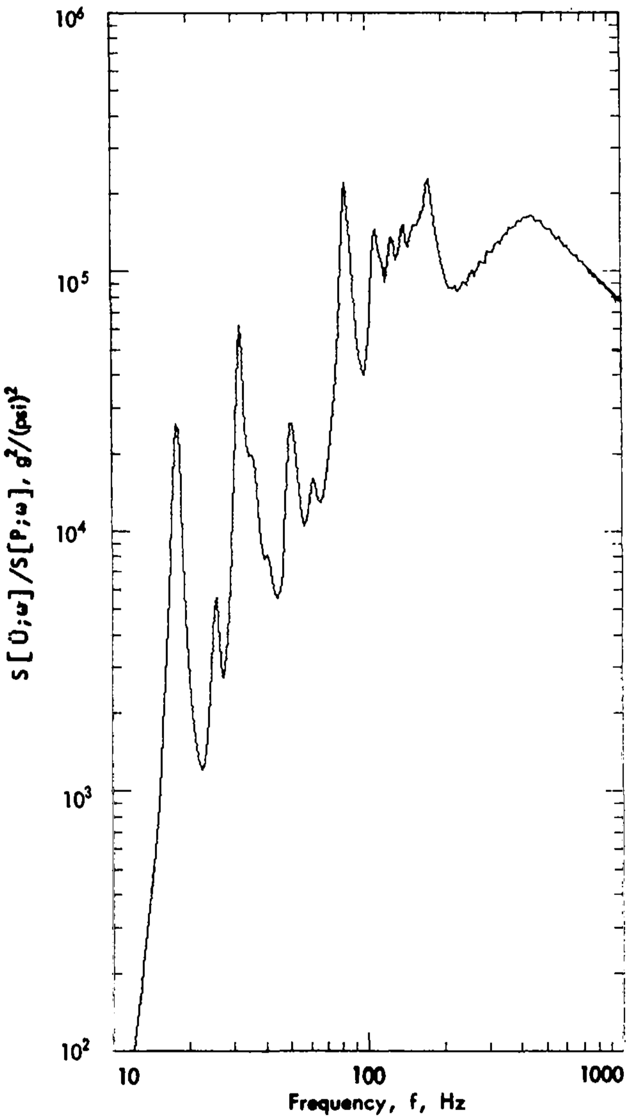

Figure 74. Effect of Stiffness Change on Acceleration Spectrum of SLA for Reverberant Field Excitation; Q = 15, D = $1.62 \cdot 10^5$ lb-in.

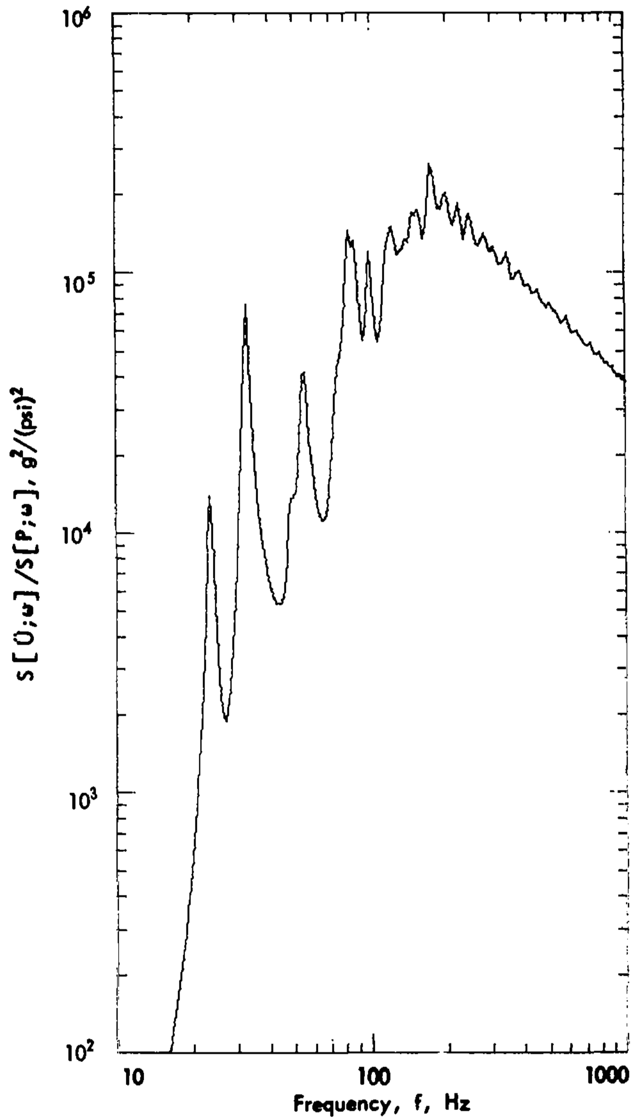

Figure 75. Effect of Stiffness Change on Acceleration Spectrum of SLA for Reverberant Field Excitation; Q = 15, D = $6.48 \cdot 10^5$ lb-in.

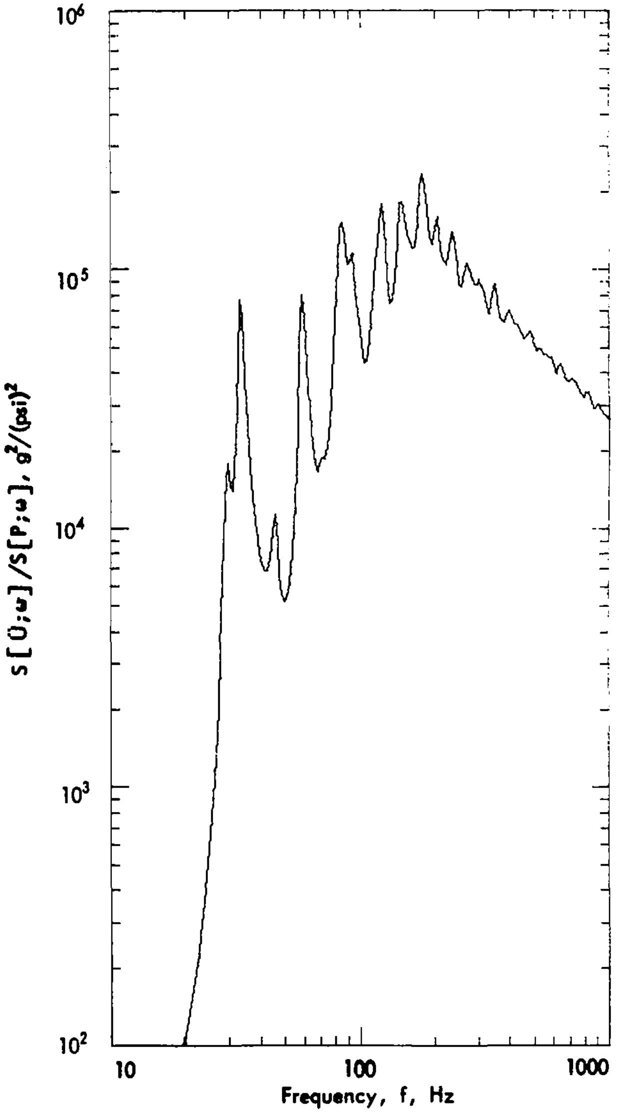

Figure 76. Effect of Stiffness Change on Acceleration Spectrum of SLA for Reverberant Field Excitation; $Q = 15$, $D = 1.296 \cdot 10^6$ lb-in.

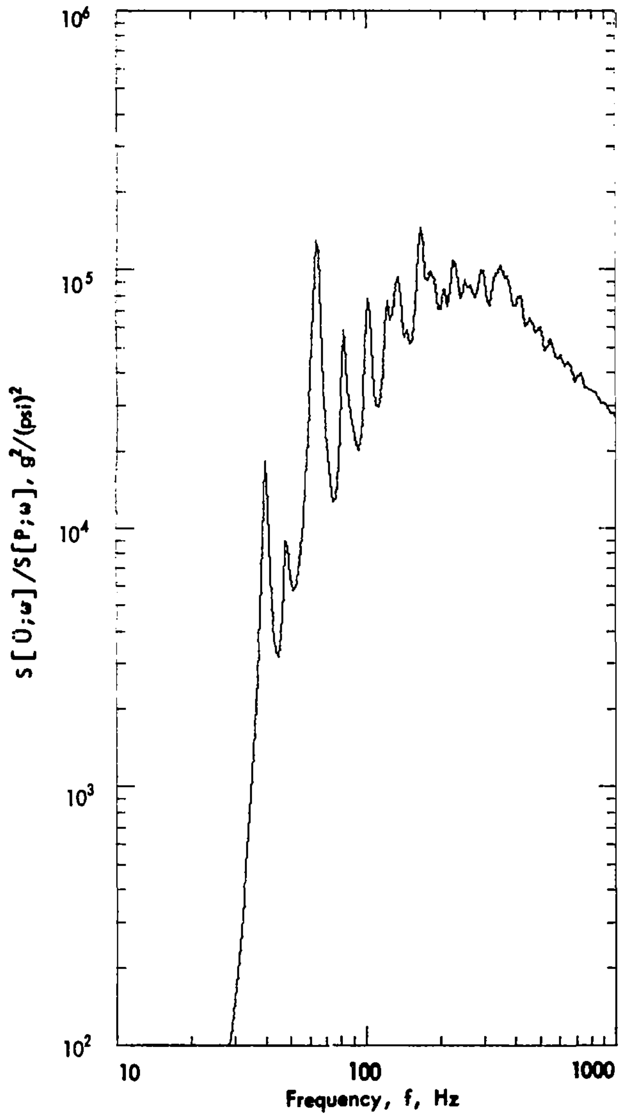

Figure 77. Effect of Stiffness Change on Acceleration Spectrum of SLA for Reverberant Field Excitation; $Q = 15$, $D = 1.296 \cdot 10^6$ lb-in., $K_e = 1.88 \cdot 10^6$ lb/in.

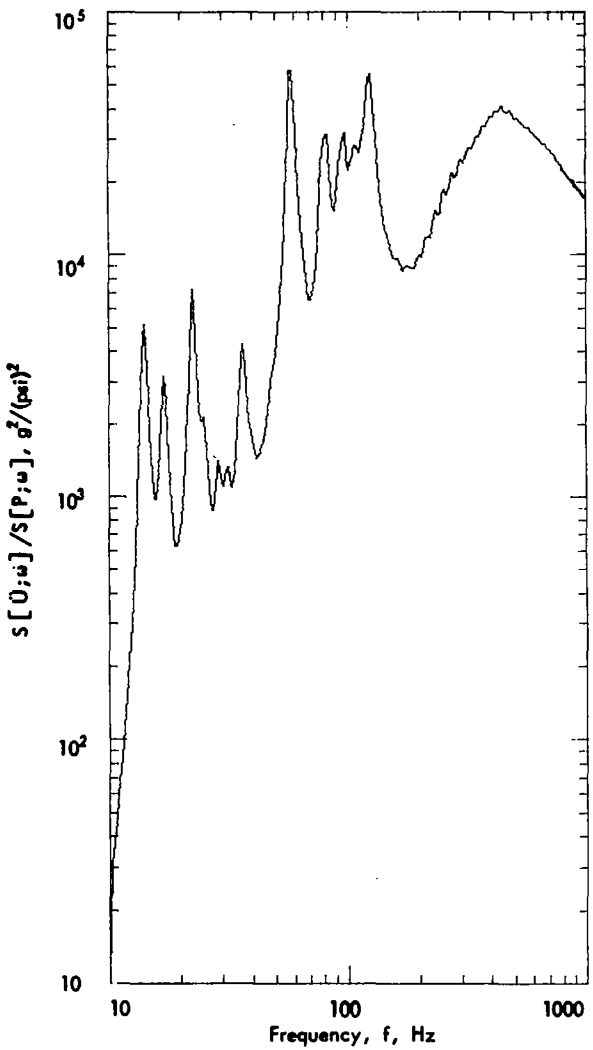

Figure 78. Effect of Surface Mass Change on Acceleration Spectrum of SLA for Reverberant Field Excitation; Q = 15, $\mu g = 0.0278$ lb/in.^{2}

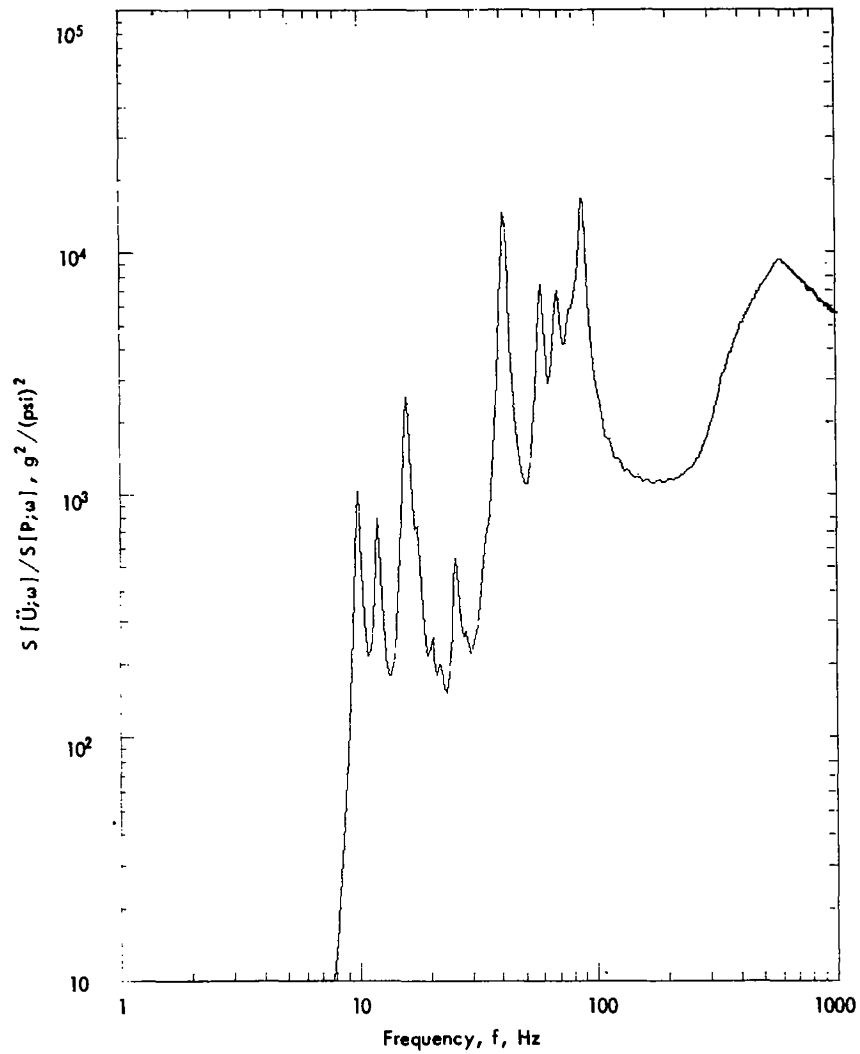

Figure 79. Effect of Surface Mass Change on Acceleration Spectrum of SLA for Reverberant Field Excitation; Q = 15, $\mu g = 0.0556$ lb/in.^{2}

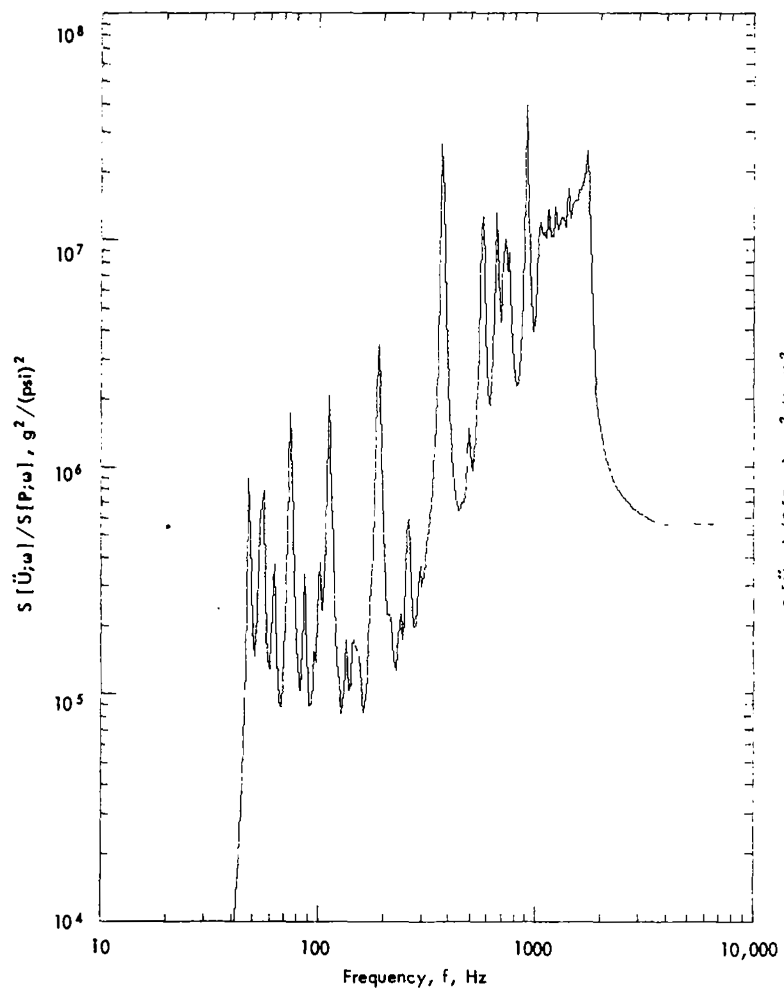

Figure 80. Acceleration Spectrum of 18 in. (Radius) by 54 in. by 0.02 in. Cylindrical Shell for Reverberant Field Excitation; Q = 30

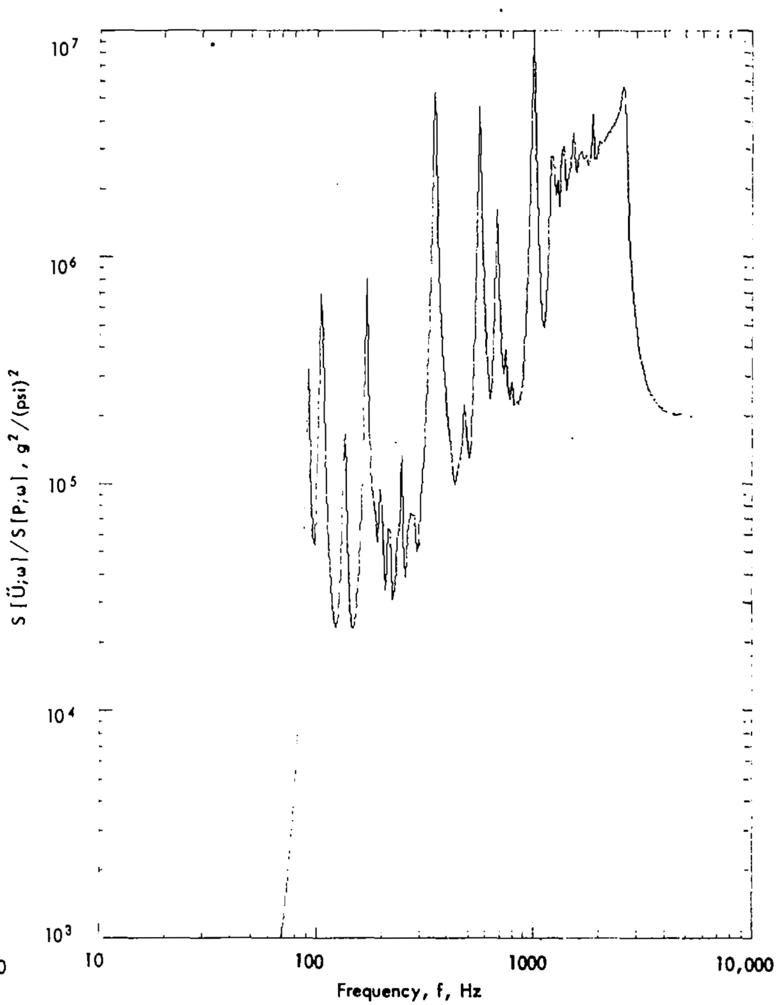

Figure 81. Acceleration Spectrum of 12 in. (Radius) by 48 in. by 0.04 in. Cylindrical Shell for Reverberant Field Excitation; Q = 30

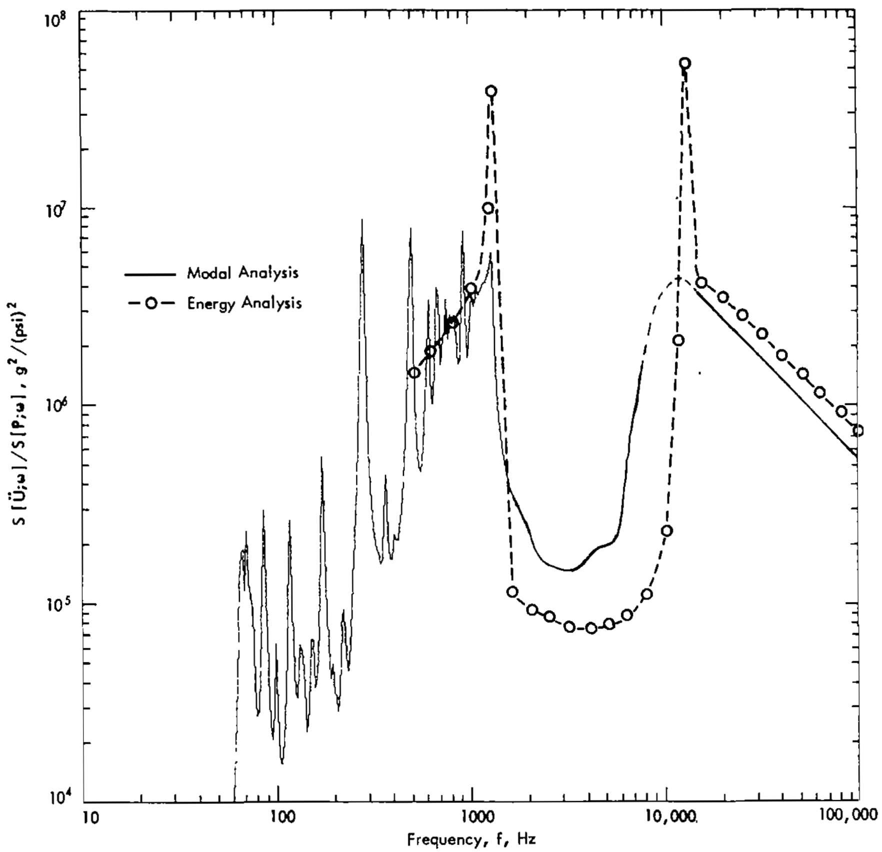

Figure 82. Acceleration Spectrum of 24 in. (Radius) by 48 in. by 0.04 in. Cylindrical Shell for Reverberant Field Excitation; Q = 30

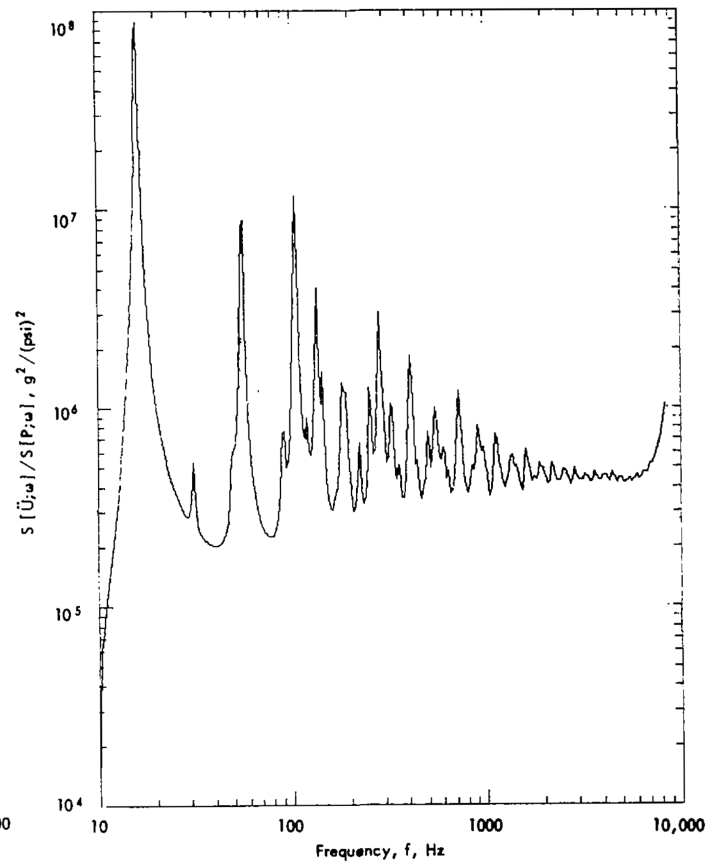

Figure 83. Acceleration Spectrum of 24 in. by 16 in. by 0.032 in. Flat Plate for Reverberant Field Excitation; Q = 30

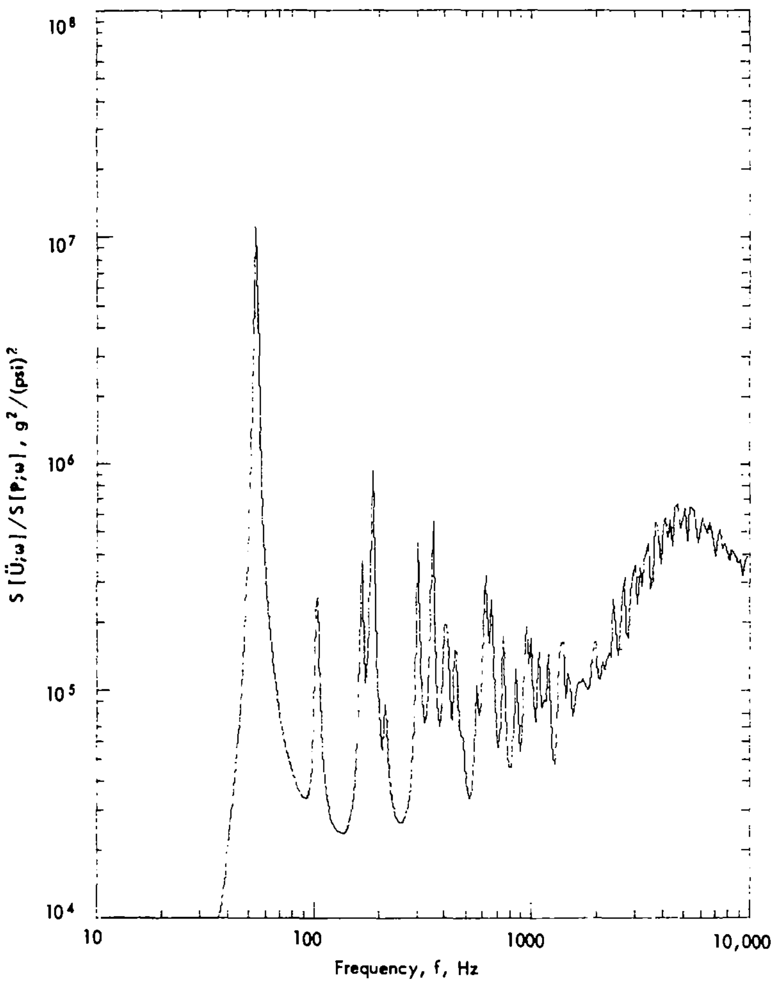

Figure 84. Acceleration Spectrum of 24 in. by 16 in. by 0.10 in. Flat Plate for Reverberant Field Excitation; Q = 30

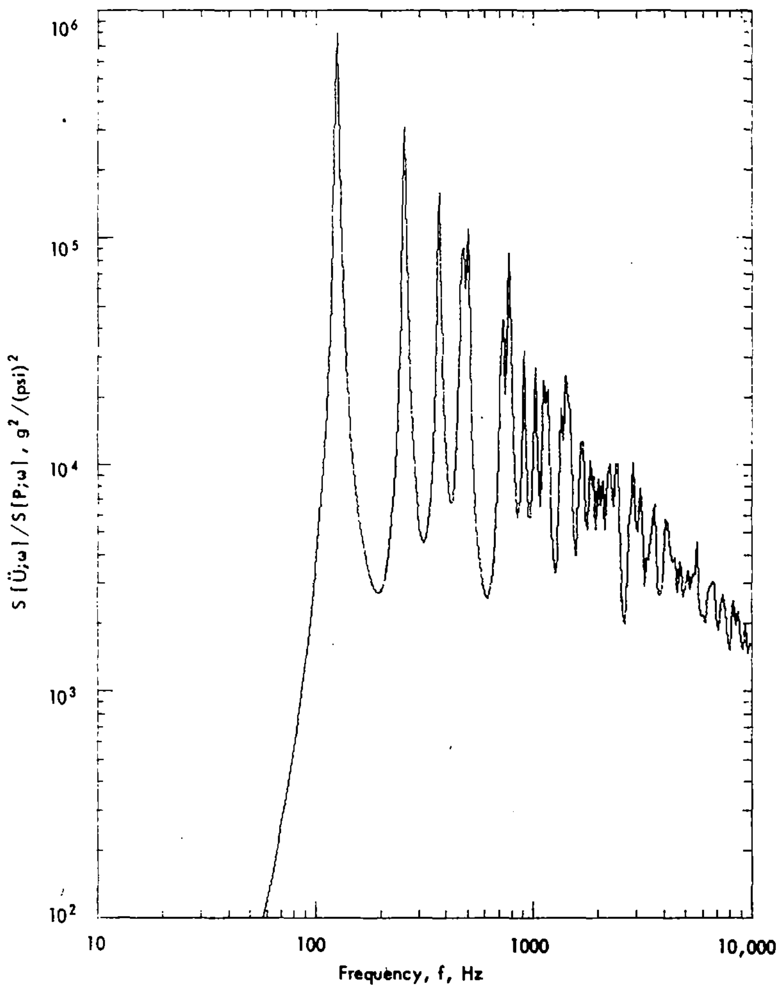

Figure 85. Acceleration Spectrum of Stiffened Flat Panel for Reverberant Field Excitation; Q = 30

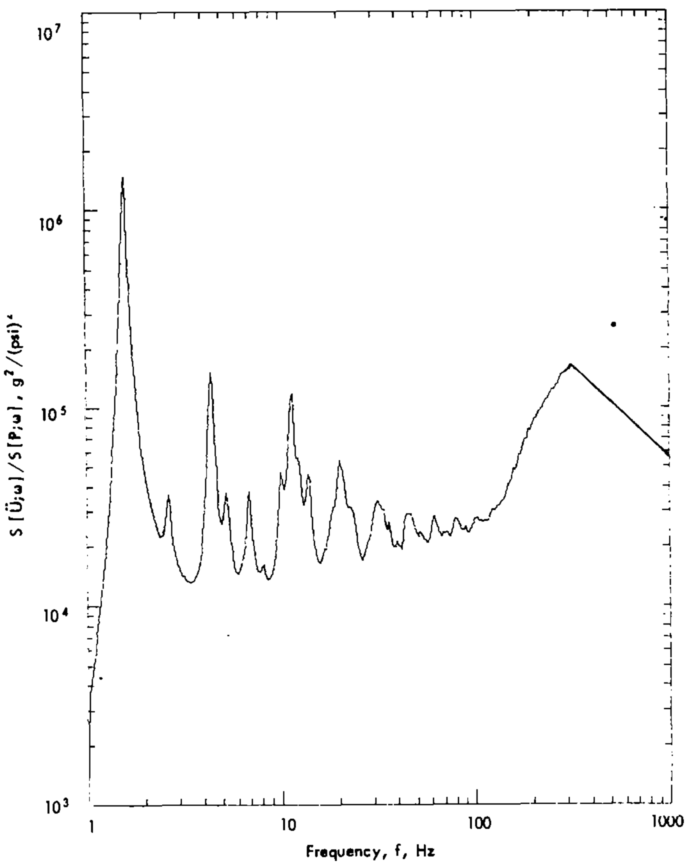

Figure 86. Acceleration Spectrum of Equivalent SLA Panel for Reverberant Field Excitation; Q = 15

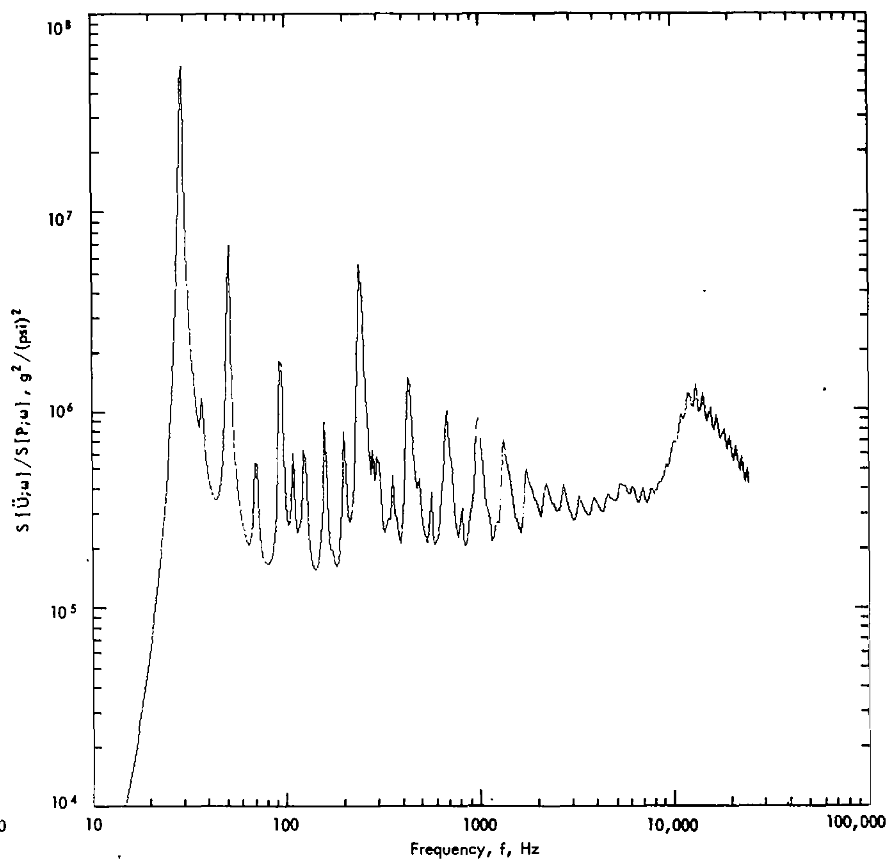

Figure 87. Acceleration Spectrum of 12 in. by 37.5 in. by 0.040 in. Flat Plate for Reverberant Acoustic Excitation; Q = 30

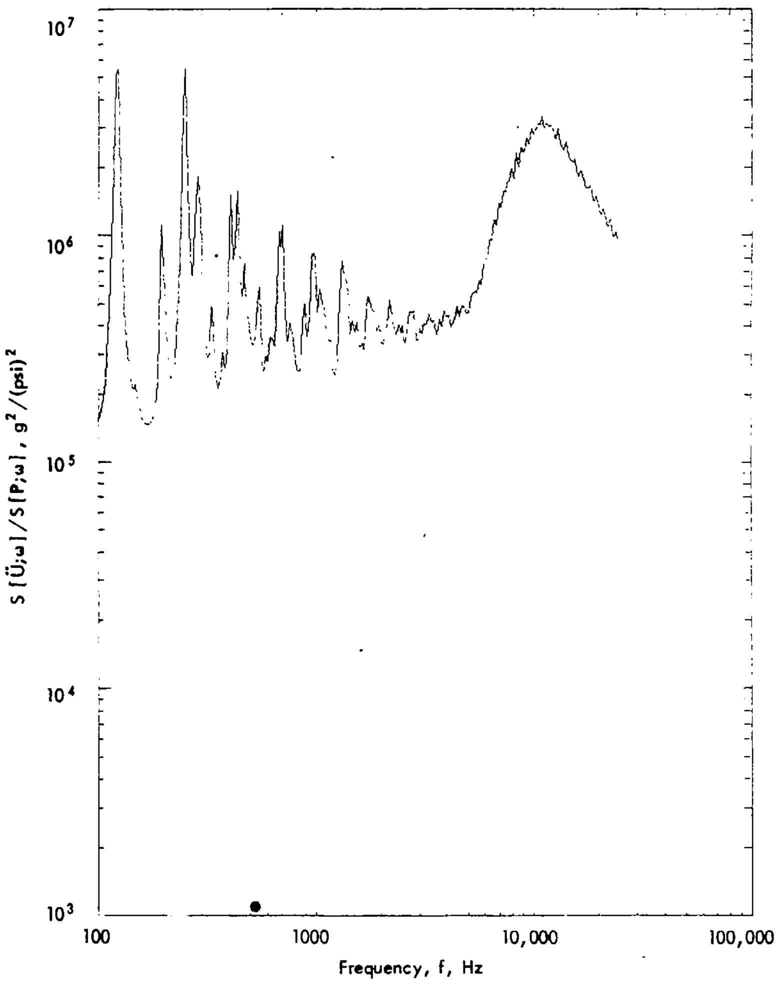

Figure 88. Acceleration Spectrum of 12 in. by 19 in. by 0.040 in. Flat Plate for Reverberant Acoustic Excitation; Q = 30

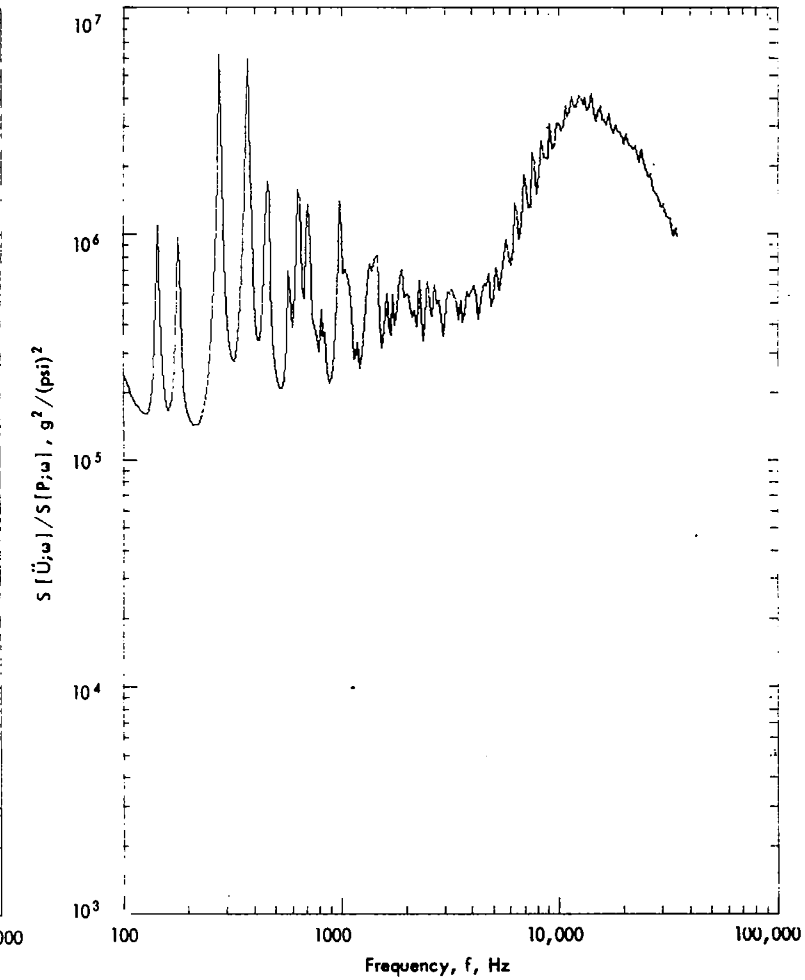

Figure 89. Acceleration Spectrum of 12 in. by 10 in. by 0.040 in. Flat Plate for Reverberant Acoustic Excitation; Q = 30

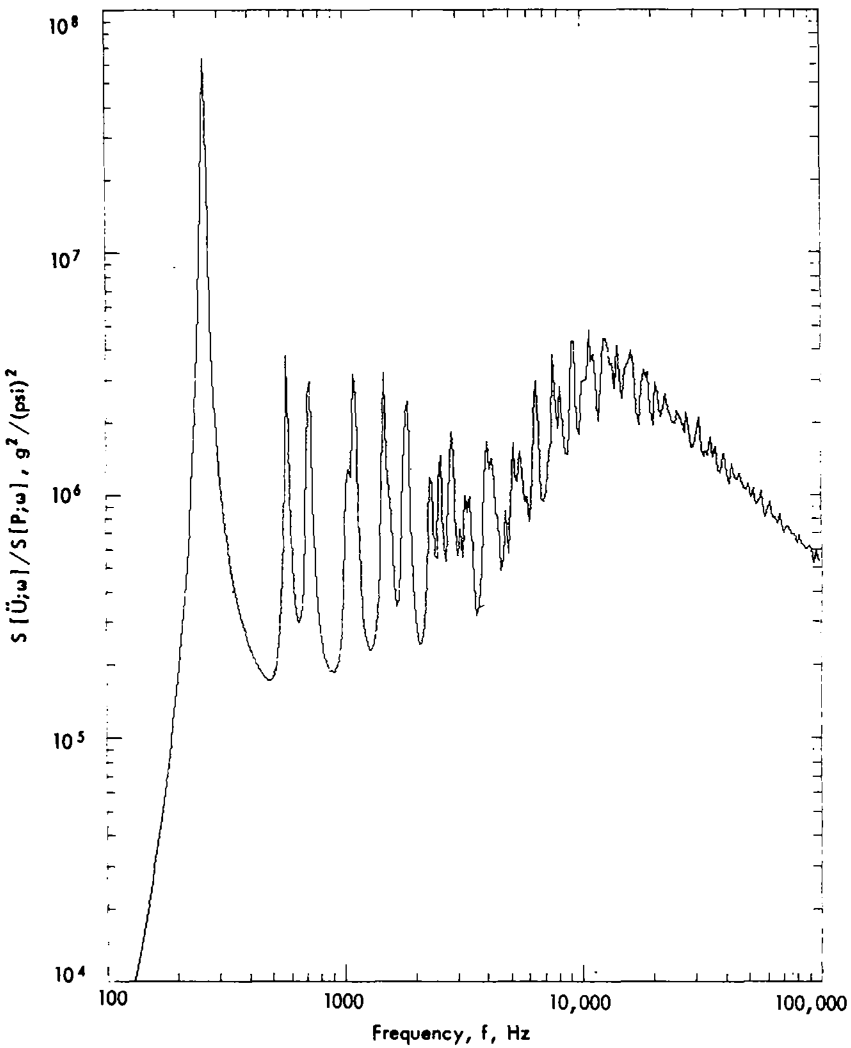

Figure 90. Acceleration Spectrum of 6 in. by 5 in. by 0.040 in. Flat Plate for Reverberant Acoustic Excitation; Q = 30

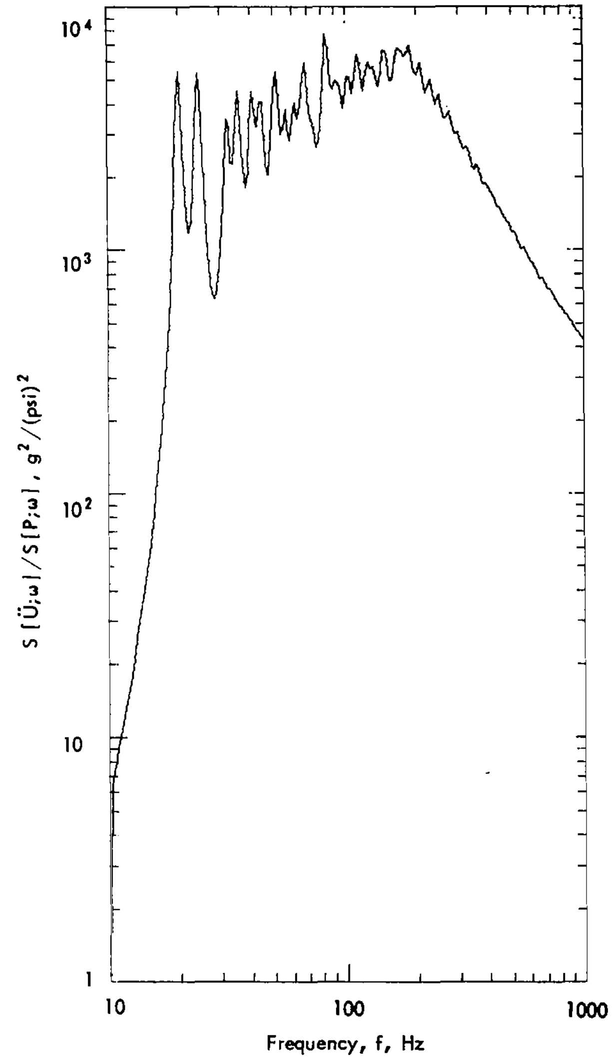

Figure 91. Acceleration Spectrum of SLA for Boundary Layer Turbulence Excitation; Mach 1, δ_b = 12.0 in., Q = 15

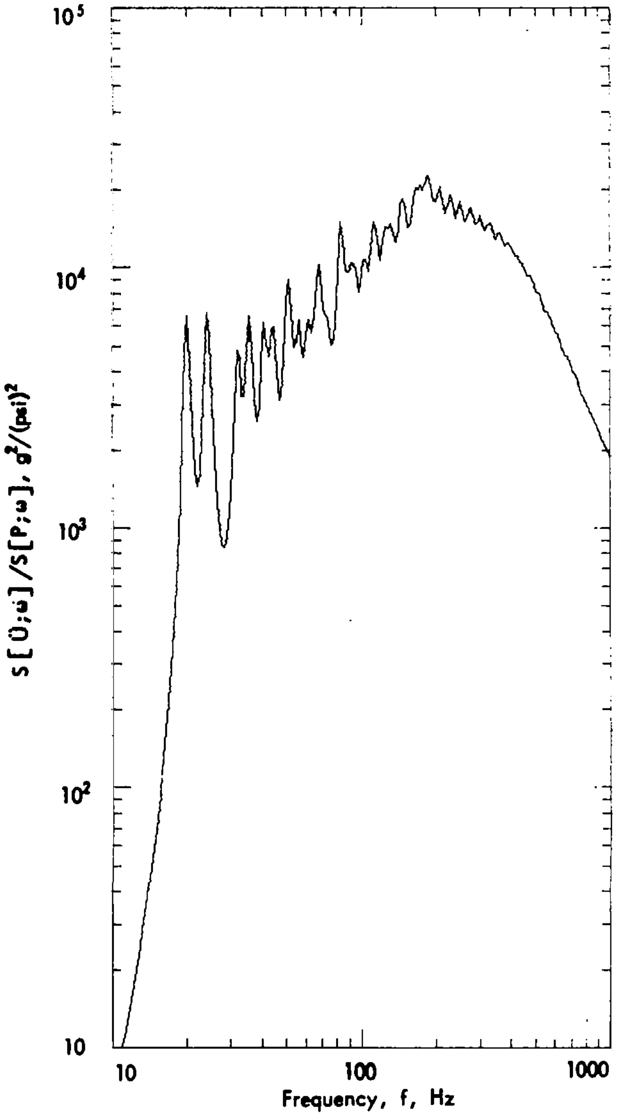

Figure 92. Acceleration Spectrum of SLA for Boundary Layer Turbulence Excitation; Mach 2, δ_b = 12.0 in., Q = 15

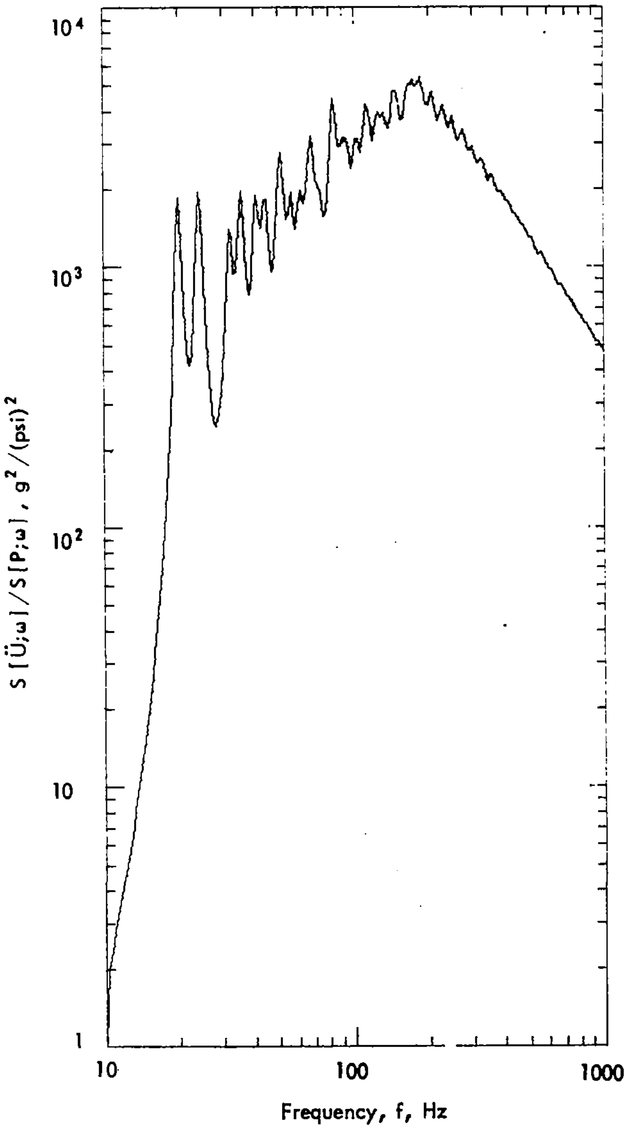

Figure 93. Acceleration Spectrum of SLA for Boundary Layer Turbulence Excitation; Mach 1, δ_b = 6.0 in., Q = 15

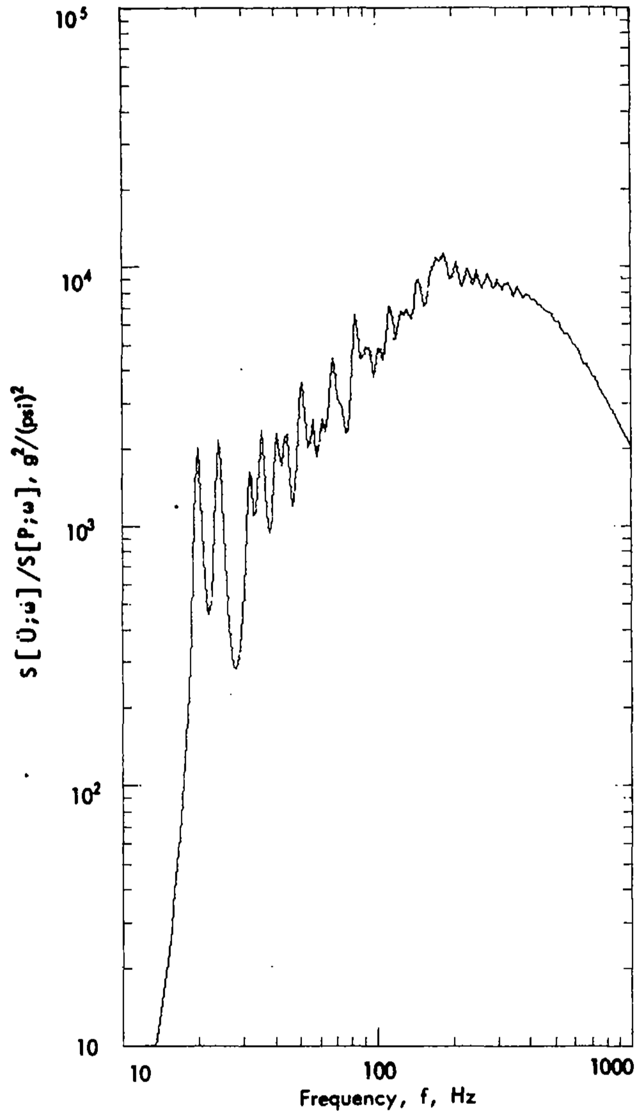

Figure 94. Acceleration Spectrum of SLA for Boundary Layer Turbulence Excitation; Mach 2, $\delta_b = 6.0$ in., $Q = 15$

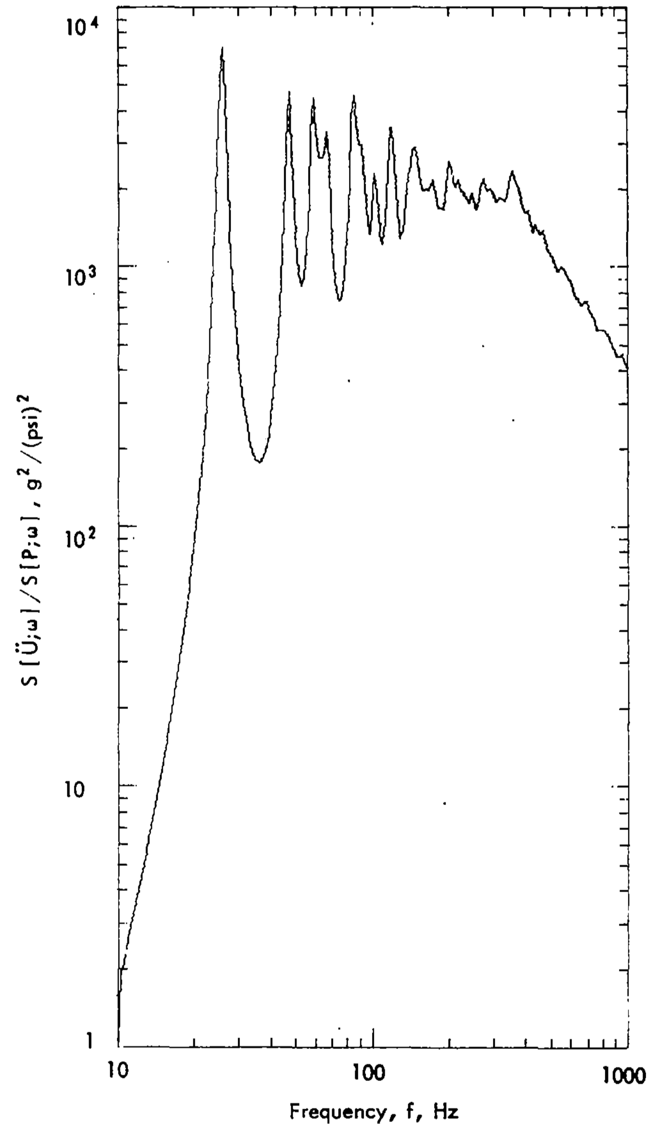

Figure 95. Effect of Radius Change on Acceleration Spectrum of SLA for Boundary Layer Turbulence Excitation; Mach 1, $\delta_b = 12.0$ in., $Q = 15$, $R = 52.0$ in.

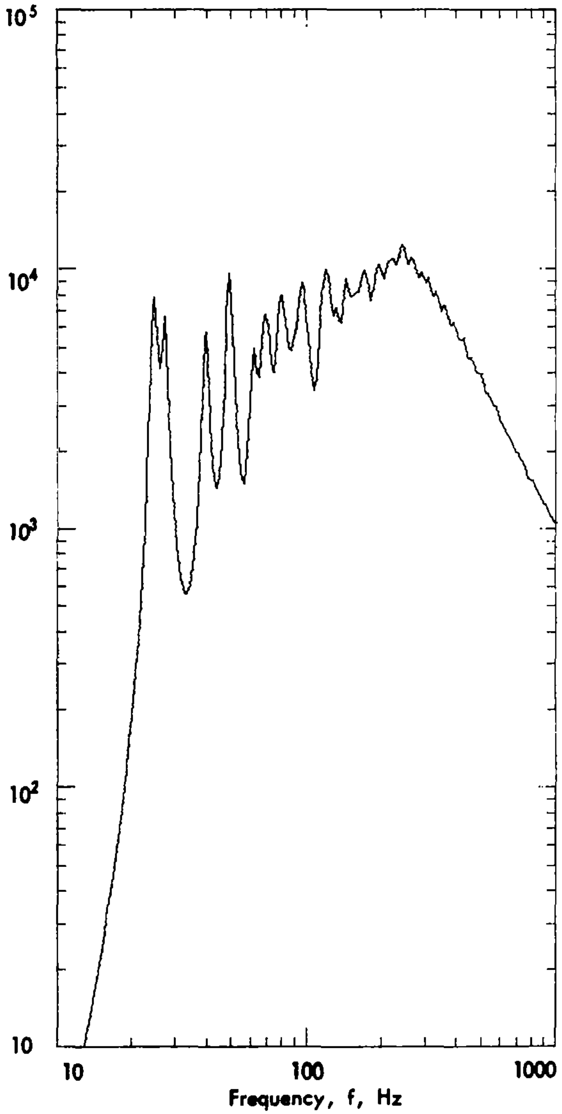

Figure 96. Effect of Radius Change on Acceleration Spectrum of SLA for Boundary Layer Turbulence Excitation; Mach 1, δ_b = 12.0 in., Q = 15, R = 78.0 in.

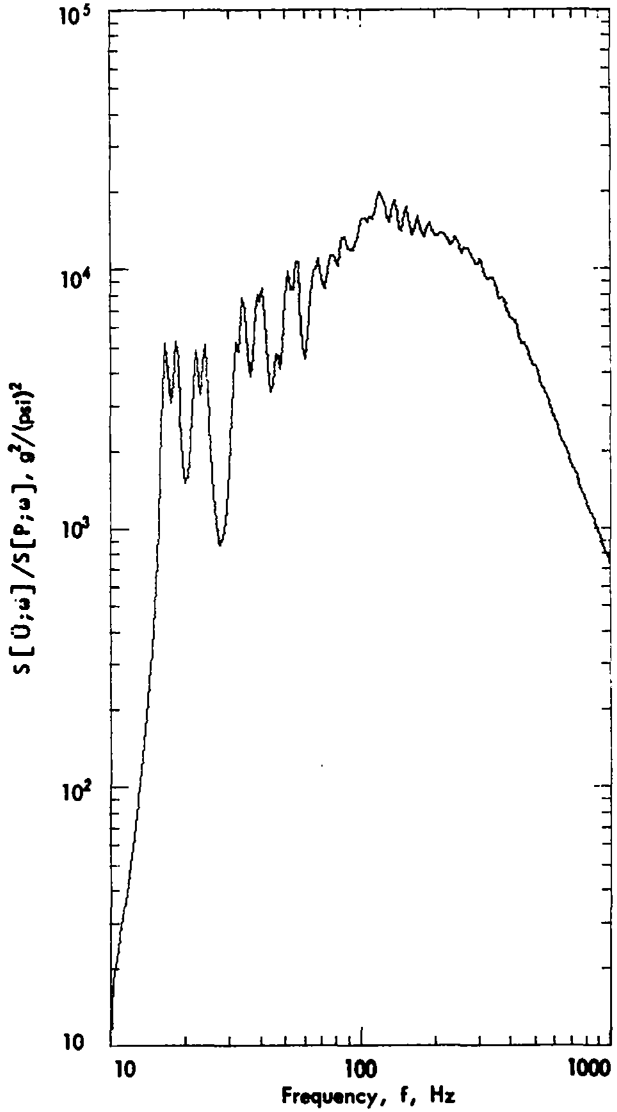

Figure 97. Effect of Radius Change on Acceleration Spectrum of SLA for Boundary Layer Turbulence Excitation; Mach 1, δ_b = 12.0 in., Q = 15, R = 156.0 in.

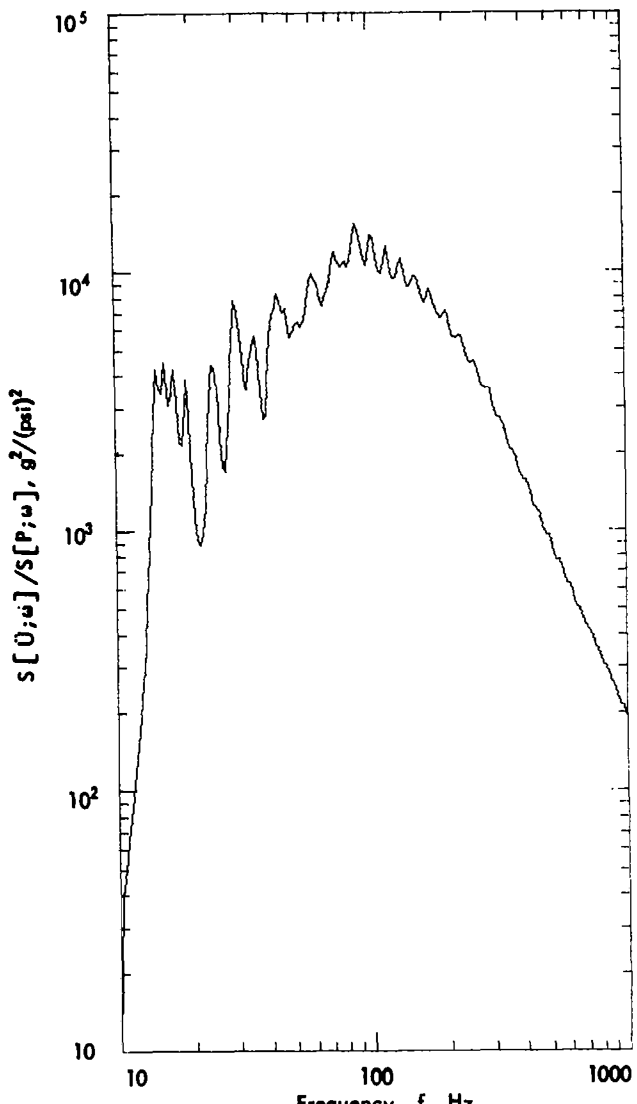

Figure 98. Effect of Radius Change on Acceleration Spectrum of SLA for Boundary Layer Turbulence Excitation; Mach 1, $\delta_b = 12.0$ in., $Q = 15$, $R = 208.0$ in.

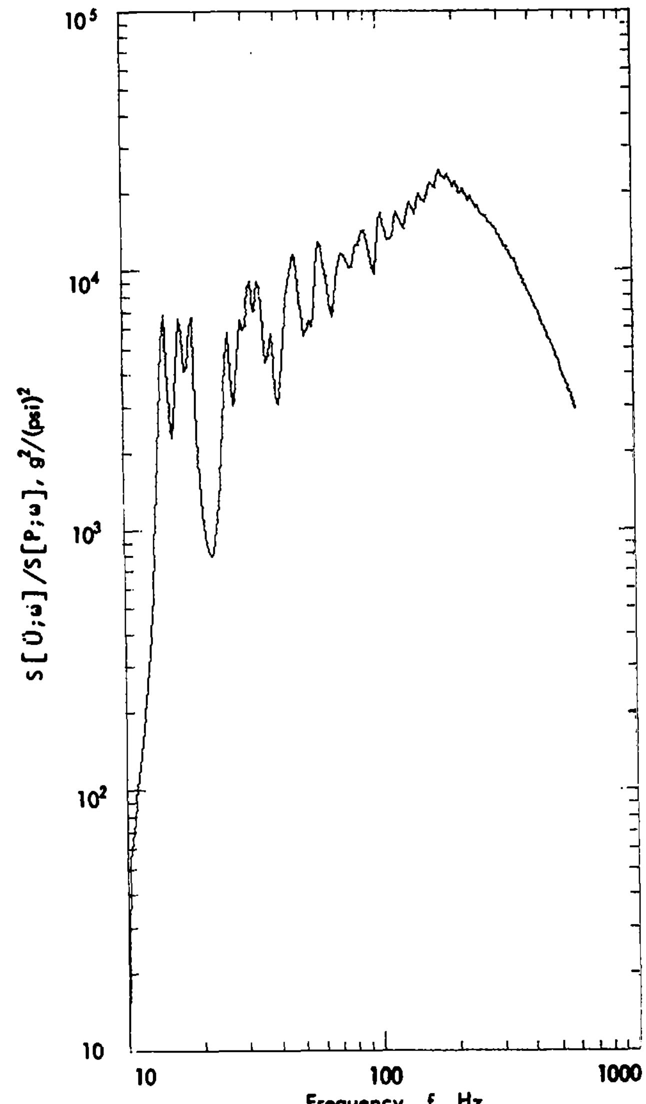

Figure 99. Effect of Radius Change on Acceleration Spectrum of SLA for Boundary Layer Turbulence Excitation; Mach 1, $\delta_b = 12.0$ in., $Q = 15$, $D = 8.10 \cdot 10^4$ lb-in.

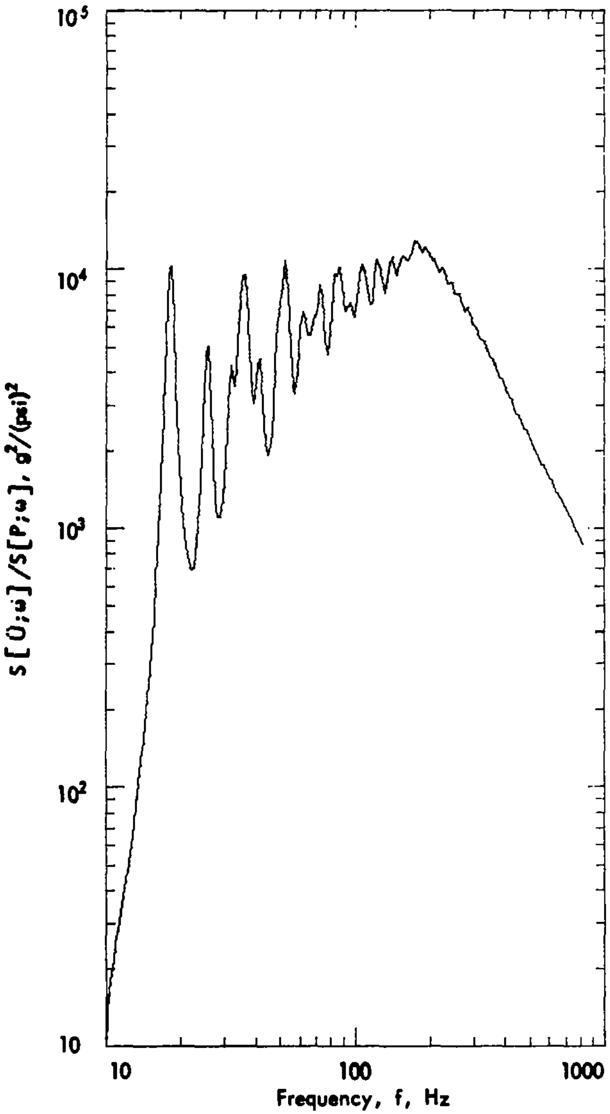

Figure 100. Effect of Stiffness Change on Acceleration Spectrum of SLA for Boundary Layer Turbulence Excitation; Mach 1, δ_b = 12.0 in., Q = 15, D = $1.62 \cdot 10^5$ lb-in.

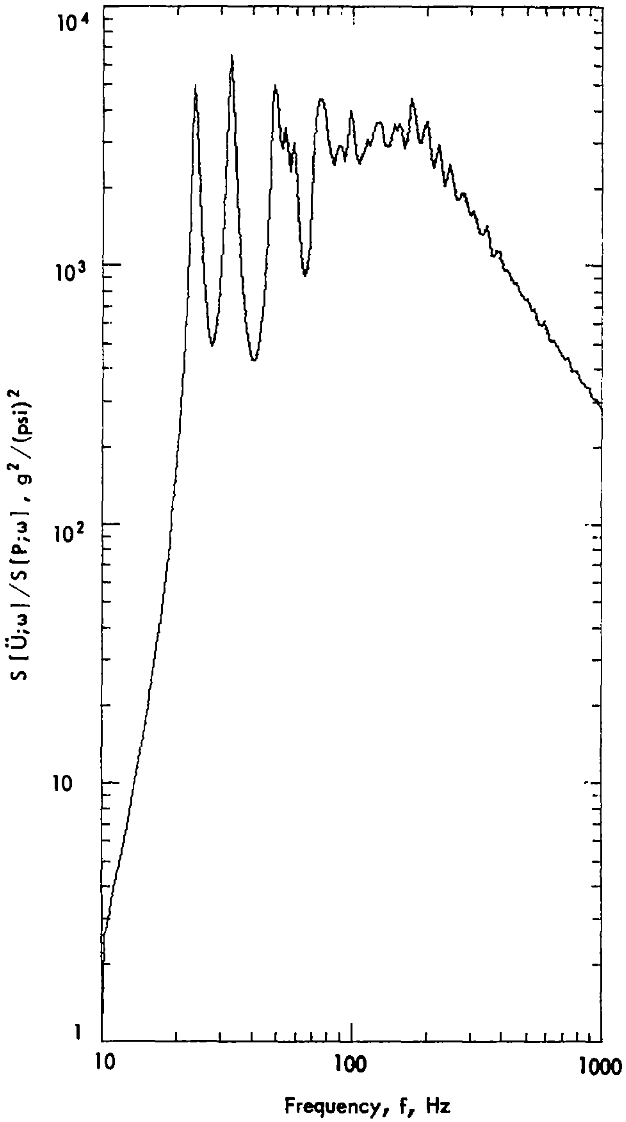

Figure 101. Effect of Stiffness Change on Acceleration Spectrum of SLA for Boundary Layer Turbulence Excitation; Mach 1, δ_b = 12.0 in., Q = 15, D = $6.48 \cdot 10^5$ lb-in.

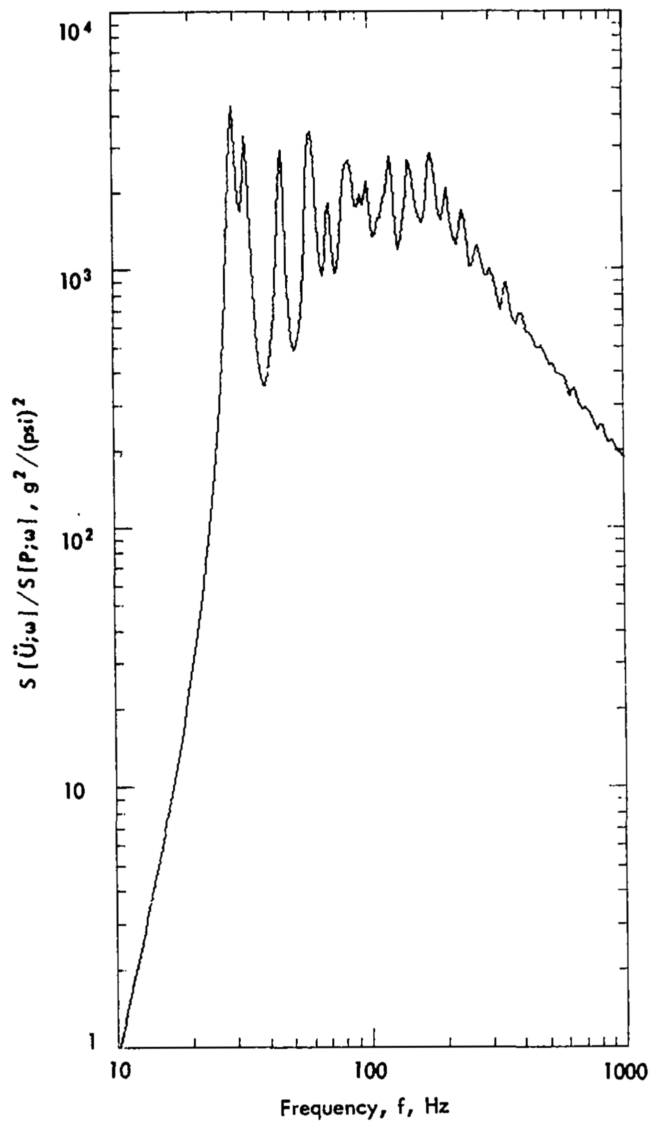

Figure 102. Effect of Stiffness Change on Acceleration Spectrum of SLA for Boundary Layer Turbulence Excitation; Mach 1, $\delta_b = 12.0$ in., Q = 15, D = $1.296 \cdot 10^6$ lb-in.

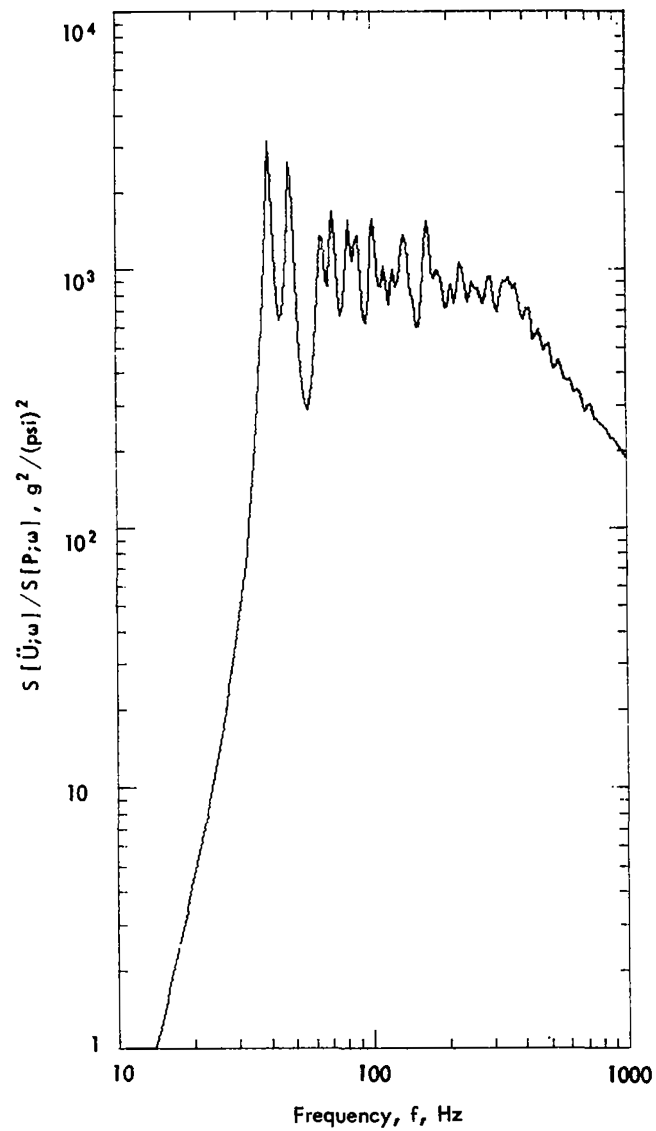

Figure 103. Effect of Stiffness Change on Acceleration Spectrum of SLA for Boundary Layer Turbulence Excitation; Mach 1, $\delta_b = 12.0$ in., Q = 15, D = $1.296 \cdot 10^6$ lb-in., $K_e = 1.88 \cdot 10^6$ lb/in.

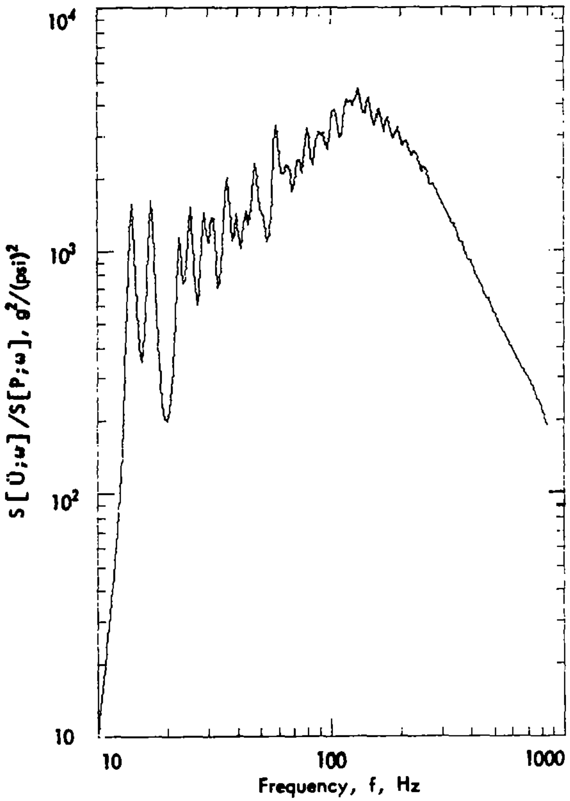

Figure 104. Effect of Surface Mass Change on Acceleration Spectrum of SLA for Boundary Layer Turbulence Excitation; Mach 1, $\delta_b = 12.0$ in., $Q = 15$, $\mu g = 0.0278$ lb/in^2

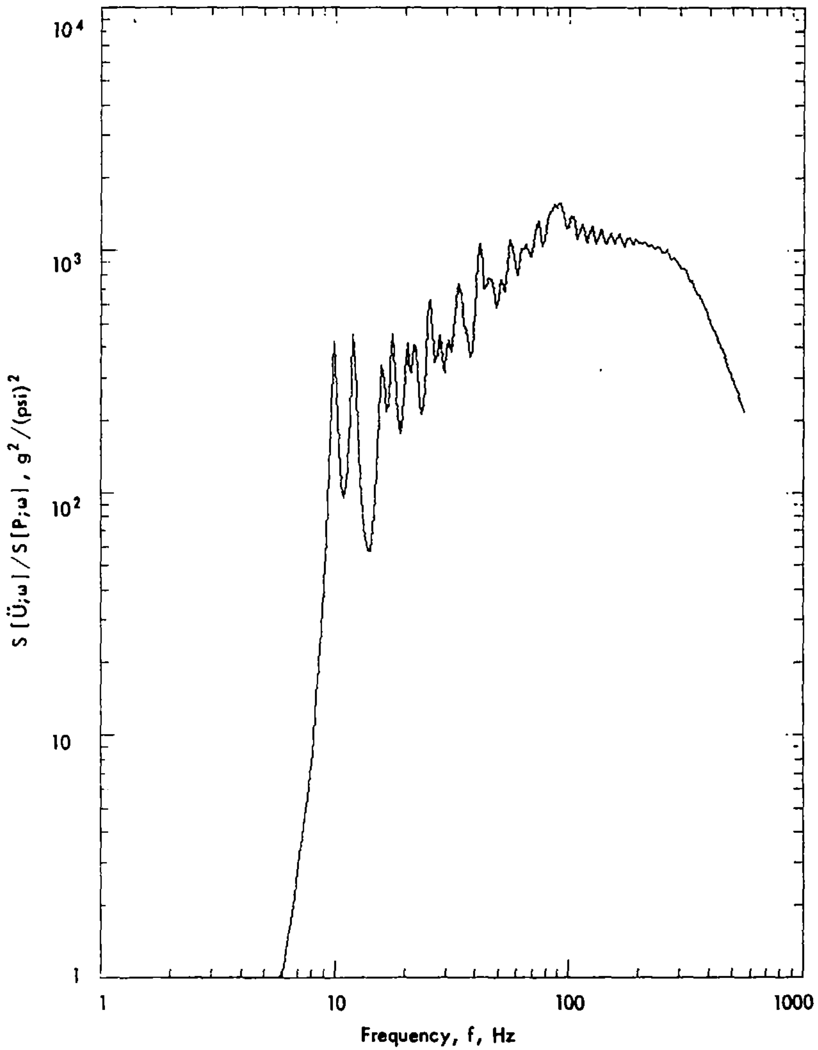

Figure 105. Effect of Surface Mass Change on Acceleration Spectrum of SLA for Boundary Layer Turbulence Excitation; Mach 1, $\delta_b = 12.0$ in., $Q = 15$, $\mu g = 0.0556$ lb/in^2

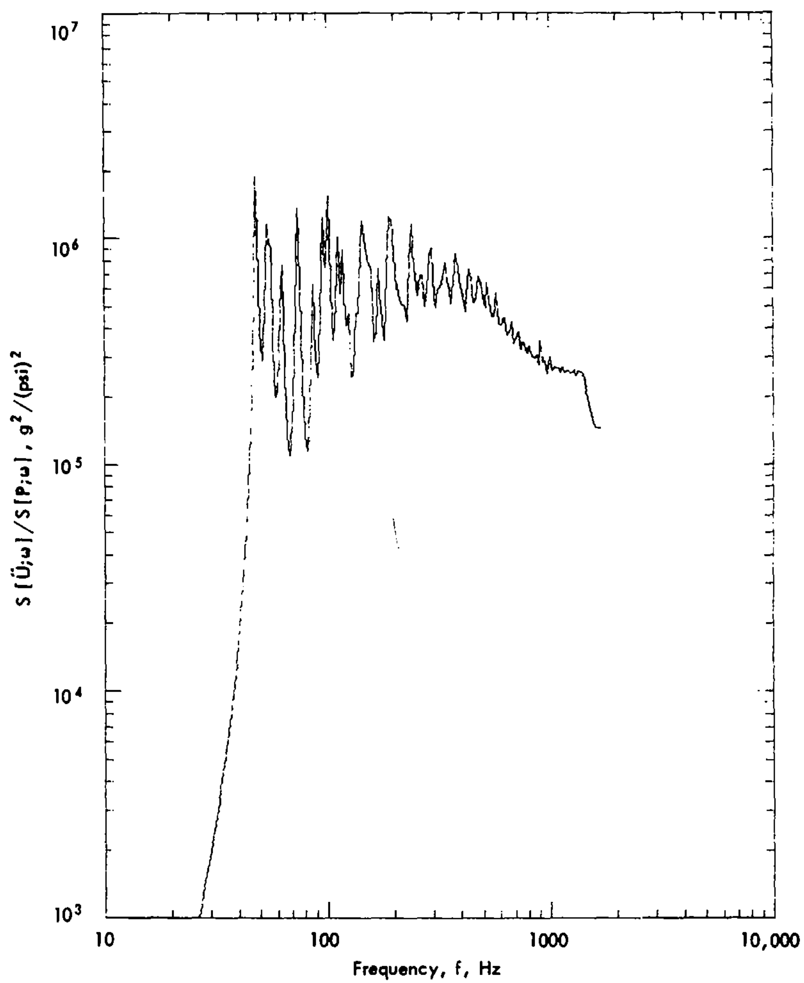

Figure 106. Acceleration Spectrum of 18 in. (Radius) by 54 in. by 0.02 in. Cylindrical Shell for Boundary Layer Turbulence Excitation; Mach $1/\sqrt{5}$, $\delta_b = 2.0$ in., Q = 30

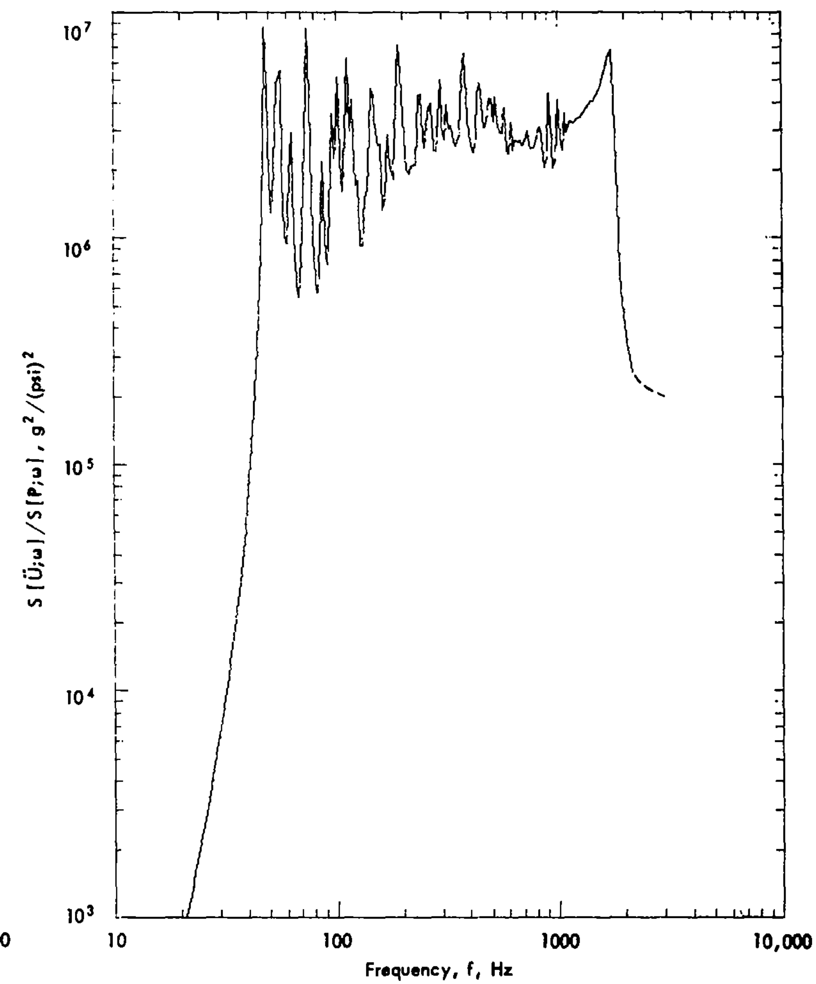

Figure 107. Acceleration Spectrum of 18 in. (Radius) by 54 in. by 0.02 in. Cylindrical Shell for Boundary Layer Turbulence Excitation; Mach 1, $\delta_b = 12.0$ in., Q = 30

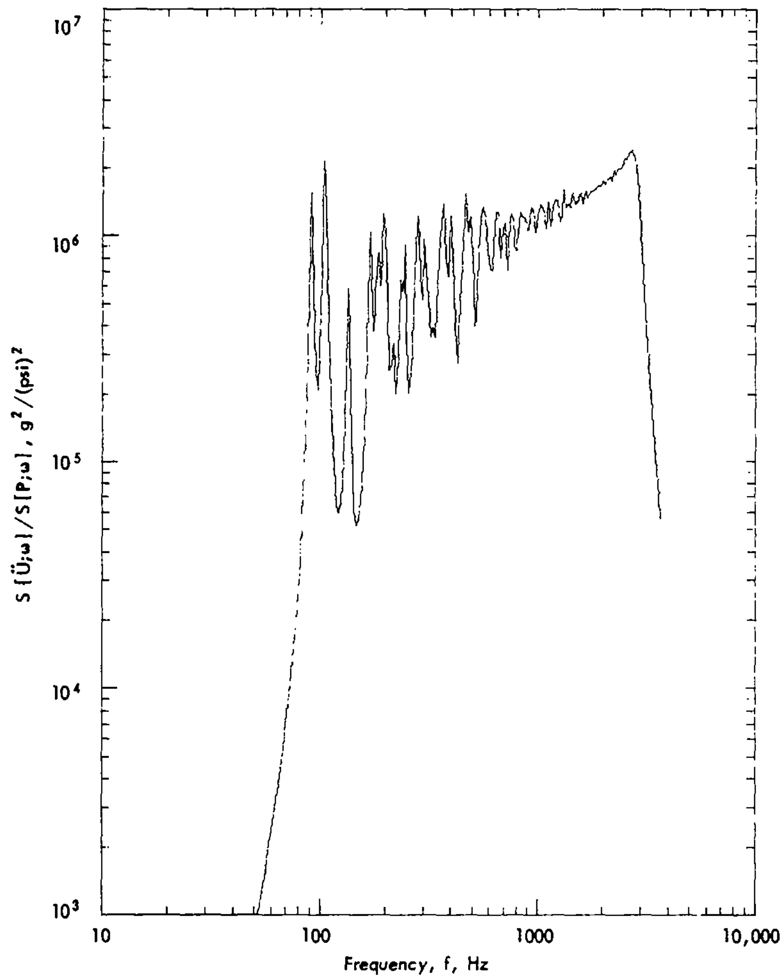

Figure 108. Acceleration Spectrum of 12 in. (Radius) by 48 in. by 0.04 in. Cylindrical Shell for Boundary Layer Turbulence Excitation; Mach 1, δ_b = 12.0 in., Q = 30

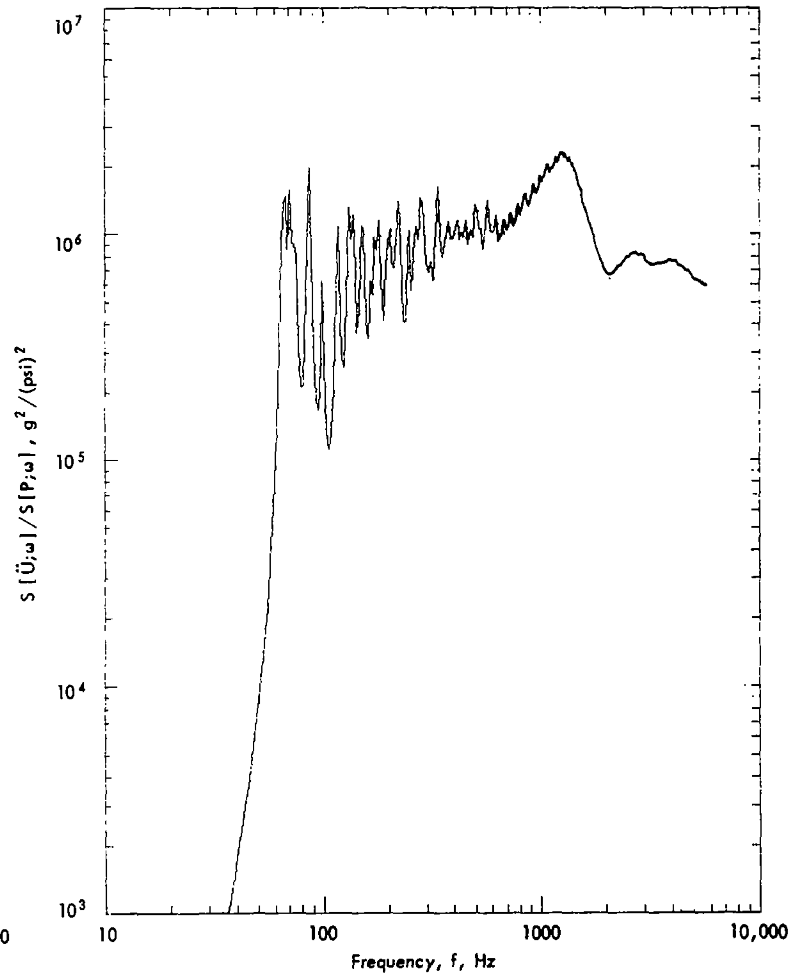

Figure 109. Acceleration Spectrum of 24 in. (Radius) by 48 in. by 0.04 in. Cylindrical Shell for Boundary Layer Turbulence Excitation; Mach 1, δ_b = 12.0 in., Q = 30

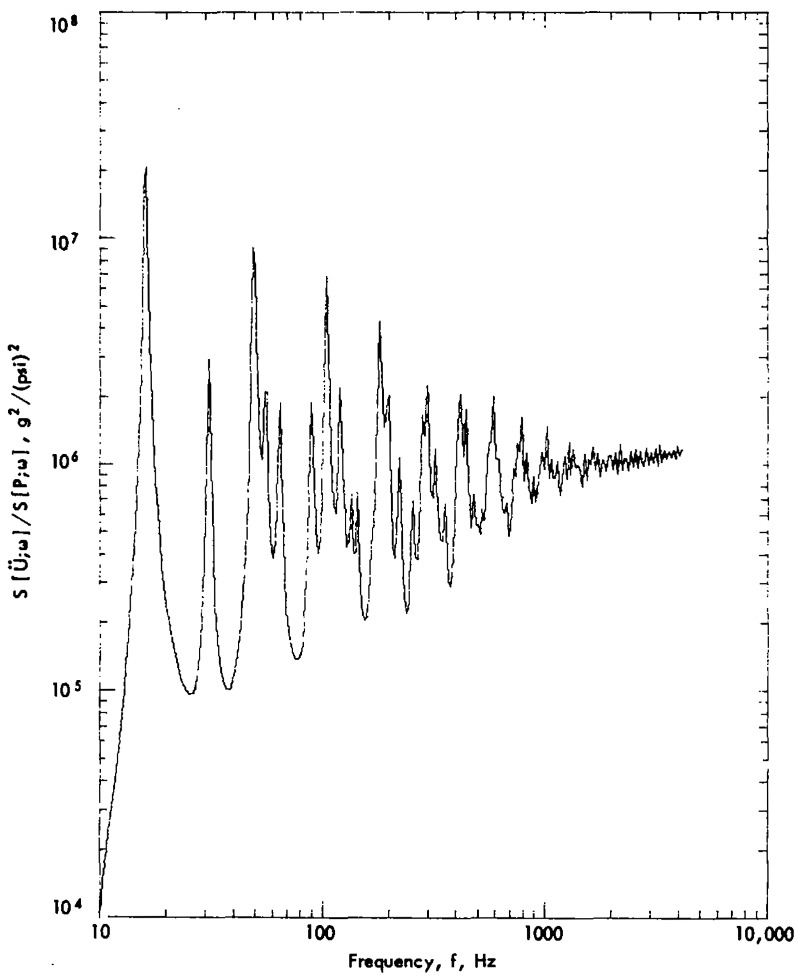

Figure 110. Acceleration Spectrum of 24 in. by 16 in. by 0.032 in. Flat Plate for Boundary Layer Turbulence Excitation; Mach 1, δ_b = 12.0 in., Q = 30

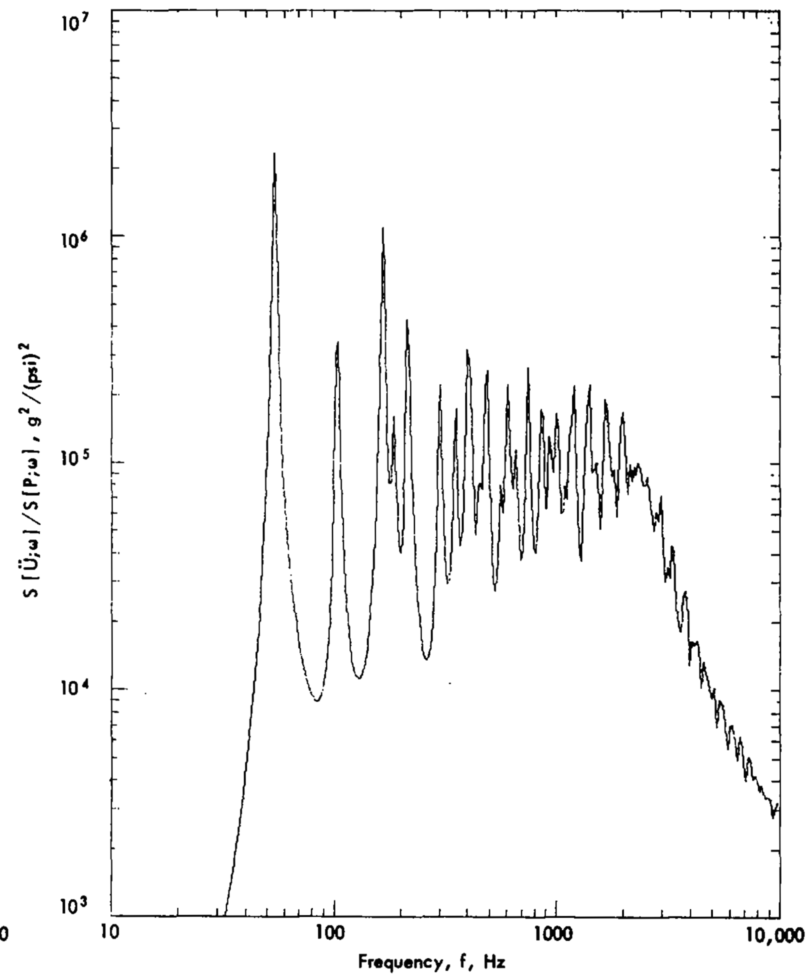

Figure 111. Acceleration Spectrum of 24 in. by 16 in. by 0.10 in. Flat Plate for Boundary Layer Turbulence Excitation; Mach 1, δ_b = 12.0 in., Q = 30

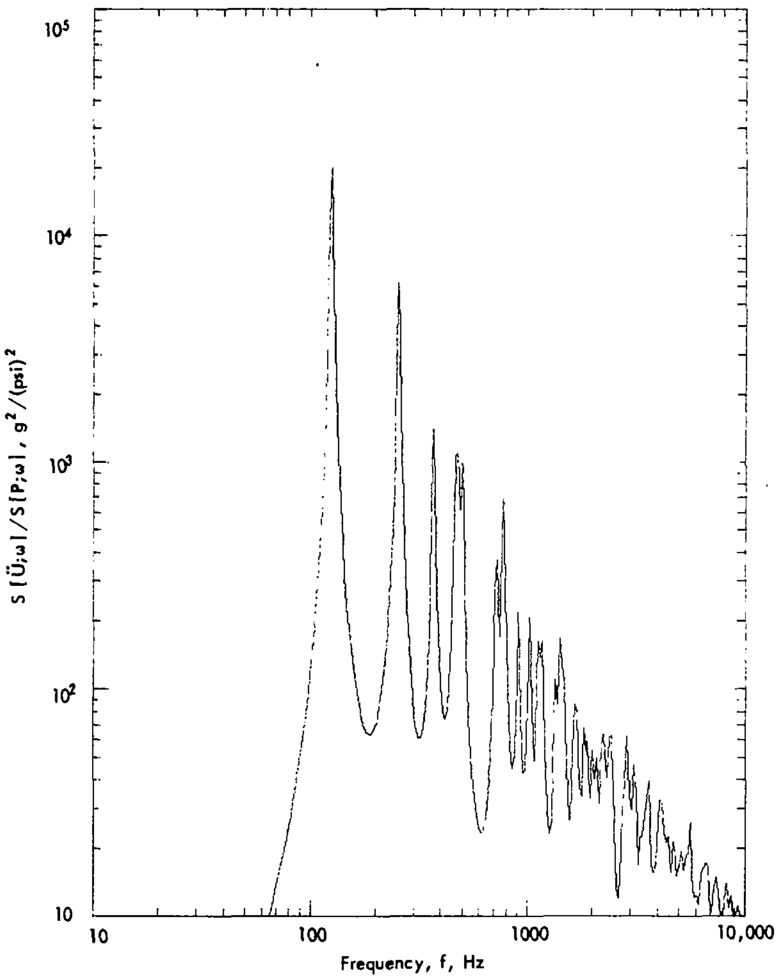

Figure 112. Acceleration Spectrum of Stiffened Flat Panel for Boundary Layer Turbulence Excitation; Mach 1, $\delta_b = 12.0$ in., Q = 30

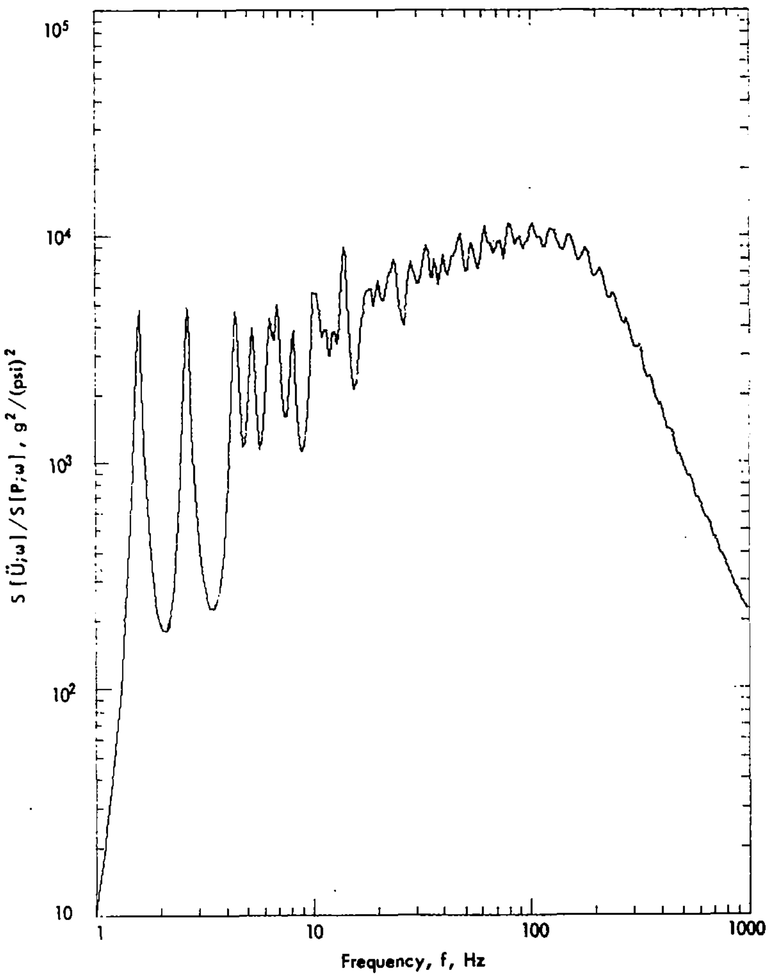

Figure 113. Acceleration Spectrum of Equivalent SLA Panel for Boundary Layer Turbulence Excitation; Mach 1, $\delta_b = 12.0$ in., Q = 15

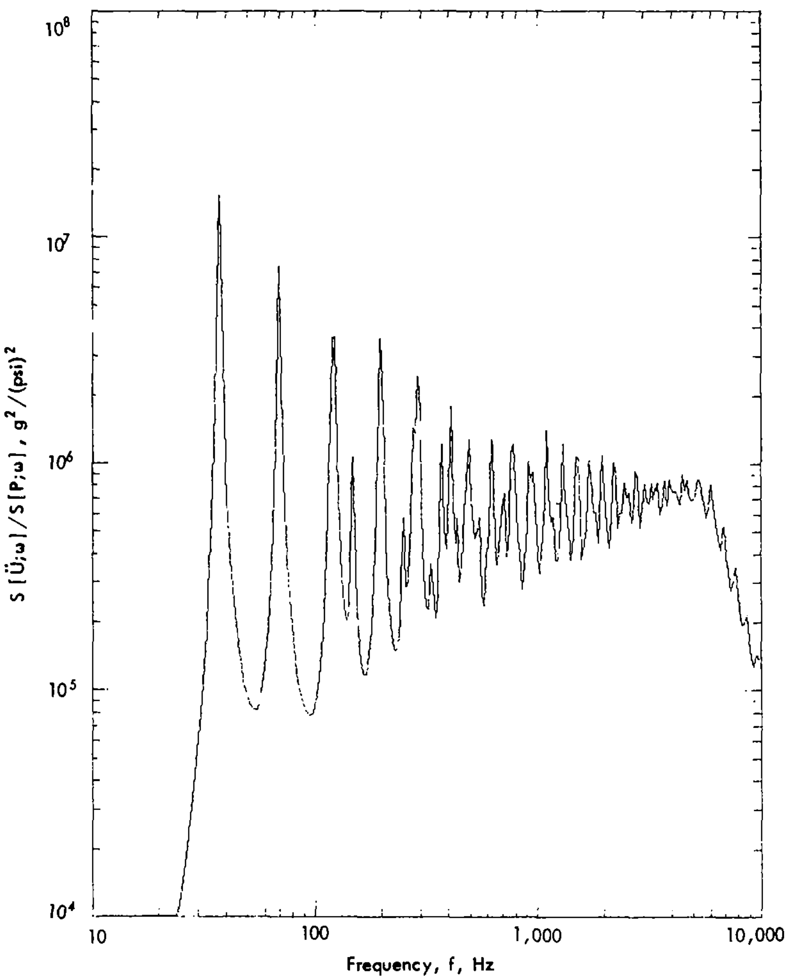

Figure 114. Acceleration Spectrum of 12 in. by 19 in. by 0.040 in. Flat Plate for Boundary Layer Turbulence Excitation; Mach 1, δ_b = 12.0 in., Q = 30

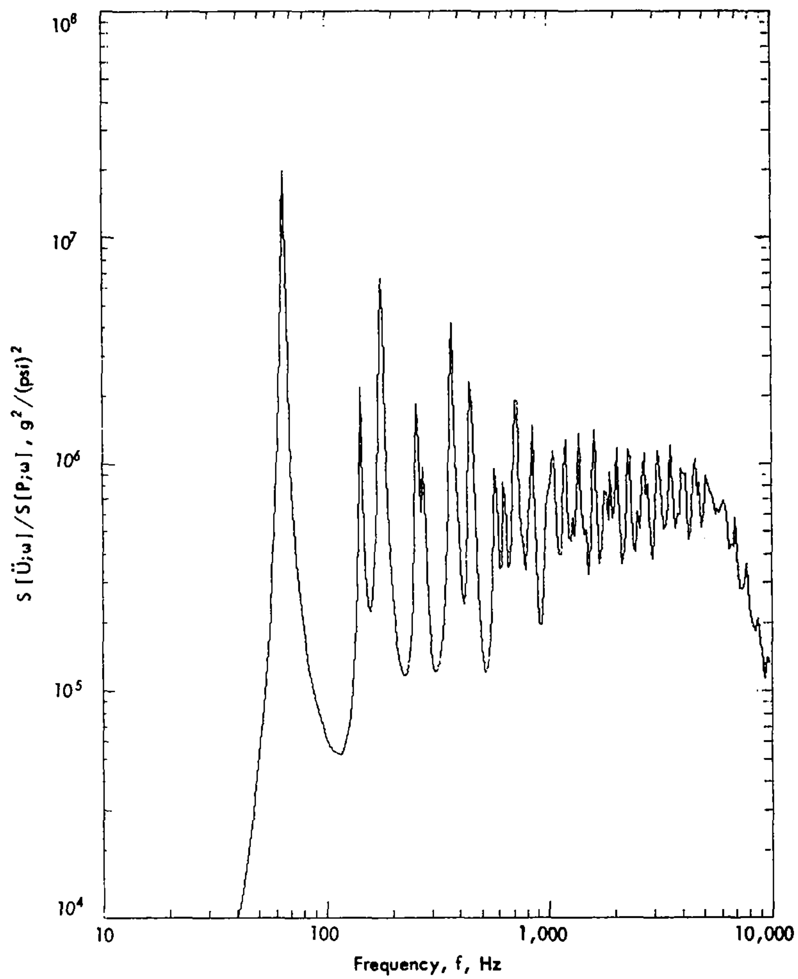

Figure 115. Acceleration Spectrum of 12 in. by 10 in. by 0.040 in. Flat Plate for Boundary Layer Turbulence Excitation; Mach 1, δ_b = 12.0 in., Q = 30

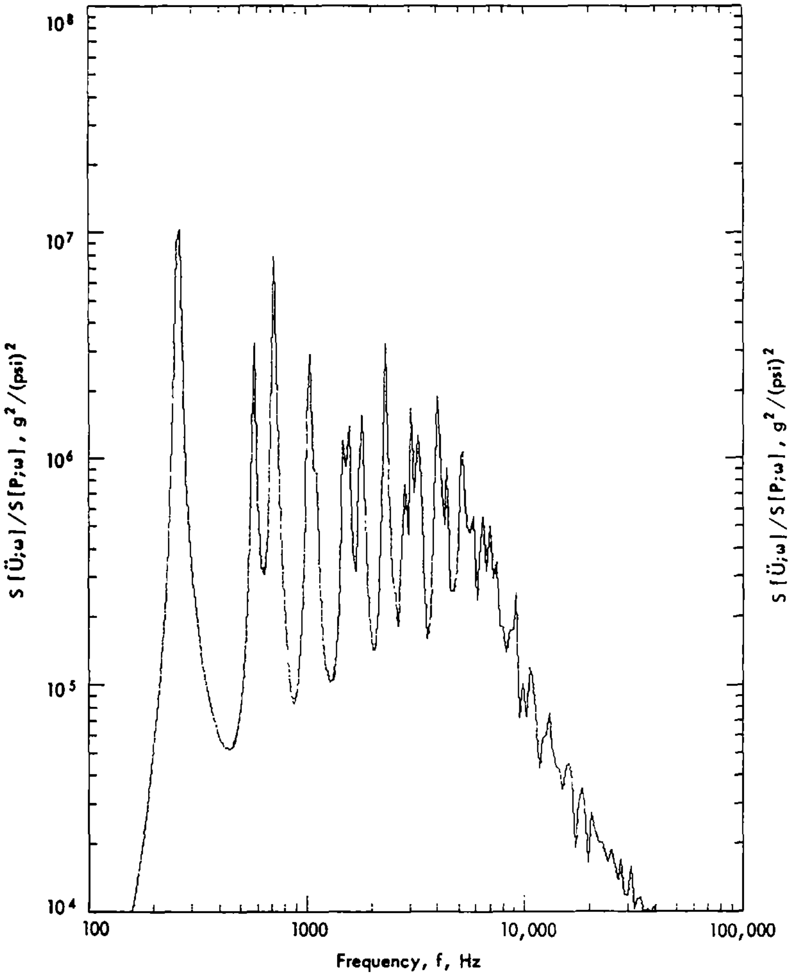

Figure 116. Acceleration Spectrum of 6 in. by 5 in. by 0.040 in. Flat Plate for Boundary Layer Turbulence Excitation; Mach 1, δ_b = 12.0 in., Q = 30

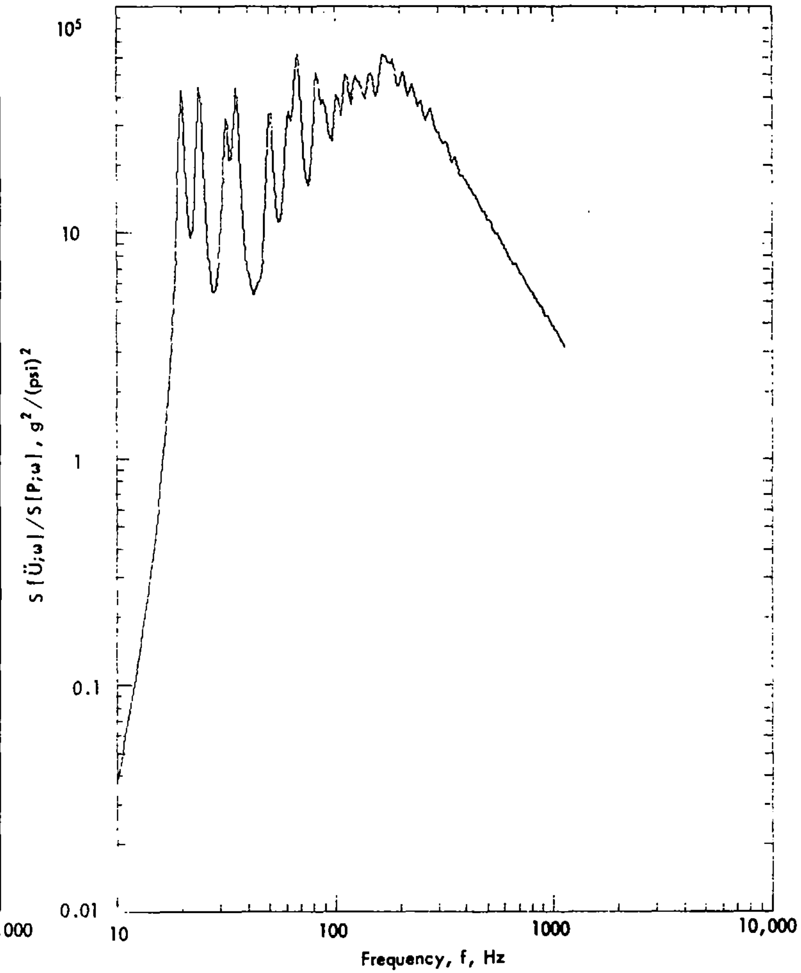

Figure 117. Acceleration Spectrum of SLA for Boundary Layer Turbulence Over 60.0 in. (Axial) x 30.0 in. Area Centered at Midheight; Q = 15, U_c = 9810 in./sec, δ_b = 12.0 in.

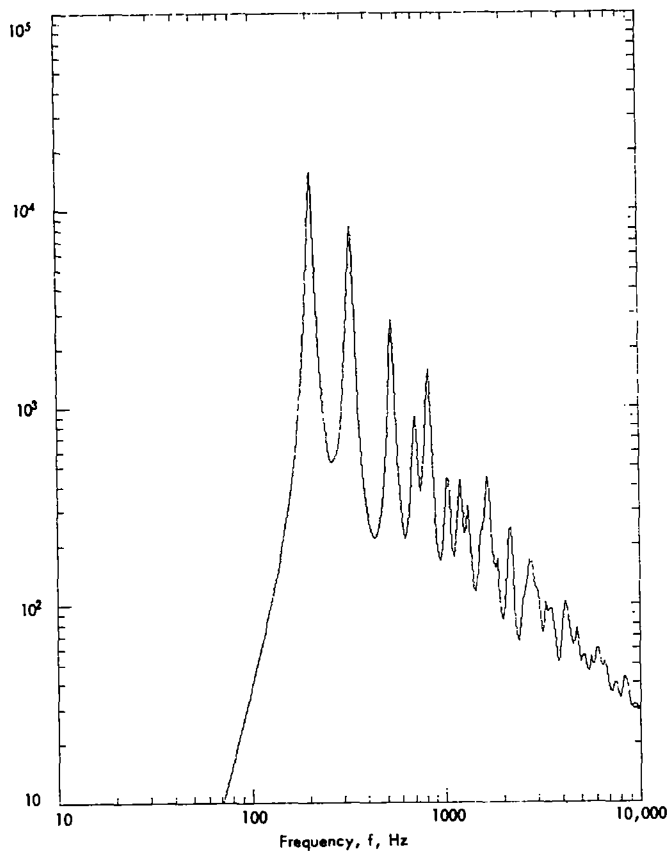

Figure 118. Acceleration Spectrum of 60.0 in. (Flow Axis) x 30.0 in. Panel Segment of SLA; Q = 15, U_c = 9810 in./sec, δ_b = 10.0 in.

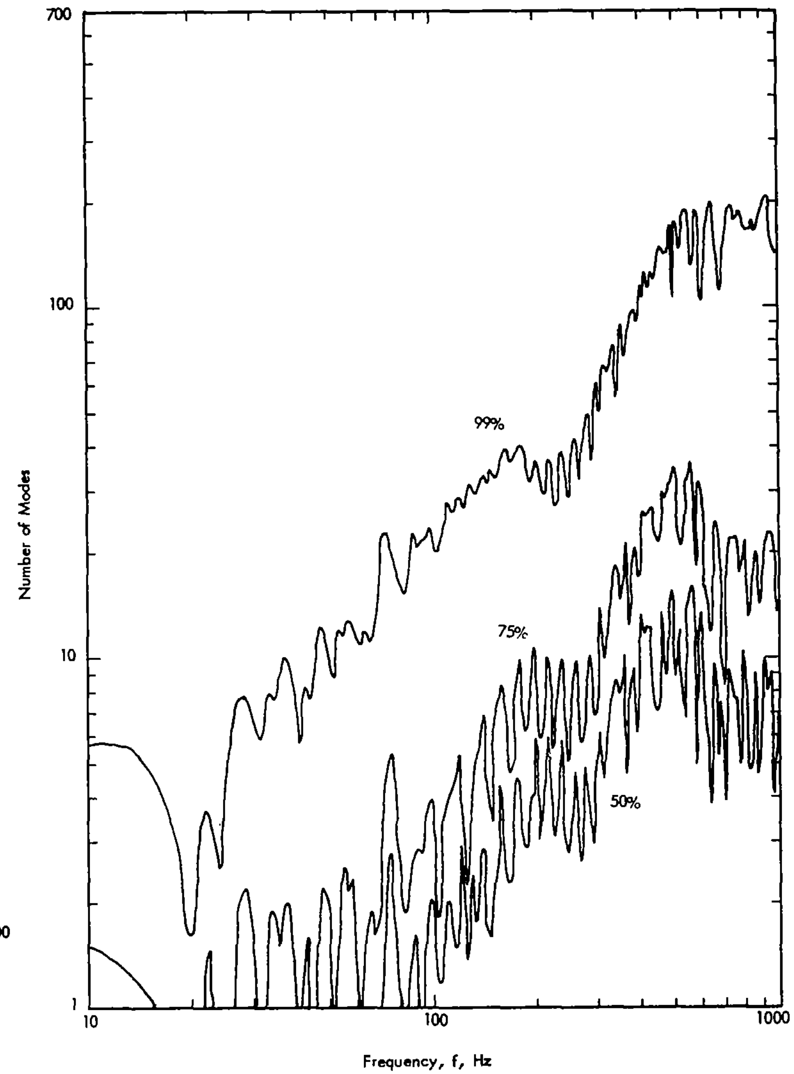

Figure 119. Number of Modes Required to Achieve Various Percentages of Total Response, SLA Structure for Sixteen Uncorrelated Ducts

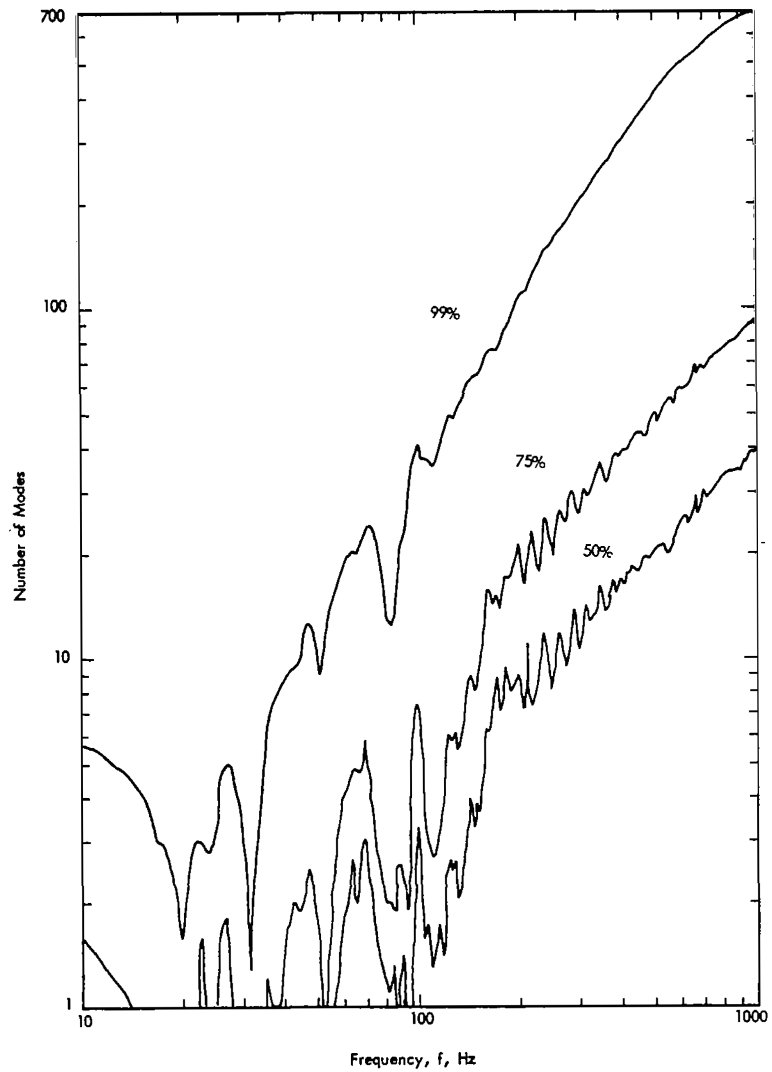

Figure 120. Number of Modes Required to Achieve Various Percentages of Total Response, SLA Structure for Reverberant Acoustic Field

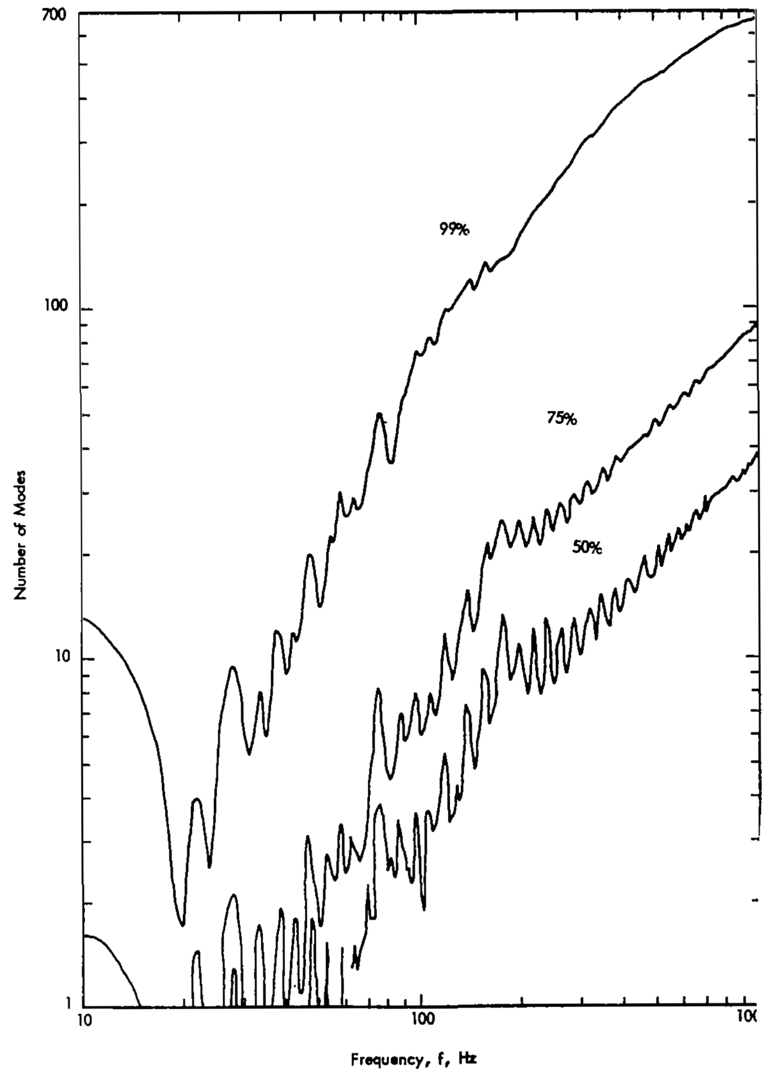

Figure 121. Number of Modes Required to Achieve Various Percentages of Total Response, SLA Structure for Boundary Layer Turbulence at Mach 1

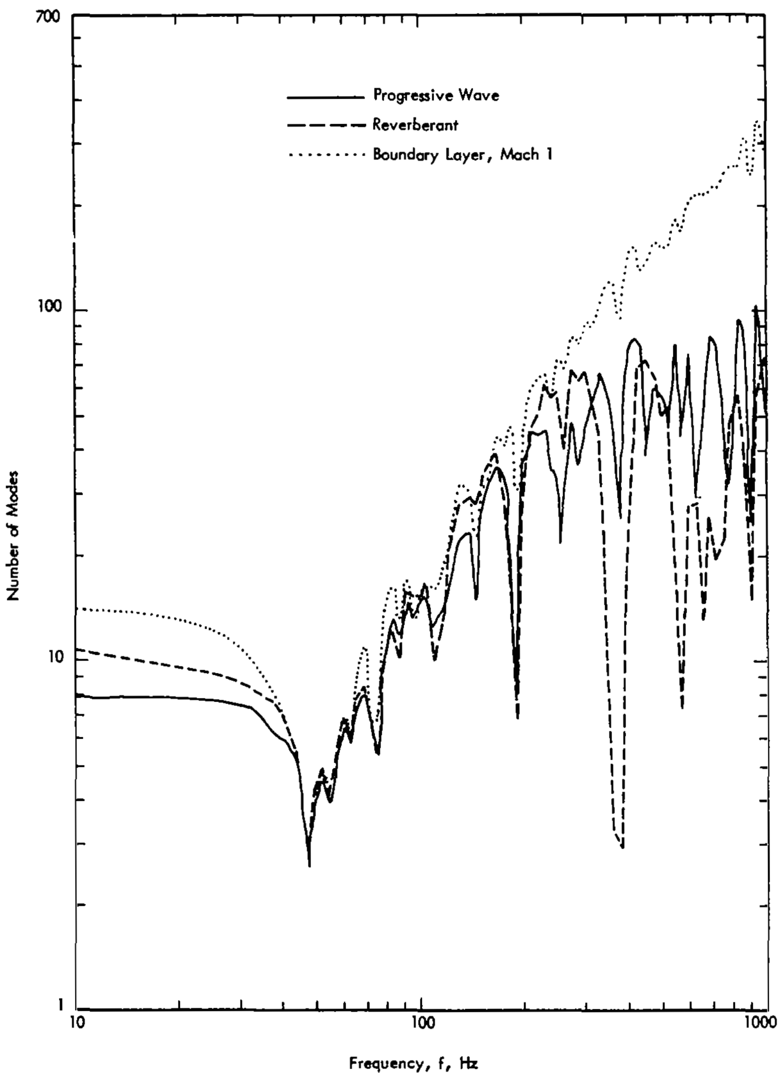

Figure 122. Number of Modes Required to Achieve 99% of Total Response for Various Excitation Fields; Republic Cylinder No. 12 (18" Radius x 54" x .020").

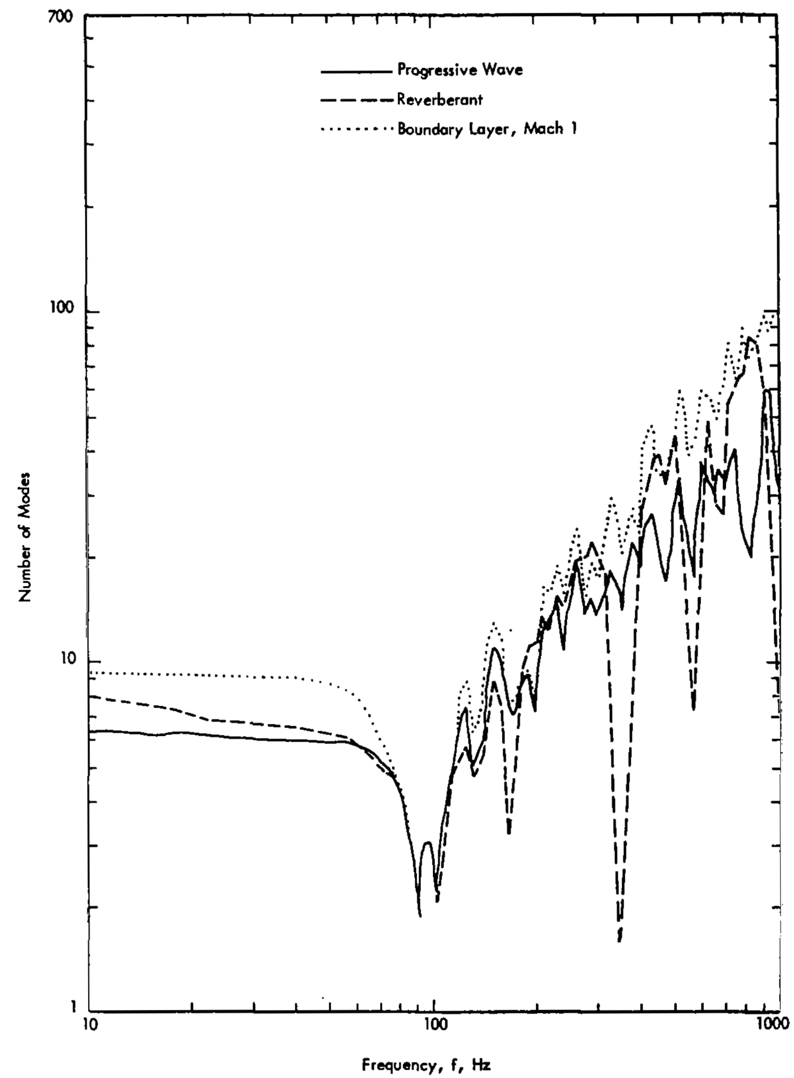

Figure 123. Number of Modes Required to Achieve 99% of Total Response for Various Excitation Fields; Uniform Cylinder (12" Radius x 48" x .040").

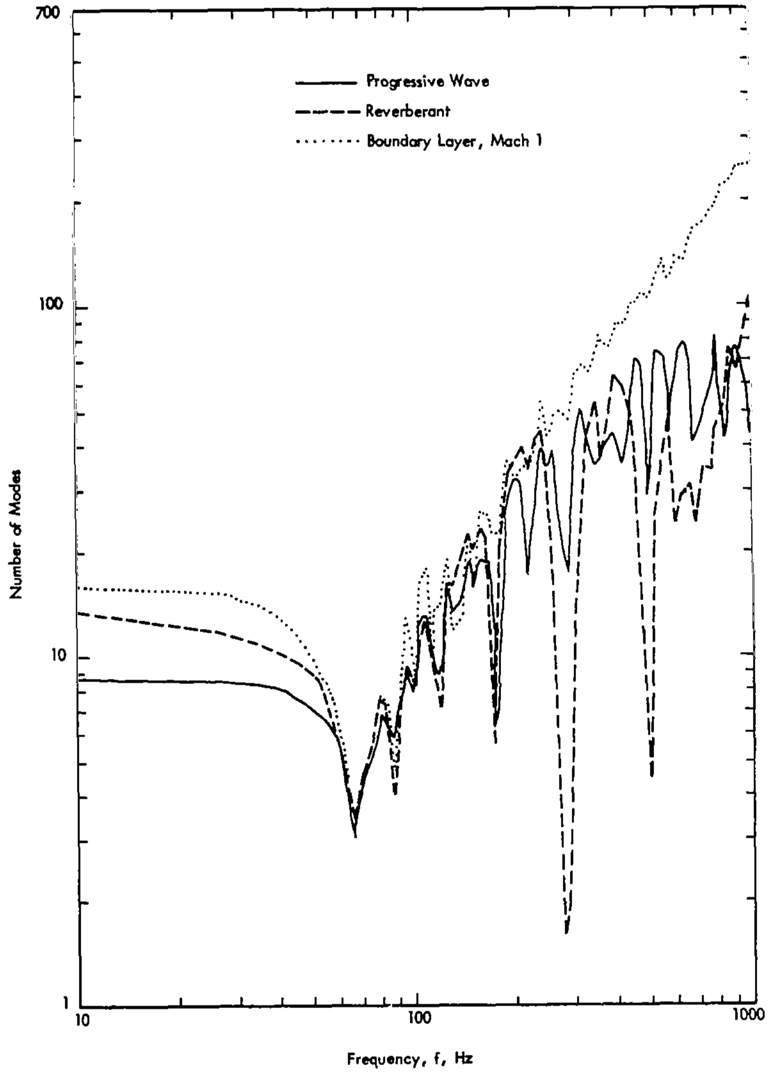

Figure 124. Number of Modes Required to Achieve 99% of Total Response for Various Excitation Fields; Uniform Cylinder (24" Radius x 48" x .040").

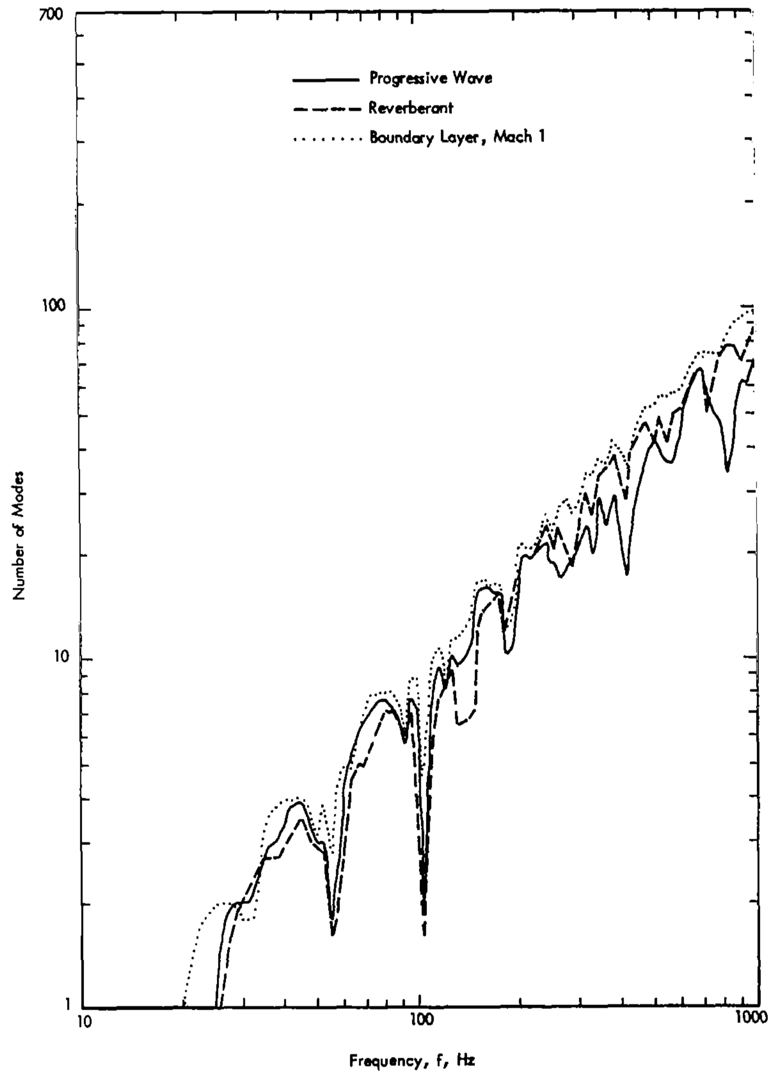

Figure 125. Number of Modes Required to Achieve 99% of Total Response for Various Excitation Fields; Flat Panel (24" x 16" x .032")

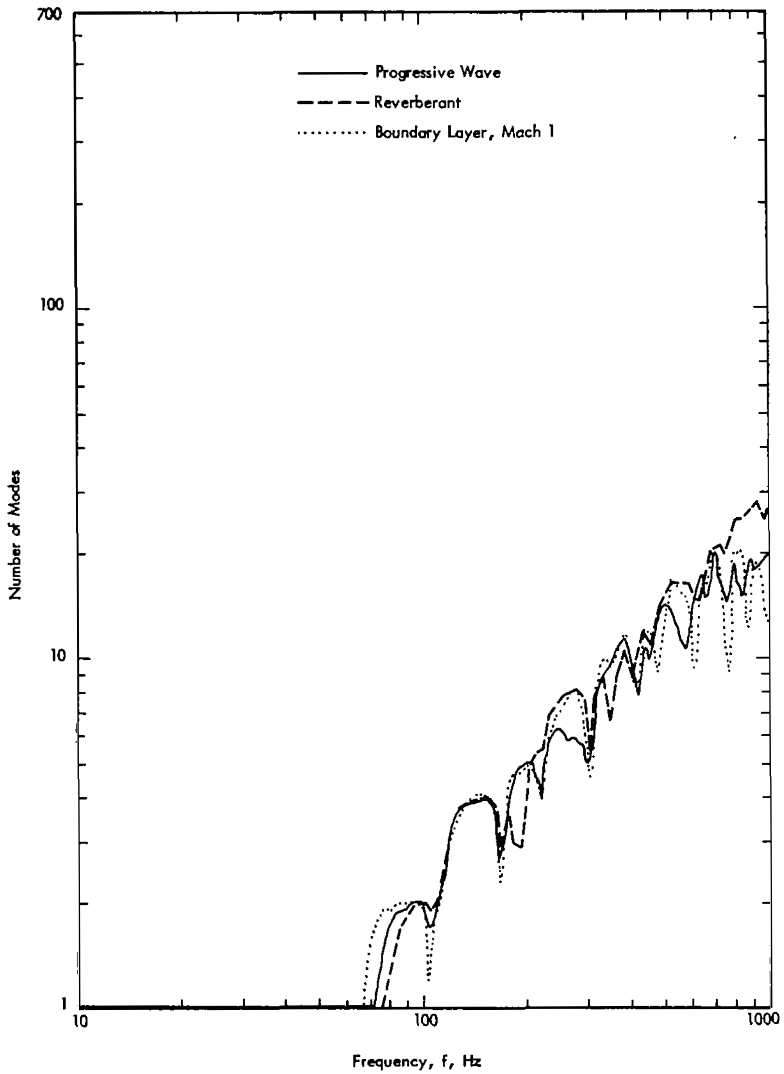

Figure 126. Number of Modes Required to Achieve 99% of Total Response for Various Excitation Fields; Flat Panel (24" x 16" x .1").

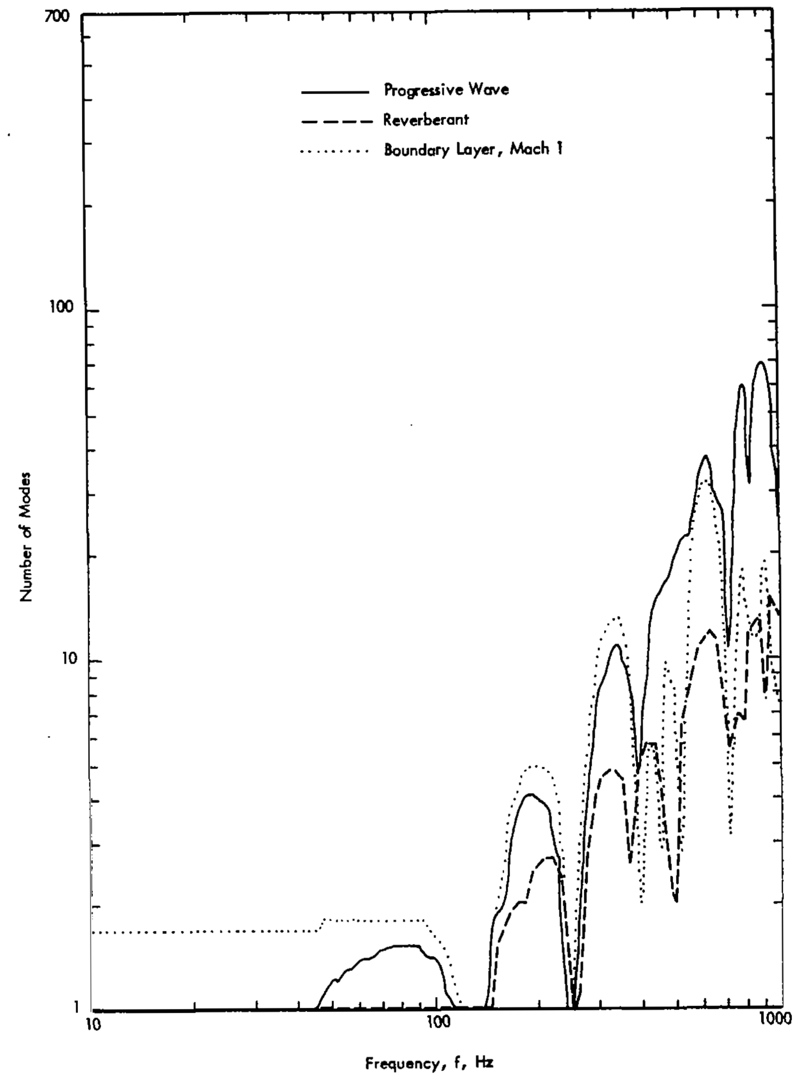

Figure 127. Number of Modes Required to Achieve 99% of Total Response for Various Excitation Fields; Stiffened Flat Panel (72.1" x 48.1").